Dissertation

submitted to the

Combined Faculties of the Natural Sciences and Mathematics
of the Ruperto-Carola University of Heidelberg, Germany

for the degree of

Doctor of Natural Sciences

Put forward by

Dipl.-Phys. Nicolai Christiansen

born in Kapfenhardt, Germany
Oral examination: 08.07.2015

Non-Perturbative Aspects of Quantum Field Theory:

From the Quark-Gluon Plasma to Quantum Gravity

Abstract.

In this dissertation we investigate several aspects of non-perturbative quantum field theory. Two main parts of the thesis are concerned with non-perturbative renormalization of quantum gravity within the asymptotic safety scenario. This framework is based on a non-Gaussian ultraviolet fixed point and provides a well-defined theory of quantized gravity. We employ functional renormalization group (FRG) techniques that allow for the study of quantum fields even in strongly coupled regimes. We construct a setup for the computation of graviton correlation functions and analyze the ultraviolet completion of quantum gravity in terms of the properties of the two- and three point function of the graviton. Moreover, the coupling of gravity to Yang–Mills theories is discussed. In particular, we study the effects of graviton induced interactions on asymptotic freedom on the one hand, and the role of gluonic fluctuations in the gravity sector on the other hand.

The last subject of this thesis is the physics of the quark-gluon plasma. We set-up a general non-perturbative strategy for the computation of transport coefficients in non-Abelian gauge theories. We determine the viscosity over entropy ratio η/s in SU(3) Yang–Mills theory as a function of temperature and estimate its behavior in full quantum chromodynamics (QCD).

Kurzfassung.

In dieser Dissertation untersuchen wir mehrere Aspekte nicht-störungstheoretischer Quantenfeldtheorie. Zwei Hauptteile dieser Arbeit beschäftigen sich mit der nicht-perturbativen Renormierung der Quantengravitation im Rahmen des Asymptotic Safety Szenarios, welches auf einem nicht-Gaussschen Ultraviolettfixpunkt beruht und eine wohldefinierte Quantisierung der Gravitationstheorie liefert. Wir bedienen uns funktionaler Renormierungsgruppenmethoden, die eine Untersuchung von Quantenfeldtheorien auch in stark gekoppelten Systemen erlauben. Wir konstruieren einen theoretischen Rahmen für die Berechnung von Gravitonkorrelationsfunktionen und untersuchen die Ultraviolettvervollständigung der Quantengravitation basierend auf den Eigenschaften der Zwei- und Dreipunktsfunktion. Darüber hinaus diskutieren wir die Kopplung von Yang–Mills Theorien und Gravitation. Im Speziellen untersuchen wir die Auswirkungen von gravitoninduzierten Wechselwirkungen auf Asymptotic Freedom auf der einen Seite, und die Rolle von gluonischen Fluktuationen auf den Gravitationssektor auf der Anderen.

Das Thema des dritten und letzten Teils dieser Arbeit ist die Physik des Quark-Gluon Plasmas. Wir konstruieren eine störungstheoretische Strategie für die Berechnung von Transportkoeffizienten in nicht-abelschen Eichtheorien. Wir bestimmen das Verhältnis von Viskosität zu Entropie η/s in SU(3) Yang–Mills Theorie als Funktion der Temperatur und präsentieren abschliessend eine Abschätzung für η/s in voller Quantenchromodynamik.

Contents

II. Yang–Mills Gravity   95

6. Basics   96

7. Quantum Gravity Contributions To Yang-Mills Theories   100

8. Yang-Mills Contributions To Quantum Gravity   109

III. The Quark Gluon Plasma and Transport Coefficients   114

9. Basics   115

Contents

CHAPTER 1

General Introduction and Structure of the Thesis

In this chapter we give a brief outline of this thesis and state the main results. This thesis consists of three main parts.

1. **Part One: Quantum Gravity**
   The first part is concerned with the quantization of gravity, Part I. It is well-known that perturbative quantization fails in the case of quantum gravity. We tackle the problem with non-perturbative renormalization group methods within the asymptotic safety scenario. The main goal in this approach is to construct a theory of quantum gravity based on a non-Gaussian ultraviolet fixed point.

   First, we give a brief introduction to quantum gravity and address the issues in standard perturbative quantization, chapter 2. A non-perturbative continuum method, namely the functional renormalization group, that forms the technical basis for our approach to quantum gravity is introduced in chapter 3. In chapter 4 we define the notion of asymptotically safe theories and put this in the context of non-perturbative quantum gravity. We review the status in the asymptotic safety scenario and discuss the standard setup for functional renormalization group equations in quantum gravity. In particular, we elaborate on the necessity of a background field and the related problems in the standard background field flows.

   In chapter 5, the more general setup of vertex expansions that allow for the calculation of fluctuation field correlation functions is constructed and applied in various approximations. The fundamental concepts and principles of this construction are formulated and developed in section 5.1. Within this framework, we present the novel notion of local RG flows of correlation functions, section 5.2. We present the general flow of the graviton propagator in this framework, section 5.3, and proof locality for the latter, subsection 5.5.1. We also generalize and formalize different expansions and projections in momentum space that are frequently used in the literature section 5.4. In section 5.5 an Einstein–Hilbert type of approximation is applied for the graviton propagator. We calculate the phase diagram and find an attractive ultraviolet

fixed point in the physical regime, thus providing further evidence for the asymptotic safety scenario. Additionally, we find a novel, attractive infrared fixed point, which is smoothly connected to the ultraviolet fixed point. For the first time, this is an approximation in quantum gravity that is ultraviolet safe, and also infrared complete. This approximation is significantly enhanced in the truncation studied in section 5.6. There, we go beyond Einstein–Hilbert truncations and include further couplings. In particular, we calculate the full momentum-dependence of the graviton and the ghost propagators by means of wave–function renormalizations that are arbitrary functions of the Laplacian. Moreover, this is the first setup in RG-gravity calculations that discriminate the different coupling parameters in the two-point function and higher order vertex functions. The momentum independent-parts of the vertex functions are constrained by a self-consistency analysis based on the hierarchy of flow equations. The resulting scaling relations turn out to be of major importance for a well-defined infrared limit. Also in this truncation we find the ultraviolet fixed point underlying asymptotic safety. In addition to that, we confirm the existence of the infrared fixed point found in the previous truncation. Moreover, an important aspect is that in this enhanced truncation the infrared fixed point has classical properties, which appear as classical scaling exponents for the dimensionless Newton constant and the dimensionless cosmological constant. As a consequence, the corresponding dimensionful quantities are really constant, meaning that we recover classical general relativity in the infrared limit. The stability of the approximation is tested for a class of regulators.

In section 5.7 we discuss the general structure of the flow of the graviton three point function, whose locality is then proven in subsection 5.8.1. This represents the first study of the three– graviton vertex with Wilsonian flow equations. The three–point function is then dynamically coupled to the propagator and the corresponding flows are derived in section 5.8 and solved in various approximations. We find further evidence for the non-Gaussian ultraviolet fixed point, with the interesting feature that in the most advanced approximation one coupling becomes irrelevant.

2. **Part Two: Yang–Mills Gravity**
   The second part section IV deals with the coupled system of Yang–Mills theory and quantum gravity. The main concern is the influence of gravitons on the fixed point in the theory of gluons and vice versa. We resolve the full momentum dependence of the gravity contributions to the running of the strong gauge coupling and find that graviton fluctuations do not destroy the property of asymptotic freedom in the ultraviolet limit. In the gravity sector, we first observe that the generic contributions of an $SU(N)$ gauge theory are local in momentum space. However, we find in a first assessment that the gravitational fixed point does not survive a large N limit.

3. **Part Three: Transport Coefficients in the Quark-Gluon Plasma**
   The topic of the third and last part, Part III, is not directly related to the ones above, since it is not concerned with the asymptotic safety scenario and Planckian and trans-Planckian ultraviolet physics. In this part we consider the quark–gluon plasma and calculate its shear viscosity over a wide range of temperatures T, from below the critical temperature T_c up to the regime where perturbation theory can be applied. The motivation for such a study, namely the creation of the quark–gluon plasma at particle

colliders and the related physical questions are discussed in section 9.1. Besides the phenomenological aspects, we provide some fundamentals in linear response theory. The strategy for calculating η/s, i.e. the ratio of shear viscosity over entropy, in a pure gluon plasma is then presented in chapter 10. The results are then given in section 10.2. We find that the viscosity over entropy ratio displays a minimum at approximately T_c. For lower temperatures, the behavior is consistent with a gluon resonance gas, while it matches the perturbative calculations for large T. Finally, we use the result in pure Yang–Mills theory for an estimate of η/s in full quantum chromodynamics.

The compilation of this thesis was carried out solely by the author. The results and presentations are largely based on work with my collaborators. Parts of this thesis are published or submitted and available as preprints: [1–4]

Part I.

Quantum Gravity, Functional Renormalization and Asymptotic Safety

Introduction to Quantum Gravity

On the one hand, the fundamental description of modern theoretical physics is based on quantum field theory, which describes the microscopic interactions of elementary particles in the framework of the standard model, [5–9]. The standard model of particle physics has been tested with impressive precision up to energy scales $E \approx 8 TeV$ and can be considered as one of the most successful theories in the history of physics. On the other hand, gravitational physics is governed by Einsteins theory of general relativity, [10]. Due to the absence of shielding effects, the force of gravity rules physics of large length scales and general relativity describes all gravitational effects that have been observed so far. The theory has proven to be able to capture phenomena like black holes and subtle effects like gravitational lensing. On smaller length scales, where electromagnetic effects become important, gravity becomes more and more difficult to detect since it is roughly forty orders of magnitude smaller then the electromagnetic force. The smallest length scale on which gravity has been tested is approximately 10^{-4}m, [11]. Nonetheless, as we will see below, dimensional analysis suggests that quantum gravity is governed by a typical energy scale, the Planck mass

$$M_{\mathrm{Pl}} \approx 10^{19}\,\mathrm{GeV}, \qquad (2.1)$$

and quantum gravitational effects are expected to become important at energies $E \approx M_{\mathrm{Pl}}$. The categorization of this immensely huge scale in the world of physics is visualized in Figure 2.1. Furthermore, general relativity predicts spacetime singularities and it is believed that quantum effects screen these classical singularities, leading to a well-behaved theory. Such a description requires a unified framework of gravitation and quantum mechanics, which is one of the outstanding questions in theoretical physics. One problem in the unification of these theories is the lack of direct access to physics of quantum gravity, as the Planck energy is much greater than all energies that can be reached with state of the art particle accelerators. As a consequence, structural and mathematical consistency are the only guiding principles in the search for a unified theory of quantum gravity. The big conceptual difference between these two theories is that the standard model arises due to quantization of classical field theories, since physical processes on very small length, or very
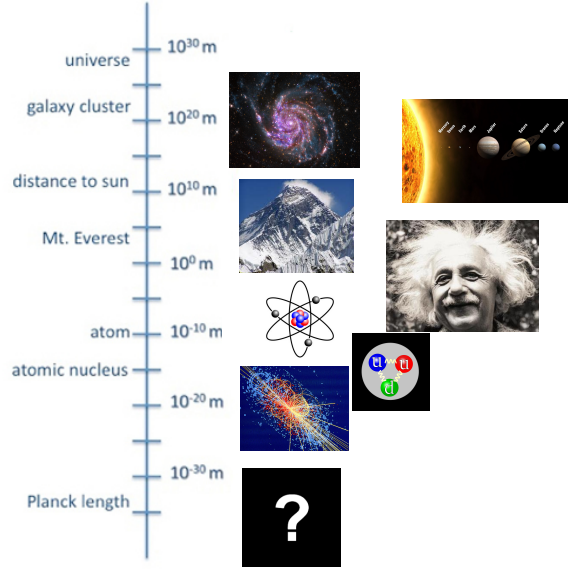
Figure 2.1.: The length scales of physic: From the largest length scales, the size of the universe itself, down to the scales of daily life, which is $\approx 1\text{m}$, via the the resolution of the LHC, $\approx 10^{-19}\text{m}$, to the known territory at the Planck length $L_{\text{Pl}} \approx 10^{-35}\text{m}$, which is the length scale that corresponds to the Planck mass.

high energy scales obey the laws of quantum mechanics. General relativity, however, is a classical field theory. No quantum effects are incorporated.

The basic principles of general relativity require a diffeomorphism invariant theory where the metric tensor carries the degrees of freedom. Note that non-metric formulations based on e.g. a vielbein field are equivalent on the classical level but may differ in the process of quantization. The classical action underlying general relativity is the famous Einstein-Hilbert action, which is constructed with the two lowest order curvature invariants. In d Euclidean spacetime dimensions it takes the form

$$S[g] = \frac{1}{16\pi G_N} \int \mathrm{d}^d x \sqrt{\det g}\, (-R(g) + 2\Lambda), \qquad (2.2)$$

where G_N is Newtons constant that describes the strength of gravitational interactions, g is the metric tensor, $R(g)$ is the Ricci scalar and Λ denotes the cosmological constant. Since the Ricci scalar contains two derivatives of the metric i.e. $R \sim (\partial g)^2$, which in turn is a dimensionless field, a simple dimensional analysis yields the mass-dimensions

$$[G_N] = 2 - d \quad , \quad [\Lambda] = 2. \qquad (2.3)$$

Therefore, in $d = 4$, which is the case that will be considered throughout this thesis, we infer $[G_N] = -2$. The mass dimension of Newton's constant implies that quantum gravity is governed by a typical energy scale, which is the Planck mass $M_{Pl} \approx 10^{19}$ GeV. The relation between Newtons constant and the Planck mass is encoded in the proportionality $G_N \sim M_{Pl}^{-2}$, where the proportionality factor is one in natural units.

The standard, and by far most developed, quantization procedure of field theories is based on perturbation theory, where n-point Greens function, which define a quantum field theory, are expanded in powers of the coupling constant. A key part in the machinery of a quantum field theory is the renormalization of ultraviolet divergences that appear at very large momenta and are mathematically rooted in ill-defined distributional products. In a renormalizable theory one can absorb these divergences by a redefinition of the fundamental fields and couplings. However, it is well-known that a coupling constant with negative mass dimension spoils renormalizibility in the framework of perturbation theory.

In perturbation theory one expands N–point correlation functions C_N as a formal power series in the *dimensionless* coupling constant, which is in the case of gravity

$$g := G_N E^2 \,, \tag{2.4}$$

where E is some typical energy scale characteristic to the process under consideration. Such an expansion can be written in a schematic way according to

$$C_N = \sum_{n=0}^{\infty} c_{N,n} g^n = \sum_{n=0}^{\infty} c_{N,n} \left(\frac{E^2}{M_{Pl}^2} \right)^n \,. \tag{2.5}$$

In typical quantum field theories the coefficients $c_{N,n}$ are divergent. However, in renormalizable field theories, one can get rid of these infinities in a meaningful way. First, one regularizes the theory with an ultraviolet-cutoff such that all quantities are finite. In a second step, the action is modified by introducing counter-terms that resemble the structure of the divergent diagrams. These counter-terms are then chosen such that they cancel the divergent parts and one is left with finite contributions only. The subtraction procedure is largely arbitrary and characterizes different renormalization schemes. The decisive point is that in perturbatively renormalizable theories, there may be infinitely many divergent coefficients[1] $c_{N,n}$, but it is sufficient to introduce finitely many counter-terms to cure all divergences order by order in perturbation theory.

However, in quantum gravity the situation is quite different. Calculating the series (2.5) with the bare Einstein-Hilbert action, one gets the expected divergences from the loop diagrams which lead to infinite contributions in the coefficients c_n. However, these divergences cannot be absorbed by finitely many counter-terms. This can immediately be seen by power counting arguments as follows. The quantities entering the loop diagrams are the graviton propagator and the multi-graviton vertices. Expanding the Einstein–Hilbert action in powers of the graviton field, we see that all graviton vertices are proportional to p^2 due to the structure of the Einstein–Hilbert action. The vertex functions will be discussed in more detail in subsection 5.1.1. Additionally, the n-th functional derivative of the Einstein–Hilbert action with respect to the metric is non-zero. Consequently, there are already infinitely many tree-level vertices in gravity. This is a distinct feature of diffeomorphism invariant theories and distinguishes quantum gravity from field theories in fixed background spacetime such as ordinary quantum electrodynamics. After a suitable rescaling of the graviton field, a perturbative n-graviton vertex is then proportional to $G^{\frac{n}{2}-1} p^2$, see Figure 2.2.

We will illustrate the structure of divergences in quantum gravity with the example of a class of diagrams containing propagators and three- and four-graviton vertices. By simple

---

[1]In super-renormalizable field theories, there are only finitely many divergent diagrams and for some order n_0 in perturbation theory all $c_{N,n>n_0}$ are finite.

$$\text{graviton propagator :} \quad \text{〜} \quad \sim \frac{1}{p^2}$$

$$\text{three} - \text{graviton vertex :} \quad \text{〜} \quad \sim \sqrt{G}p^2$$

$$\text{four} - \text{graviton vertex :} \quad \text{〜} \quad \sim Gp^2$$
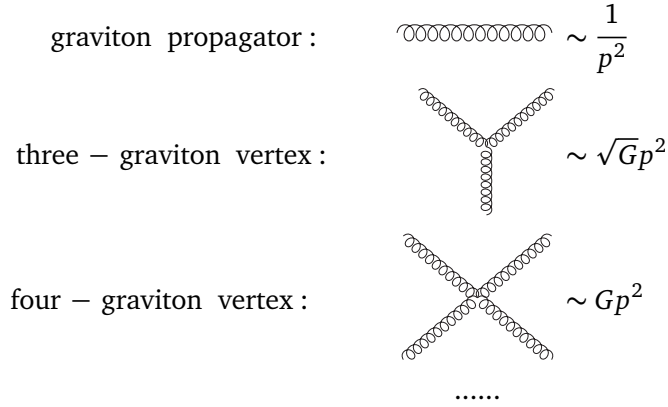
......

Figure 2.2.: Perturbative graviton propagator and vertices. Note that all vertices are proportional to p^2 and that there are already on tree-level infinitely many graviton vertices.

power counting with the graviton propagator and vertices, one can see that such a diagram diverges with the ultraviolet cutoff as Λ^γ in the limit where the ultraviolet cutoff Λ goes to infinity. The exponent γ is called the degree of divergence and is given by

$$\gamma = 2 - 2N + \#(\text{three} - \text{graviton vertices})f_3 + \#(\text{four} - \text{graviton vertices})f_4 \,, \qquad (2.6)$$

where N is the number of external lines, i.e. this indicates to which correlator C_N this diagram contributes, and

$$f_i = P - d + i \,. \qquad (2.7)$$

In the above equation P is the maximum number of derivatives in the vertex, and d the number of spacetime dimensions. As we have already argued above, $P = 2$ for all graviton vertices. From the above relations for the degree of divergence γ, one can see that at higher loop order for a correlator of constant order N, the degree of divergence gets worse and worse since the number of graviton vertices increases. A higher degree of divergence means that the counter-term that is necessary in order to absorb this divergence needs to be of higher order in momentum. However, such terms are not present in the original action and therefore each higher order introduces genuinely new divergences. Consequently, one needs infinitely many counter-terms, which in turn come along with infinitely many free parameters that need to be measured by experiments [2]. This momentum structure and the power-counting just reflects the negative mass dimension of Newtons coupling, which can therefore be regarded as the root of the perturbative non-renormalizibilty of quantum gravity. It is clear that a theory with infinitely many free parameters lacks predictive power and cannot be considered as fundamental.

The one-loop divergences have been calculated for the first time by t'Hooft and Veltman [12], and the non-renormalizibility at the two-loop level has been shown explicitly by Goroff and Sagnotti, [13]. These results constitute the famous ultraviolet problem of quantum gravity

---

[2]More precisely, one needs to introduce infinitely many renormalization conditions that need to be fixed with experimental input

that hampers the quantization of general relativity and represents one of the great problems in theoretical physics.

A theory of quantum gravity based on a classical action containing all fourth-order derivative terms can be renormalized to all orders in perturbation theory, as was shown by K.Stelle [14]. Nonetheless, the resulting quantum theory faces serious violations of the perturbative notion of unitarity and does therefore also not qualify as a fundamental UV-completion of quantum gravity. Interestingly, it was shown that once infinitely many higher derivative operators are included, unitarity can be restored, [15]. However, the bare action is in this case an infinite series of operators, which leads one back to the problem of predictivity.

Nevertheless, perturbative quantum gravity is perfectly acceptable as an effective field theory at energies well below the Planck scale. This can be seen from the perturbative expansion (2.5) of correlation functions. For energies $E << M_{\text{Pl}}$, higher order terms are negligible, and one can simply ignore the problems arising due to the infinitely many free parameters since their contributions to transition amplitudes are completely irrelevant. Perturbative quantum gravity in the framework of effective field theory was put forward by J.Donoghue, for reviews see [16,17]. An important result produced in this approach are the leading order quantum corrections to the Newtonian potential [18], analogous to the Uehling potential in quantum electrodynamics that encodes the quantum corrections to Coulombs law. Still, this theory lacks a satisfying ultraviolet completion.

These problems initiated a vast amount of new developments, even entirely new theories such as string theory or loop quantum gravity. These theories are based on concepts and assumptions that go far beyond everything that has been verified experimentally. Therefore one might ask for a more conservative approach to quantum gravity. An approach with less assumptions and without any need to introduce new, unknown physics at some very high energy scale.

This is the main intention behind the asymptotic safety scenario. It addresses the obvious weak point in the standard quantum field theoretical approach to gravity, namely the perturbative nature. The basic idea is that the ultraviolet limit in quantum gravity is governed by a non-trivial fixed point that cannot be accessed by standard perturbation theory. A fixed point appears as a point in theory space where the renormalization group flow becomes independent of the momentum scale, which is signaled by zeroes of the beta function. In this case all couplings tend to finite values in the ultraviolet limit. This construction requires knowledge of the non-perturbative scale dependence of the couplings. The method of choice in a continuum approach in order to tackle this problem is the functional renormalization group, which will be introduced in the next section.

The Functional Renormalization Group

3.1. Notation

Before introducing the functional renormalization group, we fix our notation and conventions. The fundamental object in quantum field theory is the field operator φ. This operator carries continuous indices, like the space-time position x or, after Fourier transform, the momentum p. Additionally, in general the field transforms non-trivially under the Poincare group or arbitrary gauge groups. This manifests in discrete index sets that describe the corresponding tensorial character. We subsume all that in a super index labeled by latin characters written as ϕ^a. Usual Lorentz indices are represented by greek characters. As a very important notational simplification for formal manipulations, a contraction over the super index implies not only summation over the discrete indices, but also integration over the continuous one, i.e. an integration over space-time in position space or over momentum in the Fourier representation. We will frequently use this notation for the graviton field, whose coefficient function are then written as $h_{\mu\nu}(x) =: h_a$ and

$$h_a h^a := \int_{\mathbb{R}^4} \mathrm{d}^4 x \, h_{\mu\nu}(x) h^{\mu\nu}(x) := \int_{\mathbb{R}^4} \mathrm{d}^4 x \sum_{\mu,\nu} h_{\mu\nu}(x) h^{\mu\nu}(x) \,, \qquad (3.1)$$

where the second definition just means that we apply Einsteins sum-convention for the contractions. Additionally, a general theory has a field content with more than one field. Hence, we define a yet more general index class that describes a vector in super-field space [1], i.e. in a theory with n different fields φ_i it is a n-dimensional vector that comprises all fields. Super-indices describing components in this vector space are labeled with latin, bold characters. Therefore we write

$$\varphi^{\mathbf{a}} = \left(\varphi^{a_1}, ..., \varphi^{a_n} \right)^{\mathbf{a}} \,. \qquad (3.2)$$

The super-field space is endowed with a metric that reflects the Grassmann nature of fermion fields, see Appendix A. Note that contraction over the most general index class also implies

---

[1]Note that the adjective "super" does not refer to supersymmetry.

cotraction over all sub-indices. For instance, in quantum electrodynamics, the super-field contains the fermion, the anti-fermion and the gauge field, $\varphi_{\mathbf{a}} = \left(\Psi, \bar{\Psi}, A\right)_{\mathbf{a}}$. As the super-metric is the tensor product of the fermionic part, which is the epsilon tensor, and the bosonic part, which is just the identity, a contraction is in this case given by

$$\varphi_{\mathbf{a}}\varphi^{\mathbf{a}} := \int_{\mathbb{R}^4} \mathrm{d}^4x\, \Psi_a(x)\bar{\Psi}^a(x) - \int_{\mathbb{R}^4} \mathrm{d}^4x\, \bar{\Psi}_a(x)\Psi^a(x) + \int_{\mathbb{R}^4} \mathrm{d}^4x\, A_\mu(x)v_3^\mu(x), \qquad (3.3)$$

where in this case the latin indices are the spinor indices. Note that in some cases we aim at contraction of indices without integration. In this case we label both classes of super-indices with capital latin letters or capital bold latin letters respectively, e.g.

$$h_A h^A := h_{\mu\nu}(x)h^{\mu\nu}(x). \qquad (3.4)$$

3.2. Flow Equations

Parts of the following are pretty standard repertoire in asymptotic safety and functional renormalization, and the presentation of these parts is partially parallel to [19].

A quantum field theory is then entirely defined by the infinite set of n-point correlation functions $\langle \varphi_{a_1} \varphi_{a_2} ... \varphi_{a_n} \rangle$. All physical observables such as cross-sections can finally be expressed in terms of these correlation functions. The calculation and determination of properties of these correlation functions is the ultimate goal in quantum field theory. The functional renormalization group is a particular implementation of the Wilsonian idea of renormalization, i.e. integrating out degrees of freedom in infinitesimal steps. In contrast to other RG-schemes, this method has the particular advantage that it does not necessarily require an interaction term that is assumed to be weak. This means that it is not based on a power series in the coupling constant and thus inherently of non-perturbative nature. In general, an exact solution to the FRG-master equation, the Wetterich equation, corresponds to a full solution of the path-integral. For reviews on functional renormalization in quantum gravity see [20–26], for general reviews and other applications see e.g. [27–41] . In order to formulate the coarse-graining procedure mathematically, one modifies the path integral with a regulator action $\triangle S_k[\varphi]$ that introduces a momentum scale k, according to which the functional integration is organized. This regulator categorizes field modes with large momenta $p^2 > k^2$ on the one hand, and $p^2 < k^2$ on the other.

The regulated path integral then takes the form

$$e^{W_k[J]} = \int D\varphi\, e^{-S[\varphi] + \triangle S_k[\varphi] + J_{\mathbf{a}}\varphi^{\mathbf{a}}}, \qquad (3.5)$$

where J is an external source term and $W_k[J]$ denotes the Schwinger functional, i.e. the generating functional of connected correlation functions. The path integral measure $D\varphi$ is a formal, infinite product of Lebesgue-measures and is assumed to be appropriately regularized with an ultraviolet cutoff Λ. In this thesis we use a renormalization group equation for the scale dependent effective action Γ_k, which is the regularized version of the full quantum effecitve action Γ. The quantum effective action is the generating functional of one-particle irreducible (1PI) correlation functions, also frequently called vertex functions. These vertex functions correspond to the fully dressed version of bare vertices in the classical action, i.e.

they arise if all quantum fluctuations are added to the tree-level vertex. S-matrix elements can then be obtained by forming trees with vertex functions.

In the end, we are interested in a flow equation that governs the scale evolution of Γ_k and describes how quantum fluctuations are included by integrating-out momentum shells Δq. For this equation to have a particular one-loop form, the regulator action needs to be quadratic in the fields,

$$\triangle S_k[\varphi] = \frac{1}{2} R_k^{\mathbf{ab}} \varphi_{\mathbf{a}} \varphi_{\mathbf{b}}. \tag{3.6}$$

with a regulator operator $R_k^{\mathbf{ab}}$. The scalar part of the regulator in momentum space is of the form

$$R_k = r_k(q^2)\delta(q - q'), \tag{3.7}$$

where $r_k(q^2)$ is a shape function that needs to have certain defining properties. First, we want to ensure infrared regularization of the theory organized by the scale parameter k. Since the regulator is quadratic in the fields, it acts like an additional mass term in the propagator that regulates infrared modes and cuts off momenta with $p < k$. Additionally, we want to recover the full quantum theory in the limit $k \longrightarrow 0$, while one wants to find the microscopic action in the limit $k \longrightarrow \infty$. In the case of a perturbatively renormalizable field theory, the latter case corresponds to the classical or bare action. In order to meet these requirements, the momentum space representation of the regulator needs to have the properties

$$\lim_{p^2/k^2 \to 0} R_k(p) > 0$$

$$\lim_{k^2/p^2 \to 0} R_k(p) = 0$$

$$\lim_{k^2 \to \Lambda^2 \to \infty} R_k(p) = \infty. \tag{3.8}$$

A modified Legendre transform then leads from the regularized Schwinger functional $W_k[J]$ to the scale-dependent effective action $\Gamma_k[\phi]$, which is a functional of the averaged field $\phi = \langle \varphi \rangle$. The derivation of the flow equation can be found in numerous publications, e.g. all the reviews cited above, and in particular in the super-index notation used in this thesis in [19, 32] and will not be repeated here. The master equation of the functional renormalization group, the so called flow equation or Wetterich equation, is a functional, partial differential equation and is given in compact form by

$$\dot{\Gamma}_k[\phi] = \frac{1}{2} G_{\mathbf{ab}} \dot{R}^{\mathbf{ab}}[\phi], \tag{3.9}$$

where we have defined the regularized version of the fully dressed propagator

$$G_{k,\mathbf{ab}}[\phi] := \gamma_{\mathbf{a}}^{\mathbf{c}} \left(\frac{\delta^2}{\delta \phi^2} \Gamma_k + R_k \right)_{\mathbf{cb}}^{-1} [\phi], \tag{3.10}$$

and introduced the notation

$$\dot{f} := k\partial_k f =: \partial_t f, \tag{3.11}$$

for the dimensionless scale-derivative of any k-dependent function f. In the following, we comment on some properties of the flow equation. The characteristics of the flow equations are presented in similar fashion in [19].

Diagramatics. The Wetterich equation (3.9) contains a contraction over the multi-index, and therefore it implies an integration over the propagator momentum. The propagator is contracted with $\dot{R}_k$. In the language of Feynman diagrams this is a loop with a regulator insertion, and hence the flow equation can be represented as in Figure 3.1 below. It is very important to mention that there is a big difference between this

$$\partial_t \Gamma = \frac{1}{2}\ \bigotimes$$

Figure 3.1.: Diagrammatic representation of the flow equation. A fully dressed propagator with regulator insertion.

representation and the Feynman diagrams one knows from perturbation theory: The quantities that appear are fully dressed, i.e. effective propagators and effective vertices that include quantum corrections.

Exactness and non-perturbative nature. As we have already mentioned, the quantum effective action Γ generates via functional derivatives the vertex functions, i.e. the 1-PI correlation functions, of arbitrary order. Consequently, it also contains all information about S-matrix elements and knowledge of the full effective action is equivalent to a full solution of the theory. Since the regulator vanishes in the limit $k \longrightarrow 0$, the scale-dependent effective action Γ_k converges towards the full effecitve action in this limit,

$$\Gamma_{k=\Lambda} \xleftarrow{k\to\Lambda} \Gamma_k \xrightarrow{k\to 0} \Gamma_{k=0} = \Gamma\,. \tag{3.12}$$

Therefore, the solution of the Wetterich equation (3.9) corresponds to a full solution of the respective quantum field theory. Indeed, this equation is derived from the path integral without any approximations and can be viewed as an equivalent formulation. In particular, it is inherently non-perturbative. One can also avoid the path integral representation from the very beginning and define a quantum field theory via the scale-dependent effective action and its flow equation.

Finiteness. The fundamental ingredients for the flow equation are the fully dressed two-point function and the regulator. A typical regulator shape function $r_k(q^2)$ that satisfies the conditions (3.8) and its scale derivative $\dot{r}_k(q^2)$ are shown in Figure 3.2.
The additional regulator term in the propagator G_k ensures infrared finiteness as the shape function typically scales like k^2 in the limit of vanishing momentum. Therefore, massless modes cannot lead to divergences in any finite RG-step,

$$\frac{1}{q^2 + r_k(q^2)} \xrightarrow{q\to 0} \frac{1}{k^2}\,. \tag{3.13}$$

Furthermore, the scale derivative of the regulator $\dot{R}^{\mathbf{ab}}$ is peaked around $q^2 \approx k^2$ and tends to zero for $q^2 \to \infty$. Consequently, each RG-step is also ultraviolet finite.
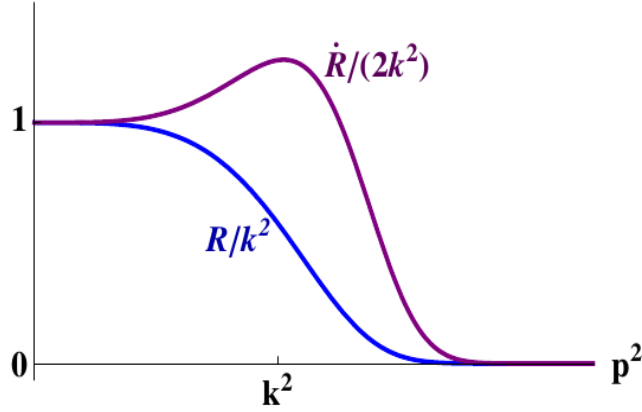
Figure 3.2.: A typical regulator shape function $r_k(p^2)$ and its scale derivative $\partial_t r_k(p^2)$. For small momenta the regulator is proportional to k^2 and thus suppresses fluctuations with $p^2 < k^2$. Moreover, one can see that the scale derivative of the regulator is peaked around $p^2 \approx k^2$, and since the flow equation is proportional to $\partial_t r_k(p^2)$, this property carries over to the flow itself. This also implies that the flow equation is sensitive to momenta $p^2 \approx k^2$. The peak property is in the flow equation even more pronounced than in $\partial_t r_k(p^2)$ itself, since the integral measure $\sim |p|^3$ further suppresses small momentum fluctuations. The figure is taken from [42].

Initial conditions. The derivation of the flow equation starts with a regularized path integral. This can be achieved with any UV regularization. Being a functional, partial differential equation, the solution of the flow equation requires a choice of boundary conditions at a scale $k = \Lambda$. For perturbatively renormalizable theories the initial condition is basically the classical action, $\Gamma_{k=\Lambda} \approx S$. More details on boundary and initial conditions will be discussed in the next section.

Renormalization and link with standard RG equations. As stated above, the functional renormalization group can be used to define a quantum field theory and due to the structure each RG-step is finite. The initial condition can then be understood as a renormalization condition known from standard renormalization theory. In this sense, the functional renormalization group represents a specific regularization and renormalization scheme.

A comparison to the well-known standard RG-schemes is very instructive. In such constructions one regularizes integrals in loop expansions and subtracts divergent contributions at an arbitrary new mass scale, usually called μ, at which one imposes renormalization conditions.

In the FRG, the construction of couplings from divergent, bare quantities is circumvented. One can rediscover such quantities in the FRG from the integrated flow. We rewrite

$$\dot{\Gamma}_k = \frac{1}{2} G_{ab} \dot{R}^{ab} = -\frac{1}{2} \partial_t \left(\log G \right)^a{}_a - \frac{1}{2} \dot{\Gamma}_k^{(2)\, ab} G_{ab} \,, \tag{3.14}$$

and integrate the above equation in order to arrive at

$$\Gamma_k = \Gamma_\Lambda - \frac{1}{2} \left(\log G \right)^a{}_a \Big|_{k'=\Lambda}^{k'=k} - \frac{1}{2} \int_\Lambda^k \mathrm{d}t \; \dot{\Gamma}_k^{(2)ab} G_{ab} \,. \tag{3.15}$$

At htis point the renormlaization becomes evident. As one can see, the boundary condition Γ_Λ explicitly enters the integrated flow. This boundary effective action is a finite quantity. The renormalization conditions for the fully integrated theory, which are imposed at a specific scale μ correspond to conditions for $\Gamma_{k=0}$. But since the flow relates Γ_Λ and $\Gamma_{k=0}$ unambiguously, the renormalization conditions translate into a constraint for the boundary condition. It is important to notice that the subtractions at the scale Λ on the right hand side are essential for regularization, since the there is no scale derivative $\dot{R}$ of the regulator that would ensure UV finiteness of the momentum integrals. In fact, at this point one can relate the FRG scheme to standard perturbative RG schemes by using the integrated n-loop flow and constructing appropriate counter-terms by fixing the Λ independent parts of Γ_Λ. This has explicitly been done, e.g in [43]. A discussion of the μ scaling of the regulated effective action in general can be found in [32, 44, 45].

The crucial point for the application to quantum gravity is of course the UV problem in the sense that we integrate out arbitrarily large momenta, i.e. we are interested in the limit $\Lambda \to \infty$. It is *not* a priori clear that Γ_Λ remains finite in this limit, since it originates from a regularized path integral and all of the above considerations have been done with a fixed Λ. This means, we ask for *global* existence of the flow. But with the insight of renormalization conditions we gained above, it is clear that this existence depends on the boundary conditions of the integral equation (3.15). Thus, from a formal point of view, the construction of a suitable boundary functional is the crucial aspect if we study the limit $\Lambda \to \infty$. How one can attack this problem within truncated flow equations in practice is the topic of the following chapters.

Link with perturbation theory As we stated in the first point, our flow equation contains in principle all non-perturbative information about the theory under consideration. In particular, it should be possible to gain back the results from perturbation theory. This is indeed the case, and it is easy to see how this works. First we write the effective action as a loop expansion

$$\Gamma = S + \sum_{n=1}^\infty \triangle \Gamma_n \,, \tag{3.16}$$

where S is the classical action and $\triangle \Gamma_n$ represents all contributions that originate from one-loop diagrams. The associated flow equation at one loop order should involve only one loop expressions on both sides of the equation. Since (3.9) already contains a loop, it is the classical action that enters in the propagator on the right hand side and we get

$$\partial_t \triangle \Gamma_{1,k} = \frac{1}{2} \left(S^{(2)} + R_k \right)_{ab}^{-1} \partial_t R_k^{ab} = \frac{1}{2} \, \partial_t \, \left(\log \left(S^{(2)} + R_k \right) \right)^a{}_a \,, \tag{3.17}$$

which one can trivially integrate to obtain

$$\triangle \Gamma_{1,k} = \triangle \Gamma_{1,\Lambda} + \frac{1}{2} \left(\log \left(S^{(2)} + R_{k'} \right) \right)^a{}_a \Big|_{k'=\Lambda}^{k'=k} \,. \tag{3.18}$$

In the limit $k \to 0$ we get via $S + \triangle\Gamma_{1,k=0}$ the well known one loop expression for the effective action. The renormalization issue in the above equation follows immediately from the general discussion above: The initial condition and subtraction at Λ in the log ensures UV finiteness.

k **microscope and effective descriptions.** In principle, the physical limit of the theory is approached for $k \longrightarrow 0$, when the regulator is removed and the standard, full quantum effective action is approached. In the full, untruncated flow, the momentum dependence of the couplings is encoded the momentum dependence of the full vertex functions. In practice, it is very difficult to calculate full momentum dependent flows. The first calculation of momentum-dependent, and even fully momentum dependent quantities in an FRG-gravity setup is actually presented in this thesis. Therefore, usually one just allows for k dependent dressed coupling parameters in order to incorporate quantum fluctuations and the dependence on external momenta is ignored. The running of couplings then always refers to the evolution with the scale k, which, being a cutoff, is a priori unphysical. Nonetheless, the locality of the flow often allows for a physical interpretation of the cutoff scale k.

The renormalization group flow defines a family of effective actions $\{\Gamma_k\}_k$, and by construction, Γ_k is particularly sensible to physics at $k \approx q$, since this is the scale where the fluctuations are integrated out. This means we can compare the flowing action with a microscope of variable resolution. For large k we gain insight about the behavior at small distances, and by successive lowering of k we average over high energy fluctuations and see the structures at larger length scales. It is now possible to identify the, a priori unphysical, RG scale k with some external parameter with dimension of mass. Imagine we have a physical situation that is governed by one scale, for instance in a two-to-two scattering process the center-of-mass energy $\sqrt{s}$, and one is interested in the behavior of physics under variation of this scale. Then one can use Γ_k for tree level calculations within an effective framework by identifying k with $\sqrt{s}$ via

$$k = f\left(\sqrt{s}\right). \tag{3.19}$$

The exact form of the function f depends on the specific process under consideration. However, a wise choice of f might lead to a good effective description.

This method is used in phenomenological applications of RG gravity to particle physics [46, 47], in cosmological applications, where one needs to link k to some cosmological parameter [48–51], or in black hole physics [52–56] .

The Hierarchy of Flow Equations. The fundamental objects that describe interactions in quantum field theories are the vertex functions. These objects determine e.g. the properties of $n-m$ particle scattering and enter the S-matrix elements. As the effective action Γ is the generating functional for these vertex functions, the latter are simply obtained by functional differentiation according to

$$\frac{\delta}{\delta\phi^{\mathbf{a_1}}}\cdots\frac{\delta}{\delta\phi^{\mathbf{a_n}}}\Gamma[\phi] =: \Gamma^{\mathbf{a_1}\cdots\mathbf{a_n}}[\phi]. \tag{3.20}$$

In order to simplify the notation, we will frequently drop the indices and denote the n-th order vertex function just as $\Gamma^{(n)}$, or as $\Gamma^{(n_1\phi_1\cdots n_m\phi_m)}$ if we consider a theory with

m different fields, and if it is important that we refer to the correlator where each field ϕ_i appears n_i times. The flow equations for the vertex functions are then obtained by functional derivatives of the Wetterich equation (3.9) with respect to the fields, i.e. by differentiation of the equation for the effective action itself. This procedure then generates the hierarchy of flow equations for the vertex functions. This infinite set of functional equations has the structure

$$
\begin{aligned}
\dot{\Gamma}_k[\phi] &= \mathrm{Flow}[\Gamma^{(2)}] \\
\dot{\Gamma}_k^{(2)}[\phi] &= \mathrm{Flow}^{(2)}[\Gamma^{(2)}, \Gamma^{(3)}, \Gamma^{(4)}] \\
\dot{\Gamma}_k^{(3)}[\phi] &= \mathrm{Flow}^{(3)}[\Gamma^{(2)}, \Gamma^{(3)}, \Gamma^{(4)}, \Gamma^{(5)}] \\
&\qquad \ldots\ldots\ldots .
\end{aligned}
\tag{3.21}
$$

One should note the important fact that the flow of the n-point vertex function depends on the vertex functions up to order $n + 2$,

$$
\mathrm{Flow}^{(n)}[\Gamma^{(2)}, ..., \Gamma^{(n+2)}] .
\tag{3.22}
$$

Note that in loose language fashion we will frequently call $\dot{\Gamma}_k^{(2)}[\phi]$ the flow equation of the propagator, although it is the equation for the inverse propagator.

Truncations and Optimization. We have seen that the implementation of coarse graining in the functional renormalization group is implemented via a regulator functional in the path integral. However, the choice of the regulator is not unique. The only requirements are the conditions (3.8). The full, exact quantum effective action $\lim_{k\to 0} \Gamma_k$ is independent of the regulator as the regulator vanishes for $\longrightarrow 0$. However, it is of crucial importance that this does not hold for the effective action at $k \neq 0$, and also not for effective actions that arise from approximate solutions of the flow equation. The latter is of particular importance as exact solutions to the flow equations are usually not possible and one has to resort to truncations. Truncations are, possibly non-perturbative, approximation schemes for the flow equation. Finding truncations that are good approximations to the full solution is usually a very difficult task. As the next part of this thesis is intensively concerned with this issue, we do not comment further on different truncation schemes at this point. However, we want to note that the non-uniqueness of the regulator can be used in order to minimize the error in approximate solutions. The business of finding regulators with such properties is called optimization and is discussed in great detail in e.g. [32, 57].

The Asymptotic Safety Scenario

4.1. Renormalization Group Flows, Fixed Points and Asymptotic Safety

Now we want to put the Asymptotic Safety Scenario in the general context of renormalization group flows and give a precise definition of an asymptotically safe theory. First, the concept of the theory space is introduced. Let us assume that our fields are functions $\phi : \mathbb{R}^n \to \mathbb{R}$ (for notational simplicity we consider scalar fields here, but the generalization to arbitrary representations such as tensorial representations is quite obvious), and that they lie in an appropriate infinite dimensional vector space, such as the Schwartz Space $\mathscr{S}(\mathbb{R}^n)$. This Schwartz Space has the nice properties that the Fourier transformation is an automorphism and that all derivatives of our fields are square-integrable. We then define the theory space $\mathscr{F}$ as all functionals $\Gamma : \mathscr{S}(\mathbb{R}^n) \to \mathbb{R}$ that respect the given symmetry, which leads to the definition

$$\mathscr{F} := \{\Gamma[\cdot] \mid \Gamma : \mathscr{S}(\mathbb{R}^n) \to \mathbb{R}, \ \mathscr{G}\Gamma[\phi] = \Gamma[\phi]\} \tag{4.1}$$

with $\mathscr{G}$ being an element of the symmetry group. Let us further assume that we have a basis in the space $\mathscr{F}$. As we have already mentioned above, the flow equation defines a family of scale-dependent effective actions $\{\Gamma_k\}_k$ with $\Gamma_k \in \mathscr{F}$. Under this requirement we can expand each Γ_k in a basis $\{F_n\}$ of $\mathscr{F}$ and write formally

$$\Gamma_k[\phi] = \sum_n \hat{g}_n(k)F_n[\phi], \tag{4.2}$$

such that such that the scale-dependence of each operator can be written as a multiplicative pre-factor. The k-dependent pre-factors $\hat{g}_i(k)$ are nothing but the dimensionless versions of the generalized running couplings $g_i(k)$ that parameterize the effective action,

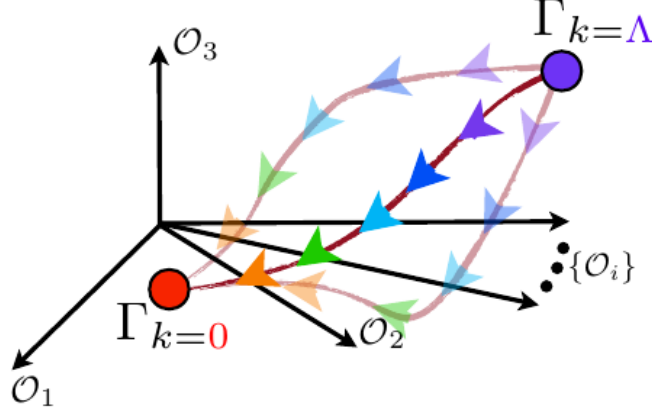$$\hat{g}_n := \frac{g_n}{k^{d_n}}, \tag{4.3}$$

Figure 4.1.: The flow in theory space. Figure taken from [42].

where d_n is the mass dimension of the coupling g_n. The evolution according to the flow equation (3.9) then generates a flow in theory space, which is graphically shown in Figure 4.1.

In general, a fixed point of the renormalization group flow is defined as a point in theory space where the dimensionless, scale-dependent effective action $\hat{\Gamma}_k[\hat{\phi}]$ is invariant under RG-transformations, i.e. invariant under a change of the RG-scale k. Note that the hat indicates the dimensionless quantities. This means that the fixed point functional $\hat{\Gamma}_k^*[\hat{\phi}]$ is defined by the property

$$\partial_t \hat{\Gamma}_k^*[\hat{\phi}] = 0. \tag{4.4}$$

In order to make the meaning of this equation more transparent, let us investigate what this means in terms of an expansion of the scale-dependent effective action in basis functionals as given in equation (4.2). Given such a parameterization, one can then obtain from the general flow equations a system of differential equations for these running couplings by appropriate projection procedures. From now on we will deal with dimensionless couplings only, and will drop the hat we have just introduced, and all couplings are dimensionless if not stated otherwise. The scale derivative of these couplings is of the form

$$\dot{g}_i(k) = \beta_i(g(k)), \tag{4.5}$$

where the vector $g(k)$ comprises all the generalized couplings $g_n(k)$. The right-hand side of these equations is nothing but the non-perturbative generalization of the β- functions that are well-known in standard quantum field theory. The fixed point condition then translates into zeros of these β-functions that are taken for the fixed point values g_n^*,

$$\beta_n(g^*) = 0 \qquad \forall\, n. \tag{4.6}$$

We further note that the structure of the beta functions for the dimensionless couplings is always of the form

$$\beta_n = -d_n g_n + \text{quantum contributions}, \tag{4.7}$$

i.e. the beta functions consist of a sum of the canonical running due to the mass dimension of the coupling, and contributions that are rooted purely in quantum fluctuations. Consequently, the fixed point condition means that the canonical running is exactly counterbalanced by the quantum fluctuations. The properties of the fixed point are determined by the stability matrix, which is obtained by linearizing the flow in the vicinity of the fixed point g^*. Let us write

$$g_n = g_{*,n} + \delta g_n, \tag{4.8}$$

which leads to a power series in δg for the beta functions,

$$\beta_n(g) = \beta_n(g_*) + \sum_m B_{mn}(g_*) \, \delta g_m + \mathcal{O}\left(\delta g_m^2\right) = \sum_m B_{mn}(g_*) \, \delta g_m + \mathcal{O}\left(\delta g_m^2\right), \tag{4.9}$$

where the first term vanishes since g_* is a fixed point, and the term linear in δg is determined by the stability matrix

$$B_{mn} = \frac{\partial \beta_n}{\partial g_m} = k \frac{\partial^2 g_n}{\partial k \partial g_m}, \tag{4.10}$$

which is a type of a hessian matrix and describes the linearized flow around the fixed point. The properties of the fixed point are discriminated by the positivity or negativity of the stability matrix, as it is well known from analysis. Therefore we diagonalize the stability matrix, since for the quadratic form B holds $B \gtrless 0$ if all eigenvalues are $\gtrless 0$. The defining equation for the eigenvalue problem is

$$B e_n = b_n e_n, \tag{4.11}$$

with eigenvectors e_n and corresponding eigenvalues b_n. We now expand the vectors g and δg in eigenvectors e_n,

$$g = \sum_n \tilde{g}_n e_n \quad, \quad \delta g = \sum_n \delta \tilde{g}_n e_n,$$

where one can of course obtain the coefficients by projections onto the eigenvectors, e.g.

$$\tilde{g}_n = \langle g, e_n \rangle. \tag{4.12}$$

By inserting this into the linearized equation (4.9) we arrive at the differential equation

$$k \frac{d}{dk} \tilde{g}_n = \delta \tilde{g}_n b_n \tag{4.13}$$

which can be solved by elementary separation of variables and using $\tilde{\delta g}_\alpha = \tilde{g}_\alpha - \tilde{g}_{*,\alpha}$ to give

$$\tilde{g}_n(k) = \tilde{g}_{*,n} + \tilde{g}_n(k_0) \left(\frac{k}{k_0}\right)^{b_n} \tag{4.14}$$

with some reference scale k_0. From this solution one can beautifully see how the sign of the eigenvalues b_n determine the stability properties of the fixed point. A UV fixed point requires $\tilde{g}_n(k) \xrightarrow{k \to \infty} \tilde{g}_{*,n} \; \forall \; n$, while for a IR fixed point this must be true in the limit $k \to 0$. Note that in general the eigenvalues b_n are complex, and the above relation then translates into a requirement for the real parts of the eigenvalues. We can therefore classify the UV stability via the positivity of B according to the following scheme:

- The fixed point is UV attractive if $\left(\mathrm{Re}\ b_\alpha\right) < 0\ \forall\ \alpha$.

- The fixed point is UV repulsive if $\left(\mathrm{Re}\ b_\alpha\right) > 0\ \forall\ \alpha$.

- The fixed point is a saddle point if none of the above is true.

This behavior can best be visualized in a one-dimensional coupling space, see figure (4.2). All
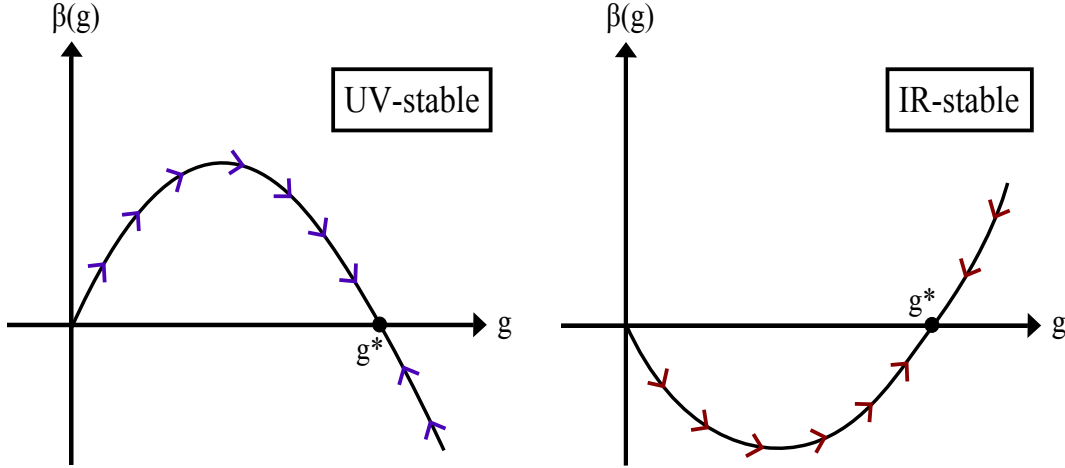

Figure 4.2.: In this schematic plot we restrict ourselves to a one dimensional coupling space. We show the beta function $\beta(g) = k d/(dk) g$ as a function of this single coupling. In this case we have only one eigenvalue which corresponds to the gradient of the curve, which in turn determines the stability properties. In the left picture the arrows point in direction of increasing k, while the opposite is true for the arrows in the right picture. The UV/IR stability can also intuitively be inferred by considering the sign of $\beta(g)$ at a given value of g. The gradient gives rise to a larger/smaller value of the coupling and drives the latter in the corresponding direction.

couplings with negative eigenvalue are called relevant, while those with positive eigenvalue are irrelevant as they die out in the direction of course graining.

The UV critical surface $\mathscr{S}_{UV}$ is defined as the hyper-surface in theory space that is built from the set of all trajectories that hit the fixed point in the limit $k \to \infty$. Consequently, its dimension $\dim\left(\mathscr{S}_{UV}\right)$ is given by the number of couplings with negative eigenvalues of the stability matrix.

The solutions (4.14) represent a complete class of trajectories and corresponding theories: one for each initial value $\tilde{g}_\alpha(k_0)$. This of course is exactly the specification of initial values that we discussed in the previous chapter.

Definition of Asymptotic Safety

In order to decide which theory is realized in nature, we have to measure a number of parameters that equals $\dim\left(\mathscr{S}_{UV}\right)$, since for attractive directions there are infinitely many initial conditions for which the couplings evolve towards the finite fixed point value. In a repulsive direction, there is exactly one initial condition, namely $\tilde{g}_n(k_0) = 0$ for which the coupling stays finite in the ultraviolet limit. The condition that the theory is tuned to the critical surface then implies that the values of these irrelevant couplings are predictions of

asymptotic safety. Obviously, a theory with $\dim\left(\mathscr{S}_{UV}\right) = \infty$ is not predictive, analogously to the case of perturbative renormalization that we have discussed in earlier.

With the background we gained in the above discussion, we can finally present a precise definition of the asymptotic safety scenario, which is now almost trivial to guess:

1. The theory contains an ultraviolet fixed point.

2. The UV critical surface of this fixed point is finite dimensional[1].

Such a theory is called *non-perturbatively renormalizable*, since the UV fixed point makes the theory well-defined for arbitrarily high momenta and the latter requirement ensures predictivity.

Some remarks concerning the notion of a asymptotically safe theory are appropriate.

First it is important to realize that this is a generalization of the perturbative renormalizability. It is clear that the relation

$$\text{perturbatively renormalizable} \implies \text{non-perturbatively renormalizable}$$

holds, while the "$\Longleftarrow$" relation is of course not true.

An asymtptotically safe theory is then a theory that has an ultraviolet fixed point with finite dimensional critical surface. This structure ensures two essential properties that one demands of a fundamental theory. First, due to the vanishing of the β functions at the fixed point, one can safely take the ultraviolet limit, since all couplings tend to finite fixed point values,

$$\lim_{k \to \infty} g_i(k) = g_i^* \qquad \forall\, i \,. \tag{4.15}$$

Consequently, the theory is free of divergences. In addition to that, a finite dimensional critical surface implies that the theory contains only a finite number of free parameters that need to be determined by experiment, namely the values of the relevant couplings at some momentum scale k_0. The irrelevant couplings are fixed by the condition that the theory is tuned to the critical surface. Thus we are left with a finite theory that has predictive power and qualifies as a truly fundamental quantum field theory. Proving asymptotic safety in non-perturbative situations is of course highly non-trivial, and in many cases with nowadays technology not possible. Rigorous proofs are possible for perturbative situations where the UV fixed point is Gaussian i.e. $g^* = 0$, or nearly Gaussian. In case of a Gaussian ultraviolet fixed point asymptotic safety reduces to the well-known special case of asymptotic freedom, where the coupling tends to zero in the ultraviolet and one is left with a free theory. Most prominently, this scenario is realized for Quantum Chromodynamics and is indicated by the negative sign of the β-function for the strong gauge coupling α_s.

For the investigation of non-perturbative regimes, one usually has to resort to truncations of the full theory. This means, that the a priori infinite dimensional theory- or coupling space is reduced to a finite number of dimensions. The specific truncation scheme representing the framework for our work will be constructed in detail in later sections. Our scheme is based on a so called vertex expansion where the effective action is expanded in a functional

---

[1]Right from the beginning of our analysis we ignored a subtlety, because the theory is really parameterized only by the essential couplings, i.e. those that are independent and cannot be absorbed by redefinitions of the fields. Hence, the analysis we presented is only completely correct if one substitutes the word "coupling" by "essential coupling". For further details see [21]

Taylor-series in the field. One can then solve the hierarchy of flow equations by truncating the expansion at some finite order n and use an ansatz for the vertex functions of order $n+1$ and $n+2$.

4.2. The Status of Asymptotic Safety in Quantum Gravity

The asymptotic safety scenario for quantum gravity was originally proposed by Steven Weinberg in 1997, [58]. However, until the formulation of the functional renormalization group for the one particle irreducible effective action by C. Wetterich in 1993, [59], there were no appropriate technical tools available in order to tackle the problem of asymptotic safety in quantum gravity. The setup of functional renormalization in quantum gravity and the first calculation were presented by M.Reuter in 1997, [60]. The most basic truncation in quantum gravity is the so-called Einstein-Hilbert truncation. This truncation is given by the classical Einstein-Hilbert action together with rescalings of the form

$$G_N \quad \longrightarrow G_{N,k} \quad , \quad \Lambda \quad \longrightarrow \Lambda_k \,, \tag{4.16}$$

which amounts to the introduction of two running couplings, while keeping just the operators present in the classical action. Moreover, all calculations are usually carried out in spacetimes with Euclidean signature, as FRG calculations in Lorentzian spacetime are notoriously difficult, see [61] for a first attempt in the Lorentzian approach to asymptotic safety. Therefore, the scale-dependent effective action in Euclidean spacetime is assumed to have the form

$$\Gamma_k[\bar{g}, h, \bar{c}, c] = \frac{1}{16\pi G_{N,k}} \int \mathrm{d}^4x \sqrt{\det g} \left(-R(g) + 2\Lambda_k \right) + \Gamma_{\text{gauge-fixing}}[\bar{g}, h] + \Gamma_{\text{ghost}}[\bar{g}, h, \bar{c}, c]\,, \tag{4.17}$$

on all scales. The diffeomorphism invariance requires a gauge fixing and is accompanied by the corresponding ghost action, which depends on the ghost field c and the anti-ghost $\bar{c}$. The gauge fixing procedure also necessitates the introduction of an unphysical auxiliary background field $\bar{g}$ and a fluctuating graviton field h. However, the reason for introducing this background field is actually twofold, since not only gauge fixing, but also the structure of the flow equation in quantum gravity usually entails a non-dynamical background. More precisely, in order to keep the one-loop structure of the flow equation, the regulator must be quadratic in the fields. However, any term invariant under diffeomorphisms of the full metric g is automatically of infinite order in g due to the canonical volume form, and also any contraction is induced by a metric. Therefore, the regulator is a function of the background field only, $R = R(\bar{g})$. This construction leads to the crucial observation that the scale-dependent effective action is a function of the background and the fluctuation field separately. The standard calculations in FRG-gravity then employ the so called background field method. The full metric is then decomposed linearly into the background h and the fluctuation $\bar{g}$ according to $g = \bar{g} + h$ and one introduces gauge transformations for both fields separately. At the end of the day one identifies $g = \bar{g}$, i.e. $h = 0$ and one then usually argues that gauge invariance is reestablished. However, we note that there are several flaws in this reasoning that will be discussed in the next section. The running of the couplings

is then extracted directly from the flow equations for the effective action by evaluating the latter at $g = \bar{g}$ e.g. on Einstein spaces, which allow for a disentanglement of curvature terms proportional to R and terms proportional Λ. In such a truncation one detects an ultraviolet fixed point with the necessary physical requirements, namely a real fixed point with $g_k > 0, \lambda_k > 0$, where have introduced the dimensionless running couplings

$$g_k := G_{N,k}\, k^2 \quad , \quad \lambda_k := \frac{\Lambda_k}{k^2} . \tag{4.18}$$

The beta functions $\big(\beta_g(g,\lambda), \beta_\lambda(g,\lambda)\big)$ define a vector-field on the two dimensional coupling space of the Einstein-Hilbert truncation. Most of the relevant properties can be visualized in the phase-diagram, which is shown in Figure 4.3.
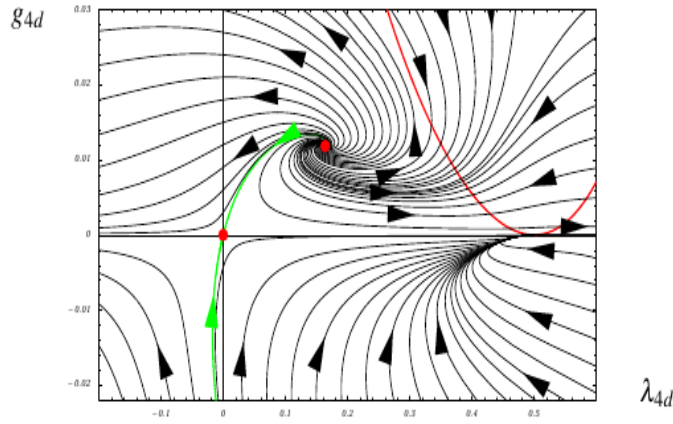

Figure 4.3.: The phase diagram of quantum gravity in the Einstein-Hilbert truncation. The arrows point from the UV to the IR direction and the fixed points are highlighted by red points and are connected by the separatrix (green). The details of this plot are discussed in the text below. The plot is taken from [62].

This plot shows the integral curves of the beta functions, i.e. the trajectories in the $g - \lambda$ plane are parameterized as $\big(g(k), \lambda(k)\big)$ and depend parametrically on the momentum scale k. The different trajectories then correspond to different initial conditions $g(k_0) = g_{\text{initial}}$, $\lambda(k_0) = \lambda_{\text{initial}}$ that are imposed at some reference scale k_0. The physical region of the phase diagram is dominated by two fixed points, namely the non-trivial ultraviolet fixed point $(g_*^{\text{UV}} \neq 0, \lambda_*^{\text{UV}} \neq 0)$, and the built-in Gaussian fixed point with $(g_* = 0, \lambda_* = 0)$. The existence of the ultraviolet fixed point is the basis for the asymptotic safety construction. The fixed point values are of course regulator and gauge-dependent. In accordance, we stress that the fixed point values of the couplings are not physical quantities. As explained in the last chapter, the properties of a fixed point are characterized by the stability matrix, i.e. the linearized flow. All background field flows in the Einstein-Hilbert truncation have in common that the critical exponents are complex. This manifests itself as a spiraling of the trajectories in the vicinity of the fixed point. The real part of the critical exponents is negative, meaning that the fixed point is ultraviolet-attractive in both directions. Since the Gaussian fixed point has one negative and one positive eigenvalue, there exists exactly

one trajectory that connects the Gaussian and the non-Gaussian fixed point, the so called separatrix, which is shown in green in Figure 4.3. Since gravity is an attractive force, the region with $g < 0$ is unphysical and will not be considered further. For positive couplings, the phase phase diagram exhibits some important properties. First of all, there is a built-in infrared attractive anti-de Sitter fixed point at $\left(g_*^{\mathrm{IR}} = 0, \lambda_*^{\mathrm{IR}} = \infty\right)$. More importantly, let us consider the physical region $(g > 0, \lambda > 0)$. The trajectories that emanate the non-Gaussian ultraviolet fixed point evolve according to the flow equation towards smaller scales. In the vicinity of the Gaussian fixed point trajectories show classical scaling behavior, namely $g_k \sim k^2$ and $\lambda_k \sim 1/k^2$, meaning that the dimensionful counterparts G_k and Λ_k are constant. This region of the phase diagram is then usually identified with the domain of classical general relativity. However, there is an important aspect of this phase diagram concerning the deep infrared. The trajectories emanating the ultraviolet fixed point that do not cross the $\lambda = 0$ line cannot be continued to $k = 0$, but hit a singular line at a finite momentum scale. This singular line is highlighted in red in the plot of the phase diagram Figure 4.3. Therefore the theory does not have a well-defined infrared limit in the background Einstein-Hilbert truncation. Consequently, this truncations does not allow for globally defined trajectories and is not infrared complete. This unsatisfactory situation turns out to be a truncation artefact and is one of the issues addressed in this thesis.

Besides this obvious failure of the truncation in the limit of large distances, the ultraviolet stability needs to be tested with enlarged and improved truncations. Additionally, the finite dimensionality of the critical surface needs to be tested, since infinite dimensionality of the latter would lead again to a theory without predictive power. This is because in an attractive direction infinitely many initial conditions lead to trajectories that flow into the fixed point and therefore an experimental input is necessary in order to pin down the physical trajectory, e.g. the measurement of the coupling at some energy scale. Consequently, an infinitely dimensional critical surface implies that the theory contains infinitely many free parameters that need to be fixed by experiment. Determining the dimensionality of the critical surface is very difficult, and for the time being even impossible. However, by including higher dimensional operators systematically, one can test the the dimensionality of the critical surface in a higher and higher dimensional theory space and use bootstrap arguments in order to support or disfavor asymptotic safety, [63–65].

There is a vast amount of work that improves the Einstein-Hilbert truncation in several directions. First of all one can extent the ansatz for the scale dependent effective action to a $f(R)$-type of theory [63–66]. On can then analyze the fixed point equation for the function f e.g. in a high order polynomial expansion polynomial expansion in the Ricci scalar. This has been done in [64] up to order R^{34}. The result is very encouraging since one finds an ultraviolet fixed point and all operators R^n with $n \geq 3$ turn out to be irrelevant. The crucial UV fixed point is confirmed in various approximations, including the coupling to gauge and matter fields [67–72], dilaton gravity [73, 74], higher derivative calculations [63, 64, 75–77], vertex expansions [1, 2, 78], geometrical flow equations [79], higher spacetime dimensions [80], unimodular gravity [81, 82] and bi-metric truncations [83–85]. There is also a rich field of phenomenological applications based on asymptotically safe quantum gravity. This includes e.g. implications for the standard model and its extensions [86, 87], black hole physics [53, 54, 88, 89], collider experiments [46, 47] and cosmology [48, 90].

4.2.1. Gauge Fixing, the Background Field and all that

A basic problem that all approaches to quantum gravity have to face is the implementation of gauge invariance, or more precisely, of diffeomorphism invariance.
Diffeomorphisms that act on the coordinates induce a transformation on the metric field, and the corresponding mappings are generated by the Lie-derivative. It is trivial to construct actions that are invariant under such mappings. For instance, the standard Einstein–Hilbert action, but also all generalizations to higher order curvature invariants are trivially diffeomorphism invariant. However, the implementation of gauge invariance in the context of quantum theories is highly non-trivial, and is even more delicate in quantum gravity where the space-time itself is a dynamical field. The first, inevitable problem in quantum field theories is that the gauge symmetry leads to equivalent field configurations along the gauge orbits. This implies an infinite over-counting of physical states in the process of quantization, and it is not even possible to define a propagator in the gauge symmetric theory as the inverse of the kinetic operator does not exist. As a consequence, one needs to introduce a gauge fixing term that breaks the symmetry explicitly. In turn, this results in an effective action that is not a gauge invariant functional of its arguments. Moreover, the notion of coarse graining in regularized theories is not a covariant formulation. The solution to these problems appears in terms of the introduction of a non-dynamical background field, which allows for the definition of a gauge invariant effective action, [91]. Moreover, we have already stated, that the introduction of a background field in the FRG-formulation of quantum gravity is necessary if one wants to retain the standard structure of the flow equation, as the regulator would be of infinite order in the full metric g if there were no background metric. The construction of the background field effective action can be outlined as follows.

In order to arrive at a diffeomorphism invariant flow equation, we introduce a background field, and use the so called background gauge.
Although this method can be applied to theories with arbitrary symmetries, we will already specialize to the case of diffeomorphism transformations, but the construction for $SU(N)$ theories is largely parallel. For the Yang-Mills analogue and further details concerning the background field formalism in general, we refer to [27, 32, 92–96] .
We have already introduced the background split which is written as

$$g = \bar{g} + h. \tag{4.19}$$

The background field $\bar{g}$ is just an auxiliary field, while the field h determines physics and represents the graviton in the particle picture. Therefore, we call h the dynamical field. It is also worth mentioning that now all functional integrals are performed with respect to h, i.e. the measure changes from $d\mu[g]$ to $d\mu[h]$.
We emphasize, that the decomposition (4.19) is, despite the equal form, quite different in spirit from a perturbative reasoning as h is in no sense a small quantity.
In the case of diffeomorphism symmetry we have a mapping under genuine transformations which acts on the dynamical fields only according to

$$\mathscr{G} : h \longrightarrow h + \mathscr{L} g$$

$$\mathscr{G} : \bar{g} \longrightarrow \bar{g} \, , \tag{4.20}$$

where $\mathscr{L}$ is the Lie derivative along an arbitrary vector field. This physical transformations cannot act on the background field since the functional measure after the background split is $d\mu(h)$, and h carries the degrees of freedom that need to be gauge fixed. All the general statements one knows from gauge theories also hold in the case of gravity: we need to get rid of the redundancies that arise from fields h which belong to the same gauge orbit. That means, we have to restrict our functional integration to exactly one representative for each equivalence class, i.e. to the manifold $M(h)/Diff(M)$, where $M(h)$ is the configuration of dynamical metric fields. Therefore, we introduce a gauge fixing term in our action and apply the Faddeev–Popov quantization. In this procedure we have to deal with the Faddeev–Popov determinant, which leads via exponentiation to the Grassman-valued ghost fields $(\bar{C}, C)$, which in turn contribute a term to the action functional.

This physical symmetry (4.20) is then of course explicitly broken by this gauge fixing procedure.

The strategy is now as follows. We introduce a auxiliary symmetry which transforms also the background field,

$$\bar{\mathscr{G}} : \bar{g} \longrightarrow \mathscr{L}\bar{g}$$
$$\bar{\mathscr{G}} : h \longrightarrow h - \mathscr{L}\bar{g} \,. \tag{4.21}$$

Note that the ghost fields which arise from Faddeev-Popov quantization are not affected by background transformations.

Then we choose a gauge fixing condition $F[\bar{g}, h] = 0$ which fixes the physical symmetry but is invariant under the combined transformations (4.20) and (4.21). This can be done if we choose a linear background gauge according to

$$F_\mu(\bar{g}, h) = \sqrt{2}\mathscr{F}_\mu^{\alpha\beta}(\bar{g})h_{\alpha\beta} \,, \tag{4.22}$$

where it is crucial that $\mathscr{F} = \mathscr{F}(\bar{g})$ is a function of the background field. A type of generalized harmonic gauge is realized by the gauge fixing functions

$$\mathscr{F}_\mu^{\alpha\beta} = \delta_\mu^\beta \bar{g}^{\alpha\gamma} \bar{\mathscr{D}}_\gamma + \frac{\alpha_2}{2} \bar{g}^{\alpha\beta} \bar{\mathscr{D}}_\mu \tag{4.23}$$

with $\bar{\mathscr{D}}$ being the covariant derivative with respect to the background connection, i.e. it is constructed from background metrics alone. Note that we have introduced a second gauge fixing parameter α_2. This gives rise to a one parameter family of gauge fixing functions and the choice of α_2 defines the orthogonal projection. In particular, the standard choice which corresponds to the usual harmonic gauge is $\alpha_2 = -1$.

The gauge fixing condition $F[\bar{g}, h] = 0$ is then implemented in the corresponding term in the action

$$S_{\text{gf}}[\bar{g}, h] = \frac{1}{2\alpha_1} \int \sqrt{-\det\bar{g}} \; \bar{g}^{\mu\nu} F_\mu(\bar{g}, h) F_\nu(\bar{g}, h) \tag{4.24}$$

with gauge fixing parameter α_1, which is the analog of the usual gauge fixing parameter in U(N) and SU(N) gauge theories. The choice $\alpha_1 = 0$ corresponds to Landau gauge and is used throughout this thesis. Note that the canonical volume form in the above integral contains the background metric. Accordingly, with (4.22) the gauge fixing term S_{gf} is quadratic in the fluctuating field.

It is not difficult to show that the above construction from the background field ensures

the crucial property that the gauge fixing action (4.24) is invariant under the combined transformations (4.20) and (4.21).

The gauge fixing leads via standard methods to a ghost term in the action that reads in the case of diffeomorphism symmetry

$$S_{\text{gh}}[\bar{g},h] = \sqrt{2} \int \sqrt{-\det\bar{g}} \; C_\mu \bar{g}^{\mu\nu} \frac{\partial F_\nu}{\partial h_{\alpha\beta}} \mathscr{L}_C \left(\bar{g}_{\alpha\beta} + h_{\alpha\beta} \right) = -\sqrt{2} \int \bar{\omega} \; C_\mu M^\mu_\nu C^\nu \,, \quad (4.25)$$

where M^μ_ν is the Faddeev-Popov operator and $\mathscr{L}_C$ is the Lie derivative that is discussed in Appendix B. The Faddeev-Popov operator is explicitly given by

$$M^\mu_\nu = \bar{g}^{\mu\alpha} \bar{g}^{\beta\gamma} \bar{\mathscr{D}}_\gamma \left(g_{\alpha\nu} \mathscr{D}_\beta + g_{\beta\nu} \mathscr{D}_\alpha \right) - \frac{1}{2}(1-\alpha_2) \bar{g}^{\alpha\beta} \bar{g}^{\mu\gamma} \bar{\mathscr{D}}_\gamma g_{\beta\nu} \mathscr{D}_\alpha \,. \qquad (4.26)$$

One can then also show that the ghost action is invariant if we combine background and physical transformations.

Let us shortly recapitulate the background gauge construction and the resulting facts. We introduced an additional symmetry for the background field, which was tuned in such a way, that the gauge fixing and the ghost term are invariant under combined transformations $(\mathscr{G} + \bar{\mathscr{G}})$. The classical action itself is trivially (or better, by construction) invariant under symmetry transformations of both types. Hence the resulting, full gauge fixed classical action with ghost term is also invariant under combined background and physical transformations. At the quantum level all of this carries over to the corresponding properties of the effective action $\Gamma[\bar{g},h]$.

We emphasize that the background transformations provide only an auxiliary symmetry and has no physical significance. It is also important to mention that the action is now explicitly a functional of two fields, namely $\bar{g}$ and h.

The crucial point is now that at the end of the calculation we let $\Gamma[\bar{g},h]$ inherit the physical symmetry by identifying the full field with the background, or equivalently by setting the fluctuating field to zero. With this procedure we arrive at the transformation property

$$0 = \left(\mathscr{G} + \bar{\mathscr{G}} \right) \Gamma[\bar{g},h]\big|_{\bar{g}=g} = \mathscr{G}\Gamma[g,g] \,. \qquad (4.27)$$

So far we did not use the framework of the FRG in the construction, but rather of quantum field theory in general. The further crucial input for the flow equation is now the regulator $\triangle S_k$ in the action. In order to ensure gauge invariance of the flow, we have to demand

$$\left(\mathscr{G} + \bar{\mathscr{G}} \right) \triangle S_k = 0 \,. \qquad (4.28)$$

As usual, one works with a cutoff that is quadratic in the dynamical field which leads to mass-like modification of the propagator and prevents the appearance of vertices $\Gamma^{(n)}$ with $n > 2$ and higher loops in the flow equation. This can be done by constructing the regulator and the volume form from the background field alone. The invariance under the combined transformations (4.20) and (4.21) then requires that $R[\bar{g}]$ transforms as a tensor under background transformations. This holds for the standard parameterization

$$\triangle S_k[\bar{g},h] = \frac{1}{2}\kappa^2 \int \sqrt{-\det\bar{g}} \; h_{\mu\nu} R^{\mu\nu\alpha\beta}_{k,hh}[\Delta_{\bar{g}}] h_{\alpha\beta} + \sqrt{2} \int \sqrt{-\det\bar{g}} \; \bar{C}_\mu R^{\mu\nu}_{k,\bar{C}C}[\Delta_{\bar{g}}] C_\nu \quad (4.29)$$

with k-dependent cutoffs operators $R_{k,hh}[\Delta_{\bar{g}}]$ for the metric field, and $R_{k,\bar{C}C}[\Delta_{\bar{g}}]$ for the ghost fields, where $\Delta_{\bar{g}}$ is the background covariant Laplacian.

With these ingredients we can write down the regularized Schwinger functional of our theory,

$$e^{W_k[J^{\mathbf{a}}]} = \int d\mu[h,\bar{C},C] e^{-S_{\mathrm{grav}}[\bar{g}+h]-S_{\mathrm{gf}}[\bar{g},h]-S_{\mathrm{gh}}[\bar{g},h,\bar{c},c]-\triangle S[\bar{g},h,\bar{c},c]+J^{\mathbf{a}}\phi_{\mathbf{a}}} \tag{4.30}$$

with super fields $\phi = (h,\bar{C},C)$, which leads to one source J_i for each field in the source term. S_{grav} is the Einstein Hilbert action, or more generally, a diffeomorphism invariant action that describes the gravitational interactions on the microscopic level. Furthermore we have the gauge fixing term S_{gf}, a ghost action S_{gh} and a cutoff $\triangle S$. We emphasize the importance of the functional dependencies of the different terms, and we stress that the dependence on the background metric $\bar{g}$ is only parametric.

Let us now write down the flow equation for the super-field $\phi = (h,C,\bar{C})$ within the background gauge framework. The general derivation form of the flow equation (3.9) allows us to write down the flow for the scale dependent effective action in quantum gravity with the given super-field space without any further effort,

$$\begin{aligned}
\dot{\Gamma}_k[\bar{g},g] &= \frac{1}{2} G_{\mathbf{ab}}[\bar{g},g] \dot{R}^{\mathbf{ab}}[\bar{g}] \\
&= \frac{1}{2}\mathrm{Tr}\left(\Gamma_k^{(hh)}+R_h\right)^{-1}\dot{R}_h - \mathrm{Tr}\left(\Gamma_k^{(\bar{C}C)}+R_{\bar{C}C}\right)^{-1}\dot{R}_{\bar{C}C},
\end{aligned} \tag{4.31}$$

where the functional arguments are again the expectation values of the quantum fields, but we dropped the $< . >$ in a slight abuse of notation. We also recall the minus sign for fermionic loops that is written explicitly in the slightly less condensed notation in the second line. The additional factor of two for the ghost part arises from the fact that we have a $G_{\bar{C}C}$ $\dot{R}_{\bar{C}C}$ and a $G_{C\bar{C}}$ $\dot{R}_{C\bar{C}}$ term in the flow.

The flaw in the background field flow equation

Despite the nice properties of the background field construction, there are several flaws and drawbacks in the standard formulation as presented above. First of all, as dictated by the principle of general covariance, the theory should be background independent. The explicit introduction of the background field $\bar{g}$ seems to spoil this property right away. A notion of background independence can be gained in the sense that one introduces a non-dynamical background metric $\bar{g}$ as an intermediate step, but the result should be independent of the specific choice of the background metric. In all truncated flows this is evidently not true, and this is surely an open problem in FRG-gravity.

Another aspect is that the gauge invariance of the standard background effective action does not imply independence of the gauge fixing condition. This drawback can be resolved by means of the geometrical fibre bundle construction of the Vilkovisky-de-Witt effective action, which is briefly discussed in subsection 5.6.2.

Moreover, there are further issues with the background field method in the context of flow equations. We have already stated, that in the standard background field formalism, the flow equation (4.31) is evaluated at vanishing fluctuation, i.e. at $h = 0$. However, the right hand

side of the flow equation (4.31) depends on the the two-point correlators of the fluctuation field h. It is important to note that the fluctuation correlation functions do not agree with the background correlations, as the effective action depends on the dynamical field and the background separately, i.e. Γ is not a functional of $g = \bar{g} + h$. As a consequence, we infer that

$$\left.\frac{\delta^2 \Gamma_k[\bar{g}, \phi]}{\delta h^2}\right|_{\phi=0} \neq \frac{\delta^2 \Gamma_k[\bar{g}, 0]}{\delta \bar{g}^2} \,, \tag{4.32}$$

and the difference is controlled by the so called modified split-identities, $[32, 70, 83, 85, 93-95, 97-99]$. In other words, one cannot simply extract dynamical couplings from the flow of the background field effective action at vanishing fluctuation fields, $\phi = 0$. This directly relates to the fact that the flow equation (4.31) for the effective action at $\phi = 0$ is not closed within the standard background field approach. In contrast to functional derivatives with respect to the fluctuation, the functional derivatives with respect to the background field hit the regulator, as R is a function of $\bar{g}$ only. Again, this dependence can be quantified by a consistency relation

$$\text{Tr}\left(G \frac{\delta^3 \Gamma_k}{\delta \bar{g} \delta g \delta g} G \, \partial_t R \right) = \text{Tr}\left(G \left(\partial_t \frac{\delta^2 \Gamma_k}{\delta g \delta g} \right) G \frac{\delta R}{\delta \bar{g}} \right), \tag{4.33}$$

similar to the split identities. The above relation follows without further assumptions from the flow equation with a background field. For a derivation see e.g. $[19, 97]$. However, in the standard flow (4.31) evaluated at $h = 0$, the above identities are not taken into account and the flow receives unphysical regulator contributions. More importantly, these unphysical contributions can spoil major physical properties such as confinement in Yang–Mills theories, $[96]$. This shows that the above discussion is not only a technical issue, but might have important consequences for observables.

We have already argued above that the background two–point function does not agree with the two–point function of the fluctuation field. This trivially generalizes for higher order correlators. As the result of the standard background field calculations is an effective action $\Gamma[\bar{g}, h = 0]$, one cannot obtain any information about e.g. the graviton three–point function, as the effective action is already evaluated at $h = 0$. This also implies that one does not have access to the momentum-dependence of the graviton correlation functions.

We conclude that the background field approximation has several drawbacks that need to be circumvented by more general constructions. This is the topic of the next chapters.

Dynamical Flows and Vertex Expansions in Quantum Gravity

5.1. Vertex expansion

We have seen in the previous section that despite some nice features, the standard background field method is not able to treat the difference between fluctuation and background fields in a satisfactorily way. In order to tackle this problem, we assume that we can expand the scale-dependent effective action in a functional power-series around a background field configuration $\bar{g}$. Then, the effective action takes the form

$$\Gamma_k[\bar{g},\phi] = \sum_n \frac{1}{n!}\Gamma^{\mathbf{a_1}...\mathbf{a_n}}[\bar{g},0]\phi_{\mathbf{a_1}}...\phi_{\mathbf{a_n}} = \Gamma_k[\bar{g},0] + \Gamma_k^{(h)a}[\bar{g},0]h_a + \frac{1}{2}\Gamma_k^{(2h)a_1a_2}[\bar{g},0]h_{a_1}h_{a_2}$$
$$+ \frac{1}{3!}\Gamma_k^{(3h)a_1a_2a_3}[\bar{g},0]h_{a_1}h_{a_2}h_{a_3} + \frac{1}{4!}\Gamma_k^{(4h)a_1a_2a_3a_4}[\bar{g},0]h_{a_1}h_{a_2}h_{a_3}h_{a_4}$$
$$+ \frac{1}{5!}\Gamma_k^{(5h)a_1a_2a_3a_4a_5}[\bar{g},0]h_{a_1}h_{a_2}h_{a_3}h_{a_4}h_{a_5} + ... + \Gamma_k^{(\bar{c}c)a_1a_2}[\bar{g},0]\bar{c}_{a_1}c_{a_2} + ...$$

$$(5.1)$$

The first and second term are of order h^0 and h^1 and do not enter the RHS of the flow equations for any $\Gamma_k^{(n)}$. A priori, the choice of the background field is completely arbitrary, although the results in a truncated theory will surely depend on the specific choice. For technical reasons we expand around a flat Euclidean background and choose $\bar{g}_{\mu\nu} = \mathbb{1}_{\mu\nu}$ as the expansion point. This choice of the expansion point also restricts the number of higher derivative operators which can contribute to the vertex functions of n-th order. For instance, the most general form of the two-point function derives from an action which includes at most $\mathcal{O}(R^2)$ operators. All higher order terms vanish after two functional differentiations and evaluation on a flat background. Terms of order R^3 and higher contribute only to vertex functions of order $n > 2$.

In the present work we use the systematic vertex expansion scheme as suggested in (5.1). The hierarchy of flow equations that has been introduced in the last section has to be truncated at finite order. This means that one can calculate the flow of a vertex function of

given order n and use an ansatz for $\Gamma_k^{(n+1)}$ and $\Gamma_k^{(n+2)}$. We will compute the full two-point correlation functions of the fluctuation fields ϕ in section 5.3, and the three–point function in section 5.7. The corresponding flows rely on the two- but also on the three-, four- and five–point functions of the fluctuation fields. Hence, we also introduce approximations for $\Gamma_k^{(4)}$ and $\Gamma_k^{(5)}$ that are consistent with the symmetries of the theory and have the correct RG-scaling.

5.1.1. Structure of the vertex functions

First of all, we have to specify the tensor structures of the vertices. In the present work, we use the classical tensor structures which arise from functional differentiation of the Einstein-Hilbert action. The gauge-fixed Einstein-Hilbert action, including the ghost part, is given by

$$S = \frac{1}{16\pi G_N} \int \mathrm{d}^4x \sqrt{\det g}\, (-R + 2\Lambda) + \int \mathrm{d}^4x \sqrt{\det \bar{g}}\, \bar{c}^\mu \mathscr{M}_{\mu\nu} c^\nu + \int \mathrm{d}^4x \sqrt{\det \bar{g}}\, \frac{1}{2\alpha_1} \bar{g}^{\mu\nu} F_\mu F_\nu\,.$$

In (2.2), G_N is the Newton constant and Λ is the cosmological constant. The Faddeev-Popov operator is given by

$$\mathscr{M}_{\mu\nu} = \bar{\nabla}^\alpha (g_{\mu\nu}\nabla_\alpha + g_{\alpha\nu}\nabla_\mu) - \bar{\nabla}_\mu\nabla_\nu\,, \tag{5.2}$$

and the linear gauge fixing conditions reads

$$F_\mu = \bar{\nabla}^\nu h_{\mu\nu} - \tfrac{1}{2}\bar{\nabla}_\mu h^\nu_{\ \nu}\,. \tag{5.3}$$

Moreover, in this work we restrict ourselves to Landau gauge, that is $\alpha_1 \to 0$. Extended ghost interactions are studied e.g. in [100, 101].

The standard Einstein-Hilbert truncation amounts to replacing the gravitational coupling and the cosmological constant in (2.2) by running couplings $G_{N,k}$ and Λ_k. The vertex functions are then given by functional derivatives of this effective action. However, this approximation turns out to be inconsistent in the physical IR limit, which will be discussed in detail later. We have also already mentioned that the basic Einstein-Hilbert truncation does not disentangle the difference between a wave-function renormalization and a running coupling, since the running of the latter is simply identified with the running of the former. Note that in Yang-Mills theory such an approximation gives a deconfining potential of the order parameter even in the confining regime, see [96, 102, 103]. In this case, it is also the non-trivial momentum-dependence of the correlation functions that plays a crucial rôle for capturing the correct non-perturbative physics. Additionally, in the UV limit, $k \to \infty$, the full momentum-dependence of correlation functions is potentially relevant. In particular, a derivative expansion implies $p^2/\text{scale}^2 \ll 1$ which relates to low energy physics. So far, these momentum-dependencies have not been taken into account.

Consequently, we construct more general vertex functions that take into account the above properties while keeping the classical tensor structures. The construction of such vertex expansions of the scale-dependent effective action was introduced in [104] and applied in the context of Yang-Mills theories. A similar truncation based on these ideas was recently applied in quantum gravity to [78]. One guiding principle in this construction is RG

invariance, i.e. invariance of the full effective action under a change of the renormalization scale μ:

$$\mu \frac{\mathrm{d}}{\mathrm{d}\mu} \Gamma = 0 \,, \tag{5.4}$$

where μ should not be confused with the running IR cutoff scale k, for a detailed discussion see [32]. In addition to that, we parameterize the vertex functions, i.e. the coefficients in the expansion (5.1) schematically as

$$\Gamma^{(n)} = Z^{\frac{n}{2}} \, \breve{\Gamma}^{(n)} \tag{5.5}$$

with a μ-independent part $\bar{\Gamma}^{(n)}$ and a μ-dependent wave-function renormalization $Z(p^2)$ of the attached fields. The above construction implies the correct scaling behavior for the fields according to

$$\mu \frac{\mathrm{d}}{\mathrm{d}\mu} \phi = \eta \, \phi \,. \tag{5.6}$$

In the present work we use a uniform wave function renormalization, $Z_h = Z_{h_i}$, for all components of the graviton. Non-uniform Z-factors will be subject to a forthcoming publication [4]. The transverse-traceless (TT) part of the full propagator is now parameterized as

$$\Gamma^{(2h)}_{\mathrm{TT}}(p^2) = Z_h(p^2)(p^2 - M^2)\Pi_{\mathrm{TT}}(p) \,, \tag{5.7}$$

with the transverse-traceless projector $\Pi_{\mathrm{TT}}(p)$, and an effective mass gap term M representing the momentum-independent part of the two-point function. We stress that this is not a physical mass term for the graviton like it is present in theories of massive gravity. As it is the background propagator that enters S-matrix elements, a massive graviton has a constant term in the background field propagator that is not related appropriately to the cosmological constant. The parameterization (5.7) above is for the fluctuation field two-point function, and this object is in general nonzero for $p \neq 0$ in the same way as the gluon acquires a non-perturbative mass gap in the infrared. Note that the Z-factors are functions of the covariant Laplacian Δ, and therefore include infinitely many terms in a covariant expansion of the effective action in powers of the Laplace operator. This is the first RG study of quantum gravity taking into account this general momentum dependence of the graviton and the ghost propagator. The fully momentum-dependent Z-factors lead to a vertex construction with the required RG scaling properties. They also embody a corresponding implicit, non-canonical momentum-dependence of the vertex functions, in line with the co-linear singularity structure of vertex functions.

Apart from these momentum-dependent wave-function renormalization dressing factors, the vertex functions acquire further scale-dependencies via quantum fluctuations. In a most general setup, modulo overall prefactors, a graviton vertex is then written in a tensor decomposition with dressing parameters as

$$\Gamma^{a_1...a_n}_k(p_1,...,p_n) \sim \sum_{i=1}^{m} g_{i,k}(p_1,..,p_n)\mathcal{T}^{a_1...a_n}_i(p_1,...,p_n) \,, \tag{5.8}$$

where the m tensors $\mathcal{T}^{(n)}_i$ form a basis for the corresponding tensor space. Using a different basis or complete set of tensors that span the tensor space leads to a redefinition of the

generalized couplings $g_{i,k}(p_1,..,p_n)$. Note that these generalized couplings depend on the RG-scale k as well as on the n-momenta p_i. The exact, physical vertex function is then obtained in the limit $k \longrightarrow 0$ and the physics of scales is then encoded in the dependence of the couplings on the external momenta. However, a truncation in this generality is beyond present technology. In fact, the investigations presented in this thesis are the first approximations that take into account momentum dependencies in the FRG approach to quantum gravity. All other truncations that can be found in the literature apply a reduction to pure k-dependence of the couplings. For the propagator the full momentum dependence is manageable and the calculation is presented in section 5.6. The first calculation of the flow of the three-point vertex is presented in section 5.7 and its momentum dependence is partially resolved.

In this thesis, the vertex functions are constructed as follows. We use the general RG-consistent scaling (5.5) with fully momentum-dependent wave-function renormalizations. Additionally, we allow for running parameters $\Lambda_k^{(n)}$ which govern the scale-dependence of the momentum-independent part of the vertex functions. This takes into account scaling properties of the vertex functions that are crucial for the global flows structure, and has not been considered before. The construction of the vertex functions also includes overall, k-dependent prefactors $G_k^{(n)}$ that are suitable generalizations of Newtons coupling. Henceforth we will call these quantities gravitational couplings. These couplings are then introduced with appropriate powers, such that in a perturbative limit, where all these couplings are equal, one regains the Einstein–Hilbert action. The tensor structures are assumed to be the classical ones. In summary, the vertex functions take the form

$$\Gamma_k^{(a_1 \ldots a_n)}(p_1, \ldots, p_n) = \prod_{i=1}^{n} \sqrt{Z_{\phi_i,k}(p_i)} \left(G_k^{(n)} \right)^{\frac{n}{2}-1} \mathscr{T}_k^{a_1 \ldots a_n}(p_1, \ldots, p_n; \Lambda_k^{(n)}), \tag{5.9}$$

with tensor structures

$$\mathscr{T}_k^{a_1 \ldots a_n}(p_1, \ldots, p_n) = S^{(a_1 \ldots a_n)}(p_1, \ldots, p_n; G_N = k^2, \Lambda \to \Lambda_k^{(n)}), \tag{5.10}$$

that arise from functional differentiation of the classical Einstein-Hilbert action S given in (2.2). We left out the functional dependence on the fields. If we leave out the functional argument, it is implicitly understood that the functional is evaluated at vanishing fluctuation fields and on a flat background. The tensor structures $\mathscr{T}_k^{a_1 \ldots a_n}$ carry not only the canonical explicit momentum-dependence of the vertex functions, but also the running parameters $\Lambda_k^{(n)}$. They are defined by

$$\mathscr{T}_k^{a_1 \ldots a_n}(p_i = 0; \Lambda_k^{(n)}) =: -2\Lambda_k^{(n)} \tilde{\mathscr{T}}^{a_1 \ldots a_n}(\delta_{\mu\nu}), \tag{5.11}$$

where $\tilde{\mathscr{T}}^{a_1 \ldots a_n}(\delta_{\mu\nu})$ is the tensor structure arising from functional differentiation of the integral of the volume form with respect to the metric tensor. The factor of -2 in the definition is introduced such that we recover the classical cosmological constant in the Einstein-Hilbert action. We emphasize again that the consistent RG-scaling of the parameters $\Lambda_k^{(n)}$ is of major importance for the transition from the UV regime to the IR regime, as well as for the stability of the IR regime. In this regime the $\Lambda_k^{(n)}$ are determined via a self-consistency analysis of the scaling behavior. Details will be presented in the corresponding results

sections. Moreover, for most parts of this thesis we use only one gravitational coupling and if not stated otherwise we identify $G_k^{(n)} \equiv G_{N,k}$. Hence, we are left with one, scale dependent gravitational coupling $G_{N,k}$ which we simply call Newtons coupling.

Such a vertex construction can also be obtained from a classical Einstein–Hilbert action as follows. We write the full metric as $g = \mathbb{1} + \check{h}$, i.e. an expansion of the metric around a flat background and a fluctuation field $\check{h}$. The classical action (2.2) can then be expanded in powers of this fluctuation in order to obtain classical vertices. Then one can use a redefinition of fields according to

$$\check{h} \longrightarrow h = \sqrt{G_N Z_h}\check{h}. \tag{5.12}$$

Note that such redefinitions of the fields are always allowed. Dressing G_N with a k-dependence, Z_h with scale and momentum dependence, and replacing Λ with $\Lambda_k^{(n)}$ at each order n in the expansion leads to vertices of the form (5.9).

An example for the above vertex construction is the scalar coefficient of the TT-two point function of the graviton,

$$Z_h(p^2)(p^2 - 2\Lambda_k^{(2)}), \tag{5.13}$$

see also (5.7). The tensor structures for the general two-point function, from which the above results via TT-projection, are given by (5.10) and arise from functional differentiation of the Einstein-Hilbert action. Equation (5.13) and (5.7) entail that $\Lambda_k^{(2)}$ is the effective graviton mass gap,

$$M_k^2 = -2\Lambda_k^{(2)}. \tag{5.14}$$

Once again, note that this mass term is neither the cosmological constant, nor a physical graviton mass.

Finally we introduce dimensionless, scale-dependent couplings, to wit

$$g := G_N k^2, \qquad\qquad \mu := M^2 k^{-2}, \tag{5.15}$$

$$\lambda := \Lambda k^{-2}, \qquad\qquad \lambda^{(n)} := \Lambda^{(n)} k^{-2}, \tag{5.16}$$

with $n \geq 3$ and $\Lambda = \Lambda^{(1)}$.

5.2. Locality

The functional renormalization group (with a momentum cutoff) is based on the idea of a successive integration of momentum shells, or, more generally, spectral shells of spectral values of the kinetic operator of the theory. In other words, it relies on the distinction of small and large momentum or spectral modes. A functional RG step implements the physics of momentum/spectral modes at a given RG scale k. Hence, all Wilsonian renormalization group equations rely on the existence of local RG steps, inherently related to local interactions.

Locality in momentum space implies in particular that the flow of a correlation function or vertices at a given momentum scale k decays relative to the cutoff scale if all momenta are taken to infinity, $p_i/k \to \infty$. This means that the change of the correlation function at some scale k compared to the norm of the correlator itself at this scale, must go to zero in

the limit of infinite external momenta. For vertices this reads schematically

$$\lim_{p_1,\ldots,p_n\to\infty} \frac{|\partial_t \Gamma_k^{(n)}(p_i)|}{|\Gamma_k^{(n)}(p_i)|} = 0\,, \tag{5.17}$$

where a projection on the scalar coefficients functions of a single tensor structure is implied. If the above condition is satisfied, the flow at some scale k for a n-point correlation function does not change the behavior of the correlation function at momenta $p \gg k$, and local coarse graining is well-defined. From a mathematical point of view, such local interactions are necessary in lattice systems for the existence of the continuum limit and similar criteria are necessary in mathematical formulations of the renormalization group [105, 106]. However, locality is not just a technical or mathematical issue, but is a very physical property of the theory. Let us illustrate the physical meaning of the locality property (5.17) with a very instructive example. Let us assume we calculate the running of a momentum-dependent coupling, say the strong coupling constant $\alpha_{s,k}(p^2)$ from e.g. the three gluon-vertex $\Gamma^{(A,\bar{c},c)}(p^2)$. In an FRG-setting, we can then set boundary conditions at an arbitrary initial scale k_0. In the case of quantum chromodynamics, one usually sets the boundary conditions in the perturbative regime, say at the mass of the Z-boson $k_0 = m_Z$. We can then integrate the flow to smaller scales and eventually arrive at the mass scale m_τ of the tau lepton with a coupling $\alpha_{s,k=m_\tau}(p^2)$. Let us assume we make a further infinitesimal RG step in order to calculate $\alpha_{s,k=m_\tau-\delta k}(p^2)$. With a well-defined coarse graining procedure one can then argue that we expect $\alpha_{s,k=m_\tau-\delta k}(p^2) \approx \alpha_{s,k=m_\tau}(p^2)$ for momenta $p^2 \gg k^2 = m_\tau^2$. However, if the locality condition for the corresponding vertex $\Gamma^{(A\bar{c},c)}(p^2)$ were not satisfied, then this integration step at the tau-mass scale could influence significantly the coupling at external momenta at the Z-mass scale, e.g

$$\alpha_{s,k=m_\tau-\delta k}(p^2 = m_Z^2) = \alpha_{s,k=m_\tau}(p^2 = m_Z^2) + \Delta\,, \tag{5.18}$$

with a possibly large correction term Δ, which is in sharp contrast to the physical picture of Wilsonian renormalization. One can make this picture completely absurd if one formulates the above argument for scales k and momenta p that are infinitely separated in momentum space, i.e. $|k - p| = \infty$

In summary, the relation (5.17) is a necessary requirement for local quantum field theories. Giving it up would pose fundamental formal problems.

It is easily proven that (5.17) applies to the standard renormalizable quantum field theories in four dimensions including non-Abelian gauge theories that involve momentum-dependent couplings.

Locality in ϕ^4 theory.

Let us consider first the illustrative example of standard ϕ^4 theory. The flow of the propagator in this theory involves just a tadpole diagram, see figure Figure 5.2. The propagator in the the loop does not carry any external momentum and the vertex is momentum independent.

As a consequence, the flow is constant a C with respect to the external momentum p. The two-point function itself, however is proportional to p^2, and the locality property (5.17) is

$$\partial_t \frac{\delta^2 \Gamma[\phi]}{\delta \phi^2} \quad : \quad$$

Figure 5.1.: The tadpole diagram that contributes to the flow of the propagator in ϕ^4 theory. We do not care about the pre-factors and the regulator here, since in this section we are interested in power counting of momenta only.

$$\partial_t \frac{\delta^4 \Gamma[\phi]}{\delta \phi^4} \quad : \quad$$

Figure 5.2.: The diagram that contributes to the flow of the four-point function in ϕ^4 theory. We do not care about the pre-factors and the regulator here, since in this section we are interested in power counting of momenta only.

trivially satisfied,

$$\lim_{p \to \infty} \frac{|\partial_t \Gamma^{(2)}_{k,\phi^4}(p)|}{|\Gamma^{(2)}_{k,\phi^4}(p)|} \sim \lim_{p \to \infty} \frac{C}{p^2} = 0 \,. \tag{5.19}$$

It is also easily checked that the flow of the four point vertex is local. The scattering diagram contributing to the flow of the four-point function is given in Figure 5.2.

In this case it is now important that *all* momenta $p_1, ..., p_4$ are taken to infinity. Then, in this diagram, one propagator in the loop carries external momenta p_1^2 and p_2^2. The two vertices in the diagram are again momentum-independent in this simple theory. The four-point function $\Gamma^{(4)}_{k,\phi^4}$ itself at a scale k is a constant C_λ and the ratio considered for locality decays as

$$\lim_{p_1,,...,p_4 \to \infty} \frac{|\partial_t \Gamma^{(4)}_{k,\phi^4}(p_i)|}{|\Gamma^{(4)}_{k,\phi^4}(p_i)|} \sim \lim_{p \to \infty} \frac{\frac{1}{p^2}}{C_\lambda} = 0 \,. \tag{5.20}$$

At his point we mention a subtlety that will become relevant later on. If we consider a configuration where two external momenta are zero, then there is one diagram in the flow where e.g. the two legs "on the right of the diagram" carry zero-momentum. In this case, momentum conservation enforces that both propagators in the loop are independent of any external momentum. As a consequence, the flow and the correlation function itself are entirely independent of the momentum. Therefore, the ratio $\partial_t \Gamma^{(4)} / \Gamma^{(4)}$ is a constant and the locality property is spoiled. The reason is obviously rooted in the fact that there is a diagram that as a finite external–momentum transfer in the loop.

Locality in Yang–Mills theory.

A less trivial example for a theory that has the locality property (5.17) is Yang–Mills theory. In Figure 5.3 we show one diagram that contributes to the flow of the propagator, and

$$\partial_t \frac{\delta^2 \Gamma[\phi]}{\delta A^2} \quad : \quad \text{\small (diagram)} \quad ,...$$

Figure 5.3.: One of the diagrams that contribute to the flow of the propagator in Yang–Mills theory. We do not care about the pre-factors and the regulator here, since in this section we are interested in power counting of momenta only.

$$\partial_t \frac{\delta^3 \Gamma[\phi]}{\delta A^3} \quad : \quad \text{\small (diagram)} \quad ,...$$

Figure 5.4.: One of the diagrams that contribute to the flow of the three–gluon vertex in Yang–Mills theory. We do not care about the pre-factors and the regulator here, since in this section we are interested in power counting of momenta only.

in Figure 5.4 one diagram that contributes to the flow of the three-gluon vertex. For the other diagrams that contain a four–gluon vertex, the momentum counting gives the same result, as can easily be verified by the reader. In Yang–Mills theory the three-gluon vertex is proportional to p, and the two-point function is as usual quadratic in momentum.

Simple momentum counting then gives rise to the structure

$$\lim_{p \to \infty} \frac{|\partial_t \Gamma^{(2)}_{k,YM}(p)|}{|\Gamma^{(2)}_{k,YM}(p)|} \sim \lim_{p \to \infty} \frac{\frac{pp}{p^2}}{p^2} = 0 \,. \tag{5.21}$$

for the flow of the two–point function and

$$\lim_{p_1,,...,p_3 \to \infty} \frac{|\partial_t \Gamma^{(3)}_{k,YM}(p_i)|}{|\Gamma^{(3)}_{k,YM}(p_i)|} \sim \lim_{p \to \infty} \frac{\frac{ppp}{p^2 p^2}}{p} = 0 \,. \tag{5.22}$$

for the flow of the three–point function. It is then easy to see that the same holds also for the flow of the four–gluon vertex. In summary, we conclude that in these two examples, the locality property is a simple consequence of power–counting.

In turn, in a similar fashion it is easy to see that a ϕ^4-theory with a momentum-dependent coupling such as $\int_x \phi^2 \partial^2 \phi^2$ does not satisfy (5.17).

Loaclity for perturbatively renormalizable field theories.

It is now quite clear how one can formulate such power–counting arguments for general field theories. Based on the insights gained from the examples for standard ϕ^4 theory and Yang–Mills theory, it is intuitively clear that this reasoning applies to all power–counting, perturbatively renormalizable quantum field theories, i.e. for theories where the couplings have only positive mass dimension,

$$[g_i] \geq 0 \,. \tag{5.23}$$

$$\partial_t \left. \frac{\delta^2 \Gamma[\bar{g}, \phi]}{\delta h^2} \right|_{\phi=0} (p^2) = -\frac{1}{2}$$

$$-2 \qquad =: \text{Flow}^{(2h)}(p^2)$$

$$\partial_t \left. \frac{\delta^2 \Gamma[\bar{g}, \phi]}{\delta c \delta \bar{c}} \right|_{\phi=0} (p^2) =$$

$$=: \text{Flow}^{(\bar{c}c)}(p^2)$$

Figure 5.5.: Diagrammatic representation of the flow of the second order vertex functions. The dressed graviton propagator is represented by a double line, the dressed ghost propagator by a dashed line, while a dressed vertex is denoted by a dot and the regulator insertion by a crossed circle.

We have indeed proven that this statement is correct. The detailed analysis will be given elsewhere.

5.3. Flow of the Graviton and the Ghost Propagators

In this section we investigate the general structure of the propagator in more detail. The corresponding general flow equation is obtained by functional differentiation of (3.9), and its diagrammatic representation is shown in Figure 5.5, where we have also introduced the notation $\text{Flow}^{(n)}$ for the right-hand side of the flow equation of the n-point correlation function.

The form of the flow equation for the two-point in terms of propagators and vertices for a general super-field ϕ is derived in Appendix B and given by (I). Due to the generality, this formula can be applied for a quantum field theory with arbitrary field content. In our case we set $\phi = (h, \bar{c}, c)$ and arrive at Figure 5.5. Note that we have omitted the tadpole contribution with a vertex of two gravitons, an anti-ghost and a ghost, since this vertex vanishes for linear gauge-fixing conditions. The building blocks of the equation are the graviton propagator $G_h = \left(\Gamma^{2h} + R_h\right)^{-1}$, which is a rank-four tensor, the ghost propagator $G_c = \left(\Gamma^{(\bar{c}c)} + R_h\right)^{-1}$, which is a rank-two tensor and the vertex functions $\Gamma^{(h\bar{c}c)}$, $\Gamma^{(3h)}$ and $\Gamma^{(4h)}$, which are rank-four, rank-six and rank-eight tensors respectively. Consequently, also the flow equation for the graviton propagator is an equation for a rank-four tensor. The propagators are obtained from an inversion of the two-point vertex function $\Gamma^{(2)}$. For the ghost propagators the corresponding tensor space is spanned by the longitudinal and the transverse vector-projectors P_T and P_L, and the inversion is almost trivial. For the graviton, however, the tensor space is much more complicated. For the inversion and a simple representation it is necessary to use an orthogonal basis of projection operators Π_i with a corresponding projector algebra. These projectors span the space of symmetric rank-four tensors that depend on one external vector, in this case the momentum p. The six projectors

$\Pi_{ab}^{(i)}(p)$, $i = 1, ..., 6$, and the technical details about the vertices and the propagators as well as their explicit representation can be found in [14, 19]. With this projector basis we can expand the two-point function as

$$\Gamma_{ab}^{(2h)}(p) = \sum_{i=1}^{6} c_i(p) \, \Pi_{ab}^{(i)}(p), \tag{5.24}$$

with some coefficients c_i that are real valued functions of the momentum. In this thesis all regulators are proportional to the respective two-point function evaluated at zero mass,

$$R_{\mathbf{ab}}(p) = r\left(\frac{p}{k}\right) \left. \Gamma_{\mathbf{ab}}^{(2)}\right|_{m=0}(p), \tag{5.25}$$

where r is a shape function that ensures the regulator properties (3.8) and depends on the dimensionless, absolute value of the momentum. In terms of contractions of the propagators and vertices the flow of the graviton two-point function can be written as

$$\text{Flow}_{\alpha\beta\mu\nu}^{(2h)} = -\frac{1}{2} \int_{\mathbb{R}^4} \frac{\mathrm{d}^4 q}{(2\pi)^4} \Gamma_{\alpha\beta\gamma\tau\iota\kappa\mu\nu}^{(4h)}(p, q, -q, -p) \, (G\dot{R}G)_{hh}^{\iota\kappa\gamma\tau}(q)$$

$$+ \int_{\mathbb{R}^4} \frac{\mathrm{d}^4 q}{(2\pi)^4} \Gamma_{\alpha\beta\gamma\tau\iota\kappa}^{(3h)}(p, q, -p - q) \, (G\dot{R}G)_{hh}^{\epsilon\delta\gamma\tau}(q) \, \Gamma_{\mu\nu\epsilon\delta\rho\sigma}^{(3h)}(-p, -q, p + q) \, G_{hh}^{\iota\kappa\rho\sigma}(p + q)$$

$$- 2 \int_{\mathbb{R}^4} \frac{\mathrm{d}^4 q}{(2\pi)^4} \Gamma_{\alpha\beta\gamma\tau}^{h\bar{c}c}(p, q, -p - q) (G\dot{R}G)_{\bar{c}c}^{\gamma\delta}(q) \Gamma_{\mu\nu\rho\sigma}^{h\bar{c}c}(-p, -q, p + q) G_{\bar{c}c}^{\tau\rho}(p + q),$$

where the first term corresponds to the tadpole diagram, the second term to the self-energy with the pure graviton loop and the third one is the ghost contribution. The contractions require extensive use of algebra. In fact, even deriving the four-graviton vertex is nothing one should do by hand. For the higher order functional derivatives of the action and the contraction of the vertices and propagators in the diagrams we use computer algebra based on FORM [107] and xTENSOR [108]. In order to obtain beta-functions for the running RG-parameters of the propagator, we have to project onto a tensor structure such that we obtain a scalar expression. As already mentioned in the previous section, in the most general case each tensor structure is equipped with its own scale-dependent RG-parameter and can be obtained by contracting the flow with the corresponding projector. However, note that the different tensor structures generically contain pure gauge degrees of freedom and therefore a careful analysis of modified Slavnov-Taylor identities is a necessary accompanist of such an approximation. In this thesis we work with a uniform wave-function renormalization Z_h for the graviton. We note that the transverse-traceless part of the graviton propagator is independent of the gauge fixing parameter. Moreover, as e.g. classical gravitational waves are purely transverse-traceless, this part is expected to carry the essential physical properties. Additionally, throughout this thesis we use Landau-de Witt gauge. This means that the overall gauge fixing parameter is taken to zero, $\alpha_1 \longrightarrow 0$. In principle, in a FRG-setting, also the gauge-fixing parameters acquire a scale-dependence. However, it can be shown that $\partial_t \alpha_1 \sim \alpha_1$. As a consequence, Landau gauge, i.e. $\alpha_1 = 0$ is a fixed point of the renormalization group flow and we do not have to consider a flow equation for the gauge fixing parameter.

The scalar transverse-traceless flow is then obtain by projection from the tensor flow according to

$$\partial_t \Gamma_{\text{TT}}^{(2h)}(p) = \frac{\Pi_{\text{TT}}^{ab}(p)\,\partial_t \Gamma_{ab}^{(2h)}(p)}{\Pi_{\text{TT}}^{ab}(p)\,\Pi_{\text{TT},ab}(p)}\,. \tag{5.26}$$

From now on, all expressions for the two-point functions relate to the TT-part and we drop the corresponding subscript. A study with all independent tensor structures will be presented elsewhere [4]. However, we stress that the transverse projection is with respect to the external momentum p only. Hence, internal propagators in the loop carry the full tensor decomposition. With the vertex parameterization presented in subsection 5.1.1, we can construct the flow equation for the propagator explicitly. After contraction of the diagrams and applying the TT-projection, the flow of the propagator takes the form

$$\partial_t \Gamma^{(2h)}(p^2) = (p^2 + M^2)\partial_t Z_h(p^2) + Z_h(p^2)\partial_t M^2 = \text{Flow}^{(2h)}(p^2), \tag{5.27}$$

with

$$\text{Flow}^{(2h)}(p^2) = G_N Z_h(p^2) \int d^4q \sum_\phi \left(\partial_t r_\phi(q^2) + \frac{\partial_t Z_\phi(q^2)}{Z_\phi(q^2)} r_\phi(q^2) \right) I_\phi(p^2, q^2, M^2, \Lambda^{(n)}), \tag{5.28}$$

where we have already dropped the subscript k, and if not stated otherwise, all generalized couplings are scale-dependent. The index $\phi = (h, c)$ labels the contributions from the gravitons and the ghosts respectively.

In the above equation, $I_\phi(p^2, q^2, \Lambda^{(n)})$ are scalar functions that arise from the contraction of the diagrams and a subsequent projection onto the TT-structure. The explicit expressions for these functions are given in Appendix C. The index n takes the values $n = 2, 3, 4$, since the diagrams on the right-hand side contain propagators, three-point and four-point vertices, and therefore there appear the corresponding coupling factors $\Lambda^{(3)}, \Lambda^{(4)}$ and the gap-parameter M^2. We also note, that according to the RG-consistent vertex construction Equation 5.9, the left-hand side is independent of the gravitational coupling, while the right-hand side is proportional to G. Moreover, since the regulator is proportional to Z, one can easily convince oneself that the left-hand side is proportional to $Z_h(p^2)$ and that wave-function renormalizations with loop momentum q in the argument appear only as a ratio $\dot{Z}(q^2)/Z(q^2)$. On the left hand-side there is one term proportional to $Z_h(p^2)$, which then drops out, and another one proportional to $\dot{Z}_h(p^2)$ that again combines into a ratio $\dot{Z}_h(p^2)/Z_h(p^2)$. Consequently, the wave-function renormalization $Z(p^2)$ does never enter a flow equation alone, but always in the combination $\dot{Z}/Z$ and the entire dependence on the wave-function renormalizations and their derivatives in equation (5.27) is encoded in the anomalous dimension $\eta_h(p^2)$ of the graviton and the anomalous dimension $\eta_c(p^2)$ of the ghost field,

$$\eta_h(p^2) := -\frac{\partial_t Z_h(p^2)}{Z_h(p^2)}, \tag{5.29}$$

$$\eta_c(p^2) := -\frac{\partial_t Z_c(p^2)}{Z_c(p^2)}. \tag{5.30}$$

This structure has important technical consequences, as will be discussed below. For the ghost sector, we apply the same strategy and arrive at the much simpler equation

$$p^2 \partial_t Z_c(p^2) = \text{Flow}^{(\bar{c}c)}(p^2). \tag{5.31}$$

Explicit expressions can be found in Appendix C.

At this point we emphasize again, that this is the first calculation in quantum gravity that takes into account the full momentum dependence of the graviton propagator and thus goes far beyond any Einstein-Hilbert truncation. The full momentum dependence is stored in the momentum dependent dressing $Z(p^2)$.

In summary, with Figure 5.5 and (5.9) the flows of the two-point functions $\Gamma^{(2)}$, i.e. the right-hand sides of the flow equations, depend on

$$\left(\eta_h(p^2), \eta_c(p^2), M^2, G_N, \Lambda^{(3)}, \Lambda^{(4)} \right), \tag{5.32}$$

while the left-hand sides contain just $\left(\eta_h(p^2), \eta_c(p^2), M^2 \right)$. It is therefore obvious that the equations for the propagators are not closed. This is exactly a reflection of the fact that the flow of the n-point function depends on the m-point functions up to order $n + 2$. There are several ways for closing the equation, one of them being the identification of different RG-parameters in a specific manner. Another one is to push the order of the vertex expansion to higher order. Such possibilities will be discussed in the next subsection below.

5.3.1. Different Closures and Truncations

We have seen that due to the structure of the coupled hierarchy, i.e. the infinite tower of flow equations, the coupling constants of the three- and four-point function appear in the flow of the propagator, but not on the left-hand side of the equation. Thus, one cannot obtain beta-functions, i.e. equations for the scale-evolution of these couplings, from the flow equation for $\Gamma^{(2)}$ alone.

We start with a basic truncation that will be generalized subsequently. This enables us to trace back the effects of different improvements of the approximation.

In section section 5.5 we present a closure that resembles an Einstein-Hilbert truncation, but is based on the flow of the propagator. Still, it is based on an identification of the couplings such that one retains only the two Einstein-Hilbert couplings G and Λ and equation (5.5) gets closed.

In section 5.6 we improve this approximation in several directions. First, we allow for a general momentum dependence of the propagator by including the momentum-dependent wave-function renormalization as presented in the general setup presented above, subsection 5.1.1, section 5.3. Second, we resolve the momentum independent parts $\Lambda^{(n)}$ of the vertices in an approximation to be explained below, and use an additional equation for the gravitational coupling G from geometrical flow equations in order to close the hierarchy.

Finally, we calculate the next level of the hierarchy by means of the flow equation for the graviton three-point function. This is presented in section 5.7 and section 5.8.

Having specified such a closing procedure, it is left to project the flow of the functional(s) onto the running of the scale-dependent couplings. We refer to this procedure as specification [109]. Analyzing and defining such procedures is subject to the next section.

5.4. Specification

The aim of a specification is to relate the truncated flow of vertex-functions to running couplings. In general, this ambiguous due to truncations, as we will argue below. The problems with different projection procedures is of course known to the community for a long time. We used the freedom of specification in [1] in the context of quantum gravity and an extensive study in ultracold-atoms is worked out in [110]. A specification is usually done with a projection in momentum space, e.g. a derivative expansion up to some finite order around some expansion point $p_\star$. Since the flow itself is in general a complicated function of momentum, the resulting flow equations depend on the truncation order and the expansion point. Consequently, the specification procedure is not unique. It is not only the expansion point $p_\star$ that is ambiguous, but one can even project different orders at different momenta. Another possibility is a finite difference at two subtraction points, which are completely in our hands. However, by including the full momentum dependence one can find unique solutions. This will be discussed in subsection 5.6.1. For all truncations in momentum space, a projection should be chosen such that the full momentum dependence is well approximated. Independent of the theory, the task of finding an appropriate specification is present in all truncated FRG-calculations, as the full momentum dependence is a priori not known. Moreover, it usually appears problem-specific in different incarnations. We now demonstrate the issue at the example of a generic propagator in a derivative expansion. For this purpose, it is convenient to work entirely in momentum space. Moreover, for notational simplicity we work with a single scalar field, however, generalization to arbitrary field content is straightforward. Quite in general, the objects entering the flow of the two-point function can then be paramterized as

$$
\Gamma_k^{(2)}(p) = Z_k(p^2)\left(p^2 + M_k^2\right)
$$
$$
\Gamma_k^{(3)}(p_1, p_2) = f_3\left(p_1, p_2, g_{3,i,k}(p_1, p_2)\right)
$$
$$
\Gamma_k^{(4)}(p_1, p_2, p_3) = f_4\left(p_1, p_2, p_3, g_{4,i,k}(p_1, p_2, p_3)\right) , \tag{5.33}
$$

where we have already used momentum conservation in order to reduce the number of momenta the vertex functions depend on. The paramterization of the two-point function is exactly as described in the vertex expansion in subsection 5.1.1, i.e. the function $Z_k(p^2)$ is a generalized wave-function renormalization that serves as a fully momentum dependent dressing function and the constant part of the propagator is characterized by a scale-dependent mass term M_k^2. The three and four-point function are arbitrary functions of the momenta (p_1, p_2) and (p_1, p_2, p_3) respectively. Additionally, they may depend on scale-dependent couplings $g_{i,k}$ that are again functions of momentum. In simple truncations, the ansatz for the three and four point vertex may look much simpler, e.g. being momentum-independent and retaining only one scale-dependent coupling $g_{4,i,k}(p_1, p_2, p_3) \equiv g_{4,k}$ as for the most archaic ansatz for a standard ϕ^4 model. However, in theories with derivative couplings, these vertex functions do depend on momentum even on tree-level, with quantum gravity and and Yang–Mills theory being prominent examples. Inserting these vertex functions into the flow of the propagator, which is given in full generality in equation (B) and for pure quantum gravity in Figure 5.5, yields an equation where both sides of the equation depend in a general fashion on the momentum p. Since this equation is then an integro-differential equation for $Z_k(p)$, quite frequently one approximates the momentum dependence. The first

study with full-momentum dependence in quantum gravity will be presented in this thesis in section 5.6 and can be found in the corresponding publication [2]. Studies of the full momentum dependence in the FRG-setting in Yang–Mills theory and QCD are presented e.g. in [111–116].

The most common approximation scheme is the derivative expansion [117]. In this approach the fully momentum-dependent wave function renormalization is expanded in powers of the momentum according to

$$Z_k(p^2) = \sum_n Z_{2n,k} p^{2n} = Z_{0,k} + Z_{2,k} p^2 + Z_{4,k} p^4 + \dots . \tag{5.34}$$

The above series is then usually truncated at some finite order n_0 and the propagator in momentum space is then a polynomial of degree $2n_0 + 2$ in p. Note that setting $Z_{0,k} \equiv Z_0 \equiv$ const. and $Z_{2n,k} = 0$ for $n \geq 1$ and setting all momenta in the higher order vertex functions to zero then corresponds to the local potential approximation (LPA).

Truncating the above series at any finite order n_0 and inserting them into the flow equation for the propagator, one is left with a polynomial in p of order $2n_0 + 2$ on the left-hand side and an arbitrary function of momentum on the right-hand side. Even if the vertex functions are also polynomials in p, the right hand-side is a general rational function of p. Consequently, the truncated flow equation is not closed with respect to the momentum structure. Strictly speaking, it is not even an equation any more. It follows immediately, that the coefficients in the derivative expansion are not uniquely determined. Therefore, any procedure that isolates the running of the scale-dependent can be used as a definition for extracting the beta-functions and they will give in general different answers. In an LPA' approximation, i.e. with a scale dependent $Z_{0,k}$ and all higher orders set to zero, the left hand side is quadratic in momentum and one can project onto the running of the scale-dependent quantities from $\Gamma^{(2)}$ via the definition

$$\partial_t Z_{0,k} := \frac{\partial^2}{\partial p^2} \text{Flow}^{(2)}(p) \Big|_{p=p_\star} \tag{5.35}$$

and

$$\partial_t \left(Z_{0,k} M_k^2 \right) := \text{Flow}^{(2)}(p) \Big|_{p=p_\star} - p_\star^2 \partial_t Z_{0,k} . \tag{5.36}$$

The simplest projection on the scale-dependent quantities on the left-hand-side is achieved by expanding the latter around $p_\star = 0$. This choice has the big advantage, that is allows for an analytical treatment if it is combined with an optimized regulator. However, the above two quantities $\partial_t Z_{0,k}$ and $\partial_t \left(Z_{0,k} M_k^2 \right)$ can just as well be obtained with $p_\star = k$, i.e. by redefining (5.35) and (5.36) via evaluation at $p = k$ instead of $p = 0$. Here it appears another subtlety, since at $p_\star \neq 0$, it actually matters if one uses two derivatives with respect to p or one derivative with respect to p^2 since

$$\frac{\partial^2 f(p)}{\partial p^2} = \frac{1}{2} \frac{\partial f(p)}{\partial (p^2)} + 4p^2 \frac{\partial^2 f(p)}{\partial (p^2)^2} . \tag{5.37}$$

Hence, the two different derivatives agree at $p = 0$ up to a proportionality factor that cancels since it appears on both sides of the flow equation. However, at $p \neq 0$ they differ. As already mentioned above, one can also define the two quantities at different $p_{\star,1}$ and $p_{\star,2}$. Such

a construction will be used in section 5.5. A generalization of the above concept of using derivatives is the finite difference projection for the part quadratic in momentum. The corresponding definition is

$$\partial_t Z_{0,k} := \frac{\left.\text{Flow}^{(2)}(p^2)\right|_{p=p_\star} - \left.\text{Flow}^{(2)}(p^2)\right|_{p=p_\bullet}}{p_\star^2 - p_\bullet^2} \,. \tag{5.38}$$

The derivative definition is then regained in the limit $p_\bullet \longrightarrow p_\star$.

5.5. Truncation I: Einstein-Hilbert type Propagator

In this section, we present the flow of the graviton propagator in a Einstein–Hilbert type of setting. This means that the scale-dependence of the effective action is entirely determined by two running couplings, namely Newtons constant and the cosmological constant. The scale-dependent gravitational coupling G_k is constructed from the graviton wave-function renormalization $Z_{h,k}$, and the momentum-independent parts of the vertex functions are all identified with the cosmological constant, $\Lambda_k^{(n)} \equiv \Lambda_k$. This procedure closes the equations (5.27) and (5.31). Additionally, in this approximation one works with a momentum-independent graviton wave-function renormalization $Z_{h,k}$ and ignores the scale dependence of the ghosts. This reduction based on identifying $\Lambda^{(n)}$ and relating the gravitational coupling G_k to $Z_{h,k}$ is used in almost all truncations in RG-gravity calculations so far. The first publications that disentangle this structure are [2, 79]. The first presentation of this idea in exactly the setup presented above in the context of gravity can be found in [118], and was used subsequently in [72, 78]. In reduced truncations, i.e. in Einstein-Hilbert type of truncations, the graviton wave function renormalization and the running Newton coupling are related via

$$G_k := \frac{G_N}{Z_{h,k}} \,. \tag{5.39}$$

Again, we emphasize that the wave-function renormalization depends only on the RG-scale k and not on the physical momentum p.

Reducing the general vertex expansion in this manner amounts to an Einstein–Hilbert truncation since in this setting all vertex functions are simply obtained by functional differentiation of the classical, gauge fixed Einstein-Hilbert action (2.2) with the replacements

$$G_N \longrightarrow G_k \quad , \quad \Lambda \longrightarrow \Lambda_k \,. \tag{5.40}$$

For the sake of completeness, we display again the basis of the Einstein–Hilbert truncation in full glory,

$$\Gamma_k[\bar{g}; h, \bar{C}, C] = \frac{Z_{N,k}}{16\pi G_N} \int \sqrt{|g|} \, (-R(g) + 2\Lambda_k) \quad + \frac{Z_{h,k}}{2\alpha_k} \int \sqrt{|\bar{g}|} \, \bar{g}^{\mu\nu} F_\mu(\bar{g}, h) F_\nu(\bar{g}, h)$$

$$- \sqrt{2} \int \sqrt{|\bar{g}|} \, \bar{C}_\mu M^\mu_{\ \nu}(\bar{g}, h) C^\nu \,. \tag{5.41}$$

Note that in the above truncation the ghost term is not dressed with a scale-dependent wave-function renormalization. As a consequence, the ghost anomalous dimension vanishes

in this approximation. In the next section we will also include not only a scale-, but also momentum-dependent ghost wave-function renormalization. Although we use such an Einstein–Hilbert effective action in this section, we emphasize that this calculation is still quite different from the standard background field Einstein–Hilbert setup, as we aim to calculate the two-point function of the fluctuation field. This is in sharp contrast to the background field approximation which is usually used in the literature and described in subsection 4.2.1. It is clear that the fluctuation field propagator cannot be obtained from the background effective action.

With the definition (5.39) of the coupling one immediately infers that

$$\frac{\partial_t G}{G} = -\frac{\partial_t Z_h}{Z_h} = \eta_h \,. \tag{5.42}$$

As usual, we suppress the argument k that indicates the scale-dependence in order to simplify the notation and G, or its dimensionless version g are scale-dependent. In terms of the dimensionless Newton coupling the above equation can be related to the beta-function of Newtons coupling as

$$\partial_t g = (2 + \eta_h)g \,. \tag{5.43}$$

Again, we see that with this closure the scale evolution of Newtons coupling is obtained from the propagator and strictly speaking it loses its precise notion as a coupling. In a similar fashion we write for the cosmological constant

$$\partial_t \lambda = -2\lambda + \eta_\lambda \,, \tag{5.44}$$

where we introduced the 'anomalous dimension' of the cosmological constant $\eta_\lambda \equiv (\partial_t \Lambda_k)/k^2$. From (5.43) and (5.44) one can see that the fixed point condition $(\partial_t g, \partial_t \lambda) = (0,0)$ is satisfied if the canonical running due to the mass dimension of G_N and Λ_k is exactly counterbalanced by the running induced by quantum fluctuations. In case of an UV fixed point, this scaling is approached in the limit $k \to \infty$, thus leading to divergence-free couplings at arbitrarily small distances. For the explicit computations we choose an optimized regulator of the form [20, 32, 119]

$$\mathcal{R}_k\left(q^2\right) = \Gamma_k^{(2)}\big|_{\lambda=0} \, r\left(q^2/k^2\right)$$
$$r(z) = (\tfrac{1}{z} - 1)\theta(1 - z), \tag{5.45}$$

which allows for a largely analytical access. It is now left to apply some specification procedure, see section 5.4, to the flow of the propagator (5.27) in order to project onto the flow of the couplings. In the spirit of the general discussion of specification prescriptions, we will use the freedom of projecting onto the running coupling in order to optimize the approximation. This means that we try to capture the most important effects of the momentum dependence of the flow. The parameter $\Lambda^{(2)} = -M^2/2$, which is in this truncation identical to the cosmological constant Λ, is defined as the momentum independent part of the propagator. Hence it is natural to apply the specification

$$\partial_t \left(Z_h \Lambda_k\right) = -\frac{1}{2} \text{Flow}^{(2h)}(p)\Big|_{p=0} \,. \tag{5.46}$$

For the projection on the running of Newtons coupling, the situation is less clear. In order to estimate the best approximation to the full momentum dependence, we first investigate the
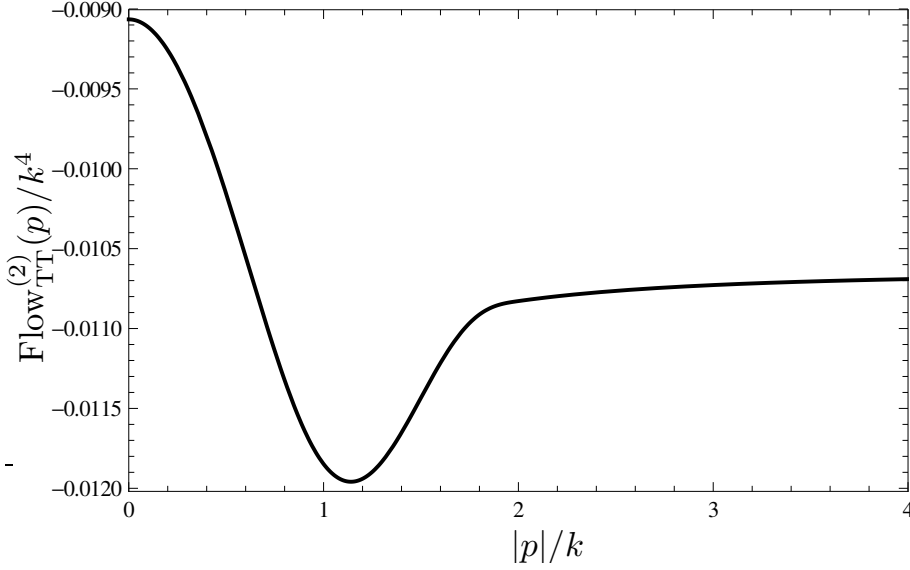
Figure 5.6.: Dependence of the flow on the external momentum p. In this plot for the parameter values $\lambda = 0$ and $\eta(q) = 0$ in the loop integral.

right-hand side of the flow equation as a function of the external momentum p^2. This is not only necessary for choosing an appropriate specification, but it is also the object of interest in the discussion of the locality with its defining property (5.17).

5.5.1. Momentum Dependence and Locality of the Propagator

In this section we prove the locality property (5.17) for the graviton propagator. This can be done completely analytically. In order to do so, we have to investigate $\text{Flow}^{(2h)}(p^2)$ in the limit $p^2 \longrightarrow \infty$. The is then compared to the behavior of the two point function $\Gamma^{(2h)}(p^2)$ itself at the same scale k. Let us first apply the power–counting arguments as presented in section 5.2 to the flow of the graviton two–point function. In a vertex construction as defined in subsection 5.1.1, the two–point function itself behaves for large momenta simply as p^2. The flow $\text{Flow}^{(2h)}(p^2)$ contains three diagrams, see Figure 5.5. The three and the four graviton vertices in these diagrams both have terms that are proportional to p^2. In the tadpole diagram there is one four–graviton vertex and only one internal propagator, which carries no external momentum. In the self energy there are two three–graviton vertices and one internal propagator that carries an external momentum. As a consequence, by power counting arguments one would expect that $\lim_{p\to\infty} \text{Flow}^{(2h)}(p^2) \sim p^2$ and therefore that the ratio $\text{Flow}^{(2h)}(p^2)/\Gamma^{(2h)}(p^2)$ goes to a constant for large momenta. This result would imply a violation of locality, (5.17). We now investigate the limit (5.17) by explicit calculation. For the sake of definiteness, we use the optimized regulator (5.45), but we stress that the results of this section are independent this choice! The investigation of locality boils down to the properties of the flow for large momenta. First we evaluate the flow numerically and display the result at the parameter value $\lambda = 0$ and without anomalous dimension under the loop integral in Figure 5.6.

The behavior of the flow shows a highly non-trivial momentum-dependence. First, in

the cutoff-regime $p \lesssim k$, it is very different from the p^2 dependence of the bare two-point function. It displays a minimum at $p \approx k$ and any derivative expansion must be taken with great care. This observation will influence the choice of specification in the next section. Moreover, we see that the the flow tends to a finite value for large momenta, in contrast to the power counting analysis above, which suggests a divergence proportional to p^2. As a consequence, the flow of the propagator satisfies locality in very non-trivial way. From the technical point of view, the root of locality in this case is a cancellation of leading terms in the large p limit of the diagrams on the right-hand side of the flow equation. As we will see, this cancellation takes place after angular integration.

In what follows, we will display the asymptotic analysis as a showcase for later calculations in some detail.

In the limit of large momenta, we can solve the flow analytically by means of asymptotic expansions. In order to do so, we consider equation (5.28), which shows the structure of the flow. The relevant part for this analysis is then the function $I_\phi(p^2, q^2, M^2, \Lambda^{(n)})$, which arises due to the contractions of the propagators and vertices in the diagrams. By splitting into the individual contributions, we can write this function as

$$I_\phi(p^2, q^2, M^2, \Lambda^{(n)}) = (\text{tadpole})_{TT} + (\text{self-energy})_{TT} \tag{5.47}$$

with

$$(\text{tadpole})_{TT} = \frac{a(p,q,y)}{\left(q^2(1 + r_k(q) - 2\Lambda_k\right)^2} \tag{5.48}$$

and

$$(\text{self-energy})_{TT} =$$
$$\frac{b(p,q,y)}{\left(p^2 + q^2 + 2pqy\right)\left(q^2(1 + r_k(q)) - 2\Lambda_k\right)^2\left((p^2 + q^2 + 2pqy)(1 + r_k(p+q)) - 2\Lambda_k\right)}, \tag{5.49}$$

where a and b are polynomials in all their arguments. These polynomials can be read off $I_\phi(p^2, q^2, M^2, \Lambda^{(n)})$. There are several important aspects to note in the above equations. First, such loop-integrals are most conveniently evaluated in four–dimensional spherical coordinates, and we can identify the angle θ between p and q with the second inclination angle θ_2 and we set $y = \cos(\theta_2)$. The integral measure is then given by

$$d^4x = dr d\phi d\theta_1 d\theta_2 r^3 \sin(\theta_1)\sin^2(\theta_2). \tag{5.50}$$

Second, since the loop integral is proportional to $\theta(k^2 - q^2)$, the integral over the absolute value q is bounded by k. As a consequence we can set the distributions $\theta(k^2 - q^2)$ in the denominator to zero. Moreover, since we are interested in the limit $p^2 \longrightarrow \infty$ we will consider an asymptotic expansion for large momenta in the usual sense that one applies a transformation $p \longrightarrow 1/p$ and then an expansion in $\epsilon := 1/p$ around $\epsilon = 0$. In such an expansion, the θ functions $\theta(k^2 - (q+p)^2)$ can be set to zero as $p >> k$ and the argument of these θ-functions is then always negative. As a result, we are left with a rational function in p,

$$\lim_{p \to \infty} \text{Flow}^{(2h)}(p^2) = \lim_{p \to \infty} \int_0^1 \int_{-1}^1 dq dy \sqrt{1 - y^2} \frac{\mathscr{P}_1(p, q, y, \lambda)}{\mathscr{P}_2(p, q, y, \lambda)} \tag{5.51}$$

where $\mathscr{P}_{1,2}$ are polynomials in p with degree

$$\deg[\mathscr{P}_1] - \deg[\mathscr{P}_2] = 2\,, \tag{5.52}$$

which is obvious from the explicit form of $I_\phi(p^2, q^2, M^2, \Lambda^{(n)})$ given in appendix Appendix C, or much simpler by the power counting arguments presented above. We write the above equation in such generality, since for any locality analysis and the corresponding asymptotic expansion the flow takes the form (5.51). In the limit of large momenta, we take into account only the leading terms in p in the denominator on the right hand-side of (5.51) and arrive at

$$\text{Flow}^{(2h)}(p^2) \overset{p\to\infty}{\sim} \frac{1}{(1-2\lambda)} \int_0^1 \int_{-1}^1 \mathrm{d}q\mathrm{d}y\, \sqrt{1-y^2}\big((5q^3(-1+4y^2)p^2 + 15q^4(-1+4y^2)p \\ + q^5 C(\lambda, y)\big)\,, \tag{5.53}$$

with some irrelevant momentum-independent constant $C(\lambda, y)$ and we have not displayed the part proportional to η_h. The term of order p is antisymmetric in y, but is integrated over the symmetric domain $y \in [-1, 1]$ and therefore drops out. This is merely a manifestation that the flow can be written as a function of p^2, i.e. after integration the odd powers of p drop out. The angular integral of the term proportional to p^2 can easily be carried out analytically by using an elementary trigonometric substitution $y = \sin(u)$ to yield

$$\int_{-1}^1 \mathrm{d}y\, \sqrt{1-y^2}(-1+4y^2) = -\frac{1}{4}\sin(2u) - \frac{1}{32}\sin(4u)\bigg|_{\sin^{-1}(-1)=-\frac{\pi}{2}}^{\sin^{-1}(1)=\frac{\pi}{2}} = 0\,. \tag{5.54}$$

As a result, the only term left in (5.53) is the term order p^0, i.e the constant term. Hence, the flow is a constant with respct to p in the limit of infinite momenta, and after elementary integration the exact asymptotic is given by

$$\lim_{p\to\infty} \text{Flow}^{(2h)}(p^2) = \frac{-20 + 42\lambda - 48\lambda^2 + (1+\lambda)\eta_h}{192\pi^2(1-2\lambda)^2}\,. \tag{5.55}$$

Since $\Gamma^{(2h)}(p^2) \overset{p\to\infty}{=} p^2$, locality is a trivial consequence,

$$\lim_{p\to\infty} \frac{\text{Flow}^{(2h)}(p^2)}{\Gamma^{(2h)}(p^2)} = 0\,. \tag{5.56}$$

5.5.2. Beta functions

Based on the results for the momentum-dependence of the flow, depicted in Figure 5.6, we have already stated, that the right-hand side of the flow equation is very different from a function $f(p^2) \sim p^2 + \text{const}$, which is the form of the propagator in the Einstein–Hilbert truncation. Therefore, a derivative expansion around $p_\star = 0$ and around $p_\star = k$ will lead to very different results. In fact, as one can see from the shape of the function, that even the sign will be different for these two expansion points. In order to find an optimized value for $p_\star$, we recall that the loop-integral on the right-hand side of the flow equation is

peaked for momenta $q \approx k$, meaning that the the flow is sensitive to physics and momentum fluctuations of the order of the cutoff. Accordingly, the propagator should resolve this domain in momentum space sufficiently precise. This improves not only the consistency of the flow, but it is also of great importance for assigning a physical meaning to the cutoff scale in the spirit of the k-microscope, see chapter 3. Due to these arguments and the structure of the propagator, we choose $p_\star = k$ for the projection on the wave-function renormalization,

$$\partial_t Z_h = \partial_p^2 \mathrm{Flow}^{(2h)}(p) \Big|_{p=k}. \tag{5.57}$$

Together with (5.46), this constitutes a bi-local projection in momentum space. The virtue of our set-up is that the running of couplings is sensitive to the global (momentum) behavior of the theory as encoded in its two-point function. In addition, the flow of the cosmological constant can be obtained completely analytically. Within this Einstein–Hilbert type truncation, the projection defined above and equation (5.27) we arrive at the explicit expressions

$$\partial_t Z_h = G Z_h \int_{\mathbb{R}^4} \frac{\mathrm{d}^4 q}{(2\pi)^4} \sum_\phi \left(\partial_t r_\phi(q^2) + \frac{\partial_t Z_\phi}{Z_\phi} r_\phi(q^2) \right) \frac{\partial^2}{\partial p^2} I_\phi(p^2, q^2, \Lambda^{(n)} \equiv \Lambda) \Big|_{p=k} \tag{5.58}$$

and

$$\partial_t \left(Z_h \Lambda_k \right) = -\frac{1}{2} G Z_h \int_{\mathbb{R}^4} \frac{\mathrm{d}^4 q}{(2\pi)^4} \sum_\phi \left(\partial_t r_\phi(q^2) + \frac{\partial_t Z_\phi}{Z_\phi} r_\phi(q^2) \right) I_\phi(p^2 = 0, q^2, \Lambda^{(n)} \equiv \Lambda), \tag{5.59}$$

where we have used $M^2 = -2\Lambda$ in Einstein–Hilbert truncations and $\phi = (h, c)$ indicates the pure graviton and the ghost contributions. In this approximation with the identification of couplings, it is of course redundant to use both, Z_h and G, as they are related by (5.39). One can also use a formulation based on G only. For convenience and in order to make contact with the standard notation used in the literature, which uses (5.43), we formulate everything in terms of the graviton anomalous dimension by rewriting the above as

$$\eta_h = -G \int_{\mathbb{R}^4} \frac{\mathrm{d}^4 q}{(2\pi)^4} \sum_\phi \left(\partial_t r_\phi(q^2) - \eta_\phi r_\phi(q^2) \right) \partial_p^2 I_\phi(p^2, q^2, \Lambda^{(n)} \equiv \Lambda) \Big|_{p=k} \tag{5.60}$$

and

$$\partial_t \Lambda = \Lambda \eta_h - \frac{G}{2} \int \mathrm{d}^4 q \sum_\phi \left(\partial_t r_\phi(q^2) - \eta_\phi r(q^2) \right) I_\phi(p^2 = 0, q^2, \Lambda^{(n)} \equiv \Lambda). \tag{5.61}$$

In the above equations there are further simplifications possible. First, we use the same regulator for the graviton and for the ghost, $r_h = r_c$. Moreover, as we use a constant, scale-independent wave-function renormalization for the ghost, its scale derivative vanishes and so does the anomalous dimension η_c. The graviton wave-function, in turn, is scale-dependent but is independent of the momentum. As a consequence, η_h can be pulled outside the integral on the right-hand side and appears as a pre-factor of the latter. We end up with an algebraic equation for the graviton anomalous dimension. Due to the optimized cutoff, the integrations in (5.61) can be carried out analytically, whereas the projection with $p_\star = k$ for
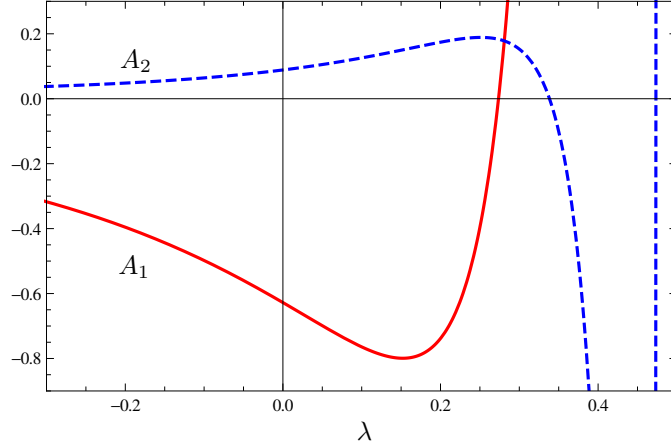
Figure 5.7.: The functions $A_1(\lambda)$ (solid red line) and $A_2(\lambda)$ (dashed blue line) in the flow of η_h (5.62). In the limit $\lambda \to 1/2$ both functions behave as $(1 - 2\lambda)^{-3}$. The function A_2 has a minimal value of -13.6 at $\lambda \approx 0.46$.

the anomalous dimensions makes the structure of the integrand difficult to handle. Typically, only derivative expansions with $p_\star = 0$ allow for purely non-numerical treatment [1]. Hence, the final beta-functions are semi-analytical. Solving these integrals and solving algebraically for η_h, and formulating everything in terms of the dimensionless quantities (5.16), the beta functions (5.43) and (5.44) take the final, integrated form

$$
\begin{aligned}
\eta_\lambda &= \eta_h \, \lambda + g \, \frac{4(1 + 2\lambda)^2 - 9}{12\pi(1 - 2\lambda)^3} - \eta_h \frac{12 - 45\lambda - 40\lambda^2}{180\pi(1 - 2\lambda)^3} + \frac{1}{\pi}, \\
\eta_h &= \frac{A_1(\lambda) g}{1 - A_2(\lambda) g} - g \frac{237\sqrt{3} - 160\pi}{240\pi^2}.
\end{aligned}
\tag{5.62}
$$

The last terms originate from the ghosts, and the functions $A_1(\lambda)$ and $A_2(\lambda)$ are known numerically and plotted in the relevant regime in Figure 5.7. With equation (5.43), the beta-function for Newtons coupling finally reads

$$
\partial_t g = 2g + g^2 \left(\frac{A_1(\lambda)}{1 - A_2(\lambda) g} - \frac{237\sqrt{3} - 160\pi}{240\pi^2} \right).
\tag{5.63}
$$

It is important to note that due to the dependence of the regulator on Z_h, the anomalous dimension appears on the right-hand-, as well as on the left-hand side of the flow equation and therefore we are left with the algebraic equation for η_h. As a consequence, we get a term proportional to $1/(1-g)$ in the anomalous dimension, which in turn enters the beta-function for g linearly. This term can then be expanded in a geometric series. As a result, β_g can be written as a power series in g, and we see that the functional renormalization group equations even in an Einstein–Hilbert truncation induce a resummation to infinite order in the coupling. We can organize the above result for Newtons coupling in a perturbative

---

[1]In principle one can give also closed expressions for $p_\star = k$, however, the result is immensely complicated an completely useless
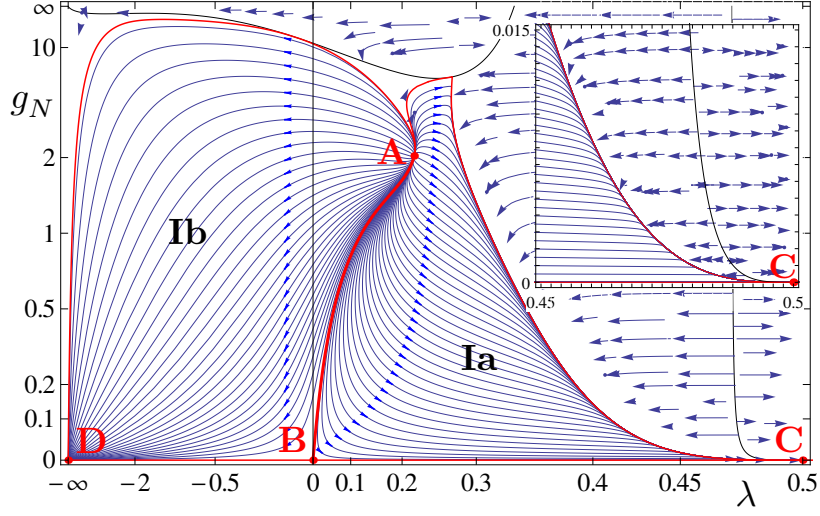
Figure 5.8.: Fixed points and phase diagram in the (g, λ)-plane. Arrows point from the UV to the IR, red lines and points mark separatrices and fçixed points, black lines signal a divergence of the flow. The inset magnifies the vicinity of C.

fashion by writing

$$\frac{A_1(\lambda)}{1 - A_2(\lambda)g} = \sum_{n=0}^{\infty} A_1(\lambda) \left(A_2(\lambda)g\right)^n \,, \tag{5.64}$$

as a geometric series.

5.5.3. Fixed points and phase diagram.

In this subsection we describe the strucutre of the phase diagram that is generated by the RG flows (5.43) and (5.44) with (5.62). As we have already explained, the phase diagram is the collection of trajectories in the (g, λ) plane. Each initial condition $(g(k_0) = g_{\text{initial}}, \lambda(k_0) = \lambda_{\text{initial}})$ fixed at some RG-scale k_0 is then in one-to-one correspondence to a trajectory. We focus on the physical regime $g > 0$. The global structure of this phase diagram displays four connected fixed points A, B, C and D in the physical regime, see Figure 9.1. The fixed point A at $(g_{N*}^{\text{UV}}, \lambda_*^{\text{UV}}) \neq (0, 0)$ denotes the asymptotically safe UV fixed point whose coordinates and scaling exponents are given in Tab. 5.1.

	g_{N*}^{UV}	λ_*^{UV}	$\lambda_*^{\text{UV}} \times g_{N*}^{\text{UV}}$	θ_1	θ_2
no ghosts	1.95	0.11	0.21	$3.09 + 2.00\,i$	$3.09 - 2.00\,i$
with ghosts	2.03	0.22	0.45	8.38	2.60

Table 5.1.: Fixed point values $(g_{N*}^{\text{UV}}, \lambda_*^{\text{UV}})$, their product, and the critical exponents $\theta_{1,2}$ of the UV fixed point without and with the ghost contributions.

It is characterised by two UV relevant real eigenvalues, which turn into a complex conjugate pair in the absence of ghost field fluctuations. A complex conjugate pair of

eigenvalues, as found in many previous studies, can be lifted via additional interactions e.g. the inclusion of higher derivative interactions. For our setup, we conclude that the degeneracy in the UV scaling of the Ricci scalar and the vacuum energy is already lifted by the ghost sector. This fully attractive UV-fixed point fulfills all requirements in order to form the basis for the UV-completion of quantum gravity in this approximation. A comparison of the fixed point values in different approaches can be found in Figure 5.9. One can see that in this approach they take values that are larger compared to other calculations. However, the fixed point values have no physical meaning, and the results obtained in the standard background flow and also in the $f(R)$ calculations are not related to dynamical quantities.

	g_*	λ_*	$\lambda_* \times g_*$	θ_1	θ_2
background flow	0.89	0.16	0.14	2.00 -2.70 i	2.00 + 2.70 i
bimetric flow	0.70	0.21	0.15	3.6 -4.3 i	3.6 + 4.3 i
geometrical flow	1.49	0.05	0.08	2.55 + 1.46 i	2.55 - 1.46 i
$f(R)$	0.97	0.12	0.12	2.50 -2.34 i	2.50 +2.34 i
this approx.	2.03	0.22	0.45	8.38	2.60

Figure 5.9.: Fixed point properties of the different flows in comparison. The result for the background flow is the one with the optimized regulator, see [24]. The results for bi-metric truncations can be found in [85]. The geometrical approach is presented in [79]. The fixed point values stated for $f(R)$ gravity are the results obtained in a polynomial expansion up to order R^{34} in [66]. The standard background flow in Einstein–Hilbert and the $f(R)$ calculations stated above are not related to dynamical quantities.

The fixed point B at $(g_{N*}^{\mathrm{IR}}, \lambda_*^{\mathrm{IR}}) = (0, 0)$ is the well-known repulsive Gauss ian IR fixed point. It corresponds to classical gravity in the IR with a vanishing dimensionless cosmological constant. The fixed point D at $(g_{N*}^{\mathrm{IR}}, 1/\lambda_*^{\mathrm{IR}}) = (0, 0^-)$ is IR attractive in both couplings and governs infrared gravity with a negative vacuum energy. In addition we find a non-trivial IR fixed point C at

$$(g_{N*}^{\mathrm{IR}}, \lambda_*^{\mathrm{IR}}) = (0, 1/2), \tag{5.65}$$

that is connected to the UV fixed point via smooth RG trajectories. It is a distinctive property of the present approach that it admits an infrared completion of quantum gravity for positive cosmological constant. Naively, one would expect classical RG-scaling in the IR fixed point regime [120], for signatures thereof see [20, 121]. Here, we find an asymptotic IR behaviour with non-classical scaling exponents $\Delta_g \approx 5.5$ and $\Delta_{(1-2\lambda)} \approx 1.8$. It implies an asymptotic weakening of gravity, see also [79]. A more detailed analysis of the infrared scaling will be presented in a more general context in the next chapter. In this setup, the non-classical scaling of the propagator is a consequence of strong IR effects. Non-classical scaling in the deep infrared might have important consequences for cosmsology and astrophysics. However, we will see in the next chapter that this non-classical scaling is likely to be a truncation artefact and disappears in more sophisticated approximations.

It is important to stress that physical short-distance initial conditions in the vicinity of the UV fixed point A leads to trajectories in the regions Ia and Ib. In region Ia all trajectories end into the new IR fixed point C with large anomalous dimensions for the graviton propagator; in region Ib the trajectories end in the IR fixed point D with classical scaling for the graviton propagator. These two regions are separated by the IR instable separatrix leading to the

Gaußian FP at B. In turn, all other trajectories terminate in singularities and have no classical regime. Hence, the strong-gravity region is shielded by the separatrices AD ($g_N \lesssim 33.5$) and AC ($g_N \lesssim 5.4$) from regions which admit an extended semi-classical regime. The fact that a strong-gravity regime is shielded dynamically by the RG flow is also present in previous global UV-IR studies [79, 122], and thus appears to be a generic feature of asymptotically safe gravity.

5.6. Truncation II: Fully momentum-dependent Propagator and the geometrical Coupling

In the last section we have presented the flow of the propagator in an Einstein–Hilbert type of truncation, which can be obtained by a specific identification of couplings in the general vertex expansion introduced in subsection 5.1.1. In this section we will improve this approximation in several ways. First, we will compute the full momentum-dependence of the propagator by taking into account the wave functions renormalizations $Z(p^2)$, i.e. they are arbitrary functions of the Laplacian. Second, we avoid the identification of the coupling and the wave-function renormalization. The latter is obtained from the propagator, while for the former we use a running coupling obtained with geometrical flow equations, see subsection 5.6.2 and [79], which serves as the coupling related to the three- and four-point function. Additionally, we resolve the constant parts $\Lambda^{(n)}$ of the vertex functions. Their running in the limit $\mu \longrightarrow -1$ is highly non-trivial and is constrained within a self-consistency analysis, subsection 5.6.3. As we have already mentioned in the presentation of the vertex construction, the fluctuation field propagator has a non-vanishing mass-gap, which is described by the parameter $-2\Lambda^{(2)} = M^2$. Once more, we stress that this is not a physical mass term for propagating gravitons that can be detected e.g. via coherent oscillations as gravitational waves. Therefore, a non-vanishing mass term of this type does not spoil the property of a force with infinite range. In summary, we solve coupled equations for the system

$$\left(\eta_h(p^2), \eta_c(p^2), M^2, G_N, \Lambda^{(3)}, \Lambda^{(4)} \right) , \tag{5.66}$$

where the constant parts $\Lambda^{(3)}, \Lambda^{(4)}$ are assumed to differ from $-\frac{1}{2}M^2$ only in the vicinity of the pole of the propagator. The justification for this approximation and its validity is discussed. In the region where they acquire a non-trivial behavior, the scaling is derived from a self-consistency analysis of the hierarchy of flow equations. In the following, we derive the flow equations for the set of couplings (5.66).

5.6.1. Integral equations for the anomalous dimensions and flow of the gap parameter.

The full-momentum dependence of the propagator that appears in our parameterization as wave-function renormalizations $Z_\phi(p^2)$ that are arbitrary functions of the momentum. As a consequence, the projection of the functional flow as well as the solution of the resulting equations requires new techniques that are quite different from the derivative expansions and the specifications presented in section 5.4. Once again, the starting point is the general equation (5.27). As we have already discussed in section 5.3, due to the structure of the

regulator, which is proportional to the wave-function renormalization, all the Z-factors in the equation for the propagator combine into anomalous dimensions $\eta_h(p^2)$. We can then write the flow as

$$\eta_h(p^2) = \frac{\partial_t M^2 - \frac{\text{Flow}^{(2h)}(p^2)}{Z_h(p^2)}}{p^2 + M^2} .$$
(5.67)

In Appendix D, we argue that under the assumption of a finite anomalous dimension, the flow of the gap paramter should be projected from an on-shell condition $p^2 = -M^2$, i.e. at the pole of the propagator, or equivalently at the zero of the two-point function. This leads to

$$
\begin{aligned}
0 &= \partial_t \left(\Gamma^{(2h)}(-M^2) \right) \\
&= \partial_t \left. \Gamma^{(2h)}(p^2) \right|_{p^2=-M^2} - \left. \partial_{p^2}\Gamma^{(2h)}(p^2) \right|_{p^2=-M^2} \partial_t M^2 \\
&= \partial_t \Gamma^{(2h)}(-M^2) - Z_h(-M^2)\partial_t M^2 .
\end{aligned}
$$
(5.68)

Solving for the running of the mass parameter, we get

$$\partial_t M^2 = \frac{\partial_t \Gamma^{(2h)}(-M^2)}{Z_h(-M^2)} .$$
(5.69)

One of the goals of this work is to evaluate the phase diagram of quantum gravity and its fixed point structure. For this reason, it is convenient to derive β- functions for the dimensionless parameters. Then, the above equation translates into

$$
\begin{aligned}
\partial_t \mu &= -2\mu + \frac{\partial_t \Gamma^{(2h)}(-M^2)}{k^2 Z_h(-M^2)} \\
&=: \beta_\mu[\eta_h, \eta_c](g, \mu, \lambda^{(3)}, \lambda^{(4)}) .
\end{aligned}
$$
(5.70)

We remind the reader the μ is just dimensionless version of M^2. The explicit form of the β-function is given in Appendix C. It is clear from (5.28) that the β-function for the running mass shows a functional dependence on the anomalous dimensions, as the latter appears as $\eta_\phi(q^2)$ in the integral over the loop momentum q. From a mathematical perspective, the functional is therefore a linear integral operator and the equation is a differential-Fredholm integral equation of the first kind.

Substituting this equation (5.69) for the running of the gap parameter in equation Equation 5.67, we obtain

$$\eta_h(p^2) = -\frac{\frac{\partial_t \Gamma^{(2h)}(p^2)}{Z_h(p^2)} - \frac{\partial_t \Gamma^{(2h)}(-M^2)}{Z_h(-M^2)}}{p^2 + M^2} [\eta_h, \eta_c] .$$
(5.71)

Note that all isolated Z- factors drop out, see (5.27). The same procedure can be applied for the ghost sector. Since there is no ghost mass, we trivially arrive from (5.31) at

$$\eta_c(p^2) = -\frac{\partial_t \Gamma^{(\bar{c}c)}}{p^2 Z_c(p^2)} [\eta_h, \eta_c] .$$
(5.72)

The explicit form of eqs. (5.71) and (5.72) is given in Appendix C. These equations for the anomalous dimensions constitute a coupled set of linear integral equations. More precisely, they are a coupled set of inhomogeneous Fredholm integral equations of the second type. This structure is reflected in the functional dependence on η_ϕ as for the running gap parameter, i.e. the functional on the right-hand side of eqs. (5.71) and (5.72) is a Fredholm integral operator. In summary, we have reduced the general flow of the propagator to set of two coupled integral equations,eqs. (5.71) and (5.72), that in turn are coupled to a differential equation, (5.69). In order to solve this system, we rewrite the integral equation for the graviton anomalous dimension in order to bring it into standard form. With pretty elementary manipulations of (5.27) we arrive at

$$\eta_h(p^2) = f(p^2) + g \int_{\mathbb{R}^4} \frac{\mathrm{d}^4 q}{(2\pi)^4} K\left(p, q, \mu, \lambda^{(n)}\right) \eta_h(q^2), \tag{5.73}$$

where the integral kernel is given by

$$K\left(p^2, q^2, \mu, \lambda^{(n)}\right) = \frac{1}{p^2 + \mu} r_h(q^2) \left(I_h(p, q, \mu, \lambda^{(n)}) - I_h(-\mu, q^2, \mu, \lambda^{(n)})\right) \tag{5.74}$$

and the inhomogeneity reads

$$f(p^2) = \frac{g}{p^2 + \mu} \int_{\mathbb{R}^4} \frac{\mathrm{d}^4 q}{(2\pi)^4} \left(\sum_\phi (\partial_t r_\phi(q^2)) \left(-I_\phi(p, q, \mu, \lambda^{(n)}) + I_\phi(-\mu, q, \mu, \lambda^{(n)})\right) \right.$$
$$\left. - \eta_c(q^2) \left(I_c(p^2, q^2, \mu, \lambda^{(n)}) - I_c(-\mu, q^2, \mu, \lambda^{(n)})\right) \right), \tag{5.75}$$

where we have now formulated everything in terms of dimensionless quantities without introducing new symbols for these objects. For instance, in a slight abuse of notation, in the above equation p denotes the dimensionless momentum instead of the dimensionful one as used in the previous equations.

Solutions of inhomogeneous Fredholm integral equation of the second kind

Fredholm integral equations of the second kind are a well-known topic in pure, as well as in applied mathematics and there are several methods in order to solve such equations. Mathematical literature that analyzes these equations in great detail can be found e.g. in the beautiful textbooks [123, 124]. A straightforward numerical solution is the so called Nystroem method that is based on discretization of the integral operator with quadratures on N points. By doing so, one obtains Riemann sums that reduce to a system of N linear equations. Moreover, if there exist a solution to equation (5.73), it can be shown by the general theory of such equations that it is unique and the discretized version converges towards this solution in the limit $N \longrightarrow \infty$. Another method that comes along with less numerical effort are iterative solutions based on the resolvent formalism and the Liouville-Neumann series. The basic idea of this approach is as follows. In order to get a feeling for such integral equations, we observe that for $g = 0$, the unique solution to (5.73) is trivially given by the inhomogeneity $f(p^2)$. Hence, if g is small in some sense, it seems reasonable that $f(p^2)$ is at least a good zeroth order approximation to the full solution $\eta_h(p^2)$, i.e.

$\eta_h(p^2) \approx \eta_{h,0}(p^2) \equiv f(p^2)$. In a first iteration step, we substitute $\eta_{h,0}(q^2)$ for $\eta_h(q^2)$ under the integral on the right hand-side of the integral equation (5.73),

$$\eta_{h,1}(p^2) = f(p^2) + g \int_{\mathbb{R}^4} \frac{\mathrm{d}^4 q}{(2\pi)^4} K\left(p, q, \mu, \lambda^{(n)}\right) \eta_{h,0}(q^2). \tag{5.76}$$

In this spirit we can construct iteratively a sequence $\left(\eta_i(p^2)\right)_{i \in \mathbb{N}}$ with

$$\eta_{h,i+1}(p^2) = f(p^2) + g \int_{\mathbb{R}^4} \frac{\mathrm{d}^4 q}{(2\pi)^4} K\left(p, q, \mu, \lambda^{(n)}\right) \eta_{h,i}(q^2). \tag{5.77}$$

The convergence properties depend on the kernel K and the coupling constant g. We observe that due to the regulator structure, the kernel K is proportional to $r_h(q^2)$, see (5.74). Therefore, the kernel is integrable with respect to the loop-momentum q. For the sake of simplicity, we will assume in the following an optimized regulator $r(q^2) \sim \theta(1 - q^2)$, where as already stated q is the dimensionless momentum. The discussion can be generalized straightforwardly to arbitrary regulators. With an optimized regulator we write $K(p, q) =: \theta(1 - q^2)\check{K}(p, q)$ As a consequence the integral in the Fredholm equation is defined on the domain $[0, 1]$ and in all equations K is substituted by $\check{K}$. Moreover, we define the angular averaged kernel

$$\langle \check{K} \rangle_\Omega(p, q, \mu, \lambda^{(n)}) := \int_{S^3} \frac{\mathrm{d}\Omega}{(2\pi)^4} \check{K}(p, q, x, \mu, \lambda^{(n)}), \tag{5.78}$$

where $\mathrm{d}\Omega$ is the canonical measure on the three-sphere. The kernel $\langle \check{K} \rangle_\Omega$ can be normed, in particular it exists its 2-norm with respect to the first two arguments

$$\left\| \langle \check{K} \rangle_\Omega \right\|_2 := \left(\int_0^1 \int_0^1 \mathrm{d}q \, \mathrm{d}p \left| \langle \check{K} \rangle_\Omega(p, q, \mu, \lambda^{(n)}) \right|^2 \right)^{1/2} \tag{5.79}$$

It can then be shown that the sequence $\left(\eta_i(p^2)\right)_{i \in \mathbb{N}}$ converges towards the full solution, i.e.

$$\lim_{i \to \infty} \eta_{h,i}(p^2) = \eta_h(p^2), \tag{5.80}$$

if the kernel is bounded as

$$\left| g \right| \left\| \langle \check{K} \rangle_\Omega \right\|_2 < 1. \tag{5.81}$$

The solution can then be written as a Liouville-Neumann series according to

$$\eta_h(p^2) = f(p^2) + g \int_{\mathbb{R}^4} \frac{\mathrm{d}^4 q}{(2\pi)^4} R\left(p, q, \mu, \lambda^{(n)}, g\right) f(q^2), \tag{5.82}$$

with the resolvent kernel

$$R\left(p, q, \mu, \lambda^{(n)}, g\right) = \sum_{i=1}^{\infty} g^{i-1} K_i\left(p, q, \mu, \lambda^{(n)}\right), \tag{5.83}$$

where K_i are the iterated kernels given by

$$K_i\left(p, q, \mu, \lambda^{(n)}\right) = \int_{\mathbb{R}^4}\int_{\mathbb{R}^4}\cdots\int_{\mathbb{R}^4}\frac{\mathrm{d}^4 q_1}{(2\pi)^4}\frac{\mathrm{d}^4 q_2}{(2\pi)^4}\cdots\frac{\mathrm{d}^4 q_{i-1}}{(2\pi)^4}K\left(p, q_1, \mu, \lambda^{(n)}\right)K\left(q_1, q_2, \mu, \lambda^{(n)}\right)$$
$$\times\cdots\times K\left(q_{i-1}, q, \mu, \lambda^{(n)}\right). \tag{5.84}$$

By truncating the resolvent series at some finite order i_0, one obtains an approximate solution to the integral equation. If the bound (5.81) is satisfied, the Liouville-Neumann series converges for any smooth initial choice $\eta_{h,0}$. One can also choose zeroth iterations that are different from the inhomogeneity $f(p^2)$. It is clear that convergence properties depend on the initial choice. For instance, if one has to correct guess for the full solution, and uses this as a starting point for the iteration, then one finds $\eta_{h,0} = \eta_{h,1}$ and one can conclude that the exact solution has been found. Additionally, there are improved iteration schemes, that increase the radius of convergence significantly. In [125], it has been proven that it exists a parameter $c \in \mathbb{R}$, such that the iteration prescription

$$\eta_{h,i+1}(p^2) = (1-c)f(p^2) + c\,\eta_{h,i}(p^2) + (1-c)\,g\int_{\mathbb{R}^4}\frac{\mathrm{d}^4 q}{(2\pi)^4}K\left(p, q, \mu, \lambda^{(n)}\right)\eta_{h,i}(q^2) \tag{5.85}$$

has a radius of convergence that is larger than the one of the standard Lioville-Neumann series, which is obtained from the improved iterations with $c = 0$.

5.6.2. The running gravitational coupling g

As we have already mentioned, we use geometrical flow equations for G_N in order to close the system of differential equations. This approach allows an inherently diffeomorphism-invariant construction of flows in quantum gravity, see [126, 127], and is based on the fiber bundle construction introduced by Vilkovisky and de–Witt, [128–132]. It has been applied to the phase structure of quantum gravity in [79], where evolution equations β_g for the dynamical coupling g, and $\beta_{\bar{g}}$ for the background coupling $\bar{g}$ are derived. In the present work we utilize the fact that the geometrical approach is directly related to the present approach in a flat background. In particular, both approaches disentangle the background from the fluctuations.

The geometrical approach to Wilsonian flows is based on the observation that the background effective action, which is constructed with a linear split $\bar{g} + h$ of the field, depends on the gauge fixing condition. Vilkovisky has shown that even in a scalar field theory without gauge-symmetry, the background effective action is not invariant under field reparameterizations. Field reparameterizations should be seen as diffeomorphisms on configuration space $\mathscr{M}$, i.e. on the manifold of fields. It can then be shown that the gauge dependence of the background effective action in the presence of gauge symmetries is a reminiscent of this reparameterization variance. The root of the problem manifests itself in the functional integro-differential equation

$$e^{\Gamma[\phi]} = \int D\varphi\, e^{-S[\varphi] + \frac{\delta\Gamma}{\delta\phi^{\mathsf{a}}}(\phi^{\mathsf{a}} - \varphi^{\mathsf{a}})}, \tag{5.86}$$

for the effective action. The difference $(\phi^{\mathsf{a}} - \varphi^{\mathsf{a}})$ is a difference of vectors at different points on the manifold and is geometrically not a well-defined object. As a result, the

effective action is not a well-defined scalar field on configuration space. The problem is solved if the problematic difference is replaced by a functional $\sigma[\phi, \varphi]$ that transforms as a vector with respect to ϕ and as a scalar with respect to φ. The field $\sigma[\phi, \varphi]$ can then be interpreted as a tangent vector in the tangent space $T_\phi \mathcal{M}$. The construction of this field requires a connection on $\mathcal{M}$, the so-called Vilkovisky-DeWitt connection. For details, we refer the reader to the literature given above. Here we just want to state that in the resulting definition of the effective action, all non-diffeomorphism invariant parts drop out. Moreover, the relation between the full metric g and the background metric $\bar{g}$ is no longer linear, but is a series in the diffeomorphism invariant part of $\sigma[\phi, \varphi]$ and involves the Vilkovisky-de-Witt connection in the contributions beyond leading order. In the linear approximation the difference $g - \bar{g}$ then reduces to the graviton field in the standard background field formulation.

The derivation of the beta functions for the coupling in [79] can be modified in order to incorporate the fully momentum-dependent anomalous dimensions computed in the present work. As a result, we are able to take into account directly effects of arbitrarily high powers of derivatives in the equations for $\beta_g, \beta_{\bar{g}}$. The anomalous dimensions enter the geometric flow equations in very much the same way as in (5.27). However, the wave-function renormalizations in [79] are momentum-independent and can be pulled outside the integrals. This is not the case in this improved set-up. Entering the equations with the momentum-dependent $\eta_\phi(p^2)$ calculated via (5.71) leads to a modification on the level of the threshold functions Φ. These modified threshold functions are given in Appendix C.

With these ingredients, the general structure of the β-function for the dynamical gravitational coupling is given by

$$\beta_g[\eta_h, \eta_c](g, \mu) = 2g + F_g[\eta_h, \eta_c](g, \mu) \,, \tag{5.87}$$

and the one for the background coupling takes the same form with g being replaced by $\bar{g}$ and an individual loop contribution $F_{\bar{g}}[\eta_h, \eta_c](\bar{g}, \mu)$. The functionals F_g and $F_{\bar{g}}$ are given in Appendix C. Note that the flow equation of the background coupling depends on the dynamical coupling via the anomalous dimensions, while the converse does not hold.

5.6.3. The couplings $\Lambda^{(n)}$

In subsection 5.1.1 we have introduced an approximation which takes into account scale-dependent couplings $\Lambda^{(n)}$ for the momentum-independent part of each vertex function. For the second order, we have identified $\Lambda^{(2)}$ as the graviton mass M^2, see (5.14). In the present section we discuss the vertices with $n \geq 3$.

The Einstein-Hilbert truncation, which identifies all $\Lambda^{(n)}$ with the cosmological constant Λ, is ill-defined in the limit $\mu \to -1$. As we will see in subsection 5.6.6, this limit is approached by physical RG trajectories in the deep IR. This regime is crucial to understand the global phase structure of Euclidean quantum gravity: the couplings $\Lambda^{(n)}$ play a distinguished role, as the related singularities arise from the momentum-independent parts of the vertex functions. In order to cure the inconsistencies of the Einstein-Hilbert truncation, we deduce the singularity structure of the couplings $\Lambda^{(n)}$ with $n \geq 3$. The full details are given in Appendix E. Essentially, the idea is to expand the right-hand sides of the flow equations for the n-point functions in powers of $1 + \mu$ and taking into account the singularities of highest

order. Thus, for $\mu \to -1_+$ we use the ansatz

$$\lim_{\mu \to -1_+} \lambda^{(n)} \sim (1+\mu)^{\alpha_n}, \tag{5.88}$$

for $n \geq 3$. We proceed by inserting this ansatz in the flow equations for $\Gamma^{(nh)}$ and analyze the generic loop integrals to leading order in the singularities that arise in the limits under consideration. Consistent scaling of both sides of the flow equations for arbitrary n leads to the relations

$$\alpha_n = \alpha_{n-2} + \alpha_4 - 1, \tag{5.89}$$

for $n \geq 5$ and

$$\alpha_4 \leq 2\alpha_3 - 1. \tag{5.90}$$

The parameter α_4 obeys the bound

$$\alpha_4 < 0. \tag{5.91}$$

The value of the parameters α_3 and α_4 cannot be obtained from the divergence analysis alone. They are dynamically determined by the flow of the three- and four-point function. This highlights again that the standard Einstein-Hilbert approximation with $\lambda^{(n)} = -\mu/2$ is inconsistent in the IR, and the non-existence of the IR fixed point cannot be inferred from such an approximation. It is also important to stress that the qualitative features of the phase diagram do not depend on the specific choice of α_3 and α_4, see subsection 5.6.7 and Appendix F. In turn, the quantitative behaviour does only mildly depend on variations of these two parameters. Their flows will be studied in a forthcoming publication [4].

Still, we can estimate α_3 based on the saturation of the inequality (5.90). Moreover, the constant parts of the vertex functions are parametrically suppressed far away from the singular regime. This entails that there it is viable to identify $\Lambda^{(n)} = \Lambda^{(2)}$ as done in all other approximations used in the literature. From these conditions one obtains $\alpha_3 \approx -1/9$. More details are given in Appendix F. In Appendix G it is shown that

$$\lambda^{(n)} = -\frac{\mu}{2}(1 + \delta\lambda^{(n)}) \tag{5.92}$$

is consistent with all constraints, where $\delta\lambda^{(n)}$ parametrizes the deviation from the Einstein-Hilbert approximation. The latter is modeled by

$$\delta\lambda^{(n)} = \mathrm{sgn}(\mu)\,\chi \left| \frac{\mu}{1+\mu} \right|^{-\alpha_n}, \tag{5.93}$$

with χ a parameter to be tuned to match the aforementioned conditions.

5.6.4. The cosmological constant

It is left to discuss the role of the cosmological constant Λ in the present construction. Written on the right hand side of the field equations, it can be interpreted as an additional source for gravity. In the classical limit, the quantum equations

$$\frac{\delta\Gamma}{\delta\phi} = J_{\mathrm{ext}}, \tag{5.94}$$

with an external source J_{ext}, reduce to the classical equations of motion. Hence, it is natural to define the cosmological constant from the one-point function, i.e. we identify $\Lambda^{(1)} = \Lambda$ as the vacuum energy. More precisely, with the vertex construction (5.9), the one-point function takes the form

$$\frac{\delta}{\delta h}\Gamma\bigg|_{g=\delta} \sim \frac{\Lambda}{\sqrt{G_N}}\sqrt{Z_h}\,. \tag{5.95}$$

Note that the one-point function does not enter the flow of higher order vertex functions. Consequently, the cosmological constant decouples from the β-functions for Newtons constant, the effective mass and the set of integral equations for the anomalous dimensions. On the other hand, these quantities obviously determine the running of the cosmological constant, i. e. the β- function for the dimensionless cosmological constant $\lambda := \Lambda/k^2$ is of the form

$$\begin{aligned}
\dot{\lambda} &= \beta_\lambda[\eta_h, \eta_c](g, \lambda, \mu) \\
&= -2\lambda + g\left(A[\eta_h, \eta_c](\mu) + \lambda B[\eta_h, \eta_c](\mu)\right).
\end{aligned} \tag{5.96}$$

The explicit form of this flow equation is given in Appendix C.

5.6.5. Regulators and stability

In order to test the quality of our truncation, we will use several regulators and vary the parameters χ and α_n introduced before. As regulators, on the one hand we use the class of exponential regulators given by

$$r_a(x) = \frac{1}{x(2e^{x^a} - 1)}, \tag{5.97}$$

where $x = p^2/k^2$ is the dimensionless squared momentum. In our analysis, we scanned the parameter range $a = \{2, 3, 4, 5, 6\}$. On the other hand, the Litim regulator, [133], is used,

$$r_{opt}(x) = \left(\frac{1}{x} - 1\right)\theta(1 - x), \tag{5.98}$$

where $\theta(x)$ is the Heaviside step function. Note that this regulator is optimized within the leading order derivative expansion but not beyond, see [32, 133]. Also, with the semi-optimized regulator the divergence analysis for the $\Lambda^{(n)}$ is slightly different from the one performed in Appendix E, but leads to similar results.

We also have scanned different values for the parameters χ and α_3 in (5.93), and we have restricted our investigation to the case of equality in (5.90). It turns out that the results do not depend on the specific choice of α_3. Note that the parameter χ is bounded from above as otherwise the parametric suppression of the $\delta\lambda$-contribution away from the singularity is lifted and the UV regime is changed. In Table E.1 in Appendix F, a table is given where the change of the UV fixed point values under a change of α_3 and χ can be ascertained.

5.6.6. Results

In this section we present our results. First, the global phase diagram is discussed. Subsequently, its UV and IR properties will be examined in more detail. In doing so, we will also make contact with older results. If not stated otherwise, all results and pictures are obtained with the specific choice of the exponential regulator r_4.

5.6.7. The phase diagram

The phase diagram for the dynamical couplings (g, μ) is depicted in Figure 5.10. We find
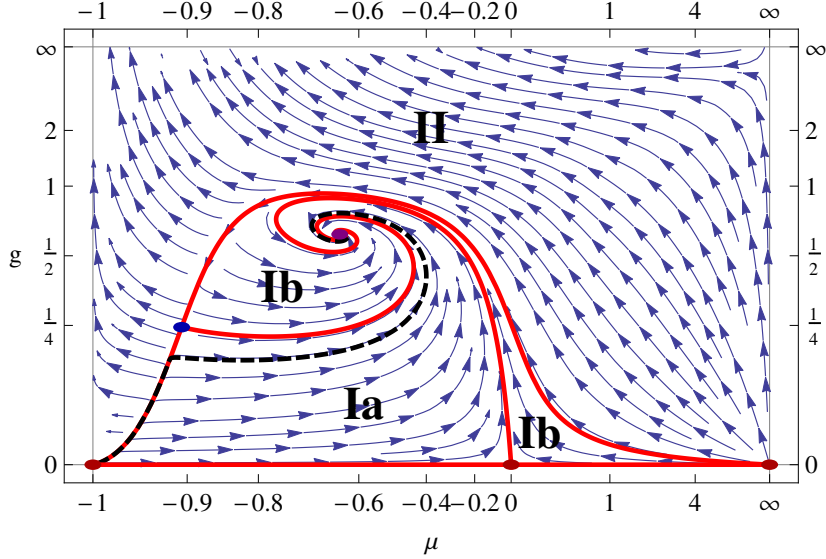
Figure 5.10.: Fixed points and global phase diagram in the (g, μ)-plane. Arrows point from the IR to the UV, red solid lines mark separatrices while dots indicate fixed points. The black dashed line is a specific trajectory that connects the UV fixed point with the non-trivial IR fixed point, which is analyzed further in the text. In analogy to [1], region Ia corresponds to trajectories leading to the massless IR fixed point, whereas region Ib leads to the massive IR fixed point. Region II is not connected to the UV fixed point, and thus physically irrelevant.
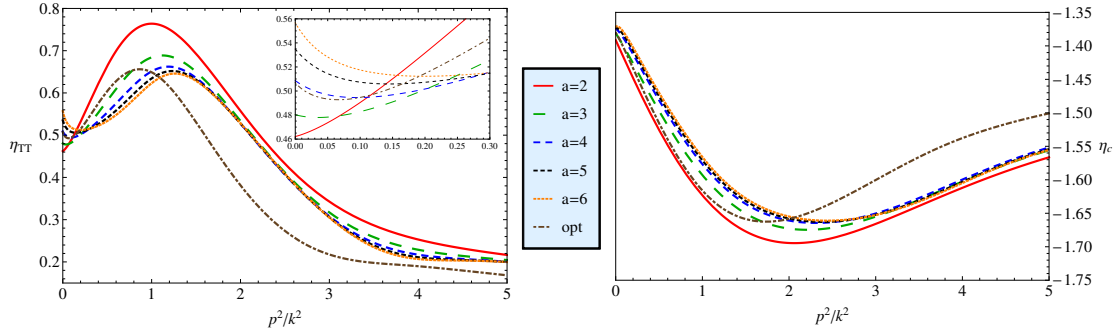
Figure 5.11.: The momentum-dependence of the anomalous dimensions of the graviton (left) and the ghost field (right) for different regulators at the respective UV fixed points. Only a weak dependence on the parameter is observed. The difference between optimized and exponential regulators is due to the fact that the modes are not integrated out at the same scale. From the fact that the quadratic external momentum terms cancel in the flow of the graviton [1], η_h goes to zero in the limit of large external momenta. The same is not true for the ghosts, where the anomalous dimension goes to a constant.

an attractive UV fixed point with coordinates

$$(g_*^{\text{UV}}, \mu_*^{\text{UV}}) = (0.614, -0.645), \tag{5.99}$$

and complex critical exponents $\theta_{1,2} = (-1.268 \pm 3.009\text{i})$. This provides further non-trivial evidence for the asymptotically safe UV structure of quantum gravity. We also find the built-in repulsive Gaussian fixed point at $(g_*^{\text{Gauss}}, \mu_*^{\text{Gauss}}) = (0,0)$, and an infrared fixed point at $(g_*^{\text{IR}}, \mu_*^{\text{IR}}) = (0, \infty)$. The most striking feature of the present phase diagram is the confirmation of the attractive IR fixed point

$$(g_*^{\text{IR}}, \mu_*^{\text{IR}}) = (0, -1), \tag{5.100}$$

which has already been found in [1], where it corresponds to a de-Sitter fixed point with $\lambda = 1/2$. This fixed point implies the global existence of trajectories connecting the UV fixed point with a finite IR fixed point. The present result is a clear confirmation that this IR fixed point is not a truncation artifact, but rather a physical property of the theory.

Importantly, it turns out to be an IR fixed point describing classical gravity. Physical initial conditions lead to globally defined trajectories that connect the non-trivial UV fixed point with the physical IR fixed point $(g_*^{\text{IR}}, \mu_*^{\text{IR}}) = (0, -1)$.

Note also that all UV-complete trajectories are also IR-complete, and end in either the massive or massless IR fixed point. In addition to this structure, there is a repulsive fixed point at $(g_*^{\text{rep}}, \mu_*^{\text{rep}}) = (0.250, -0.905)$. This fixed point was also found in [79]. All essential features do not depend on the choice of the regulator $r(x)$, and there are only minor quantitative changes induced by variations of the latter. The variation of the UV fixed point values under a variation of the vertex model parameters χ, α_3, (5.93) is given in Table E.1 in Appendix E.

5.6.8. UV regime

a	2	3	4	5	6	opt
μ_*	-0.637	-0.641	-0.645	-0.649	-0.651	-0.489
g_*	0.621	0.622	0.614	0.606	0.600	0.831
$\bar{g}_*$	0.574	0.573	0.567	0.559	0.553	0.763
λ_*	0.319	0.316	0.316	0.318	0.319	0.248
EVs	-1.284	-1.284	-1.268	-1.255	-1.244	-1.876
	$\pm 3.247\text{i}$	$\pm 3.076\text{i}$	$\pm 3.009\text{i}$	$\pm 2.986\text{i}$	$\pm 2.974\text{i}$	$\pm 2.971\text{i}$
	-2	-2	-2	-2	-2	-2
	-1.358	-1.360	-1.360	-1.358	-1.356	-1.370

Table 5.2.: UV fixed point values and eigenvalues for different regulator parameters a, and the optimized regulator, with parameter values $\alpha_3 = -0.1$ and $\chi = 0.1$.

Let us further investigate the properties of the UV fixed point. First of all, the existence of the fixed point does not depend on the specific choice of the regulator. Moreover, it is attractive in all four directions investigated here. Furthermore, even though the

critical exponents of the dynamical quantities (g, μ) are complex, the ones of the physical background couplings $(\overline{g}, \lambda)$ are real. This was also found in [1] and [78]. Notice that the eigenvalue corresponding to $\overline{g}$ is exactly -2, which can be immediately inferred from the specific structure of the background coupling flow equation. Also, the eigenvalue corresponding to λ is inherently real, as its flow equation is a polynomial of order one in the cosmological constant. All these points are summarized in Table 5.2.

The connection to earlier results is drawn in Table 5.3. The present results support the qualitative reliability of the Einstein-Hilbert type approximations in the UV regime.

	here	[20]	[1]	[79]	[84]	[78]	Table 5.7
$\overline{g}_*$	0.763	1.178	2.03	0.966	1.055	1.617	1.684
λ_*	0.248	0.250	0.22	0.132	0.222	-0.062	-0.035
$\overline{g}_* \lambda_*$	0.189	0.295	0.45	0.128	0.234	-0.100	-0.059

Table 5.3.: Comparison of the UV fixed point coordinates with earlier results for the optimized cutoff. Parameter values are $\alpha_3 = -0.1$ and $\chi = 0.1$. Methods of the references (in order): background approximation [20], bi-local projection [1], geometric approach [79], bi-metric approach [84]. The mixed approach is applied in [78] and is also discussed in the last paragraph of this subsection, Table 5.7.

The couplings as functions of the RG scale k along one selected trajectory (marked as a dashed black line in the phase diagram) are shown in Figure 5.13. One can see how the couplings tend to their finite fixed point values in the UV. The IR regime will be discussed below.

A further quantity of interest is the anomalous dimension. The momentum-dependence of both graviton and ghost anomalous dimension is given in Figure 5.11 for all used regulators at their respective UV fixed point. As one can see, only quantitative differences occur. The graviton anomalous dimension is of the order of 0.5, whereas the ghost anomalous
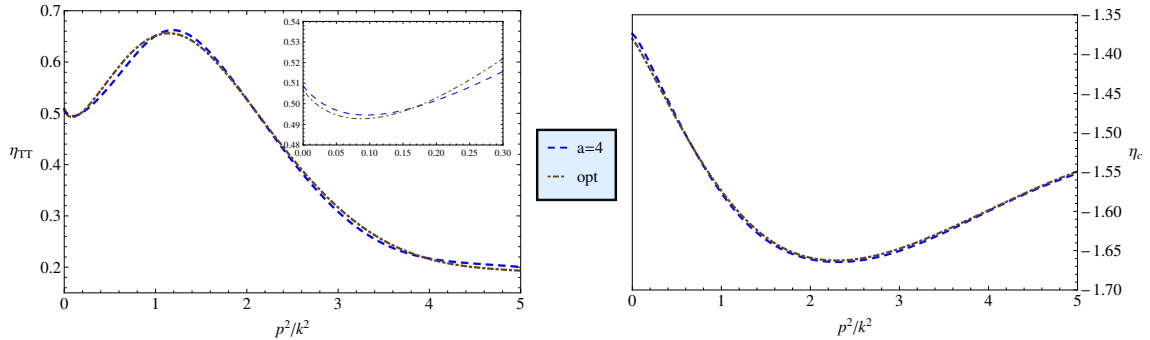
Figure 5.12.: The momentum dependence of the graviton and the ghost anomalous dimension with the exponential regulator with $a = 4$ on the one hand, and the optimized regulator with the cutoff-rescaling (5.101) on the other.

dimension is of the order of -1.5. The difference between exponential and optimized regulators is due to the fact that the regulators integrate out modes at different scales. Consequently, the effective cut-off scale is regulator-dependent. A formal discussion of

scale-optimization can be found in [32], and is applied in the context of finite temperature Yang-Mills theory in [115]. For instance, for the exponential cutoff $r_a(x)$ with $a = 4$, we find that if one rescales

$$k_{\text{opt}} \to 1.15\, k_{\text{opt}}\,, \tag{5.101}$$

the momentum-dependence of the anomalous dimension with a optimized regulator matches the one obtained with an exponential regulator, see Figure 5.12. In general, we observed that the (TT-part of the) graviton anomalous dimension is positive, however there are indications that this does not remain so when the other degrees of freedom of the graviton receive an individual anomalous dimension [4]. On the other hand, the ghost anomalous dimension is strictly negative, as was already found in [134] and [135]. We also note that the anomalous dimensions are not the leading contribution to the flow. This means that by setting $\eta(q^2) = 0$ on the RHS of the flow (5.28), one captures all qualitative properties dicussed here. Hence, the anomalous dimensions only constitute correction effects while the leading term on the RHS of the flow equations is the one proportional to $\dot{r}$. In the ghost sector this pattern is even more pronounced, and dynamical ghost effects on the phase diagram and the running couplings are very small.

Derivative expansion: We close this section with a discussion of the stability of the (covariant) derivative expansion which is the standard approximation scheme used so far. The first calculation of the graviton anomalous dimension has been presented in [1] within the FRG. There, the flow is projected at $p = k$. In the work [78] a derivative expansion around $p = 0$ is performed. The full results in the present study show a strong momentum dependence of the correlation functions as well as their flows in the cut-off regime with $p^2/k^2 \lesssim 1$. Such a strong momentum dependence of the flows either requires higher orders in the derivatives or a non-local expansion that works-in the information of momenta close to zero and those close to $p^2/k^2 = 1$, see [1, 110, 115].

Note that there is a strong cut-off dependence of the graviton anomalous dimension at the UV fixed point for small momenta $p^2/k^2 \lesssim 0.05$, see Figure 5.11. The occurance of this regime is presumably related to the mass-scale set by the fixed point value of μ. Here we investigate its impact on the value of η_h in the leading order of the derivative expansion. We also consider a variation of the expansion point. We also use the present results with full momentum-dependence in order to investigate the reliability of the derivative expansion. There, the computation of the anomalous dimension requires

$$\frac{\partial_{p^2}\dot{\Gamma}_k^{(2h)}}{Z} = -\eta + \frac{\dot{Z}'}{Z}(x + \mu) + \frac{Z'}{Z}(2\mu + \dot{\mu})\,, \tag{5.102}$$

e.g. at vanishing momentum, $x = p^2/k^2 = 0$. On the other hand, the momentum derivative of η gives the relation

$$\frac{\dot{Z}'}{Z} = -\eta' - \frac{Z'}{Z}\eta\,. \tag{5.103}$$

Inserting (5.103) in (5.102) leads to

$$\frac{\partial_{p^2}\dot{\Gamma}_k^{(2h)}}{Z} = -\eta - \eta'(x + \mu) + \frac{Z'}{Z}\left[(2-\eta)\mu - \eta\, x + \dot{\mu}\right]\,. \tag{5.104}$$

a	2	3	4	5	6	opt
η_{der}	0.46	0.48	0.51	0.54	0.56	0.51

Table 5.4.: Anomalous dimension η_{der} in the lowest order derivative expansion derived from the full flow.

a	2	3	4	5	6	opt
η_{der}	0.44	0.50	0.58	0.66	0.74	0.61

Table 5.5.: Full anomalous dimension η_{der} in the lowest order derivative expansion derived from the full flow.

In the lowest order derivative expansion, that is $\Gamma_k^{(2h)} = Z_k(p^2 + m^2)$, the anomalous dimension η_{der} is given by (minus) (5.104) evaluated at $x = 0$. Moreover, the lowest order implies $Z' = 0$ and we simply arrive at

$$\eta_{\text{der}} = \eta(0). \tag{5.105}$$

For the regulators used in the present work this leads to anomalous dimensions listed in Table 5.4. However, the full lowest order derivative expansion takes into account the Z'-terms on the right hand side. At vanishing momentum there is the relation

$$\frac{Z'}{Z}\bigg|_{x=0} = \frac{1}{2}\eta'\bigg|_{x=0}. \tag{5.106}$$

This is easily derived from

$$Z_k(p^2) = Z_{k_0}(p^2)\exp\left\{-\int_{k_0}^{k}\frac{d\bar{k}}{\bar{k}}\eta_{\bar{k}}(p^2)\right\}, \tag{5.107}$$

where both k and k_0 are in the scaling regime. The latter condition implies that $Z'/Z = Z_{\bar{k}}'/Z_{\bar{k}}(0)$ and $\eta' = \eta_{\bar{k}}'(0)$ are independent of $\bar{k} \in [k_0, k]$. Then we conclude that at $x = 0$ we have

$$\frac{Z_k'}{Z_k} = \frac{Z'}{Z}\frac{k^2}{k_0^2} + \frac{1}{2}\eta'\left(1 - \frac{k^2}{k_0^2}\right), \tag{5.108}$$

for all k, k_0 in the scaling regime and we are led to (5.106). Hence, in the scaling regime (with $\dot{\mu} = 0$) the full anomalous dimension in the derivative expansion at $x = 0$ is given by

$$\eta_{\text{der}} = \eta\left(1 + \frac{1}{2}\eta'\mu\right), \tag{5.109}$$

leading to Table 5.5. These results seem to be much more stable then the approximation (5.105).

To complete the present reliability analysis of Taylor expansions in momenta p^2, we also investigate expansions about a general expansion point $p = \alpha k$. We present results for the

α	0	0.25	0.5	0.75	1	1.15
η_{der}	0.57	0.50	0.39	0.25	0.074	-0.016

Table 5.6.: Anomalous dimension η_{der} in the standard derivative expansion with optimized regulator in an expansion around $p = \alpha k$ with $(\mu = 0, g = 1)$.

optimized regulator and evaluate the anomalous dimension for $g = 1, \mu = 0, \eta_c = 0$. The conclusions of this study do not depend on the choice of these parameters. As one can see, the anomalous dimension of the graviton in a derivative expansion strongly depends on the specification parameter α. This relates to the fact that such an expansion only works well if the full flow of the propagator shows a mild momentum dependence. This is not the case for the flow of the graviton two-point function, see [1]. In general, even the sign of the anomalous dimension depends on the specification parameter. We conclude that a derivative expansion in quantum gravity with $\alpha = 0$ has to be used with great caution.

Effect of identifications of couplings in the UV: As already mentioned, the present approximation is the first work that employs individual running couplings for the momentum-independent part of each vertex function. In particular, the graviton mass term should not be identified with the cosmological constant. Still, we have shown, that the full expansion with momentum-dependent wave function renormalizations and a mass term for the fluctuating graviton h provides UV fixed point results in qualitative agreement with that of the standard background field approach, if we identify the mass a posteriori with (minus 1/2 of) the cosmological constant. Within such an identification we have a deSitter fixed point.

For completeness, we also have investigated a mixed approach: We use a flat anomalous dimension η_h in a derivative expansion about vanishing momentum, or a momentum-dependent one, $\eta_h(p^2)$, for the fluctuating graviton. In turn, the flows of the graviton mass and the Newton coupling g are extracted from the flow of the cosmological constant and the Newton coupling in the background field approximation. This can be interpreted as an intermediate step towards the full approximation studied here. Interestingly this leads to a very small and negative fixed point value for the cosmological constant, see also [78] for such a mixed expansion with a flat anomalous dimension. Our fixed point results for the case with a flat anomalous dimension are given in Table 5.7. They are in qualitative agreement with the results of [78]. Notably, the results in the mixed approach deviate from both, the background field results and that of the full approximation introduced in the present work. We have also checked that this originates in the identification of the mass term with the cosmological constant, the given alternative choices for the flow of the Newton constant do not alter this result.

5.6.9. IR regime

The non-trivial IR fixed point is located at $(g, \mu) = (0, -1)$. The most important feature is that it is a classical one, i.e. the essential couplings scale classically and all quantum

a	2	3	4	5	6	opt
g_*	1.68	1.72	1.75	1.77	1.80	1.68
λ_*	-0.064	-0.076	-0.088	-0.100	-0.110	-0.035
η_h^{der}	0.81	0.93	1.03	1.14	1.24	0.86
η_c^{der}	-1.08	-1.05	-1.04	-1.03	-1.01	-0.75

Table 5.7.: Fixed point values g_* and λ_* and anomalous dimension η_{der} at this fixed point in the mixed approach.

contributions vanish: The gravitational couplings and the cosmological constant scale as

$$g, \bar{g} \sim k^2, \qquad\qquad \lambda \sim k^{-2}, \qquad\qquad (5.110)$$

and the anomalous dimensions vanish,

$$\eta_h \to 0, \qquad\qquad \eta_c \to 0, \qquad\qquad (5.111)$$

see Appendix H. This leads to flow trajectories that connect the asymptotically safe UV regime for $k \to \infty$ and short distances, with a classical IR regime for $k \to 0$ and large distances. Since μ approaches a finite value in the limit $k \to 0$, the dimensionful mass $M^2 = \mu k^2$ vanishes in the deep IR. Moreover, the scaling of Newton's coupling (5.110) allows us to identify a scale in the following way. As g (or $\bar{g}$) scales classically, the coefficient of proportionality, say C, is nothing else than the Newton constant, because

$$G_N = g k^{-2} = C k^2 k^{-2} = C. \qquad\qquad (5.112)$$

Thus, scales are measured in units of the Planck mass, $M_{Pl}^2 = 1/C$. The physical trajectory is then fixed by measuring the relevant couplings, that is the (background) Newton constant
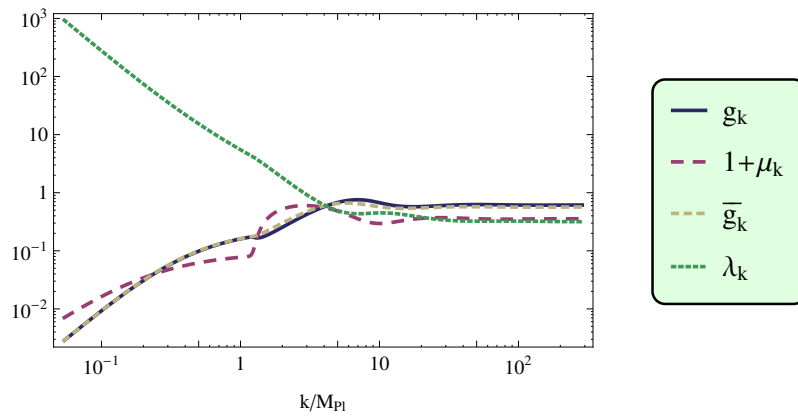
Figure 5.13.: The running couplings as functions of the renormalization scale k in units of the Planck mass. In the UV the couplings tend to their finite fixed point values. As one follows the trajectories down to the IR, one can see the scaling behaviour in the vicinity of the IR fixed point.

and cosmological constant, at a given scale. In Figure 5.13 one can see both, the classical scaling in the IR as well as the vanishing of the β-functions in the vicinity of the UV fixed point for large k. The classical scaling regime extends roughly up to one order of magnitude below the Planck scale. This implies the absence of quantum gravity effects for energies $E \ll M_{\text{Pl}}$, as it is expected in a theory without a large volume compactification of extra-dimensions. Note also that the difference between the two couplings g and $\bar{g}$ is hardly visible, which justifies to some extent the background approximation for the Newton constant.

5.7. Flow of the Three-Point Function

In the next sections we will improve our setting by including the flow equation of the graviton three-point function. This enables us to set up a consistent, coupled hierarchy for the two- and the three point function and the related couplings in quantum gravity. This calculation is the first study of the three graviton vertex in the asymptotic safety scenario. In the setting of the vertex expansions this is the third order of the coupled hierarchy of flow equations, and the first order that allows for a genuine calculation of a coupling constant.

The general structure of the flow equation in super field space is derived in Appendix I. Since in this section we are interested in pure quantum gravity, the field content is once more given by the graviton, the ghost and the anti-ghost. Therefore, again we set $\phi = (h, \bar{c}, c)$ and specify this field-vector in the general equation in Appendix I. The resulting equation is given in diagramatical language in figure Figure 5.14.

$$\partial_t \left. \frac{\delta^3 \Gamma}{\delta h^3} \right|_{\phi=0} (\mathbf{p}) = -\frac{1}{2} \quad + 3 \quad - 3$$

$$+ 6 \quad \equiv Z_h^{3/2} \text{Flow}^{(3)} \tag{5.113}$$

Figure 5.14.: Diagrammatic depiction of the flow of the three-graviton vertex. Double lines represent graviton propagators, dashed lines ghost propagators, filled circles denote dressed vertices whereas crossed circles are regulator insertions.

5.7.1. Kinematical Configurations

The first step in the setup of the three point function is the discussion of the kinematical configuration. Obviously, for the propagator this issue is not present since momentum conservation fixes kinematics uniquely. The three point-function, however, depends on the external momenta (p_1, p_2, p_3), where p_3 can be eliminated using momentum conservation.

The dependence on the external momenta can then be parameterized by the absolute values of the remaining two momenta $|p_1|$, $|p_2|$ and the angle θ_{12} between them. In the following we will always consider momentum configurations where we set $|p_1| = |p_2| =: p$. In particular, we consider two momentum configurations that will be used in order to define a gravitational coupling from the three-point function.

1. **The asymmetric configuration** In this case we set the angle $\theta_{12} = \pi$, which corresponds to the limit $p_3 \longrightarrow 0$ and $p_1 = -p_2$. Physically, it is tempting to interpret this momentum configuration as a limit of soft-graviton radiation. Note that due to the limiting process that is involved in this configuration, there remain some ambiguities, namely the angle between p_3 and p_1 can be chosen arbitrarily, and the specific value then corresponds to an initial configuration from which the limit $p_3 \longrightarrow 0$ is taken. This issue will have some consequences in the projection procedure, since the notion of transversality is not well-defined without further input about the limiting procedure in this case. Moreover, due to the asymmetry, the flow equation in needs to be symmetrized with respect to the external momenta. This symmetrization is always implicitly understood when we talk about the asymmetric configuration. The simplicity of this asymmetric configuration has two important technical advantages. First, the contractions of the diagrams are much simpler, since one can set one external momentum to zero from the onset. Second, in order to carry out the loop integrations, we have to define a coordinate system in four- dimensional Euclidean space, most conveniently four-dimensional spherical coordinates. Since in this configuration there are only two non-zero momenta which are aligned in one direction in four-dimensional space, there is only one free angle in the kernels of the loop integrals, which is the angle between the loop momentum q and the external momentum $p_1 = -p_2$. This angle can then be identified with one of the angles in the measure of the spherical coordinates and there is only one non-trivial angular integration, i.e. this is analogous to the case for the loop integrals for the propagator.

2. **The symmetric configuration** In this setup we choose a maximally symmetric configuration, which means that all momenta have equal norm, $|p_1| = |p_2| = |p_2| = p$ and with the same angle between all three momenta. This implies $\theta_{12} = \frac{2\pi}{3}$. In this configuration, the position in of the three external momenta in four dimensional Euclidean space-time requires two angles, and the same is true for the relation between an arbitrary vector and an external momentum. Hence, the there are two non-trivial angular integrations in the loop integral. However, since this is the balanced configuration, it is intuitively clear that this might be the best setting for defining a momentum-independent coupling g_k from the flow.

5.8. Truncation III: The coupled Hierarchy

In this section we analyze the fully coupled system of the two- and the three–point function of the graviton. This means that the flow of the three point function feeds back into the veritces that enter the two–point function. Still, as the flow of the three–point function depends on the four and five graviton vertex, the hierarchy of flow equations needs to be truncated and we close the equations via the identifications $\Lambda^{(3)} \equiv \Lambda^{(4)} \equiv \Lambda^{(5)}$ and

$G^{(3)} \equiv G^{(4)} \equiv G^{(4)} \equiv G_N$. We are then confronted with a coupled system of equations for the scale–dependent generalized couplings

$$\left(\eta_h, \eta_c, M^2, G_N, \Lambda^{(3)} \right). \tag{5.114}$$

In order to determine the running of these couplings from the flow $\dot{\Gamma}^{(3h)}$, one has to specify the projection on the tensor structure. For the two-point function, the tensor projection is based on an orthogonal tensor decomposition, see (5.26). We would like to find an analog construction for the three-point function. The three point function in gravity is a rank six tensor depending on two external momenta (after using momentum conservation) and has a very rich tensor structure. In principle, one could use a complete set of orthogonal projectors and calculate all corresponding contributions. This however, is a very extensive task and not all of these tensor structures are physical. Therefore, a detailed study of Slavnov-Taylor identities is a necessary accompanist of such a calculation. Moreover, to our knowledge there is yet no such basis explicitly given in the literature, although the construction strategy is in principle clear. Nevertheless, giving such an orthogonal basis explicitly is very laborious due to the overflowing tensor algebra. In this work, we construct a canonical projector that is expected to capture the leading physical effects and is most compatible with the tensor structures chosen in our approximation. The tensor structures $\mathcal{T}^{A_1 \cdots A_n}(p_1, \ldots, p_n; \Lambda_n)$ defined in (5.10) are given by variations of the classical, gauge fixed Einstein-Hilbert action. Therefore, all $\mathcal{T}^{A_1 \cdots A_n}$ are at most quadratic in the field momenta $(p_1, \ldots, p_n)$. Furthermore, they decompose into the sum of a momentum-independent part and a part which is quadratic in the momenta. Thus, for the three point function the tensor structure can be written as

$$\mathcal{T}^{A_1 A_2 A_3}(p_1, p_2, p_3; \Lambda_n) = \Lambda_n \mathcal{T}^{A_1 A_2 A_3}(0, 0, 0; 1) + \mathcal{T}^{A_1 A_2 A_3}(p_1, p_2, p_3; 0). \tag{5.115}$$

By factoring out Λ_n in the first term, both tensor parts on the RHS of (5.115) are independent of any coupling parameter or k-dependent quantity, in particular they are independent of Λ_n. In the case $n = 3$ which is relevant here, we will use the momentum dependent tensor part $\mathcal{T}^{A_1 A_2 A_3}(p_1, p_2, p_3; 0)$ to construct an operator Π_G to project the flow of $\Gamma^{(3)}$ onto the flow of G_3. Similarly, an operator Π_Λ is obtained from the momentum-independent tensor part $\mathcal{T}^{A_1 A_2 A_3}(0, 0, 0; 1)$. In direct analogy, Π_Λ will be employed for the projection onto the flow of Λ_3. Moreover, in analogy to the construction for the two-point function, we associate all external legs with transverse-traceless gravitons. The coefficient functions of projectors with these properties are then given by

$$\Pi_G^{ABC}(p_1, p_2, p_3) := \Pi_{TT}^{AA'}(p_1) \Pi_{TT}^{BB'}(p_2) \Pi_{TT}^{CC'}(p_3) \mathcal{T}^{A'B'C'}(p_1, p_2, p_3; 0), \tag{5.116}$$

and

$$\Pi_\Lambda^{ABC}(p_1, p_2, p_3) := \Pi_{TT}^{AA'}(p_1) \Pi_{TT}^{BB'}(p_2) \Pi_{TT}^{CC'}(p_3) \mathcal{T}^{A'B'C'}(0, 0, 0; 1), \tag{5.117}$$

where Π_{TT} is the transverse-traceless projector for symmetric rank-four tensors. Note that the multi-indices with capital letters used above do not include the continuous index part and are in this case just an abbreviation for two ususal Lorentz indices, $A = \{\mu_1 \mu_2\}$. Hence, there is also no integration implied. Both operators $\Pi_{G/\Lambda}$ act on rank 6-tensors via full contractions and return scalar expressions. Applying this to the flow equation for the graviton three-point function, the transverse traceless projectors in (5.116) and (5.117) ensure transverse traceless external graviton legs of the vertex. This running TT-vertex is then contracted

with the tensor structure of the momentum-dependent part of $\Gamma^{(3h)}$ for projection on the running coupling G, and with the momentum-independent part for projection on Λ. In summary, we obtain two scalar flow equations by fully contracting the tensor equations with the coefficient functions of the projectors defined above, and taking the limit of external momenta to zero for the $\Lambda^{(3)}$ flow,

$$
\dot{\Gamma}_G^{(3)}(p_1,p_2,p_3) := \left(\Pi_G^{ABC}\, \dot{\Gamma}_{ABC}^{(3h)} \right)(p_1,p_2,p_3) = \left(\Pi_G^{ABC}\, \mathrm{Flow}_{ABC}^{(3h)} \right)(p_1,p_2,p_3)
$$
$$
=: \mathrm{Flow}_G^{(3h)}(p_1,p_2,p_3) \qquad (5.118)
$$

and

$$
\dot{\Gamma}_\Lambda^{(3)} := \lim_{(p_1,p_2,p_3)\to 0} \left(\Pi_\Lambda^{ABC}\, \dot{\Gamma}_{ABC}^{(3h)} \right) = \lim_{(p_1,p_2,p_3)\to 0} \left(\Pi_\Lambda^{ABC}\, \mathrm{Flow}_{ABC}^{(3h)} \right) =: \mathrm{Flow}_\Lambda^{(3h)} \qquad (5.119)
$$

The scalar flows of the three point function then take the form

$$
\mathrm{Flow}_{G/\Lambda}^{(3)}(p_1,p_2,p_3) = Z^{\frac{1}{2}}(p_1) Z^{\frac{1}{2}}(p_2) Z^{\frac{1}{2}}(p_3) G^{\frac{3}{2}} \int_{\mathbb{R}^4} \frac{\mathrm{d}^4 q}{(2\pi)^4} \sum_\phi \left(\dot{r}_\phi(q^2) - \eta_\phi(q^2) r_\phi(q^2) \right)
$$
$$
\times F_{G/\Lambda,\phi}(p_1,p_2,p_3,q,G_n,\Lambda_n),
$$
$$
(5.120)
$$

where $n \in \{3,4,5\}$ and a sum over species of fields $i \in \{h,c\}$. As it is the case for the flow of the propagator, the right-hand side of the flow is just a function of the anomalous dimension

$$
\eta_\phi(p^2) := -\dot{Z}_i\phi(p^2)/Z_\phi(p^2), \qquad (5.121)
$$

since all wavefunction renormalisations organize in such ratios. We also note that the contributions encoded in $F_{G/\Lambda,\phi}$ originate from the diagrams displayed in Figure 5.14, which are symmetrized with respect to the interchange of external momenta. Unfortunately, these integral kernels are way too lengthy to display for general kinematical configurations, as already the corresponding kernel I_ϕ for the two–point function are quite complicated. Now, we need to relate $\mathrm{Flow}_G^{(3)}$ and $\mathrm{Flow}_\Lambda^{(3)}$ to the flow of the couplings G_3 and Λ_3, respectively. For the two kinematical configurations described in subsection 5.7.1, namely the asymmetric and the symmetric configuration. Let us consider the flow of the gravitational coupling G first. We observe that in both configurations, there is only one non-zero absolute value of momentum, the external momentum p. The projector Π_G is proportional to p^2 and $\dot{\Gamma}^{(3h)}$ has a term that is also proportional to p^2 and a constant term proportional to $\Lambda^{3)}$. Moreover, the projectors are independent of t, and therefore

$$
[\partial_t, \Pi_{G/\Lambda}] = 0. \qquad (5.122)
$$

As a result, in any of the two configurations $\Gamma_G^{(3)}(p_1,p_2,p_3)$ is necessarily of the form

$$
\Gamma_G^{(3)}(p_1,p_2,p_3) = \partial_t \left(Z^{\frac{1}{2}}(p_1^2) Z^{\frac{1}{2}}(p_2^2) Z^{\frac{1}{2}}(p_3^2) G^{\frac{1}{2}} \left(A p^4 + B\, \Lambda^{(3)} p^2 \right) \right), \qquad (5.123)
$$

with some combinatorical coefficients A and B that arise from the contraction of the tensors and depend on the kinematical configuration that is chosen. Due to the projector, the

right-hand side of the flow is proportional to p^2 and this factor can be divided out. The concept of specification, as it is presented in section 5.4 in detail for the propagator, is of the same importance for the three-point function and will be further investigated below. It is clear from equation (5.123), that we can obtain a flow equation for G with a finite difference projection at subtraction points $p_\star$ and $p_\bullet$, i.e. we evaluate both sides of the flow equation at $p_\star$ and at $p_\bullet$ and subtract the resulting equations, see also (5.38). Combining (5.123) and (5.120) with such a projection we arrive at flow equations which read for the dimensionless gravitational coupling

$$
\begin{aligned}
\partial_t g =& 2g + g \frac{\sum_{i=1}^3 \left(\eta(p_{i,\star}^2)p_\star^2 - \eta(p_{i,\bullet}^2)p_\bullet^2 \right)}{p_\star^2 - p_\bullet^2} + g \frac{B\Lambda^{(3)}}{A} \frac{\sum_{i=1}^3 \left(\eta(p_{i,\star}^2) - \eta(p_{i,\bullet}^2) \right)}{p_\star^2 - p_\bullet^2} \\
&+ g^2 \frac{2}{A} \frac{1}{p_\star^2 - p_\bullet^2} \left(\int_{\mathbb{R}^4} \frac{\mathrm{d}^4 q}{(2\pi)^4} \sum_\phi \left(\dot{r}_\phi(q^2) - \eta_\phi(q^2)r_\phi(q^2) \right) F_{G/\Lambda,\phi}(p_i, q, G_n, \Lambda_n) \right) \Bigg|_{p_\bullet}^{p_\star}.
\end{aligned}
\tag{5.124}
$$

In the above equation $p_{i,\star} = p_\star \; \forall i$ and $p_{i,\bullet} = p_\bullet \; \forall i$ in the symmetric configuration since all external momenta have the same norm p. In the antisymmetric configuration there is one zero-external momentum, say $p_3 = 0$, and therefore $p_{3,\star} = 0$ and $p_{3,\bullet} = 0$, while $p_{i,\star} = p_\star$ and $p_{i,\bullet} = p_\bullet$ for $i = \{1, 2\}$. This finite difference projection is quite general, as all derivative definitions of the coupling can be obtained since in the limit $p_\bullet \longrightarrow p_\star$ the finite differences approach the derivative $\frac{\partial}{\partial p^2}\big|_{p=p_\star}$.

In analogous fashion we derive the equation for the constant part $\lambda^{(3)}$ of the three–point function. In this case, however, it is quite natural to project at $p = 0$, as we are interested in the momentum–independent part. Following these lines, we evaluate equation (5.119) at vanishing external momentum. For the dimensionless coupling the resulting equation is then given by

$$
\partial_t \lambda(3) = -2\lambda^{(3)} + \frac{3}{2}\eta_h(0)\lambda^{(3)} - \frac{1}{2}(\frac{\partial g}{g} - 2)\lambda^{(3)} + \frac{96\pi}{5}\pi \mathrm{Flow}_\Lambda^{(3h)}.
\tag{5.125}
$$

5.8.1. Locality of the Three-Point Function

In subsection 5.5.1 we have shown that the flow of the graviton propagator satisfies the locality condition (5.17), and have also presented the general structure of such asymptotic expansion of flow equations. In this section we apply these techniques in order to investigate the behavior of the three point function for large momenta. The first step in the analysis is the projection on the scalar coefficient of the tensor structure, which is described in the previous section. As this study is concerned with the momentum dependence of the flow, we consider the projection with the operator Π_G that projects on the momentum-dependent part of the flow. Hence, the object under investigation is the ratio $\partial_t \Gamma_G^{(3)}(p_1, p_2, p_3)/\Gamma_G^{(3)}(p_1, p_2, p_3)$ for large momenta. From the general construction of the vertex functions, one immediately infers that all graviton vertices have p_i^2 as the leading large momentum behavior. Together with the diagrams contributing to the flow of the three-point function, depicted in Figure 5.14, naive power–counting as presented in section 5.2, yields $\mathrm{Flow}_G^{(3h)}(p_1, p_2, p_3) \sim p_i^4$ in the

limit of infinite momenta. Note that the fourth power in p is rooted in the fact that the projector Π_G itself is quadratic in momenta, and the tensorial flow is also proportional to p_i^2. As one can infer from equation (5.123), the three point function $\Gamma_G^{(3)}$ projected with Π_G resembles this behavior and also behaves as p_i^4. Therefore, as expected for perturbatively non-renormalizable, locality can only be established by non-trivial cancellations in the flow.

We have also seen in the discussion of locality in ϕ^4 theory, that the condition that *all* momenta go to infinity might be of major importance in these questions. For the flow of the propagator this is of course trivial since momentum conservation implies that there is only one external momentum in the propagator. For the three-point function, we have defined in subsection 5.7.1 two different kinematical configurations, namely the asymmetric configurations and the symmetric configuration. While the latter allows for a limit with all external momenta going to infinity, the first has one external momentum that is set to zero from the onset. We perform the analysis exactly along the lines presented in subsection 5.5.1, and indeed, we find that there is no cancellation in the asymmetric configuration and

$$\lim_{p \to \infty} \frac{\partial_t \Gamma_{G,\text{asymmetric}}^{(3)}(p)}{\Gamma_{G,\text{asymmetric}}^{(3)}(p)} = \text{const.}, \tag{5.126}$$

which is a non-local flow.

For the symmetric configuration the situation is different. In this case, the individual diagrams have the asymptotic expansion

$$-\frac{1}{2} \quad \quad \overset{p \to \infty}{=} -\frac{752 g^2 \pi^2}{19} p^4 \int_0^1 \mathrm{d}q q^3 \frac{2 + \eta_h(q^2)(-1+q^2)}{(1+\mu)^2} + p^2 \,\text{const.}$$

$$\tag{5.127}$$

$$3 \quad \quad \overset{p \to \infty}{=} \frac{1232 g^2 \pi^2}{19} p^4 \int_0^1 \mathrm{d}q q^3 \frac{2 + \eta_h(q^2)(-1+q^2)}{(1+\mu)^2} + p^2 \,\text{const.} \tag{5.128}$$

$$-3 \quad \quad \overset{p \to \infty}{=} -\frac{480 g^2 \pi^2}{19} p^4 \int_0^1 \mathrm{d}q q^3 \frac{2 + \eta_h(q^2)(-1+q^2)}{(1+\mu)^2} + p^2 \,\text{const.}$$

$$\tag{5.129}$$

Figure 5.15.: Asymptotic contributions of the diagrams in the flow of the three-graviton vertex.

As one can see, there is a fantastic cancellation of the leading order terms! Note that this cancellation takes place after angular integration and integration over the absolute value of the momentum is not necessary. The leading order terms in the asymptotics are independent of $\lambda^{(3)}$, since the highest power terms are created when terms $\sim p^2$ from each vertex are
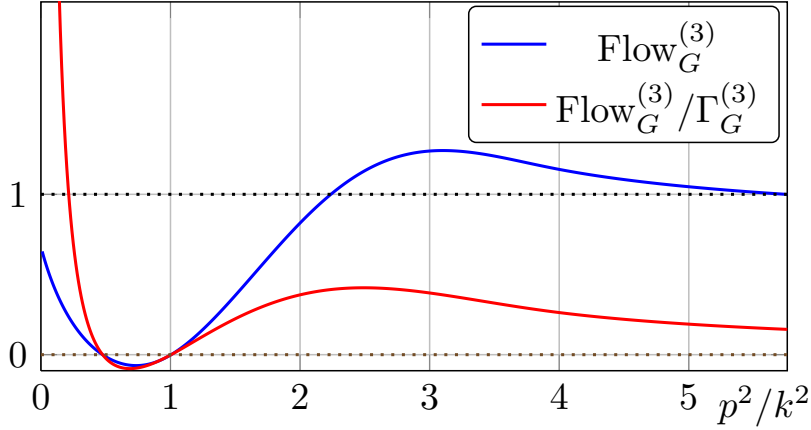
Figure 5.16.: Typical flow of $\Gamma_G^{(3)}$, after dividing out the trivial $1/p^2$ factor stemming from the projector, as a function of p^2 (blue curve). The red curve shows the locality of the flow in momentum space where it decays rapidly with p^2.

contracted, and these parts do obviously not contain the momentum independent part $\lambda^{(3)}$, which contribute only the the sub-leading terms. This cancellation of the leading order p terms in the flow of the three point function obviously has the consequence

$$\lim_{p \to \infty} \frac{\partial_t \Gamma_{G,\text{symmetric}}^{(3)}(p)}{\Gamma_{G,\text{symmetric}}^{(3)}(p)} = 0, \qquad (5.130)$$

leading to a local renormalization group flow of the graviton three-point function. The momentum dependence for arbitrary values of the momentum p can of course not calculated analytically, but numerically. The result is shown in Figure 5.16, and one can beautifully see the locality of the flow.

As a generalization, we have also proven locality for a more general kinematic setup. More precisely, the property (5.17) does indeed hold independently of the angle θ_{12} between the vectors p_1 and p_2. The exact asymptotics are are somehow lengthy and the exact form does not matter, hence we only state that

$$\lim_{|p_1|=|p_2|=p \to \infty} \frac{\partial_t \Gamma_G^{(3)}(p, \theta_{12})}{\Gamma_G^{(3)}((p, \theta_{12}))} = 0 \quad \forall \, \theta_{12}, \qquad (5.131)$$

and for $\theta_{12} = \pi$ the results reduce to Figure 5.15.

For a sensible choice of a specification procedure, that appears as the freedom of choosing $p_\star$ and $p_\bullet$ in (5.124), it is very important to investigate the momentum dependence more closely. For this reason, we solve the loop integrals of the flow over a grid in the external momentum p, the mass-gap parameter μ and the constant parts $\lambda^{(3)}$ of the vertex functions. A selection for different parameter values is shown in Figure 5.17.

First, we note that locality manifests itself as $\lim_{p \to \infty} \Gamma_G^{(3)} = \text{const}$ and, as we have already argued, it is a property of the flow for any value of of $\lambda^{(3)}$. Only the specific value of the constant depends of the value of the latter.
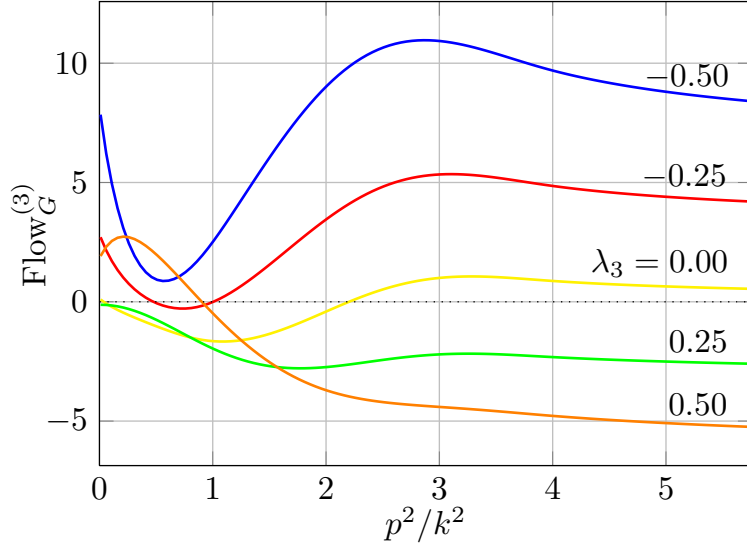
Figure 5.17.: Momentum dependence of the flow of the graviton three–point function in the symmetric kinematical configuration and for $\mu = -0.3$ and different values of $\lambda^{(3)}$. One can see that locality of the flow holds for any value of $\lambda^{3)}$, as explained in the text.

5.8.2. Beta Functions: The Asymmetric Case

We have seen in the last section that in the asymmetric configuration the flow of the three–point function lacks locality in momentum space. It is also important to note that the momentum dependence as depicted in Figure 5.17 shows a highly non-trivial behavior similar to the graviton two–point function, see Figure 5.6, which makes a derivative expansion around $p = 0$ highly questionable. Hence, a beta–function for Newtons coupling that originates in a flow in the asymmetric configuration and a derivative at $p = 0$ seems to be untrustworthy. However, there are reasons for exactly such a setup. First of all, derivative expansions around $p = 0$ are simply the only projections that yield an analytical flow equation. In addition to that, if one aims at a fully analytical system of flow equations, also the wave-function renormalization of the two–point function must momentum–independent and be projected with a derivative at $p = 0$, as opposed to the "optimized" derivative procedure used in (5.57). Then, if the two–point function is projected in such a way, the vertices that enter the flow of the two–point function, shown in Figure 5.5, have one leg with zero momentum, which is exactly the situation in the asymmetric configuration. Consequently, one might argue that in a setup where all beta functions are extracted from flows of the n–point functions at $p = 0$, then the asymmetric configuration is somehow self-consistent. In summary, we then obtain a system of differential equations for the scale–dependent quantities (5.114), where the constant parts M^2 and $\Lambda^{(3)}$ are obtained by evaluating the corresponding n–point function at $p = 0$ and the momentum–dependent parts η and G_N are obtained via a specification with derivative projections at $p = 0$. Concerning this specification in combination with an optimized regulator of the form (5.45), there is a technical remark in order. The p derivatives hit the θ functions in the propagators that carry an external momentum and produce δ–functions. After evaluation at $p = 0$, one is left with distributional products of the form $\theta(x)\delta(x)$, which need to be handled with great

care. A precise analysis of how to treat such expressions can be found in [19]. In summary, we solve equations (5.124) with $p_\bullet \longrightarrow p_\star \longrightarrow 0$, (5.125), (D.8) and (D.9). After loop integrations, we arrive at the corresponding analytic flow equations that are displayed in Appendix J. As we have already discussed in subsection 5.5.2, a first access to such equations can be obtained by discarding the anomalous dimensions entirely. As a consequence, the resummation terms in the beta-functions for g and $\lambda^{(3)}$ vanish, and β_g is a polynomial of degree two in the coupling g, i.e. this is a beta–function that is essentially of perturbative form. Moreover, as we already discussed in subsection 5.5.2, an anomalous dimension with a $p = 0$ specification is questionable.

The fixed point analysis is performed in the standard way by looking for zeros $g_*, \mu_*, \lambda^{(3)}_*$ for the beta functions $\beta_g, \beta_\mu, \beta_{\lambda^{(3)}}$. Such a fixed point analysis shows that in this approximation the system does *not* exhibit a non-Gaussian UV-fixed point in the physical regime! And this fixed point structure remains unchanged upon inclusion of anomalous dimensions.

As a result, we state that this approximation does not exhibit a sensible UV-completion. However, this is expected since the momentum–dependence is poorly reflected in $p = 0$ projections. Due to the argument presented above, projections at finite momenta seem to be much more accurate, but are self-consistent with the symmetric kinematical configuration. Consequently, we discard this approximation due to the lack of locality and an insufficient resolution of the momentum–dependence.

5.8.3. Beta Functions: The Symmetric Case

In the last subsection we have seen that the asymmetric configuration seems inappropriate for several reasons. On the contrary, the symmetric configuration can potentially capture much more of the momentum–dependence and, as an important factor, the flow exhibits locality. The system of flow equations for the generalized couplings $\left(\eta_h, \eta_c, M^2, G_N, \Lambda^{(3)}, \right)$ can then be derived, as usual, for different specifications and approximations, with a first approximation consisting of vanishing anomalous dimensions and the full system with fully-momentum–dependent anomalous dimensions and corresponding integral equations in the two–point sector.

Derivative Expansion at vanishing Momentum

As a first approximation we resort again to the simplest case, namely the derivative expansion at vanishing momentum. This results in the equations (5.124) with $p_\bullet \longrightarrow p_\star \longrightarrow 0$, (5.125), (D.8) and (D.9), i.e. formally the same equations as in the previous subsection 5.8.2, but this time with β_g originating in from $\partial_t \Gamma^{3h)}$ in the symmetric kinematical configuration. As in the asymmetric case, the loop integrals can be carried out analytically. The equations derived from the two–point function remain the same so do the equations for the constant part $\lambda^{(3)}$ of the vertex, since the latter is not affected by the configuration of the external momentum. The analytic beta-function for the gravitational coupling is given in Appendix J. The first step is again to neglect the anomalous dimensions. The fixed point analysis yields a non-Gaussian UV-fixed point with coordinates

$$\left(g_*^{\mathrm{UV}}, \lambda_*^{(3)\,\mathrm{UV}}, \mu_*^{\mathrm{UV}} \right) = (0.57, -0.16, -0.16) \,. \tag{5.132}$$

However, it is important to note that this fixed point has only two UV-attractive directions, since the eigenvalues of the stability matrix read

$$(\theta_1, \theta_2, \theta_3) = (-1.5 + 1.8\,i, -1.5 - 1.8\,i, 1.6)\,. \tag{5.133}$$

The fact that this fixed point is not fully attractive, is a priori not a problem from the conceptual point of view, since the very definition of the asymptotic safety scenario requires a finite dimensional hypercritical surface, which means that there are only a finite number of UV-attractive directions allowed, as explained in the general discussion of asymptotic safety in chapter 4. Nevertheless, it is somehow surprising based on the results in section 5.6. Interestingly, this fixed point will turn out to be the physical one, as it survives all improvements of the approximation that will be presented below. The canonical improvement of the setup above is the inclusion of scale-dependent wave–function renormalizations, i.e. non-vanishing anomalous dimensions. Concerning the momentum dependence of the propagator, the lesson from section 5.5 and section 5.6 is quite clear: An anomalous dimensions projected via a specification with a derivative at $p = 0$, i.e. with $p_\bullet \longrightarrow p_\star \longrightarrow 0$ in equation (5.38) is untrustworthy for the graviton propagator. Consequently, we apply the finite difference presented in section 5.6. Before enhancing this setup, we analyze how anomalous dimensions enter the loop integrals, and how the full momentum–dependence can be approximated.

Approximation to fully momentum-dependent anomalous dimensions

As presented in section 5.6, the solution with a fully momentum dependent anomalous dimension requires the solution of an integral equation coupled to the system of differential equations. The anomalous dimension $\eta(p^2)$ is then used at each scale k in the solution of the differential equation as $\eta(q^2)$ in the loop integrals for the couplings, e.g. (5.120). This structure of the anomalous dimension in FRG-based beta-functions is generic if the regulator is proportional to a momentum-dependent wave-function renormalization. The dependence on the anomalous dimensions is then always stored in integrals of the form $\int \mathrm{d}q q^3 \eta(q^2) f(q, ...)$, with some functions f that depend on further couplings and external momenta. Due to the general properties of the regulator, we know that the integrands are peaked at $q \approx k$. This structure is very pronounced as the low momentum modes are highly suppressed due to the factor q^3 in the integral measure. Moreover, any anomalous dimension should be a moderate correction and not the dominant factor in the integral, since its implementation depends on the regulator. As a consequence, the integrals are well-approximated by an upper bound

$$\int \mathrm{d}q q^3 \eta(q^2) f(q, ...) \lessapprox \eta(p^2 = k^2) \int \mathrm{d}q q^3 f(q, ...)\,. \tag{5.134}$$

Using the above estimate in the equation for the anomalous dimension itself, the aforementioned integral equation (5.73) whose solution is discussed in subsection 5.6.1, this describes an approximation to $\eta_1(p^2)$ beyond the zeroth order approximation.

Derivative Expansion+ at vanishing Momentum

Now we use the same system of equations as in the case for the derivative expansions at vanishing momentum (without "+"), but this time with anomalous dimensions approximated

as discussed above, signaled by the "+" label at the derivative expansion. This improvement generates only quantitative corrections to the fixed point structure, namely the non-Gaussian fixed point with two UV-attractive and one UV-repulsive direction survives and changes its fixed point coordinates to

$$\left(g_*^{\mathrm{UV}}, \lambda_*^{(3)\,\mathrm{UV}}, \mu_*^{\mathrm{UV}}\right) = (0.61, 0.012, -0.43,) \tag{5.135}$$

with critical exponents

$$\left(\theta_1, \theta_2, \theta_3\right) = (-1.3 + 4.6\,i, -1.3 - 4.6\,i, 5.9)\,. \tag{5.136}$$

The anomalous dimensions at the fixed point take the values

$$\left(\eta_{h*} = 1.0, \eta_{c*} = -0.8\right)\,, \tag{5.137}$$

which is in qualitative agreement with the fully momentum–dependent anomalous dimensions calculated in section 5.6.

Finite Differences

The highly non-trivial momentum dependence of the flow of the three–point function is depicted in Figure 5.17. Due to this highly non-trivial momentum dependence of the flow, a fully momentum-dependent coupling $g(p^2)$ would be the deluxe-solution for the specification problem for the gravitational coupling. However, this turns the beta-function β_g for the coupling into an integro-differential equation, which in turn is then coupled to the integral equation for η_h and to the differential equations for μ and $\lambda^{(3)}$. In the spirit of optimization of some specification procedure, we utilize the generalization of derivative projections, namely finite differences. The general finite difference projection for the running of the gravitational coupling is already presented in equation (5.124). Based on the locality of flow equations in momentum space, or more precisely the peak structure in the loop integrals, the finite difference with $p_\star = k$ and $p_\bullet = 0$ in (5.124) is expected to approximate the full momentum-dependence reasonably. This choice has a big advantage over the derivative at $p = k$, since it is sensitive to global properties of the flow and is hence not affected by local inaccuracies. As usual, we first study the system with anomalous dimensions set to zero. This means we solve the coupled equations (5.124) with $p_\star = k$ and $p_\bullet = 0$, (5.125), and (D.8).

In the approximation described above, we obtain a very interesting phase diagram that is worth some discussion. A visualization of the phase diagram in the three–dimensional $(g, \lambda^{(3)}, \mu)$ space, i.e. a collection of trajectories $(g(k), \lambda^{(3)}(k), \mu(k))$ for different initial conditions, is shown in Figure 5.18. In the ultraviolet we find a fully attractive non-Gaussian fixed point with the coordinates

$$\left(g_*^{\mathrm{UV,1}}, \lambda_*^{(3)\,\mathrm{UV,1}}, \mu_*^{\mathrm{UV,1}}\right) = (0.98, 0.29, -0.33)\,, \tag{5.138}$$

and critical exponents

$$\left(\theta_1, \theta_2, \theta_3\right) = (-4.0 + 0.9\,i, -4.0 - 0.9\,i, -3.3)\,, \tag{5.139}$$
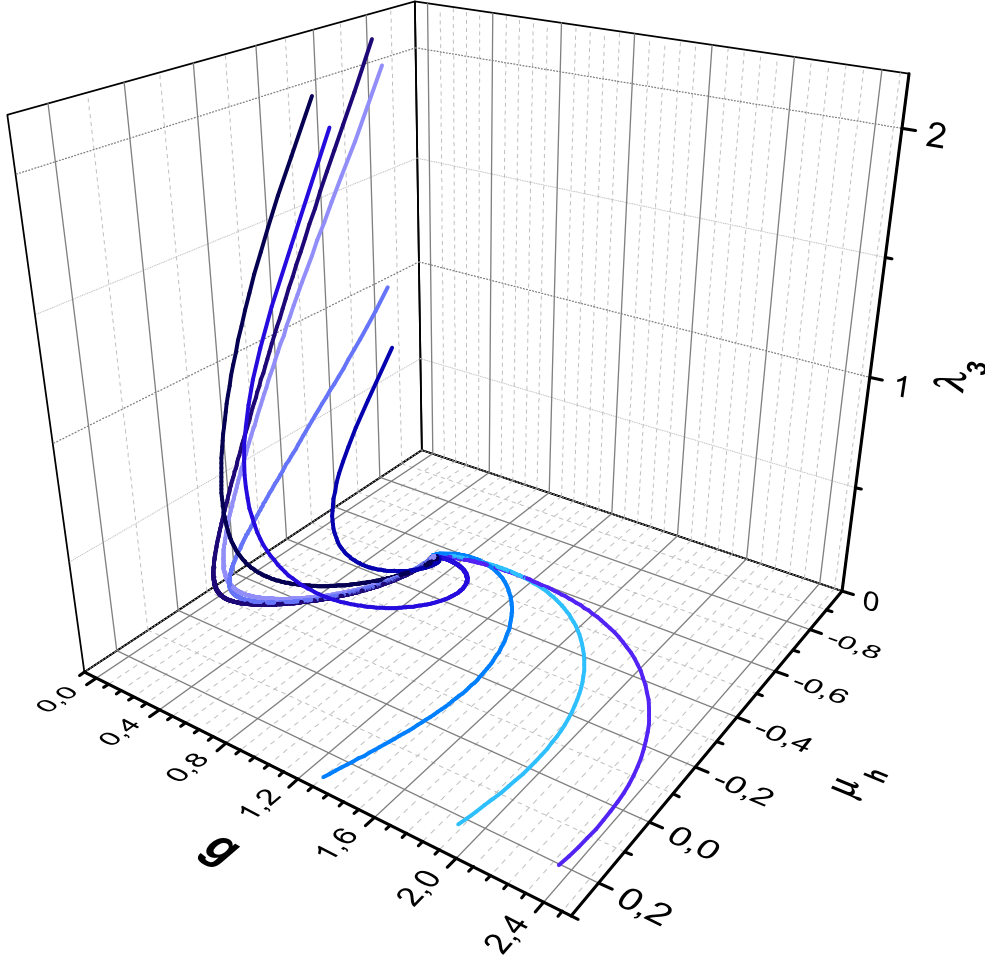
Figure 5.18.: Phase diagram with a finite difference specification for the gravitational coupling.

i.e. the three negative real parts of the eigenvalue indicate that the fixed point has three UV-attractive directions. This phase diagram has some striking similarities with the one obtained in section 5.6. First of all, the product $g_* \mu_* \approx 0.39$, to which one can attribute at least some physical meaning since explicit scale dependencies cancel, is quite close to the one obtained the in section 5.6, where we found $g_* \mu_* \approx 0.32$.

In addition to the fully attractive ultraviolet fixed point, we rediscover the fixed point found in the approximations with projections at $p = 0$, namely the fixed point with two UV-attractive and one UV-unstable direction. In this approximation the fixed point coordinates read

$$\left(g_*^{\mathrm{UV},2}, \lambda_*^{(3)\,\mathrm{UV},2}, \mu_*^{\mathrm{UV},2} \right) = (0.96, -0.024, -0.35) \,, \tag{5.140}$$

and critical exponents

$$\left(\theta_1, \theta_2, \theta_3 \right) = (-2.1 + 2.4\,i,\ -2.1 - 2.4\,i,\ 5.8) \,. \tag{5.141}$$

Interestingly, the eigenvector belonging to the positive eigenvalue, i.e. UV-repulsive direction, points mostly in the $\lambda^{(3)}$ direction. The importance of this fixed point will become clear

later, as it is the only fixed point that is found in all approximations with the running of the coupling defined from the three-point function.

Also the flows towards the infrared have interesting properties. The trajectories emanating the ultraviolet have two basins of infrared attraction. One class of trajectories flows towards the infrared fixed point

$$\left(g_*^{\mathrm{IR}}, \lambda_*^{(3)\,\mathrm{IR}}, \mu_*^{\mathrm{IR}}\right) = (0, \infty, -\infty)\,, \qquad (5.142)$$

which is the anti-de Sitter fixed point that is built-in in the fundamental structure of the equations, similar to the Gaussian fixed point. This can easily be seen, as the loop integrals on right hand sides of the flow equations are all proportional to $1/(1+\mu)^{\#}$, with $\#$ being the number of internal propagators. As a consequence, all the loop terms vanish in the limit $\mu \longrightarrow \infty$ and we are left with

$$\partial_t g = 2g \qquad , \qquad \partial_t \mu = -2\mu\,, \qquad (5.143)$$

with the solutions

$$g(k) \sim k^2 \qquad , \qquad \mu \sim \frac{1}{k^2}\,. \qquad (5.144)$$

The other class of trajectories are all attracted by the non-trivial infrared fixed point

$$\left(g_*^{\mathrm{IR}}, \lambda_*^{(3)\,\mathrm{IR}}, \mu_*^{\mathrm{IR}}\right) = (0, 1, \infty)\,, \qquad (5.145)$$

which has already been found for the first time in an Einstein–Hilbert type of truncation in section 5.5, and more generally in section 5.6. In the reduced approximation section 5.5, this infrared fixed point has non-classical scaling properties, while in section 5.6, the infrared analysis shows that this fixed point is induced by self-consistency conditions and that disentangling the cosmological constant λ and the constant parts of the vertices $\lambda^{(n)}$ opens the possibility for an infrared fixed point that is classical in the cosmological constant and the gravitational coupling. In approximations where the three–point function is not resolved, the trajctories hit a singularity at latest when they approach the attractor line $\mu = -1$ at finite g. In section 5.5 the self-consistency analysis creates the attractive infrared fixed point such that the singularity is avoided and the flows are driven towards $g = 0$. As we have already pointed out, the necessity for the infrared analysis arises due to the truncation of the hierarchy of flow equations, in particular the infrared-scaling of the constant parts $\lambda^{(n)}$ needs to be resolved properly. In the present approximation the the flow of $\lambda^{(3)}$ is captured dynamically. As a consequence, the the attractor line $\mu = -1$ shrinks to the point $(g, \mu) = (0, -1)$, which is the pole of the propagator. Once the trajectories approach this point, all the scaling arguments presented in section 5.6 hold and the existence of the infrared fixed point at $\left(g_*^{\mathrm{IR}}, \lambda_*^{(3)\,\mathrm{IR}}, \mu_*^{\mathrm{IR}}\right) = (0, \infty, -1)$ is guaranteed. An important fact is that also in this system, the non-trivial infrared fixed point exhibits classical scaling, namely

$$g(k) \sim k^2 \qquad , \qquad \lambda \sim \frac{1}{k^2}\,. \qquad (5.146)$$

with the cosmological constant defined as in subsection 5.6.4. The cosmological constant has been ignored so far in this analysis as it decouples from the flow and has no influence on the phase diagram shown above. As a reminder, we note that this decoupling is rooted in the fact that the cosmological constant is defined from the one–point function, which does not enter
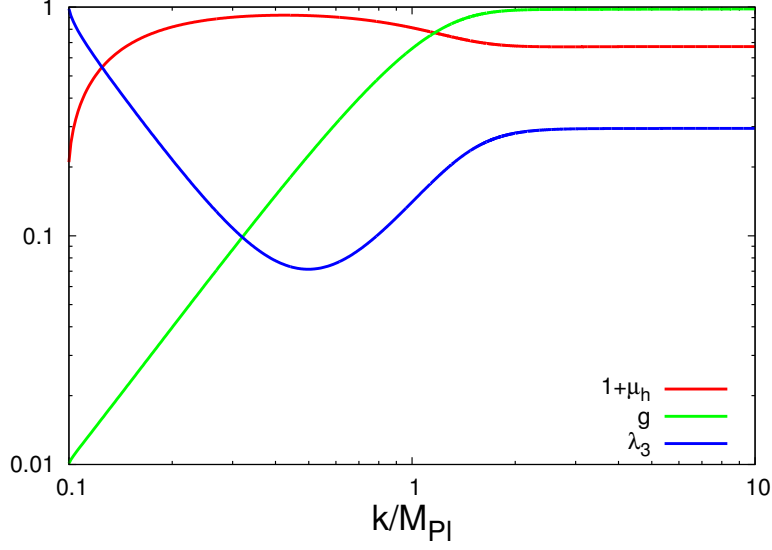
Figure 5.19.: The couplings as a function of k/M_{Pl}.

the flow of the higher order vertex functions. As in subsection 5.6.9, the classical scaling of the gravitational coupling allows us to define a physical scale, namely the Planck mass. In Figure 5.19 we show typical trajectories $(g(k), \lambda^{(3)}(k), \mu(k))$ of the generalized couplings. One can see that the couplings tend to their ultraviolet fixed point values for $k \gg M_{\text{Pl}}$ and behave as dictated by the physical infrared fixed point in the limit $k \ll M_{\text{Pl}}$. We also stress the impressive fact, that the flow of $\lambda^{(3)}$ calculated from the three–point function diverges as predicted by the infrared analysis, where we estimated a behavior $\lambda^{(3)} \overset{\mu \to -1_+}{\sim} (1+\mu)^{-\frac{1}{9}}$, see subsection 5.6.3, Appendix E and Appendix F.

In summary, this approximation seems to fulfill all necessary conditions: The ultraviolet is dominated by a non-Gaussian fixed point. Thus, this framework provides a sensible UV completion of quantum gravity. Moreover, there are globally defined trajectories that hit an infrared fixed point with classical properties, which means that we recover general relativity in the limit $k \longrightarrow 0$. However, we have already mentioned that the fully attractive ultraviolet fixed point will disappear after enhancement of the approximation and the UV-fixed point with one repulsive direction will be the physical one.

Finite Differences $+$

As in the paragraph above, the "+" indicates that we are now including anomalous dimensions with an approximated momentum-dependence described by (5.134). We now observe, that the fully attractive non-Gaussian ultraviolet fixed point $\left(g_*^{\text{UV},1}, \lambda_*^{(3)\,\text{UV},1}, \mu_*^{\text{UV},1} \right)$ is lost, and only the fixed point $\left(g_*^{\text{UV},2}, \lambda_*^{(3)\,\text{UV},2}, \mu_*^{\text{UV},2} \right)$ with two ultraviolet attractive directions survives this enhancement of the approximation. We continue to label this fixed point with an upper index 2. The coordinates of this fixed point are now given by

$$\left(g_*^{\text{UV},2}, \lambda_*^{(3)\,\text{UV},2}, \mu_*^{\text{UV},2} \right) = (0.60, 0.10, -0.57,) , \tag{5.147}$$

and critical exponents

$$\left(\theta_1, \theta_2, \theta_3\right) = \left(-0.52 + 4.1\,i,\, -0.52 - 4.1\,i,\, 12\right). \tag{5.148}$$

It is striking that the pair of complex conjugate exponents have now a very small real part, while the positive eigenvalue is huge. Usually such large critical exponents are a hint that some higher order corrections influence the lower order terms in a way that is not captured properly, and the eigenvalues decrease once the truncation is improved in the correct way. As hint in this direction we find that the fixed point values are very stable against variations of the form $\lambda^{(4)} = \lambda^{(3)} + \epsilon$ with a small parameter ϵ, but the third, positive eigenvalue changes a lot. An analogous behavior was found in [66] for the eigenvalue of the R^2 term, whose eigenvalue is significantly lowered once R^3 terms are included. However, the sign of the eigenvalue is not expected to change.

5.8.4. Finite Differences $++$, or fully momentum-dependent Anomalous Dimensions and the State of the Art.

In the light of the results of the previous paragraphs, we provide a further improvement of the truncation. This time, we use fully momentum dependent anomalous dimensions, indicated by the "$++$". This is the most advanced approximation in this chapter, and in terms of resolution of vertex functions and momentum-dependencies by far the most refined one in the subject of asymptotic safety. For the sake of completeness, we summarize once again all equations that are used for this computation. The equation for the gravitational coupling g is given by (5.124), and is now used with a finite difference with $p_\star = 1$ and $p_\bullet = 0$, or in the limit $p_\bullet \longrightarrow p_\star$ as a derivative at $p = k$. This equation is coupled to the one for the constant part of the vertex functions $\lambda^{(3)}$, (5.125) and the gap-parameter μ of the graviton (5.70). Moreover, the anomalous dimensions of the graviton and the ghost enter all these equations with their full momentum dependencies, which are determined by solving the coupled integral equations (5.71) and (5.72).

With this setup, we can confirm the existence of the non-Gaussian ultraviolet fixed point $\left(g_*^{\mathrm{UV},2}, \lambda_*^{(3)\,\mathrm{UV},2}, \mu_*^{\mathrm{UV},2}\right)$, with two ultraviolet attractive, and one repulsive direction. A fixed point analysis yields for the finite difference in the g equation the values

$$\left(g_*^{\mathrm{UV},2}, \lambda_*^{(3)\,\mathrm{UV},2}, \mu_*^{\mathrm{UV},2}\right) = \left(0.66, 0.11, -0.59, \right), \tag{5.149}$$

and critical exponents

$$\left(\theta_1, \theta_2, \theta_3\right) = \left(-1.4 + 4.1\,i,\, -1.4 - 4.1\,i,\, 13\right). \tag{5.150}$$

This is in impressive agreement with the results in the previous paragraph, where we used the estimate (5.134) for the anomalous dimensions. This quantitative agreement is expected, as we have already argued that the approximation (5.134) is usually well-justified due to the structure of the integral kernels.

For the derivative specification at $p = k$ we obtain

$$\left(g_*^{\mathrm{UV},2}, \lambda_*^{(3)\,\mathrm{UV},2}, \mu_*^{\mathrm{UV},2}\right) = \left(0.56, -0.01, -0.37, \right), \tag{5.151}$$

and critical exponents with the values

$$(\theta_1, \theta_2, \theta_3) = (-1.2 + 2.2\,i, -1.2 - 2.2\,i, 4.8)\,. \tag{5.152}$$

The fixed point values for g and μ are only weakly affected by this change of the projection point. The fixed point value for $\lambda^{(3)}$ is still small, but now with opposite sign. Suspiciously, this is exactly the coupling that points mostly in the unstable direction. The corresponding critical exponent is now smaller by a factor of roughly 2.7, and therefore one is tempted to favor the derivative over the finite difference.

Summary and interpretation of the results.

Due to the surprising and interesting results of this section, we summarize and interpret our findings. We have solved the coupled hierarchy of the graviton two- and three–point function in various approximations. The main result is, that there is one non-Gaussian ultraviolet fixed point that is present in all approximations. Most importantly, it is present in the most refined approximation "finite differences ++". Hence, we will attribute to this fixed point physical relevance. The fixed point values and critical exponents in different approximations are summarized in Table 5.8. This ultraviolet fixed point is equipped with two negative and one positive critical exponent. As a consequence, there are two attractive and one repulsive direction, where the latter is mostly in the direction of $\lambda^{(3)}$. This repulsive direction implies that the corresponding parameter is ultraviolet *irrelevant*! This is a very encouraging result for asymptotic safety, as there are only finitely many relevant parameters allowed in the full theory. See the general discussion in chapter 4. Therefore, if one found more and more relevant parameters upon inclusion of further generalized couplings and improved truncations, this would put asymptotic safety in bad shape. In contrast, our findings support the asymptotic safety conjecture. The appearance of this irrelevant eigenvalue is in great accordance with the complementary high-level background field studies in $f(R)$ gravity, [63, 64, 66], where only the operators R^0, R, R^2 generate relevant eigenvalues.

method	$p_\star = 0, \eta \equiv 0$	$p_\star = 0, \eta_k$	$p_\star = k, \eta \equiv 0$	$p_\star = k, \eta_k$	$p_\star = k, \eta_k(p^2)$
g_*	0.57	0.61	0.96	0.6	0.66
$\lambda^{(3)}_*$	-0.16	0.02	-0.2	0.10	0.11
μ_*	-0.16	-0.43	-0.35	-0.57	-0.59
θ	-1.5, 1.6	-1.3 ,5.9	-2.1,5.8	-0.5,12	-1.4,13

Table 5.8.: The fixed point values and critical exponents of the physical non-Gaussian ultraviolet fixed point obtained in different approximation schemes. The label $p = p_\star$ indicates a projection of the three–point function with a derivative at zero if $p_\star = 0$, or a finite difference at $p = 0$ and $p_\star = k$. Moreover, we used approximations without anomalous dimensions, scale–dependent anomalous dimensions and fully momentum–dependent anomalous dimensions. For the eigenvalues we display only the real part of the complex conjugate pair. As one can see, including an anomalous dimensions properly changes the sign of $\lambda^{(3)}_*$.

The infrared properties of trajectories that hit this ultraviolet fixed point are under current investigation and will be presented in a forthcoming publication.

5.8.5. General remarks on locality.

We close this part with a discussion of the locality property introduced in section 5.2. We have argued, that the notion of locality as defined in (5.17) is a crucial property of renormalization group flows, and all perturbatively renormalizable are local by simple power counting arguments. For perturbatively non-renormalizable theories, locality is based on on-trivial cancellations. We found such cancellations for the two- and three–point function of the graviton. We also state that this holds for the Yang–Mills contributions to these correlators, which will be shown in subsection 8.1.2. Moreover, we have found that the same is true for matter contributions, [136]. These intriguing results raise the question of the fundamental reason for the cancellations that lead to local flows in perturbatively non-renormalizable field theories. We have already observed that locality is spoiled in e.g. $\int_x \phi^2 \partial^2 \phi^2$ theories, as there is no way that the leading order terms cancel against each other. In gravity, this is possible due to the contractions of tensor structures. Hence, it is tempting to attribute the locality property to diffeomorphsim invariance. In this spirit, it would be very interesting to see if the "lifted" version of the above counterexample is local, namely a $\int_x \sqrt{\det g} \, \phi^2 \Delta \phi^2$ theory with a Laplace-Beltrami operator, as such a theory is clearly diffeomorphism invariant. In general, it would then be the question if diffeomorphism invariance is a necessary or a sufficient condition for local flows. Both cases have interesting consequences, as for the former, one could use locality as a construction principle and forbid all terms that generate non-local flows, justified by the fundamental principle of locality. On the other hand, if diffeomorphism invariance is sufficient, one could conclude that a general theory of quantum gravity is local.

Part II.

Yang–Mills Gravity

Basics

6.1. Introduction and Motivation

Yang–Mills theories are gauge theories based on the Lie group SU(N). Describing the weak and the strong interactions, they form the basis of the standard model of particle physics. A striking feature of Yang–Mills theories is asymptotic freedom, meaning that the theory is governed by a Gaussian fixed point in the ultraviolet. This implies that gluon interactions weaken for high energies and that perturbation theory is applicable. In fact, the great success of the standard model, which is able to describe high-precision data from collider experiments, is possible only due to the rapid decrease of the relevance of higher order terms in the perturbative series for energies $E \gg \Lambda_{\mathrm{QCD}}$. The weakening of interactions is encoded in the energy dependence of the Yang–Mills coupling α, which in turn is signaled by a strictly negative sign of the beta function. However, it is well known that fermions contribute with a positive sign to the running of the gauge coupling,

$$\beta_\alpha = -2(\frac{11}{3}N_c - \frac{2}{3}N_f)\frac{\alpha^2}{4\pi}, \tag{6.1}$$

where we have displayed only the one-loop contributions and N_c are number the of colors, while N_f is the number of fermion flavors. One can see that there is a critical number of fermion flavors above which the positive contributions to the beta function dominate. This implies that asymptotic freedom is lost.

Due to the non-perturbative nature of ultraviolet quantum gravity, not that much is known about the coupling of gravitons to gluons at very high energies. In the context of the asymptotic safety scenario, a question of major importance is if the graviton–gluon interactions preserve the property of asymptotic freedom, since in the end one is interested in an ultraviolet completion of the entire standard model. On the other hand, one has to make sure that the gravitational fixed point survives in the fully coupled system of Yang–Mills gravity.

A first access to this system has been gained in first order perturbation theory [137–142] by treating gravity as an effective field theory [18]. The main message of these calculations is

that the sign of the Yang–Mills beta function is not altered by graviton fluctuations. However, in such an effective field theory approach, all statements are reliable only for energies $E \ll M_{\text{Pl}}$. A first non-perturbative study using functional renormalization techniques within pure background flows confirmed this result [68]. A subsequent FRG-study with a vertex expansion up to second order draws similar conclusions [70], but asymptotic freedom is present only if the fixed point values in the gravitational sector obey the bound $\lambda_* < \frac{1}{8}$. However, the aforementioned work does not resolve the momentum dependence of the propagator sufficiently. In this part of the thesis we test the stability of the Yang–Mills gravity system including the general momentum dependence of the gluon propagator.

6.2. The Setup

Gravity couples to any source of energy. In any diffeomorphism invariant theory the integral measure is proportional to $\det g$, which generates automatically interactions with gravitons. Moreover, any contraction is generated by the metric tensor that acts on vectors and therefore also leads to vertices of gravitons with the respective field. As a result, the coupling of Yang Mills theory to gravity is automatically implied in the classical Yang-Mills action

$$
\begin{aligned}
S_{\text{YM}} &= \frac{1}{4} F_{\mathbf{a_1 a_2}} F^{\mathbf{a_1 a_2}} \\
&= \frac{1}{4} \int_{\mathbb{M}} \mathrm{d}^d x \sqrt{-\det g}\, g_{\alpha \alpha'} g_{\beta \beta'} \mathrm{Tr}\left[F^{\alpha' \beta'} F^{\alpha \beta} \right],
\end{aligned} \tag{6.2}
$$

with the standard non-Abelian field strength tensor, or curvature form $F_{\mathbf{a_1 a_2}}$ and the trace in color-space. We use the functional renormalization group in order analyze the coupled system of quantum gravity and quantum Yang-Mills theory, in particular the ultraviolet behavior. We use the setup of vertex expansions as presented in section 5.1. The scale dependent effective action that contains the graviton–gluon interactions is then expanded analogously to (5.1) in powers of the fluctuation fields,

$$
\Gamma_k[\bar{g}, \phi] = \sum_n \frac{1}{n!} \Gamma^{\mathbf{a_1 \cdots a_n}}[\bar{g}, 0] \phi_{\mathbf{a_1}} \cdots \phi_{\mathbf{a_n}},
$$

where now the field content is enlarged to $\phi = \left(h, \bar{c}, c, A, \bar{c}_{\text{YM}}, c_{\text{YM}} \right)$ with with the gluon field A, Yang–Mills ghosts $\left(\bar{c}_{\text{YM}}, c_{\text{YM}} \right)$ and background fields $\bar{g}, \bar{A}$. However, the gauge-fixing and ghost terms do not contribute to the graviton–gluon interactions, as the graviton ghost and gauge fixing term is independent of A by construction, and the Yang–Mills ghost sector depends on the background metric only. Since we take functional derivatives with respect to the fluctuation fields in order to generate graviton–gluon interactions, we can neglect the ghost-sector. The auxiliary background field is arbitrary and is chosen as $\bar{\phi} = \left(\bar{A} = 0, \bar{g} = \mathbb{I} \right)$. We then split the effective action into a pure gravity part, the ghost and gauge fixing parts, and the terms that contains gluon self-interactions and the gluon–graviton interactions,

$$
\Gamma_k = \Gamma_{k,\text{grav}} + \Gamma_{k,\text{YM}-\text{grav}} + \Gamma_{k,\text{ghost}} + \Gamma_{k,\text{gauge}}, \tag{6.3}
$$

where we have already noted that the last two terms are of no relevance here. The pure gravity part of the effective action $\Gamma_{k,\text{grav}}$ is constructed exactly as presented in chapter 5.

For the parts involving gluons, we are guided by asymptotic freedom, namely that for high energies, also the full quantum effective action for Yang–Mills theory is given by the classical Yang–Mills action modified with a scale–dependent wave–function renormalization. Consequently, our truncation for $\Gamma_{k,\text{YM}-\text{grav}}$ is based solely on Equation 6.2. We employ the same vertex construction that we have already used in the pure gravity sector. Moreover, the diagrams that describe the graviton–gluon interactions of course also contain the graviton propagator. With these three ingredients the relevant part of the scale–dependent action takes the form

$$
\begin{aligned}
\Gamma_{k,\text{YM}-\text{grav}}[\bar{g},h,A] + \Gamma_{k,\text{grav}-\text{prop}}[\bar{g},h] &= \Gamma^{(AA)\,\mathbf{a_1 a_2}} A_{\mathbf{a_1}} A_{\mathbf{a_1}} + \Gamma^{(hh)\,\mathbf{a_1 a_2}} h_{\mathbf{a_1}} h_{\mathbf{a_2}} \\
&+ \Gamma^{(AAh)\,\mathbf{a_1 a_2 a_3}} A_{\mathbf{a_1}} A_{\mathbf{a_2}} h_{\mathbf{a_3}} + \Gamma^{(AAhh)\,\mathbf{a_1 a_2 a_3 a_4}} A_{\mathbf{a_1}} A_{\mathbf{a_2}} h_{\mathbf{a_3}} h_{\mathbf{a_4}} \\
&+ \mathcal{O}\left(h^3 A^2\right),
\end{aligned}
\tag{6.4}
$$

The terms that we have not written down are of higher order in h and A and, as we will see below, do not enter the flow equations of the gluon and graviton propagators nor of the graviton three–point function, which will be the objects of interest. With the approximation described above, the vertices in momentum space and with standard index notation are then given by

$$
\Gamma^{(AA)}_{\mu\nu}(p_1,p_2) = Z_A^{\frac{1}{2}}(p_1) Z_A^{\frac{1}{2}}(p_2)\ \left.\frac{\delta^2 S_{\text{YM}}}{\delta A^\mu(p_1)\delta A^\nu(p_2)}\right|_{A=0,h=0},
\tag{6.5}
$$

which is the gluon two–point function,

$$
\Gamma^{(AAh)}_{\mu\nu\alpha_1\alpha_2}(p_1,p_2,p_3) = Z_A^{\frac{1}{2}}(p_1) Z_A^{\frac{1}{2}}(p_2) Z_h^{\frac{1}{2}}(p_3^2) G^{\frac{1}{2}}\ \left.\frac{\delta^3 S_{\text{YM}}}{\delta A^\mu(p_1)\delta A^\nu(p_2)\delta h^{\alpha_1\alpha_2}(p_3)}\right|_{A=0,h=0},
\tag{6.6}
$$

which describes interactions of two–gluons and one graviton, and finally the two gluon–two graviton vertex

$$
\begin{aligned}
\Gamma^{(AAhh)}_{\mu\nu\alpha_1\alpha_2\beta_1\beta_2}(p_1,p_2,p_3,p_4) =&\, Z_A^{\frac{1}{2}}(p_1) Z_A^{\frac{1}{2}}(p_2) Z_h^{\frac{1}{2}}(p_3^2) Z_h^{\frac{1}{2}}(p_4^2) G \\
&\times \left.\frac{\delta^4 S_{\text{YM}}}{\delta A^\mu(p_1)\delta A^\nu(p_2)\delta h^{\alpha_1\alpha_2}(p_3)\delta h^{\beta_1\beta_2}(p_4)}\right|_{A=0,h=0},
\end{aligned}
\tag{6.7}
$$

with scale- and momentum-dependent wave–function renormalizations Z_A for the gluon and Z_h for the graviton and a scale-dependent gravitational coupling G. The graviton two–point function $\Gamma^{(hh)\,\mathbf{a_1 a_2}}$ is the usual one from the previous sections. There are several important things to note concerning the vertices.

- First, due to the F^2 approximation, the vertex expansion is maximally of fourth-order in A, while the $\det g$ factor generates infinite orders in h. However, only the terms that we have written down explicitly in (6.4) will contribute to the graviton–gluon interactions in the flow equations, and these terms are maximally quadratic in A. Consequently, the non-Abelian parts in the F^2 term are irrelevant since they are of order three and higher. This means, that modulo trivial color factors δ^{ab}, the vertices defined above are identical for SU(N) and U(1) gauge theories! This enables us to make also some statements about quantum electrodynamics.

- The following is a more technical issue. In principle, the derivatives in the curvature form $F^{\mu\nu}$ are covariant derivatives with respect to the Levi-Civita connection. However, since $F^{\mu\nu}$ is antisymmetric, and the Christoffel-symbols symmetric in the paired index, the latter cancel against each other and the covariant derivatives can be replaced by partial derivatives.

In the end, we are interested in the gravitational corrections to the Yang–Mills beta–function β_α for the running of the strong coupling constant, and the Yang–Mills contributions to the scale-dependence in the gravity sector. The beta-functions of the latter have been discussed in great detail in chapter 5. In the Yang–Mills sector, we can make use of the fact that in the background field formalism and in the perturbative domain, the renormalization of the gluon wave–function renormalization and of the coupling constant are related as [91]

$$Z_g = Z_a^{-\frac{1}{2}}.$$ (6.8)

The running of the coupling is then determined by

$$\partial_t g_{\mathrm{YM}} = \beta_{g_{\mathrm{YM}}} = \frac{1}{2}\eta_A g_{\mathrm{YM}}$$ (6.9)

with the standard definition of the anomalous dimension

$$\eta_A := -\frac{\partial_t Z_A}{Z_A}.$$ (6.10)

Quantum Gravity Contributions To Yang-Mills Theories

In this section we are interested in the gravitational corrections to the running of the gauge coupling. The key question is if the graviton–gluon interaction spoil, or preserve the property of asymptotic freedom in the gauge sector. If asymptotic freedom was lost, this would be a serious problem for the asymptotic safety scenario, as we ultimately seek for a UV–completion of all forces. We have seen in the last chapter, that the running of the gauge coupling can be calculated from the gluon wave–function renormalization. As a consequence, the object under investigation is the flow of the gluon two–point function, or more precisely, the graviton contributions to the flow of the gluon two–point function. This equation is obtained from the general equation (I) by specifying the field content above. The full flow can be written as

$$\partial_t \Gamma^{(AA)} = \triangle_A \text{Flow}^{(AA)} + \triangle_h \text{Flow}^{(AA)}, \tag{7.1}$$

where the first term contains glue fluctuations only, while the second term is induced by gravity mediated interactions. The diagrammatic form of the second term is given in Figure 7.1.

$$\triangle_h \text{Flow}^{(AA)} = -\frac{1}{2} \quad$$

$$\tag{7.2}$$

Figure 7.1.: Diagrammatic depiction of gravitational contributions to the flow of the Yang–Mills propagator. The wiggly lines are gluon propagators, and the double line represent graviton propagators.

This split is reflected in a corresponding split of the anomalous dimension

$$\eta_A = \triangle_A \eta_A + \triangle_h \eta_A. \tag{7.3}$$

Asymptotic freedom is then signaled by a negative sign of the gluon anomalous dimension as the beta-function for the coupling is proportional to η_A. We know that the pure glue contributions $\triangle_A \eta_A$ are negative. Hence, the question whether asymptotic freedom is preserved in the Yang–Mills gravity system boils down to the sign of the gravity contributions $\triangle_h \eta_A$. For a negative sign it is clear that

$$\triangle_h \eta_A < 0 \quad \Longleftrightarrow \quad \text{asymptotic freedom preserved}. \tag{7.4}$$

If the sign is positive instead, it is clear that asymptotic freedom may be spoiled. Since $\triangle_h \text{Flow}^{(AA)} \sim G$, this is the case if the gravitational coupling grows larger than some critical value.

7.1. Gravitational corrections to the Yang–Mills beta-function and Asymptotic Freedom

As we have already discussed in great detail in the gravity sector, the projection and approximation of the momentum–dependence is of great importance if the right-hand side of the flow equations shows a non-trivial behavior. With the construction of the effective action (6.4), and an optimized regulator (5.45) for both, gluons and gravitons, we obtain after transverse projection

$$\triangle_h \text{Flow}^{(AA)} = Z_A(p^2) G \int_q \left((-\eta_A(q^2) r(q^2) + \dot{r}(q^2)) f_A(q, p, \mu) \right.$$
$$\left. + (-\eta_h(q^2) r(q^2) + \dot{r}(q^2)) f_h(q^2, p^2) \right), \tag{7.5}$$

where the first term originates in the diagram with a regulator in the gluon propagator and the second one in the two diagrams with a regulator insertion in the graviton propagator. The left-hand side is simply given by

$$\partial_t \Gamma^{(AA)} = p^2 \partial_t Z_A(p^2). \tag{7.6}$$

7.1.1. Bounds for Asymptotic Freedom

We investigate the the sign of the gravitational contributions to the running of the Yang–Mills propagator. In the fully coupled system, these contributions are of course functions of the running parameters of the gravity sector, which in turn depend on the truncation. It is therefore interesting to evaluate $\eta_{A,h}$ with a parametric dependence on the gravity parameters, in order to obtain general conditions under which asymptotic freedom is guaranteed.

In a first approach, we drop the momentum-dependence of the gluon wave-function renormalization and use finite difference or derivative projections according to (5.38). In a derivative expansion one assumes a momentum independent wave-function renormalization Z_k, and one can pull the anomalous dimensions on the RHS outside the integral.

Derivative at $p = 0$

The simplest choice is the derivative at $p = 0$, i.e. $p_\star = 0$ in (5.35). In this case we can solve the loop-integrals analytically, in the same fashion as in the pure gravity case. We obtain the analytic result

$$\triangle_h \, \mathrm{Flow}^{(AA)} = -\frac{g}{8\pi} \left(-\frac{\eta_A}{1+\mu} + \frac{4(1+2\mu)}{(1+\mu)^2} + \frac{\eta_h}{(1+\mu)^2} \right). \tag{7.7}$$

It is important to note that on the right-hand side, the full gluon anomalous dimension appears. For the analysis of asymptotic freedom, we are interested in the high-energy limit, where we know that the pure glue-part of η_A, namely $\triangle_A \eta_A$ vanishes. Therefore, assuming a fixed point in the gravitational sector, we are left with the ultraviolet limit

$$\lim_{k \longrightarrow \infty} \triangle_h \eta_A = \frac{g_*}{1 - \frac{g_*}{8\pi(1+\mu_*)}} \left(\frac{4 + 8\mu_* + \eta_{h*}}{8\pi(1+\mu_*)^2} \right). \tag{7.8}$$

The above function has a zero where it changes sign at the critical value

$$\mu_{*,\mathrm{crit}} = \frac{1}{8}(-4 - \eta_h). \tag{7.9}$$

Moreover, there is a pole at $\mu_* = -1 + \frac{g_*}{8\pi}$ with another sign change for the regimes to the left and to the right of the pole. However, this sign change at the pole can be neglected, as all fixed point values g_* that have been calculated so far have values $g_* \approx 1$. For fixed point values of this order the pole is located at $\mu_* \approx -1 + \frac{1}{8\pi} \approx -0.96$, which in turn is a fixed point value that is very unusual. Therefore, we assume the overall pre-factor in (7.8) to be positive. Then, $\lim_{k \longrightarrow \infty} \triangle_h \eta_A \gtrless 0$ for $\mu_* \lessgtr \frac{1}{8}(-4 - \eta_h)$. A check of this result is obtained by comparing with [70], where these contributions have been calculated in such a derivative expansion, but with an Einstein–Hilbert truncation in the gravity sector, which means that the graviton wave-function renormalization is related to the coupling according to (5.39), which enforces $\eta_{h*} = -2$. Moreover, $\mu = -2\lambda$ in this approximation. Using these identifications, we obtain exactly the result in [70] with the bound $\lambda_{*,\mathrm{crit}} < \frac{1}{8}$ for asymptotic freedom to be maintained. In our more general case, the anomalous dimension of the graviton is not fixed by the fixed point condition for Newtons coupling. The fixed point value for the gap-parameter where the gravitational contributions change sign is plotted against the graviton anomalous dimension, i.e. (7.9), in figure Figure 7.2. There are some bounds on anomalous dimensions for well-defined theories. From a mathematical point of view $\eta < 4$ is required such that the correlation functions are tempered distributions. Moreover, $\eta < 2$ is necessary that the regulator in flow equations maintains its properties. Hence, the range of $\eta \in (-2, 2)$ seems reasonable. From the results obtained in chapter 5, we learn that typical values for the graviton anomalous dimension are roughly given by $\eta_h \approx 1$. For such anomalous dimensions we obtain critical values of $\mu_{*,\mathrm{crit}} \approx -0.6$, which is the region where one expects the ultraviolet fixed point to be located.

We conclude that in this simplest approximation the stability of asymptotic freedom is not guaranteed, but depends strongly on subtle effects in the gravity sector. In the following, we investigate how this picture changes in more elaborate approximations and specifications.
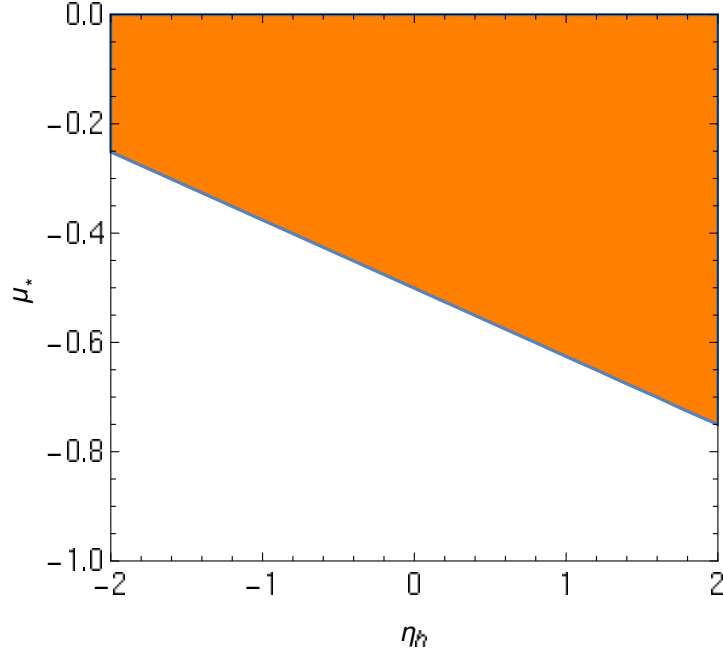
Figure 7.2.: The critical fixed point value $\mu_{*,\mathrm{crit}}$ where the anomalous dimension η_A of the gluon changes sign due to the gravitational contributions. The critical value $\mu_{*,\mathrm{crit}}$ is the boundary line between the colored and the white region. In the colored region $\mathrm{sgn}(\eta_{A,h}) = -1$, while the white region indicates $\mathrm{sgn}(\eta_{A,h}) = +1$. In the first case asymptotic freedom is maintained, while it is lost in the latter one.

General Derivatives

We now generalize the definition of the anomalous dimension η_A to derivatives at arbitrary points $p = p_\star$ in (5.35) and redo the analysis as described above. For such specifications the results are numerical. We evaluate the flow equation for values $p_\star \in [0,1]$ and find very encouraging results, as for "optimized" specifications where the momentum dependence of the flow in the vicinity of the cutoff scale k is resolved, the graviton interactions do not change the sign of the Yang–Mills beta function, but rather support the the weakening of the gauge coupling in the flow towards the ultraviolet. More precisely, the region of the parameter space where $\mathrm{sgn}(\eta_{A,h}) = +1$ and asymptotic freedom is lost, gets smaller and smaller for values of $p_\star \gtrsim 0.5$, and finally the boundary line of the critical value $\mu_{*,\mathrm{crit}}(\eta_h)$ disappears from the "physical" regime. Already for $p_\star \approx 0.75$ we find $\mathrm{sgn}(\eta_{A,h}) = -1$ for all values of μ and η_h, and therefore asymptotically free gluons also in the presence of quantum gravity. These results, are shown in Figure 7.4.

General Finite Differences

We have seen above that for a suitable definition of the gluon wave-function renormalization via derivatives, namely if the derivative is taken at momenta at the order of the cutoff, asymptotic freedom is guaranteed. In order to test the stability of these results, we generalize the derivative-definition to finite differences as described by (5.38). We choose one

(a) Derivative specification with $p_\star = 0.25$

(b) Derivative specification with $p_\star = 0.5$

(c) Derivative specification with $p_\star = 0.75$

(d) Derivative specification with $p_\star = 1$
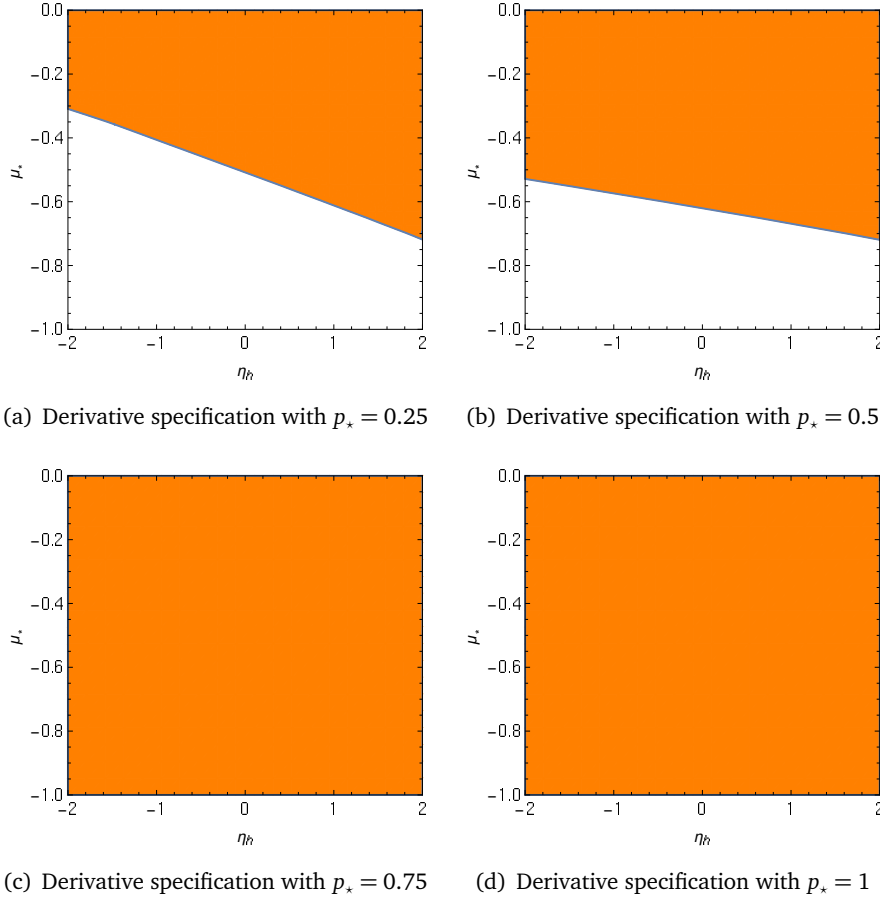
Figure 7.3.: As in Figure 7.2 for the $p = 0$ derivative, in these plots we show $\mathrm{sgn}(\eta_{A,h}) = -1$ as the colored region and $\mathrm{sgn}(\eta_{A,h}) = +1$ in white in the (μ, η_h)-parameter space. The boundary line is the critical value $\mu_{*,\mathrm{crit}}$.

subtraction point at vanishing momentum, i.e. $p_\bullet = 0$ and vary $p_\star$ in the range from zero to one. The corresponding results are represented in Figure 7.4. The findings are very similar to the ones with the derivative definition and substantiate the stability of the specification. In the next paragraph, we investigate the full momentum dependence in order to check whether the validity of the optimization conjecture that the full result is best approximated by projections that are sensitive to fluctuations at the cutoff scale.

Full Momentum Dependence

By including the full momentum dependence we solve the full integral equation obtained by (7.5) and (7.6). For this task, we employ the iterative method that leads to the Liouville-Neumann series that was presented in the context of the graviton propagator in subsection 5.6.1. As a result, we obtain $\eta_A(k, p^2)$, which depends on k via the gravitational coupling, the anomalous dimension η_h of the graviton and the gap-parameter μ. With this

(a) Derivative specification with $p_\star = 0.5$

(b) Derivative specification with $p_\star = 0.75$

(c) Derivative specification with $p_\star = 1$
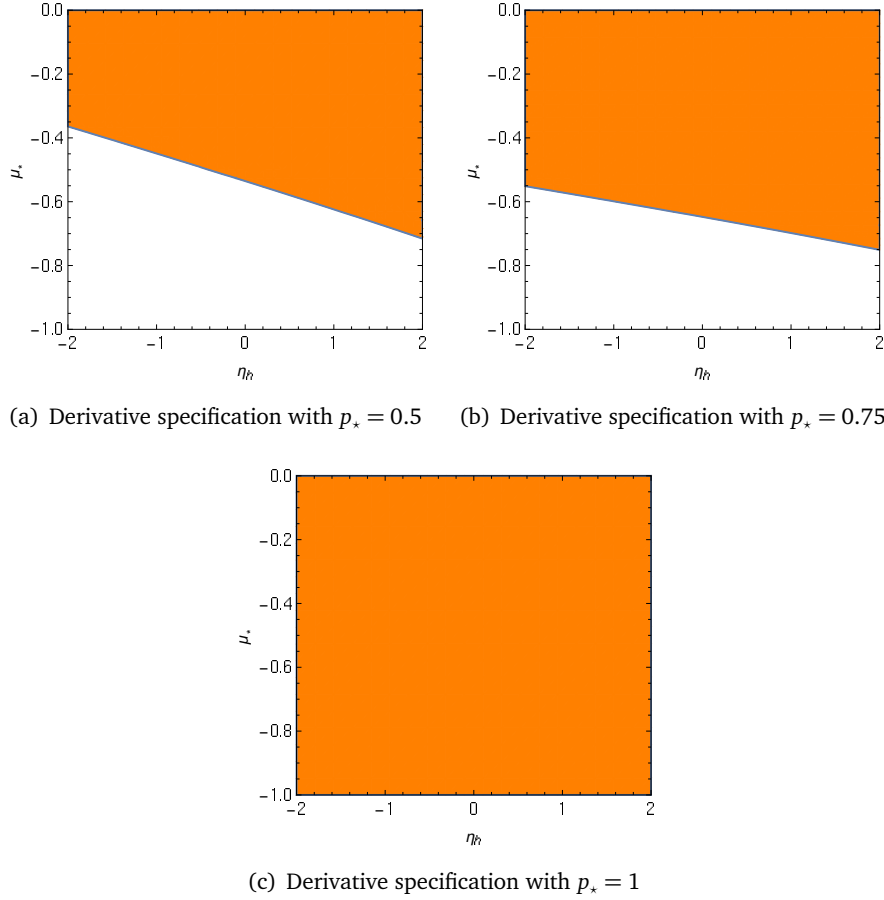
Figure 7.4.: We use the same color-coding as in Figure 7.2 and . The plots show the results for $p_\star = 0.5$, $p_\star = 0.75$ and $p_\star = 1$.

anomalous dimension one can then define a one parameter coupling that depends only on the RG-scale k via the generalization of equation (6.9) with the prescription

$$\partial_t g_{\mathrm{YM}} = \beta_{g_{\mathrm{YM}}} = \frac{1}{2}\eta_A(k, p^2 = k^2)g_{\mathrm{YM}}. \tag{7.10}$$

In Figure 7.5, we plot $\eta_A(k, p^2)$ for some specific parameter values. All these plots are obtained for $g = 0.5$, however, we stress that the sign does not depend on this choice as the result is a power series in g. We investigate the iterations, where we have always assumed a constant function $\eta_0 = \mathrm{const.}$ as a first approximation. We then plot the first, second and third order and find rapid convergence in all cases, which is expected as we have checked that the kernel in (7.5) generates a very large radius of convergence. The third iteration is for this choice of η_0 not even visible any more, since the corresponding curve lies exactly on top of the second iteration. The convergence and the dependence on the zeroth order iteration are analyzed in more detail in Figure 7.7. There, we depict the iterative solutions for different initial functions η_0. We observe that in all cases we find convergence in the

(a) Momentum dependence for $\mu = 0$. The zeroth iteration is a constant function.

(b) Momentum dependence for $\mu = -0.2$. The zeroth iteration is a constant function.

(c) Momentum dependence for $\mu = -0.5$. The zeroth iteration is a constant function.

(d) Momentum dependence for $\mu = -0.7$. The zeroth iteration is a constant function.
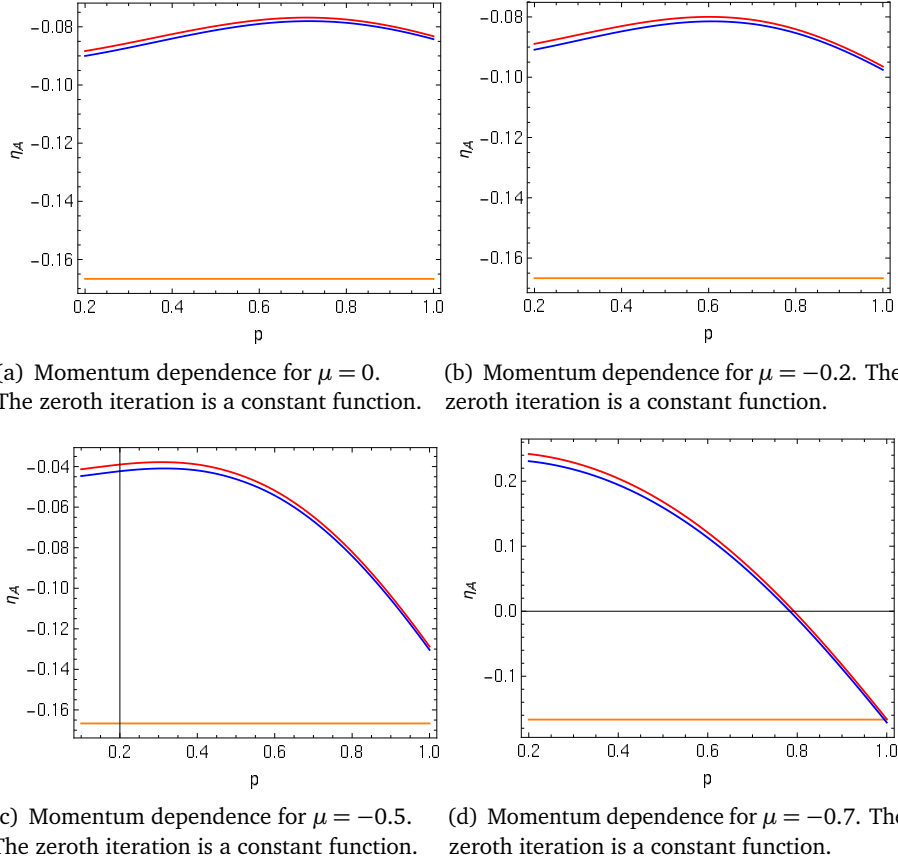
Figure 7.5.: The full momentum dependence of the gravity contributions to the anomalous dimension η_A for different paramter values of the gap parameter μ and for $g = 0.5$ and $\eta_h = 0.5$. We show the zeroth iteration (orange curve), which is of course an arbitrary function and then the first (blue curve) and second (red curve) iteration.

second order of the iteration. In the first three examples, (a), (b) and (c), we have chosen well-behaved functions that have average values of the order of the final solution. As a result, the third order iteration is indistinguishable from the second order. In example (d), the average value of the function is much larger. In this case the first iteration is not a good approximation and has a different sign for small momenta. There is a minimal difference between the second and the third iteration, which is hardly visible, and convergence is perfectly ensured. Even with a zeroth order iteration that has a different pole-structure, the result turns out to be convergent. It is clear that an initial function with a singularity that is not too strong can lead to a smooth limit of the iteration as the singularity is screened by the integral measure. However, in this case the first iteration still resembles the pole structure and is a good approximation for large momenta only.

In spirit of the plots in the last paragraph, we depict $\text{sgn}(\eta_{A,h})$ in Figure 7.7 as a function of the external momentum p and the parameters of the graviton propagator η_h and μ. For a negative sign, indicated by the colored region, asymptotic freedom is preserved and we find that this is indeed the case for the definition Equation 7.10.
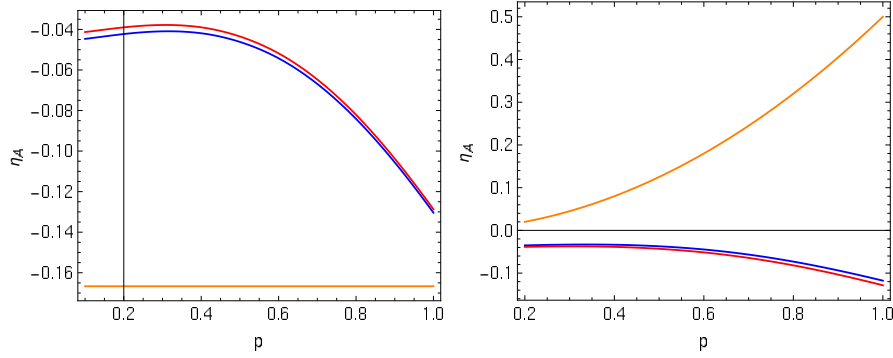
(a) Momentum dependence for $\mu = 0$. The zeroth iteration is a constant function.

(b) The zeroth iteration is in this case the function $\eta_0 = 0.5p^2$
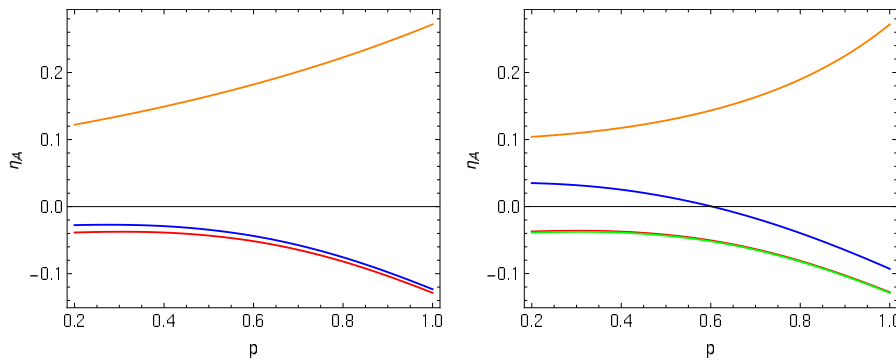
(c) The zeroth iteration is the exponential $\eta_0 = 0.1e^x$.

(d) The zeroth iteration is the exponential $\eta_0 = e^{x^2}$. This function is rescaled by a factor of 0.1.
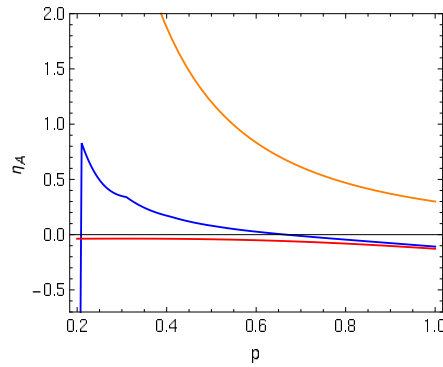
(e)The zeroth iteration is given by $\eta_0 = \frac{1}{p^2}$.

Figure 7.6.: The full momentum dependence of the gravity contributions to the anomalous dimension η_A for different for typical fixed point parameter values parameter $\mu = -0.5$, $g = 0.5$ and $\eta_h = 0.5$, bur for different initial functions η_0 for the iteration process. We show this zeroth iteration as an orange curve, then the first (blue curve), second (red curve) and third (green curve) iteration.
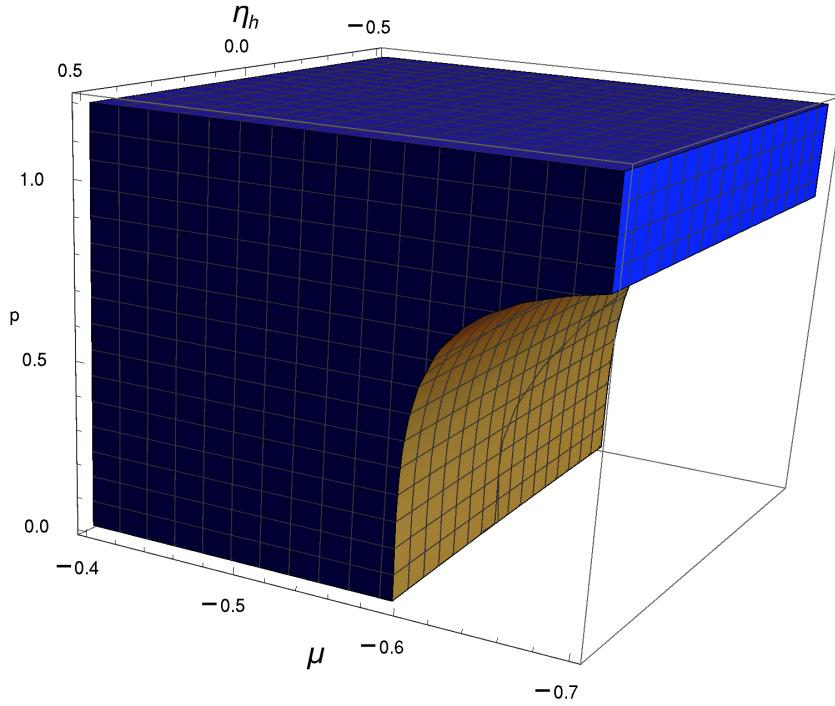
Figure 7.7.: Signum of the gravity contributions to the gluon anomalous dimension, i.e. $\mathrm{sign}\,\eta_{A,h}$ as a function of η_h and μ and the external momentum p. The colored region indicates $\mathrm{sign}\,\eta_{A,h} < 0$

The main results of this chapter can be summarized as follows. For the beta-function as defined in equation (7.10), the graviton contributions to the running of the Yang–Mills coupling are strictly negative, hence supporting asymptotic freedom. Moreover, we find that with derivative or finite difference projections of the wave–function renormalization the full momentum dependence is indeed nicely approximated if the projection resolves fluctuations $p \approx k$.

Yang-Mills Contributions To Quantum Gravity

In the last chapter we have investigated the quantum gravitational corrections to the running of the Yang–Mills coupling. This chapter is concerned with the converse situation, namely the impact of gluonic fluctuations on the gravity sector.

For the results in this chapter, we want to add that these are very recent calculations that are not checked sufficiently. Hence, everything in the following is preliminary.

8.1. Beta Functions

We have seen in the last part of this thesis, Part I, that there are several ways to define a running gravitational coupling, with the definition via the the three–point function being the most advanced and refined one, and in the sense of vertex expansions the only one that is directly related to multi-graviton interactions. In this chapter we want to investigate the gluonic vertex corrections. Moreover, there are of course gluon corrections to the running of the graviton propagator. These Yang–Mills corrections to the graviton two and three–point function split in an analog way as the gravity corrections to Yang–Mills theory in the last chapter, since for any n-point function the structure is

$$\text{Flow}^{(nh)} = \triangle_h \text{Flow}^{(nh)} + \triangle_A \text{Flow}^{(nh)}, \tag{8.1}$$

with pure graviton contributions $\triangle_h \text{Flow}^{(nh)}$ and the gluon induced term $\triangle_A \text{Flow}^{(nh)}$. In diagrammatic language the Yang–Mills contributions are given in Figure 8.1 and Figure 8.2.

A generic beta-function for the gravitational coupling including Yang-Mills corrections is then of the form

$$\partial_t g = 2g + g^2 \left(A_h(\lambda^{(n)}) + \eta_h B_h(\lambda^{(n)}) + C_A + \eta_A D_A \right), \tag{8.4}$$

where A_h and B_h originate in pure graviton contributions while C_A and D_A are generated by diagrams with internal gluon propagators. These gluon–induced corrections are the direct Yang–Mills contributions i.e. the Yang–Mills contributions to the running of the three-point function. We also assume momentum-independent anomalous dimensions throughout

$$\triangle_A \text{Flow}^{(2h)} = -\frac{1}{2} \quad \text{[diagram]} \quad + \quad \text{[diagram]} \tag{8.2}$$

Figure 8.1.: Diagrammatic depiction of the gluon contributions to the flow of the graviton propagator. The wiggly lines are gluon propagators, and the double line represent graviton propagators.

$$\triangle_A \text{Flow}^{(3h)} = -\frac{1}{2} \quad \text{[diagram]} \quad + 3 \quad \text{[diagram]} \quad - 3 \quad \text{[diagram]}$$

$$\tag{8.3}$$

Figure 8.2.: Diagrammatic depiction of the gluon contributions to the flow of the graviton three–point function. The wiggly lines are gluon propagators, and the double line represent graviton propagators.

this chapter. Moreover, the Yang–Mills contributions to the graviton propagator enter the above beta-function (8.4) via the graviton anomalous dimension η_h and the flow of the gap-parameter $\mu = -2\lambda^{(2)}$. These equations have the general form

$$\eta_h = g(E_h(\lambda^{(n)}) + \eta_h F_h(\lambda^{(n)}) + G_A + \eta_A H_A) \tag{8.5}$$

and

$$\partial_t \mu = -2\mu + \eta_h \mu + g(I_h(\lambda^{(n)}) + J_h(\lambda^{(n)})\eta_h + K_A + \eta_A L_A), \tag{8.6}$$

where again all pure gravity contributions are labeled with an index h and the one generated by gluons with an index A. Note that all the Yang–Mills contributions do not depend on μ, as the corresponding diagrams do not involve graviton propagators, see Figure 8.1 and Figure 8.2. In particular, this implies that these terms have no $1/(1 + \mu)$ singularity in the limit $\mu \longrightarrow -1$. Furthermore, in contrast to the gravity corrections to the running of the gauge coupling, all these diagrams contain a closed gluon loop and hence all the factors in the above equations with an index A are proportional to $N_c^2 - 1$.

8.1.1. Contributions to the Propagator

The gluon contribution to the graviton propagator has already been studied in a derivative expansion around $p = 0$ in [143]. However, the author has already found that this projection is insufficient due to the non-trivial momentum-dependence of the flow, which is
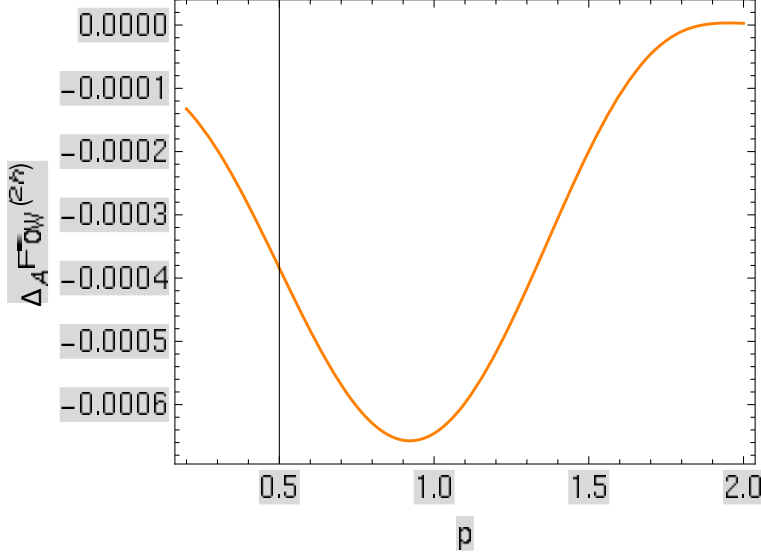
Figure 8.3.: The momentum dependence of $\triangle_A \mathrm{Flow}^{(2h)}$ for $\eta_A = 0$ on the right-hand side of the flow.

characterized by a dip at $p \approx k$. We have shown in [1], see also subsection 5.5.1, that this structure is resembled by the full flow, i.e. by the graviton contributions and that projections at momentum scales close to the cutoff are necessary. We have re-derived the momentum dependence of $\triangle_A \mathrm{Flow}^{(2h)}(p^2)$ and the result is depicted in Figure 8.3.

As in the setup in the last section, we use an optimized cutoff. For the the projection at $p = 0$, we re-derive the result in [143] and obtain for the momentum independent part

$$\triangle_A \mathrm{Flow}^{(2h)}(p^2 = 0) = (N_c^2 - 1)\frac{1}{60\pi}\eta_A. \tag{8.7}$$

Surprisingly, this contribution is proportional to η_A. This, however, is only the case for an optimized regulator. The momentum dependent part in a general finite difference projection is of the form

$$\frac{\triangle_A \mathrm{Flow}^{(2h)}\Big|_{p=p_\star} - \triangle_A \mathrm{Flow}^{(2h)}(p^2)\Big|_{p=p_\bullet}}{p_\star^2 - p_\bullet^2} = g Z_h (N_c^2 - 1)(\alpha_{p_\star,p_\bullet} + \beta_{p_\star,p_\bullet}\eta_A), \tag{8.8}$$

where $\alpha_{p_\star,p_\bullet}$ and $\beta_{p_\star,p_\bullet}$ depend on the specification, but once the latter is fixed are pure numbers. This is rooted in the fact that there are only internal gluon propagators and graviton-gluon vertices and both do not depend on $\lambda^{(n)}$. For $p_\bullet = 0$ and $p_\star \longrightarrow p_\bullet$, i.e. a derivative at $p = 0$, we obtain

$$\alpha = \beta = -\frac{1}{12\pi} \approx -0.027. \tag{8.9}$$

Due to the momentum strucutre of thre flow, the sign of $\alpha_{p_\star,p_\bullet}$ and $\beta_{p_\star,p_\bullet}$ changes for optimized specifications with $p_\star \approx k$. More precisely, we obtain for the derivative at $p = k$

$$\alpha \approx 0.54. \tag{8.10}$$

and

$$\beta \approx -0.3. \tag{8.11}$$
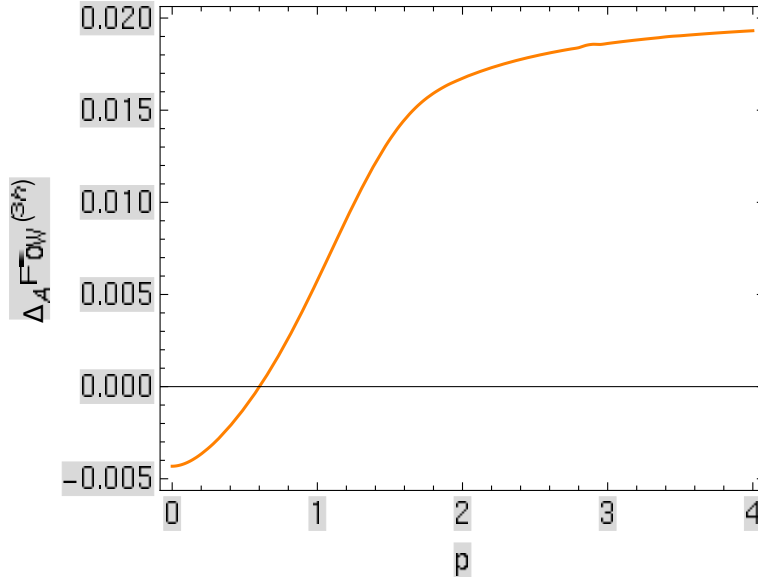
Figure 8.4.: The momentum dependence of $\triangle_A\text{Flow}^{(3h)}$ for $\eta_A = 0$ on the right-hand side of the flow.

8.1.2. Contributions to the Three–Point Function

The contributions to the three–point function enter the general equation (5.124) for the beta–function of the gravitational coupling g as additional terms in the function $F_{G/\Lambda,\phi}(p_i, q, G_n, \Lambda_n)$, since this encodes the right-hand side of the flow equation. Now the sum over the fields includes the gluon field A. As usual, in order to get reliable results, an analysis of the momentum dependence is necessary. For this task we resolve the full momentum dependence of the contributions $\triangle_A\text{Flow}^{(3h)}(p^2)$. The only approximation is that we drop the momentum-dependence of the gluon wave–function renormalization under the loop integrals. The result is shown in Figure 8.4.

Interestingly, the contributions to the three point function are in the cutoff regime $p \lesssim k$ very well approximated by a function $c_1 + c_2 p^2$ with constants c_1 and c_2. We also note that this behavior is independent of η_A. Therefore, results are quite independent from the specification procedure, since any derivative or finite difference with arbitrary $p_\star$ and $p_\bullet$ in (5.124) just returns the coefficient c_2 and the quadratic approximation to the flow is sufficient in this case. As a result, we obtain

$$\frac{\triangle_A\text{Flow}^{(3h)}\Big|_{p=p_\star} - \triangle_A\text{Flow}^{(3h)}(p^2)\Big|_{p=p_\bullet}}{p_\star^2 - p_\bullet^2} = g^{\frac{3}{2}} Z_h^{\frac{3}{2}}(N_c^2 - 1)(\gamma + \delta\eta_A), \qquad (8.12)$$

where γ and δ are almost independent of $p_\star$ and $p_\bullet$ and

$$\gamma \approx 0.3, \qquad (8.13)$$

and

$$\delta \approx -0.1. \qquad (8.14)$$

Remark on Locality

At this point we add the important remark, that $\triangle_A \text{Flow}^{(2h)}$ as well as $\triangle_A \text{Flow}^{(3h)}$ tend to constants in the limit $p \longrightarrow \infty$, see Figure 8.3 and Figure 8.4. As a consequence, these terms do not spoil locality of the flow of the graviton two- and three–point function, which was proven in subsection 5.5.1 and subsection 5.8.1. In summary, we assert

$$\lim_{p \to \infty} \frac{\partial_t \Gamma^{(2h,3h)}_{G,\text{Gravity+YM}}(p)}{\Gamma^{(2h,3h)}_{G,\text{Gravity+YM}}(p)} = 0 \,, \tag{8.15}$$

i.e. the full flows of the graviton two- and three–point functions including Yang–Mills corrections are local in the sense defined in section 5.2.

8.1.3. Large N limit

As the above calculations are only preliminary results, we do not aim at a complete analysis of the impact of the Yang–Mills contributions on the fixed point structure. However, we note the positive sign of the leading term γ in (8.12). In turn, this term contributes with a positive sign to the running of the gravitational coupling via C_A in (8.4). In a large N-limit, gluonic fluctuations dominate the loop contributions. This is intuitively clear and is quantified by $\triangle_A \text{Flow}^{(3h)} \sim N_c^2$. As a consequence, we obtain in a large N limit a positive loop contributions to the beta function, see (8.4), and a first guess is

$$\dot{g} = 2g + g^2 \left(\text{loop contributions}\right) \overset{N_c \to \infty}{\approx} 2g + g^2 C_A \,, \tag{8.16}$$

with $C_A > 0$. This implies that the the fixed point condition cannot be satisfied for positive Newton constant.

Part III.

The Quark Gluon Plasma and Transport Coefficients

Basics

9.1. Heavy Ion Collisions, The Quark–Gluon Plasma and Transport Phenomena

Quantum Chromodynamics has proven to be a very powerful theoretical framework for the description of strong interactions. It is the accepted theory of quarks and gluons and is part of the standard model of particle physics. The theory shows striking properties such as confinement, chiral symmetry breaking and asymptotic freedom. These mechanisms lead to a very rich phenomenology and a very interesting phase diagram, whose global structure is still unknown, [144, 145]. In equilibrium, the partition function of QCD depends on the external parameters temperature T and quark-chemical potential μ. Therefore, the phase diagram can be visualized in a two-dimensional plane, see Fig. 9.1.

One of the most interesting and most investigated aspect is the confinement-deconfinement phase transition at the critical temperature T_c. More precisely, it is a first order phase transition in pure Yang–Mills theory, while it is crossover in full quantum chromodynamics. Since this is the relevant feature for this thesis, I will focus in the following exclusively on this property. At temperatures below T_c, quarks and gluons are confined into hadronic bound states, which are the effective degrees of freedom of low energy QCD. This regime is inherently non-perturbative and therefore requires suitable methods such as lattice QCD, functional methods or effective models. For temperatures above the critical temperature, quarks and gluons exist as unbound color-charged particles in the the quark-gluon plasma (QGP). Additionally, for very high temperatures when all relevant momenta are sufficiently large, the coupling gets small and perturbation theory becomes applicable since all quantities can be expanded in a power series in the coupling.

Experimental access to the phase diagram can be gained with heavy ion collisions in particle accelerators. The heavy ion programs at RHIC [147, 148] and at the LHC [149] explore the physics of the quark-gluon plasma. In order to understand the relevance of transport coefficients, in particular of the shear viscosity, I briefly discuss the phenomenology of heavy ion collisions. A heavy ion collision is a time-dependent process that can be divided
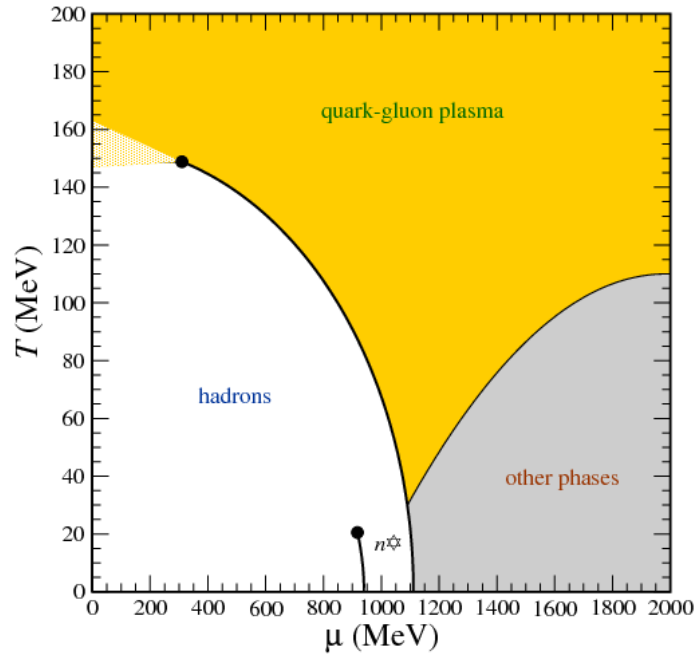
Figure 9.1.: Possible sketch of the phase diagram of QCD. Figure taken from [146].

into several stages. Schematically, the time-evolution is depicted in Fig. 9.2.
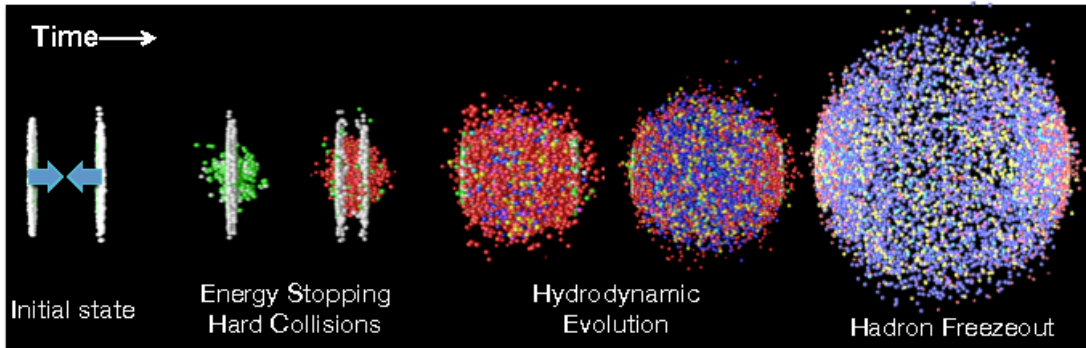
Figure 9.2.: Time evolution of a heavy ion collision. Figure taken from [150].

The heavy ions collide at very high energy as Lorentz-contracted pancakes. In this collision the partons interact in a complicated way and form a quark-gluon plasma heavily out of equilibrium. Experimental data indicates that this state of matter equilibrates on time scales of $t_{eq} \approx 1\text{fm}/c$. As the matter expands further, it cools down, reaches the critical temperature and hadronizes. Interestingly, the phase transition temperature coincides with the chemical freezout, [151]. Finally, these hadrons escape the collision vertex further and reach the detector. However, we can gain information about the quark gluon plasma, i.e. the intermediate stage of the evolution, by studying the elliptic flow coefficients, which arise due to breaking of spherical symmetry of the collision. Fig. 9.3 shows the geometry of a heavy ion collision. Usually the nuclei do not collide head-on, but with a finite impact parameter b.

Therefore, only matter in an almond-shaped, or almost elliptical, area gets compressed and heated up, see Fig. 9.4.
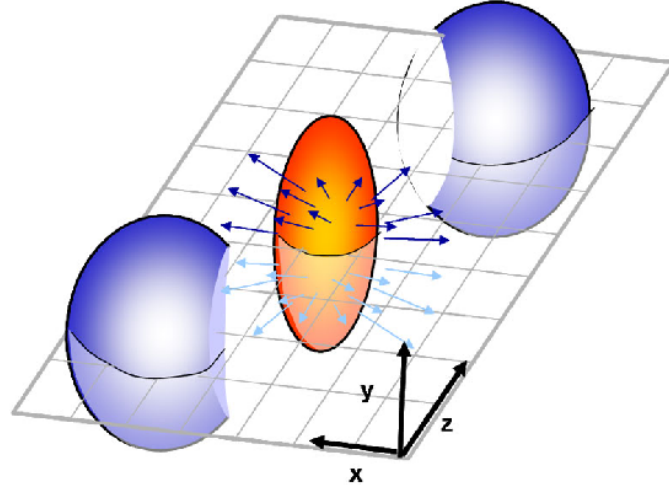
Figure 9.3.: The x-z reaction plane in a heavy ion collision. The plane is spanned by the beam direction z and the vector of the impact parameter b. The figure is taken from [152].
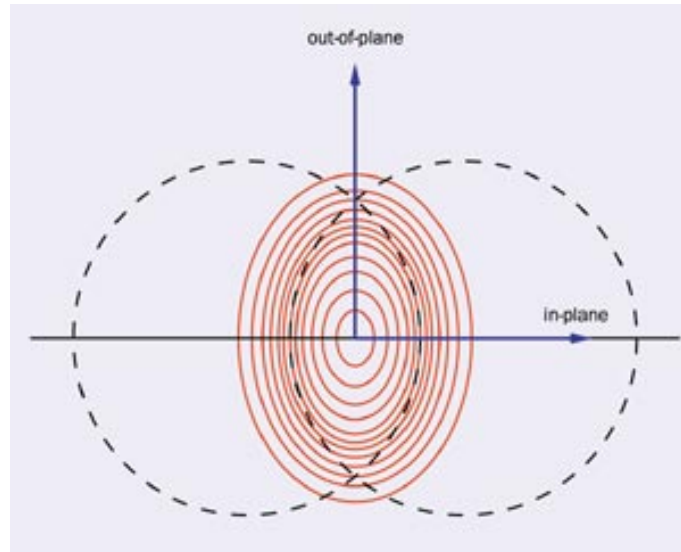
Figure 9.4.: The almond-shaped collision region in a non-central heavy ion collision. Figure taken from www.cerncourier.com.

Because of the gradients in this spatial anisotropy of the initial state, the final state shows a corresponding momentum anisotropy. This momentum anisotropy can be quantified with the anisotropic flow coefficients v_n. These coefficients are defined by a Fourier expansion of the momentum distribution in terms of the angle between the direction in the reaction plane and the the out-of plane direction. The first coefficient v_1 in this expansion is known as the directed flow, while the second coefficient v_2 is called the elliptic flow. The elliptic flow is one of the most important observables in heavy-ion collisions and is directly related with

transport coefficients. Having in mind the picture of the hot and dense matter as a plasma, one might be tempted to describe the collective behavior of the system with hydrodynamics. And indeed, experimental results indicate that the expansion of the many-body system created in heavy-ion collisions is well-described by hydrodynamics. However, at high p_T ideal hydrodynamics fails and viscous effects need to be taken into account. The dynamics of the expansion of a plasma depends on the transport coefficients as a measure for the deviation from ideal hydrodynamics. Consequently, the asymmetry in momentum space can be related to the transport coefficients of the plasma. And indeed, it turns out that viscous hydrodynamics fits the observed data quite well, [153–155]. Therefore, the determination of transport coefficients in the QGP is of great interest. In particular, the shear viscosity is the quantity that is directly related to the data of v_2 extracted from experiment, [156–159]. More precisely, it is the viscosity over entropy ratio η/s that is directly proportional to the efficiency of the conversion of the initial spatial anisotropy into a momentum anisotropy of the final state.

Moreover, experimental data show that the quark gluon plasma close to the critical temperature is governed by a very small value for η/s, meaning that it is very close to a perfect fluid. Since the viscosity is proportional to the mean free path, which in turn is inversely proportional to the cross section, these results indicate that the quark gluon plasma is strongly coupled close to the phase transition.

The viscosity over entropy ratio η/s is not only of great phenomenological interest, but it is also a fascinating playground for purely theoretical considerations. As we have already mentioned above, the high temperature regime $T \gg T_c$ is governed by a small coupling and can be described by perturbative techniques such as hard thermal loop resummations. However, since the QGP behaves non-perturbatively in the vicinity of the critical temperature, where the minimum for η/s is expected [160, 161], other methods are necessary in order to describe the quark gluon plasma over a range of temperatures from below T_c up to the weakly coupled regime. A universal lower bound for η/s of $1/4\pi$ was conjectured in [162] using the AdS/CFT correspondence. Indeed, measurements of the elliptic flow v_2 indicate a value for η/s which is of the order of this lower bound [153]. The bound has been tested theoretically with several methods for the QGP [163–169], but also for other potentially perfect liquids, such as ultracold atoms [170–172].

However, the calculation of transport coefficients is a hard problem. The fluctuation-dissipation theorem relates the transport coefficients via Kubo relations to spectral functions of the energy–momentum tensor, which is inherently a real-time quantity and cannot be obtained directly from Euclidean correlation functions. However, the direct calculation of real-time correlation functions represents a notoriously difficult problem in non-perturbative approaches to quantum field theory such as lattice techniques and functional methods. Even though first computations in this direction have been performed e.g. in [173, 174], we shall utilize Euclidean correlation functions and a numerical analytic continuation.

9.1.1. The strategy

In this part of the thesis we study the shear viscosity over entropy ratio η/s in pure $SU(3)$ Landau gauge Yang-Mills (YM) theory within the approach set-up in [163]. We considerably generalize the approach, also aiming at quantitative precision. We use a Kubo relation in order to express the viscosity of the non-Abelian plasma in terms of a two–point correlation

function of the energy-momentum tensor (EMT) and apply an exact functional relation that allows a representation of this correlation function in terms of full propagators and vertices of the gluon field. We use a real-time representation of this EMT-correlator, and consequently it involves real-time gluon propagators that can be expressed in terms of their spectral functions. These gluon spectral functions are obtained from Euclidean propagators via analytic continuation with maximum entropy methods, [175]. We are then left with loop–integrals at finite temperature over the spectral functions, internal gluon vertices and an external vertex that couples the EMT to the gluons. As a result, we obtain the shear viscosity η as a function of temperature. Combining this with lattice data for the entropy, we calculate the famous η/s ratio. Finally, we use these results in pure Yang–Mills theory in order to estimate the viscosity over entropy ration in full QCD.

The analysis covers the entire temperature range from the glueball regime below the critical temperature T_c, up to the ultraviolet where perturbation theory is applicable. In particular, this resolves the non-perturbative domain at temperatures $T \lesssim 2T_c$. We provide a global, analytic fit formula for η/s which extends the well-known perturbative high-temperature behavior to the non-perturbative temperature regime.

9.2. Hydrodynamics

In this section we give a brief summary of the most important concepts and equations necessary for understanding hydrodynamics in the context of heavy-ion collisions and the quark-gluon plasma. Since we need a relativistic formulation in order to describe heavy-ion collisions, we focus on relativistic hydrodynamics.

9.2.1. Ideal Hydrodynamics

A (quantum) many-body system can be described as a continuum if the fluid approximation is valid. This means that, small volume elements are characterized by constant physical quantities. In particular, the ensemble is in local thermal equilibrium.

In order to match these conditions, one must be able to establish the following hierarchy of scales in the system. Let l_{MFP} be the mean-free path of the particles, L the overall macroscopic scale and l the scale of the fluid elements. Then, for hydrodynamics to be applicable the hierarchy

$$l_{\mathrm{MFP}} \ll l \ll L, \tag{9.1}$$

must hold. This translates to the statement that after small external perturbations the relaxation time is much smaller than any other typical time scale of the system. The underlying microphysics can be understood in terms of (quantum) kinetic theory, where the above conditions mean that the underlying phase-space distributions are given by, or immediately relax to the equilibrium distributions.

The hydrodynamic equations are then consequences of conservation laws. The conserved quantities are given by the energy-momentum tensor T and the conserved charges J. For an energy-momentum tensor $T_{\mu\nu}$ and conserved currents J_μ the conservation laws take the form

$$\partial_\mu T^{\mu\nu} = 0 \quad , \quad \partial_\mu J^\mu = 0. \tag{9.2}$$

The energy-momentum tensor can now be expanded in derivatives. Ideal hydrodynamics, i.e. the local equilibrium assumption, implies that T and J do not contain any derivatives, which means that ideal hydrodynamics corresponds to a zeroth order derivative expansion. Moreover, in a relativistic formulation, Lorentz invariance dictates the general form of these objects, once the hydrodynamic variables are specified. In the relativistic case a convenient choice for the hydrodynamic variables is the energy density ϵ, pressure p, the fluid four-velocity $u_\mu = (\gamma, \gamma v)_\mu$ with $u^\mu u_\mu = 1$, and the local charge density n that describes the conserved currents. Therefore, the only covariant tensors at hand are u^μ and the metric $g^{\mu\nu}$. Additionally, in the local rest frame, the component T^{00} should be the energy density and the momentum density vanishes, while the spacelike components are simply the pressure. With these requirements the energy-momentum tensor for an ideal relativistic fluid reads

$$T_0^{\mu\nu} = (\epsilon + p)u^\mu u^\nu - p\, g^{\mu\nu} = \epsilon u^\mu u^\mu - p\mathscr{P}^{\mu\nu}\,, \tag{9.3}$$

with the transeverse projector

$$\mathscr{P}^{\mu\nu} = g^{\mu\nu} - u^\mu u^\nu\,. \tag{9.4}$$

The conserved currents can be written as

$$J^\mu = nu^\mu\,. \tag{9.5}$$

Using the above expressions in the conservation laws, one can write down the fluid equations

$$u^\mu \partial_\mu \epsilon = -(\epsilon + p)\partial_\mu u^\mu \tag{9.6}$$

and

$$u^\mu \partial_\mu n = -n\partial_\mu u^\mu\,. \tag{9.7}$$

In the non-relativistic limit the above equations reduce to the well-known continuity equation and the Euler equation. Due to the normalization condition for the fluid four-velocity, the above equations actually constitute only five independent relations for six unknowns. The system of equations is then closed with the equation of state (EoS) $p(\epsilon, n)$, that relates pressure, energy density and number density. Moreover, we note that entropy is a conserved quantity in ideal hydrodynamics. More precisely, the covariant entropy current $s^\mu = su^\mu$ is conserved. This can be seen as follows. Using $s = (\epsilon + p)/T$, the divergence of the entropy current can be written as

$$\partial_\mu s^\mu = u^\mu \frac{1}{T}\partial_\mu(\epsilon + p) + u^\mu(\epsilon + p)\partial_\mu \frac{1}{T} + \frac{\epsilon + p}{T}\partial_\mu u^\mu\,. \tag{9.8}$$

Now we compare this with the spatial derivative of the energy momentum tensor in the direction of the fluid velocity

$$\begin{aligned} u_\nu \partial_\mu T^{\mu\nu} &= u_\nu u^\nu u^\mu \partial_\mu(\epsilon + p) + (\epsilon + p)u_\nu \partial_\mu(u^\mu u^\nu) - u^\mu \partial_\mu p \\ &= u^\mu \partial_\mu(\epsilon + p) + (\epsilon + p)\partial_\mu u^\mu + u^\mu(\epsilon + p)T\partial_\mu \frac{1}{T}\,, \end{aligned} \tag{9.9}$$

where we have used the normalization of the fluid four-velocity and that $u_\nu \partial_\mu u^\nu = 0$, which follows from $\partial_\mu(u^\nu u_\nu) = 0$. Additionally, we have utilized the Gibbs Duhem relation in order to rewrite the derivative of p in terms of a derivative of $1/T$

$$\mathrm{d}p = -(\epsilon + p)T\,\mathrm{d}\left(\frac{1}{T}\right)\,. \tag{9.10}$$

Putting the pieces together we arrive at

$$\partial_\mu s^\mu = \frac{1}{T} u_\nu \partial_\mu T^{\mu\nu} = 0 \,, \tag{9.11}$$

because of the conservation law for the energy momentum tensor. This saturates the bound given by the second law of thermodynamcis which states

$$\partial_\mu s^\mu \geq 0 \,. \tag{9.12}$$

Including dissipative effects, i.e. in viscous hydrodynamics, the entropy is no longer conserved and strictly larger than zero. In order to include these dissipative effects, one needs to take into account derivative terms in the energy momentum tensor.

9.2.2. Viscous Hydrodynamics

Dissipative effects correspond to small perturbations from local equilibrium. On the microscopic level this means that the phase space distribution functions deviate from its equilibrium form. On the level of the effective description in terms of hydrodynamics, they appear as additional terms proportional to derivatives of the fluid velocity in the energy-momentum tensor. Neglecting the heat conductivity, the leading order modifications define the transport coefficients shear-viscosity η and bulk-viscosity ζ that enter the energy-momentum tensor as

$$T_1^{\mu\nu} = -\eta\, \theta^{\mu\alpha}\theta^{\nu\beta} \left(\partial_\alpha u_\beta + \partial_\beta u_\alpha - \frac{2}{3} \eta_{\alpha\beta} \partial\gamma u^\gamma \right) - \zeta \theta^{\mu\nu} \partial_\gamma u^\gamma \,, \tag{9.13}$$

with

$$\theta^{\mu\nu} = \eta^{\mu\nu} + u^\mu u^\nu \,. \tag{9.14}$$

The total energy momentum tensor up to first order is then given by

$$T^{\mu\nu} = T_0^{\mu\nu} + T_1^{\mu\nu} \,. \tag{9.15}$$

Intuitively, the shear viscosity describes the friction force between neighbouring fluid layers that move with relative speed to each other. Thus it is plausible that

$$\eta \sim \text{density} \times \text{velocity} \times l_{\text{MFP}} \,. \tag{9.16}$$

From a microscopic point of view, the mean free path is inversely proportional to the cross section, which in turn is directly proportional to the coupling strength. Therefore, we conclude that $\eta \sim 1/f(g)$, where f is some monotonically increasing function.

9.2.3. Linear Response Theory, the Fluctuation Disspiation Theorem and Kubo relations

The main goal of this part of the thesis is the calculation of the viscosity over entropy ratio η/s in the quark-gluon plasma. For this task it is necessary to find a way to determine η/s in a non-Abelian plasma from the microscopic, underlying quantum field theory. As we have already mentioned, in this work we want to make use of the Kubo formulas, which are based

on the fluctuation-dissipation theorem and linear response theory and relate correlation functions to transport coefficients.

Linear response theory is applicable if a medium is subject to a small perturbation that drives the system slightly out of equilibrium, i.e. if the answer to the small disturbance is a also only a small effect.

Assume we perturb the system with a real, external source field $\tilde{\xi}(x^0, x) = \epsilon\,\xi(x^0, x)$. We further assume, as we are interested in linear response, that the change of any expectation value of an essentially self-adjoint operator A is linear in ξ, or to put it differently, we assume $\epsilon \ll 1$ and ignore higher order terms in the external perturbation and work in a linear approximation. Hence, we can infer the perturbation to take the form

$$\delta\langle A(x^0, x)\rangle := \langle A(x^0, x)\rangle\big|_{\xi} - \langle A(x^0, x)\rangle\big|_{\xi=0} = \int \mathrm{d}^3x'\mathrm{d}x'^0\, \mathcal{R}(x^0, x, x'^0, x')\,\tilde{\xi}(x'^0, x'),$$

(9.17)

where we have defined the kernel $\mathcal{R}(x^0, x, x'^0, x')$. This kernel is called the response function. Additionally, we want the system to be translation invariant. In this case the response function can only depend on the differences $x^0 - x'^0$ and $x - x'$. In this case, (9.17) is the convolution $\mathcal{R} * \tilde{\xi}$ and the Fourier transform $\mathscr{FT}[\cdot]$ of the same is just the pointwise product. Consequently, we get

$$\mathscr{FT}\left[\delta\langle A(x^0, x)\rangle\right] = \delta\langle A(p^0, p)\rangle = \mathcal{R}(p^0, p)\,\tilde{\xi}(p^0, p).$$

(9.18)

This implies that the response is ultra-local in momentum space: if we perturb the system with frequency p^0, then the deviation is also characterized by the very same frequency. Non-local effects can only be described within non-linear response theory. Since the external source field ξ and the expectation of A are mappings to the real numbers, the response function $\mathcal{R}(x^0 - x'^0, x - x')$ must also be real-valued. However, the Fourier transform will be complex,

$$\mathcal{R}(p^0, p) = \operatorname{Re}\mathcal{R}(p^0, p) + i\operatorname{Im}\mathcal{R}(p^0, p).$$

(9.19)

Let us now investigate the physical interpretation of the response function. Obviously, the imaginary part can be written as

$$\begin{aligned}
\operatorname{Im}\mathcal{R}(p^0, p) &= -\frac{i}{2}\left(\mathcal{R}(p^0, p) - \mathcal{R}^*(p^0, p)\right) \\
&= -\frac{i}{2}\int \mathrm{d}x^0 e^{ip^0 x^0}\left(\mathcal{R}(x^0, p) - \mathcal{R}(-x^0, p)\right).
\end{aligned}$$

(9.20)

Thus we can infer that the imaginary part of the response function arises due to effects that are not invariant under the transformation $t \longrightarrow -t$, i.e. not invariant under time reversal. Microscopic laws of physics, such as fundamental scattering processes, are typically invariant under time reversal. However, it is well-known that dissipative effects are not invariant under this transformation. Therefore, the imaginary part of the response function is also called its dissipative part. The relation to n-point functions in quantum field theory will become clear below.

Let us now shortly comment on causality and its implications for the response function. Causality means that any action cannot affect the past. In our case, this means that the

system reacts only to perturbations that are in the past relative to the time of observation. Mathematically, this causality condition translates into

$$\mathscr{R}(x^0, x) = 0 \quad \forall \ x^0 < 0. \tag{9.21}$$

This implies some important properties for the Fourier transform. We Fourier transform the zero-component according to

$$\mathscr{R}(x^0, \cdot) = \mathscr{F}\mathscr{T}\{\mathscr{R}(p^0, \cdot)\} = \int_{\mathbb{R}} \frac{\mathrm{d}p^0}{2\pi} e^{-ip^0 x^0} \mathscr{R}(p^0, \cdot). \tag{9.22}$$

Furthermore, we assume a sufficiently fast decaying response functions in momentum space. More precisely, we require any response function to have the property

$$\mathscr{R}(p^0, \cdot) \overset{p^0 \to \infty}{\leq} \frac{1}{p^0}. \tag{9.23}$$

Then we can analytically continue the integral and for $t < 0$ close the the contour in the upper-half of the complex plane. Due to the causality condition (9.21), this integral must be zero. By the residue theorem we can then conclude that the response function has no poles in the upper-half of the complex plane, i.e. $\mathscr{R}(p^0, \cdot)$ is an analytic function of its first argument on $\mathscr{H}^+$. Therefore, the causality condition implies analyticity and vice versa.

This analyticity property ensures relations between the real and imaginary parts of the response function, namely the Kramers-Kronig relations, which are well-known as an expression of causality. By standard calculus in complex analysis, we obtain the Kramer-Kronig relations as

$$\operatorname{Re}\mathscr{R}(p^0, \cdot) = \mathscr{P} \int_{\mathbb{R}} \frac{\mathrm{d}p'^0}{\pi} \frac{\operatorname{Im}\mathscr{R}(p'^0, \cdot)}{p'^0 - p^0}, \tag{9.24}$$

and

$$\operatorname{Im}\mathscr{R}(p^0, \cdot) = -\mathscr{P} \int_{\mathbb{R}} \frac{\mathrm{d}p'^0}{\pi} \frac{\operatorname{Re}\mathscr{R}(p'^0, \cdot)}{p'^0 - p^0}, \tag{9.25}$$

where $\mathscr{P}\int$ denotes the principal value. Using the Sokhotskj-Plemelj theorem, we can obtain the important equation

$$\mathscr{R}(p^0, \cdot) = \lim_{\epsilon \to 0} \int_{\mathbb{R}} \frac{\mathrm{d}p'^0}{\pi} \frac{\operatorname{Im}\mathscr{R}(p'^0, \cdot)}{p'^0 - p^0 - i\epsilon}, \tag{9.26}$$

which tells us that the entire response function can be reconstructed from its dissipative part.

Now we proceed with the derivation of the fluctuation dissipation relation from the basic assumptions of linear response theory. We write the perturbation to the Hamiltonian as

$$H_{\mathrm{pert}} = \epsilon \xi A, \tag{9.27}$$

with $\epsilon \ll 1$ being the control parameter of perturbation theory. Furthermore we assume that the perturbation is switched off in the limits $x^0 \longrightarrow \pm\infty$, i.e. H_{pert} is an operator with compact domain in x^0, e.g. $H_{\mathrm{pert}}(x^0) = 0$ if $x^0 < x_i$ or $x^0 > x_f$. Expectations in presence of

the source are labeled with the field ξ. The time evolution operator that evolves interaction picture states from x_0^0 to x^0 is then constructed as

$$U(x^0, x_0^0) = T e^{-i \int_{x_0^0}^{x^0} dx'^0 H_{\text{pert}}(x'^0)}. \tag{9.28}$$

We now take the limit $x_0^0 \longrightarrow -\infty$, such that the system is unperturbed at x_0^0 according to our assumptions, and we further consider times $x^0 > x_i$ The density matrix evolves as

$$\rho(x^0) = U(x^0, -\infty) \rho(x_0^0) U^\dagger(x^0, -\infty). \tag{9.29}$$

Then we can use the cyclicity of the trace and the time evolution in order to express the expectation of an operator A at x^0 in terms of the unperturbed expectation and a deviation in first order perturbation theory according to

$$\begin{aligned}
\langle A(x^0, \cdot) \rangle \big|_\xi &= \text{Tr} \rho(x^0) A(x^0) \\
&= \text{Tr} \rho(x_0^0) U(x^0, -\infty) A(x^0) U^\dagger(x^0, -\infty) \\
&= \langle A(x^0, \cdot) \rangle \big|_{\xi=0} + i \int_{-\infty}^{x^0} dx'^0 \, \langle [H_{\text{pert}}(x'^0), A(x^0)] \rangle \big|_{\xi=0} + \mathcal{O}(\epsilon^2)
\end{aligned} \tag{9.30}$$

Therefore the change in the operator defined in (9.17) is given by

$$\delta \langle A(x^0, x) \rangle = i\epsilon \int_{-\infty}^{\infty} \theta(x^0 - x'^0) \, \langle [A(x'^0), A(x^0)] \rangle \big|_{\xi=0} \, \xi(x'^0), \tag{9.31}$$

where the theta function is introduced in order to extend the range of integration to $+\infty$. Comparing this with the definition of the response function in (9.17), we obtain

$$\mathcal{R}(x^0, x, x'^0, x') = -i\theta(x^0 - x'^0) \, \langle [A(x^0, \cdot), A(x'^0, \cdot)] \rangle \big|_{\xi=0}. \tag{9.32}$$

We see that the response function is nothing but the retarded Greens function without presence of an external source. The above equation (9.32) is a version of the fluctuation dissipation theorem, as it relates the response function, i.e. the central quantity of linear response theory, to correlation functions, which describe fluctuations. From the fluctuation dissipation theorem it is still a quite lengthy, and a bit tedious, calculation leading to explicit Kubo-relations for transport coefficients, [176–178]. In this work we need the Kubo relation for the shear viscosity, which will be presented below.

Shear Viscosity in Yang–Mills Theory and QCD

As we have already mentioned, the main goal in this part of the thesis is the computation of the viscosity over entropy ratio η/s in SU(3) Yang–Mills theory and full QCD. We will compute the former explicitly and gain access to the latter by an appropriate transformation procedure.

10.1. The Strategy in more detail

In this section we want to present our strategy and the technical setup for calculating the the viscosity over entropy ratio in Yang–Mills theory in some detail.

The Kubo Relation

From the fluctuation dissipiation theorem, one can derive the Kubo relation for the shear viscosity, which is given by

$$\eta = \lim_{\omega \to 0} \frac{1}{20} \frac{\rho_{\pi\pi}(\omega, \vec{0})}{\omega}, \tag{10.1}$$

where

$$\rho_{\pi\pi}(\omega, \vec{p}) = \int \frac{d^4x}{(2\pi)^4} e^{-i\omega x_0 + i\vec{p}\vec{x}} \langle [\pi_{ij}(x), \pi_{ij}(0)] \rangle, \tag{10.2}$$

is the spectral function of π_{ij}, which in turn is the spatial, traceless part of the energy-momentum tensor and reads

$$\pi_{ij}(x) = T_{ij} - \frac{1}{3}\delta_{ij}T^m_m. \tag{10.3}$$

We emphasize that the above Kubo formula contains an expectation in real-time that cannot simply be calculated in Euclidean field theory.

Given this relation, one needs to compute the spectral function of the energy-momentum tensor. In SU(3) gauge theory the spatial, traceless EMT in momentum space is explicitly given by

$$\pi_{ij}(p) = \text{tr}[F_{\mu i} * F^\mu_j](p) - \frac{1}{3}\delta_{ij}\text{tr}[F_{\mu m} * F^{\mu m}](p), \tag{10.4}$$

where $*$ denotes the convolution, as in the last section.

It is immediately clear that the energy-momentum tensor is a composite operator of the fundamental gluon field A. As a consequence, we need to compute correlation functions of composite operators.

The Magic Formula

A correlation function of a general composite operator $\Phi_{\mathbf{c}}[\varphi_{\mathbf{a}}]$ can be represented in terms of the fundamental field [32],

$$\langle \Phi_{\mathbf{c}}[\varphi_{\mathbf{a}}] \rangle = \Phi_{\mathbf{c}}[G_{\mathbf{ab}} \frac{\delta}{\delta \phi_{\mathbf{b}}} + \phi_{\mathbf{a}}], \tag{10.5}$$

where we remind the reader that $\phi = \langle \varphi \rangle$ is the expectation of the operator φ. The above equation can be interpreted as a generalized Dyson–Schwinger equation for composite operators. In order to get a feeling for this condensed representation, we apply it in an almost trivial case where the composite operator is just the two–point function of a scalar field,

$$\Phi_{ab}[\varphi] = \varphi_a \varphi_b . \tag{10.6}$$

In this case

$$\langle \Phi_{ab}[\varphi] \rangle = \left(G_{ac} \frac{\delta}{\delta \phi_c} + \phi_b \right) \left(G_{ad} \frac{\delta}{\delta \phi_d} + \phi_b \right) \mathbb{1} = G_{ab} + \phi_a \phi_b \tag{10.7}$$

which is of course a well-known expression. We have written out explicitly a $\mathbb{1}$ in the expression above, such that the derivative operators at the rightmost return zero. Usually this identity operator is dropped in the notation, but is always implicitly understood. In our study, we apply the magic formula (10.5) to the composite operator

$$\Phi_{ij}[\hat{A}] = \pi_{ij}[\hat{A}] \pi_{ij}[\hat{A}], \tag{10.8}$$

whose expectation is then given by

$$\langle \pi_{ij}[\hat{A}] \pi_{ij}[\hat{A}] \rangle = \pi_{ij}[G_{A\phi_k} \cdot \frac{\delta}{\delta \phi_k} + A] \pi_{ij}[G_{A\phi_k} \cdot \frac{\delta}{\delta \phi_k} + A], \tag{10.9}$$

where $\phi = (A, c, \bar{c})$ denotes the expectation value of the fluctuation (super-)field $\hat{\phi}$, e.g. $A = \langle \hat{A} \rangle$, and $G_{\phi_i \phi_j} = \langle \hat{\phi}_i \hat{\phi}_j \rangle - \langle \hat{\phi}_i \rangle \langle \hat{\phi}_j \rangle$ denotes the propagator of the respective fields. The energy–momentum tensor can then be expanded in powers of the gluon field, which is just a finite sum

$$\pi_{ij} = \sum_{n=2}^{4} \frac{1}{n!} \frac{\delta^n \pi_{ij}}{\delta A_{a_1} ... \delta A_{a_n}} A_{a_1} ... A_{a_n}, \tag{10.10}$$

where the derivatives of π with respect to the field are interpreted as vertices coupling the EMT to n gluon fields. Inserting this in (10.9) then yields a diagrammatic representation in terms of a finite number of diagrams involving full propagators and vertices, see Fig. 10.1 for the types of diagrams appearing in the full expansion up to two-loop order. As there are at most A^4 terms in the EMT π, the structure of (10.9) implies that the maximal loop order of the diagrams is six.

We emphasise that (10.9) is an exact relation whose finite diagrammatics should not be confused with a perturbative expansion in an infinite series of Feynman diagrams.
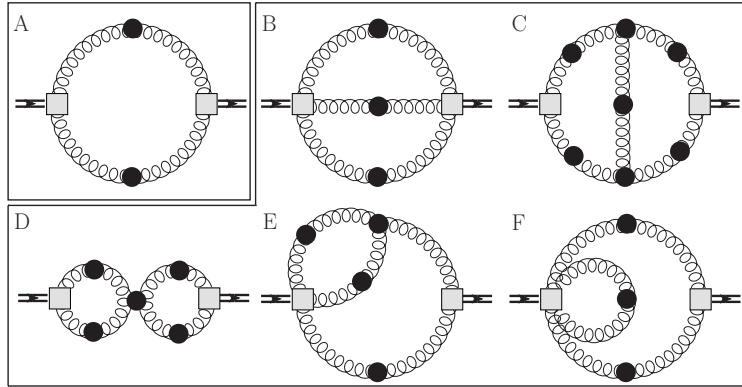
Figure 10.1.: Types of diagrams contributing to the correlation function of the energy momentum tensor up to two-loop order; squares denote vertices derived from the EMT; all propagators and vertices are fully dressed.

The propagators and internal vertices, which arise from functional derivatives of the full propagator in (10.9), are fully dressed. However, the RG-invariance of the left hand side of (10.9) only carries over to right hand side if also the external vertices derived from the EMT are dressed with appropriate wave-function renormalisation factors and running couplings. This argument is supported by the flow equation for the EMT itself, which can be derived from the flow equation for composite operators [32], where full vertices are generated during the flow. More heuristically, this can also be seen in a skeleton expansion. Therefore, on a diagrammatic level only up to 3-loop diagrams with dressed external vertices appear.

The Schwinger–Keldysh Formalism, Correlation- and Spectral Functions

As we are interested in the spectral function of the energy–momentum tensor, which is inherently a real–time object, the natural framework for such a calculation is the real-time formalism based on the Schwinger-Keldysh closed time path. Within such a setup one never has to resort to Euclidean field theory. The Schwinger–Keldysh formalism is capable of describing even non-equilibrium situations, [179–182]. The necessity of the closed time path arises due to the fact that in general situations, one cannot simply relate the Hilbert spaces at $t = -\infty$ and $t = +\infty$ in the sense that the vacuum states differ just by a phase factor, which is needed in order to construct the well-known path integral representation for S-matrix elements in zero-temperature quantum field theory. By implementing the Kubo-Martin-Schwinger (KMS) condition, the theory then describes a quantum field theory in equilibrium at finite temperature, [183–187]. We have seen in subsection 9.2.2 and subsection 9.2.3, that the transport coefficients can be calculated within linear response theory. In particular, this means that we have to consider only close-to-equilibrium situations and the correlation functions that enter the fluctuation dissipation relations can be calculated in thermal equilibrium. Hence, we deal with finite temperature field theory in the following. Note that one could also use the Euclidean Matsubara formalism for finite temperature field theories and apply an analytical continuation afterwords in order to gain a Minkowski-space correlation function. We will not do so and use the more elegant formulation in real-time.

In finite temperature field theory correlation functions of any operator A are quantum

statistical averages with the equilibrium density matrix ρ_{eq} defined as

$$\langle A \rangle := \frac{\text{Tr}\left\{\rho_{\text{eq}} A\right\}}{Z}, \tag{10.11}$$

with

$$\rho_{\text{eq}} = e^{-\beta H} \tag{10.12}$$

and with the inverse temperature $\beta := 1/T$ and the partition function $Z := \text{Tr}\,\rho_{\text{eq}}$.

In the real-time path integral formulation, the generating functional takes form

$$Z[J_C] = \int \mathrm{d}\phi_C\, e^{i \int_C \mathrm{d}x \left\{ \mathscr{L}(x) + J_C(x) \circ \phi_C(x) \right\}}, \tag{10.13}$$

where the fields live on the Keldysh contour C, whose non-trivial part, namely the time direction, is depicted in Figure 10.2.
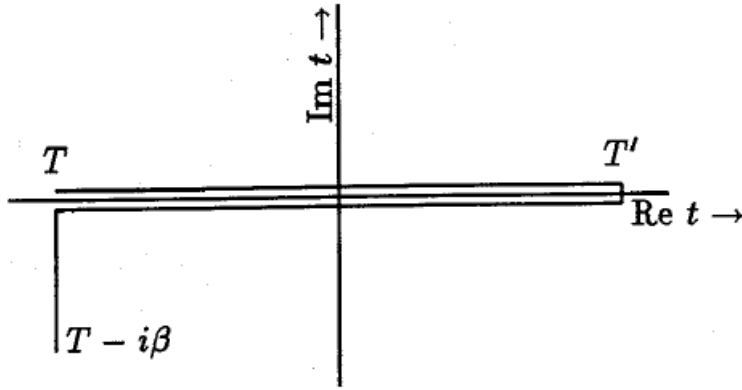
Figure 10.2.: The closed time path at finite temperature. Figure taken from [188].

The time path has the properties that it runs from $t = -\infty$ to $t = +\infty$, and is then reflected and runs backwards. It can be shown that the vertical segment factorizes and thus can be ignored, see [183, 188]. Nevertheless, the fact that we work at finite temperature is manifested in the KMS condition for correlation functions

$$\langle A(t)B(t') \rangle = \langle B(t')A(t + i\beta) \rangle, \tag{10.14}$$

see [183, 189]. The price to pay for the real-time formulation is the doubling of the Hilbert space and a corresponding doubling of field degrees of freedom. This doubling is also inherent to the formulation of real-time finite temperature correlation functions in thermofield dynamics, which is based on the definition of a thermal vacuum state and an operator algebra that reflects the thermal properties, [190–192]. In the closed time path formulation, one distinguishes two branches of the time contour, conventionally denoted

by $+/-$, along with separate fields and sources. Correlation functions thus become matrix valued, as there are correlations between fields defined on the different parts on the time contour, labeled by a corresponding branch index. For the two-point function

$$G = \begin{pmatrix} G_{++} & G_{+-} \\ G_{-+} & G_{--} \end{pmatrix}, \tag{10.15}$$

these components are defined by

$$
\begin{aligned}
G_{-+}(x,y) &:= -i \langle \varphi_-(x)\varphi_+(y)\rangle =: G_>(x,y) \\
G_{+-}(x,y) &:= -i \langle \varphi_-(y)\varphi_+(x)\rangle =: G_<(x,y) \\
G_{++}(x,y) &:= -i \langle T\varphi_+(y)\varphi_+(x)\rangle =: G_F(x,y) \\
G_{--}(x,y) &:= -i \langle \tilde{T}\varphi_-(y)\varphi_-(x)\rangle =: G_{\tilde{F}}(x,y),
\end{aligned}
\tag{10.16}
$$

where T denotes the time ordering operator and $\tilde{T}$ the anti-time ordering operator. Using the definition of the retarded propagator, one obtains

$$G_R(x,y) = G_{++}(x,y) - G_{+-}(x,y). \tag{10.17}$$

The spectral function is now defined as

$$\rho := G^{-+} - G^{+-}. \tag{10.18}$$

The entire theory of spectral representations in the real-time formalism is developed in Appendix K. This appendix is based on my internal notes, [193], which were already presented in similar fashion in [175]. As important results we state the relations

$$
\begin{aligned}
G^{\pm\pm}(\omega,\vec{p}) &= F(\omega,\vec{p}) \pm i\left(n(\omega)+\tfrac{1}{2}\right)\rho(\omega,\vec{p}), \\
G^{+-}(\omega,\vec{p}) &= -i\,n(\omega)\rho(\omega,\vec{p}), \\
G^{-+}(\omega,\vec{p}) &= -i\,(n(\omega)+1)\rho(\omega,\vec{p}),
\end{aligned}
\tag{10.19}
$$

where $n(\omega) = 1/(\exp(\omega/T)+1)$ denotes the Bose distribution function and $F(\omega,\vec{p})$ is given as a principal value integral,

$$F(\omega,\vec{p}) = PV \int\limits_{-\infty}^{\infty} d\bar{\omega}\, \frac{\rho(\bar{\omega},\vec{p})}{\omega - \bar{\omega}}. \tag{10.20}$$

It is important to note, that all elements of the propagator matrix can be expressed by the spectral function alone. Moreover, in thermal equilibrium the KMS relation relates the off-diagonal parts of the propagator via

$$G^{+-}(\omega,\vec{p}) = e^{-\beta\omega}G^{-+}(\omega,\vec{p}), \tag{10.21}$$

which is also proven in Appendix K. Hence we find for the spectral function of the energy momentum tensor

$$\rho_{\pi\pi}(\omega,\vec{p}) = (1 - e^{-\beta\omega})G^{-+}_{\pi\pi}(\omega,\vec{p}). \tag{10.22}$$

Inserting the above identity into (10.1), this implies

$$\eta = -\frac{\beta}{20} G_{\pi\pi}^{-+}(0,0).$$
(10.23)

The Loop Diagrams

In the paragraph above we have shown that the computation of the viscosity can be reduced to a computation of one, off-diagonal, component of the EMT two–point function. For this correlator we then apply the magic formula (10.9). Thus, we have to specify these external branch indices in the diagrammatic expression for the EMT two–point function which is shown in Figure 10.1. It is clear, that the gluon propagator is now also a 2×2 matrix with respect to the branch indices and that the multi-indices in (10.9) include these indices and a corresponding summation. In this work we present the full two-loop diagrammatics shown in Fig. 10.1. There are five types of two-loop diagrams arising from the expansion (10.9): Sunset (B), Maki-Thompson (C), Eight (D), Squint (E), one-loop with vertex correction (F). The branch indices of the external vertices are fixed by (10.23) as $-+$, whereas we sum over internal branch indices. Thus, unlike in the one-loop case, at two-loop level principal value parts of propagators with equal branch indices can occur, which leads to divergent contributions. However, at two-loop level, these divergent contributions can explicitly be shown to cancel due to a left-right symmetry after combining appropriate diagrams. This is no longer true beyond two-loop, where diagrams with divergent sub-diagrams arise.

The non trivial input in these diagrams are then the gluon spectral functions and the temperature and momentum dependent running gauge coupling $\alpha_s(q,T)$. The former are obtained from Euclidean correlation functions via maximum entropy methods, which will very briefly be discussed below. The latter is extracted from the ghost-gluon vertex via the dressing functions $z_{\bar{c}Ac}, Z_c, Z_T$ of the ghost-gluon-vertex, the ghost propagator and the transverse gluon propagator, respectively as

$$\alpha_s(q,T) = \frac{z_{\bar{c}Ac}^2(q,T)}{4\pi Z_T(q,T) Z_c(q,T)^2},$$
(10.24)

with data taken from [115]. Following the discussion above, all couplings that appear in the vertices are fully dressed running couplings. For each two-loop diagram we study the integrand of the viscosity integral as a function of one of the loop four-momenta $(q_0, \vec{q})$, integrating out the other one. It turns out that all integrands are peaked in the vicinity of some diagram-dependent value $(q_{0,\text{max}}, \vec{q}_{\text{max}})$. The running couplings $\alpha_s(q,T)$ are then evaluated at a momentum $q_{\text{max}}(T) = \sqrt{q_{0,\text{max}}^2 + \vec{q}_{\text{max}}^2} \approx 7\,T$ to minimise the impact of the neglected momentum dependence of the vertices. This implicitly defines a temperature-dependent vertex coupling $\alpha_{s,\text{vert}}(T) = \alpha_s(7\,T, T)$.

Gluon Spectral functions and Maximum Entropy Method

The non-perturbative gluon propagator can be calculated from methods that do not rely on an expansion in a small coupling parameter. However, we have already stated that such methods like lattice gauge theory or functional methods are usually set up in Euclidean spacetime and Minkowski formulations are not straightforward. Here, we use spectral functions from Euclidean FRG data obtained in [115]. We want to add the comment that all

the results can also be obtained with lattice data and one finds only minor differences [163]. As the maximum entropy method is not part of this thesis, we will just briefly comment on this issue. For details about the maximum entropy method and the properties of the gluon spectral functions we refer the reader to [163, 175, 194, 195].

The starting point is that we assume given data for the Euclidean propagator $G(it)$, which is related to the spectral function $\rho(p^0)$ via the integral equation

$$G(\tau = it) = \int \frac{\mathrm{d}p^0}{2\pi} K(\tau, p^0) \rho(p^0), \tag{10.25}$$

with a known kernel $K(\tau, p^0)$. The goal is then the inversion of the integral equation, which is not unique. Moreover, the Euclidean propagator is known only numerically, e.g. as a set of discrete points with uncertainties obtained from lattice simulations or numerical evaluation of flow equations, as in our case. However, one has some additional analytical constraints, namely the spectral function in the perturbative limit, i.e. the asymptotic behavior of $\rho(p^0)$ for large p^0. The task is then to find an approximation to $\rho(p^0)$ with the perturbative input on the one hand, and the discrete set of data on the other hand. The naive approach of using simple interpolation functions for the data fails miserably. The maximum entropy method then optimizes the result by, loosely speaking, ensuring an optimal implementation of the ultraviolet condition.

10.2. Results: The viscosity over entropy ratio

Applying the above strategy, we can calculate the loop integrals in order to obtain the desired result, i.e. the viscosity over entropy ratio as a function of temperature even in the non-perturbative regime.

η/s in SU(3) Yang–Mills theory.

Fig. 10.3 shows the full two-loop result for η/s employing the lattice entropy density from [196] including all diagrams from Fig. 10.1.

The data shows, as expected on general grounds, a clear minimum at $T_{\min} \approx 1.26\, T_c$. The minimal value $\eta/s(T_{\min}) = 0.14$ is well above the AdS/CFT bound, where the error bars represent the combined systematic errors from MEM and the FRG calculation. The lattice data [166, 167] is in good agreement with our results, supporting the reliability of both methods. The inset in Fig. 10.4 shows the comparison to the one-loop calculation [163], illustrating the very good agreement around T_c. This confirms the argument concerning the optimisation of the RG scheme around T_c, which was put forward in [163]. Consistent with this reasoning, only at larger temperatures the deviation between the two calculations becomes significant and the relative size of the two-loop contribution grows with temperature. For large temperatures the dominant two-loop contributions arise from the Maki-Thompson and the Eight, see Fig. 10.4, that resum classes of ladder diagrams. This is consistent with the conventional picture in perturbative expansions where ladder resummations are required to obtain the correct result for the viscosity [197, 198]. Note that diagrams with overlapping loops are potentially suppressed as the spectral functions are peaked in a narrow region in momentum space. Due to the additional phase space suppression, we expect that
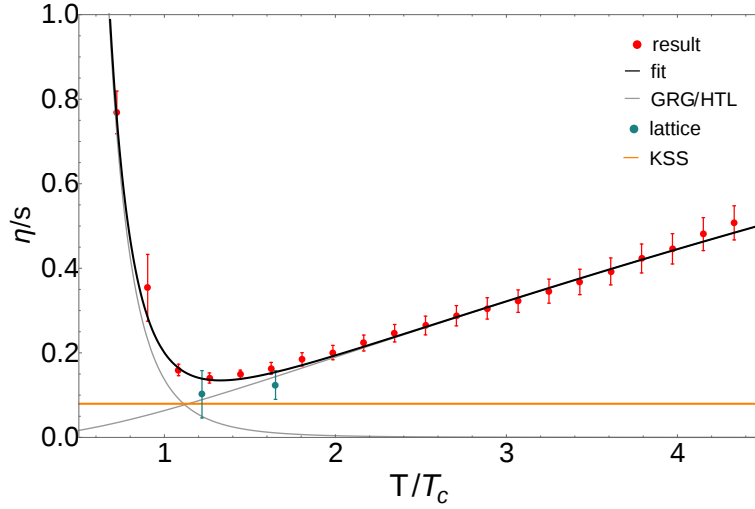
Figure 10.3.: Full Yang-Mills result (red) for η/s in comparison to lattice results [166, 167] (blue) and the AdS/CFT bound (orange). In addition, the plot shows the analytic fit given in (10.28) and its two components. The ratio η/s shows a minimum at $T_{\min} \approx 1.26\,T_c$ with a value of 0.14.

diagrams with more than two loops are negligible. We have checked this suppression in a first assessment of three-loop diagrams.

For understanding the physical picture underlying the temperature behavior, we provide a global fit function for $\eta/s(T)$. Additionally, such an analytic fit function is well-suited for phenomenological applications. This parametrization has to cover temperature ranges corresponding to vastly different physical situations. At large temperatures $T \gg T_c$ the degrees of freedom are gluons which can eventually be treated perturbatively. By contrast, at small temperatures $T \lesssim T_c$ YM theory can effectively be described as a glueball resonance gas (GRG). Finally, there is a transition region between these two asymptotic regimes whose description requires non-perturbative techniques.

In the high temperature regime, perturbation theory is applicable and η/s is given as a function of the strong coupling α_s only. It turns out that the hard-thermal loop (HTL) resummed data [199] is well-described by the functional form

$$\frac{\eta}{s}(\alpha_s) = \frac{a}{\alpha_s^\gamma}, \tag{10.26}$$

with an overall coefficient a and a scaling exponent $\gamma \approx 1.6$. We aim at extracting a non-perturbative extension of the above parametrization based on our data. In the region $T_c - 3\,T_c$ strong correlations become important and perturbation theory breaks down. This raises the question of a suitable running coupling as there is no unique definition of α_s beyond two-loop. A quasi-particle picture suggests that an appropriate choice of α_s can be deduced from a heavy quark potential [200, 201].

An analytic expression for a coupling that generates a linearly rising static quark potential at large distances is given by [202–204]

$$\alpha_{s,HQ}(z) = \frac{1}{\beta_0} \frac{z^2 - 1}{z^2 \log z^2}, \tag{10.27}$$
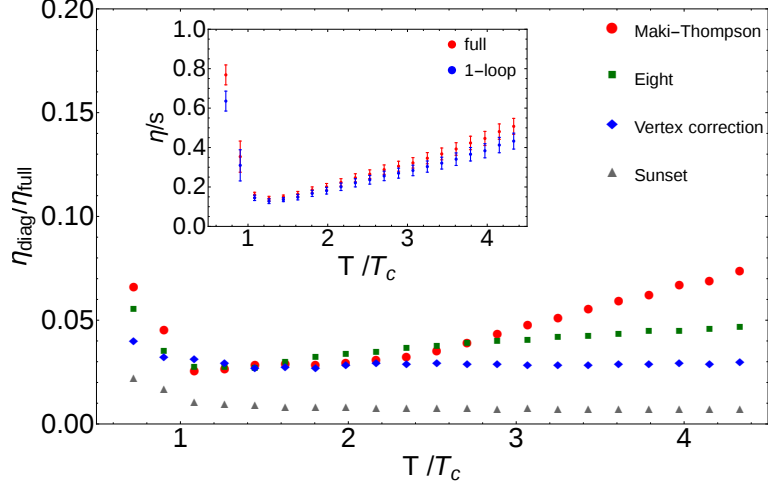
Figure 10.4.: Relative contributions from different diagram types to the two-loop viscosity as a function of temperature. The squint contribution is orders of magnitude smaller and not shown. The inset shows the comparison to the one-loop result [163].

where z denotes a dimensionless momentum variable. At large momenta it approaches the one-loop running coupling, where $\beta_0 = 33/(12\pi)$ denotes the coefficient in the one-loop beta-function of pure $SU(3)$ Yang-Mills theory. The scale identification is implemented by regarding $\alpha_{\text{s,HQ}}$ as a function of $z = c\,T/T_c$ with a scale identification factor c. By construction, the divergence of (10.27) at zero momentum leads to a vanishing contribution of (10.26) to η/s at zero temperature. As an estimate for a lower bound for a reasonable high-temperature fit, we consider the trace anomaly as a hint from QCD thermodynamics, which starts to develop a T^4 behaviour for $T \gtrsim 2\,T_c$ [205]. Using $T > 3\,T_c$ as a conservative estimate, our data is well-described by the scaling form (10.26) with the running coupling (10.27) and parameters $a = 0.15$ and $c = 0.66$. One should note that whereas the heavy quark potential coupling takes a rather large value $\alpha_{\text{s,HQ}}(cT/T_c)|_{T=T_c} \approx 1.77$ at T_c, the vertex coupling $\alpha_{\text{s,vert}}(T_c) \approx 0.76$ corresponding to a value of $\alpha_{\text{s,vert}}^{\overline{\text{MS}}}(T_c) \approx 0.35$, after conversion to the $\overline{\text{MS}}$ scheme [206], is comparably small. This supports the validity of resummation arguments at moderately large temperatures but also underlines the non-uniqueness of the definition of a running coupling in the nonperturbative regime around T_c. It turns out that the fit (10.26) can be extended to even lower temperatures $T \gtrsim 1.8T_c$, where it is still in very good agreement with our data, see Fig. 10.3. Note, that the fitting with the vertex coupling $\alpha_{\text{s,vert}}$ fails for temperatures below $3\,T_c$. These findings hint at the validity of a quasi-particle picture even at considerably low temperatures.

Below the critical temperature the effective degrees of freedom change from gluons to glueballs. The glueball spectrum can be calculated using the formalism put forward in this work [207]. Hence, the present YM calculation is also capable of describing glueball resonances. Therefore one expects an algebraic decay of η/s with temperature similar to a hadron resonance gas [160, 161]. Due to the small number of data points and the comparably large error bars below T_c, no precise determination of the exponent δ in the power law is possible. We construct a global fit function by superposing a power law behaviour at small temperatures with the extrapolated high temperature behaviour (10.26),

i.e. a global parametrisation of the form

$$\frac{\eta}{s}(T) = \frac{a}{\alpha_{s,HQ}^{\gamma}(c\,T/T_c)} + \frac{b}{(T/T_c)^{\delta}} \,. \tag{10.28}$$

With $a = 0.15$, $b = 0.14$, $c = 0.66$, $\delta = 5.1$ and $\gamma = 1.6$ as given above, this fit describes our data very well, see Fig. 10.3. The best-fit value $\delta = 5.1$ lies in the expected range for a hadron resonance gas [161], where for example a pion gas leads to an exponent of 4.
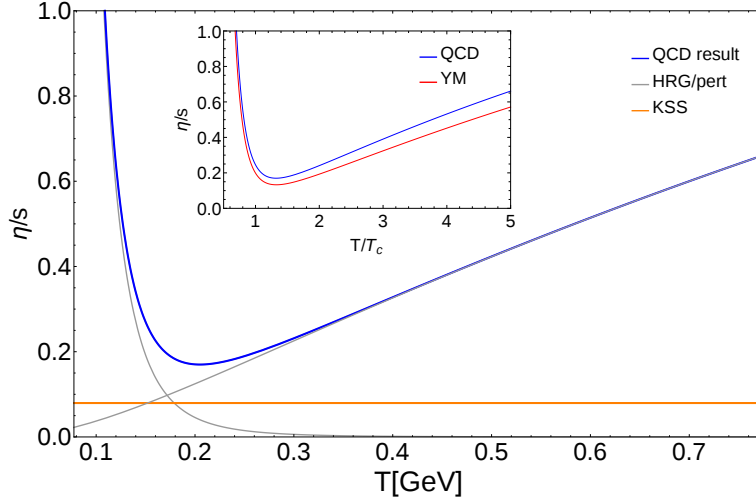
Figure 10.5.: Estimate for η/s in QCD which shows a minimum at $T_{\min} \approx 1.3\,T_c$ at a value of 0.17. The inset shows the comparison to the YM results for temperatures normalised by the respective critical temperatures.

Estimate for η/s in full QCD.

The analytic fit function (10.28) for η/s in YM theory enables us to provide a first estimate of η/s in full QCD, again based on the idea of superposing a low and a high temperature behaviour term. The procedure consists of three separate steps. Firstly, one has to take into account the difference in scales and the running couplings in YM and QCD. This involves replacing the coefficient β_0 in (10.27) by its QCD value, $\beta_{0,QCD} = (33 - 2N_f)/(12\pi)$. Additionally, one has to set a scale by fixing the ratio of the running couplings in YM and QCD at a certain point. In our setup the characteristic scale is the critical temperature T_c. For the phase transition to the confinement phase to take place, the strong coupling usually needs to exceed a certain critical value $\alpha_s(T) = \alpha_{\mathrm{crit}}$. On general grounds one can argue that the critical values in YM theory and QCD are of comparable size. This argument is supported by the fact that the values of α_{crit} for the vertex couplings tend to coincide. Consequently, we impose the condition

$$\alpha_{s,HQ}^{N_f=0}(c\,T/T_c)\Big|_{T=T_c} = \alpha_{s,HQ}^{N_f=3}(c_{QCD}\,T/T_c)\Big|_{T=T_c} \,. \tag{10.29}$$

This matching condition fixes the scale factor to the value $c_{QCD} = 0.79$. Secondly, one has to take into account genuine quark contributions that are not encoded in the change of the

running couplings. Denoting the quark contributions to viscosity and entropy as $\Delta\eta$ and Δs respectively, we write

$$\frac{\eta}{s}\bigg|_{\text{QCD}} = \frac{\eta_{\text{YM}} + \Delta\eta}{s_{\text{YM}} + \Delta s} = \frac{\eta}{s}\bigg|_{\text{YM},\alpha_s^{\text{YM}}\to\alpha_s^{\text{QCD}}} \cdot \left(\frac{1 + \frac{\Delta\eta}{\eta_{\text{YM}}}}{1 + \frac{\Delta s}{s_{\text{YM}}}} \right), \qquad (10.30)$$

and estimate the ratios $\Delta\eta/\eta_{\text{YM}}$ and $\Delta s/s_{\text{YM}}$ using leading order perturbative results. For $N_f = 3$ we find $\Delta\eta/\eta_{\text{YM}} \approx 2.9$ [208, 209] and $\Delta s/s_{\text{YM}} \approx \frac{21}{32}N_f \approx 2.0$ [210, 211], leading to an overall correction factor of approximately 4/3. Finally, in the low temperature regime one has to replace the pure glueball resonance gas by a hadron resonance gas, which also decays algebraically with temperature. In this work we use the data given in [212].

In summary, the final fit for QCD takes the form (10.28), but with the following QCD parameters replacing the corresponding YM values: $a_{\text{QCD}} \approx 4/3\,a$ for the high-temperature part and $b_{\text{QCD}} = 0.16$, $\delta_{\text{QCD}} = 5$. Additionally the full QCD $\alpha_{s,\text{HQ}}^{N_f=3}(c_{\text{QCD}}T/T_c)$ with $c_{\text{QCD}} = 0.79$ replaces the pure-glue beta-function, whereas the perturbative exponent $\gamma = 1.6$ remains unchanged. Note that a continuation of the fit to very high energies requires taking into account the quark flavor thresholds appropriately.

This procedure yields the final result shown in Fig. 10.5. Plotted in terms of temperatures normalised by the respective critical temperatures, the QCD curve is shifted slightly upwards compared to the YM result, see the inset of Fig. 10.5. The general shape resembles the one of the YM result and shows a minimum at $T_{\text{min}} \approx 1.3\,T_c$ with a value 0.17.

Summary and Conclusions - We have computed the shear viscosity over entropy density ratio in pure YM theory over a large temperature range. The setup is based on an exact functional relation for the spectral function of the energy-momentum tensor involving full gluon propagators and vertices. The only input are the gluon spectral function and the running coupling α_s. As a highly non-trivial result, the global temperature behaviour of η/s can be described as a direct sum of a glueball resonance gas contribution with an algebraic decay at small temperatures, and a high temperature contribution consistent with HTL-resummed perturbation theory. Finally we provide a first estimate for η/s in QCD.

Part IV.

Summary, Conclusions and Outlook

Quantum Gravity

We have presented a novel setup for renormalization group investigations within the asymptotic safety scenario for quantum gravity, chapter 5. This construction allows for the investigation of the properties of graviton correlation functions and the related scale-dependent couplings. We have introduced the notion of locality for renormalization group flows as a fundamental property in the spirit of the Wilsonian idea of coarse graining, section 5.2. Subsequently, this property is proved for the two- and three–point function in quantum gravity, section 5.3 and subsection 5.8.1. We define scale-dependent generalized couplings related to the aforementioned correlators, in particular for Newtons constant and the cosmological constant, but also for quantities that do not appear in the classical Einstein–Hilbert action but emerge purely out of quantum fluctuations, such as the graviton wave–function renormalization and the constant parts of the n–point graviton vertices. The non-perturbative beta functions for all these couplings are derived in various approximations. We confirm the existence of a non-Gaussian ultraviolet fixed point, section 5.5, section 5.6, section 5.8. Thus, we find further evidence for asymptotic safety in quantum gravity. In our most advanced approximation the fixed point is described by two relevant and one irrelevant direction, section 5.8, in contrast to our earlier findings where all directions are attractive. Interestingly, this fixed point with one UV-repulsive direction is found in all our approximations that include the graviton three–point function. This repulsive direction is very encouraging for the general perspective of asymptotic safety in quantum gravity, as an acceptable fixed point in the full theory needs to be described by only finitely many attractive directions. These results are even more emboldening as one finds in $f(R)$ truncations that all operators with $n \geq 3$ are irrelevant.

In addition to asymptotically safe ultraviolet physics, our approximations show a novel, attractive infrared fixed point that smoothly connects to the non-Gaussian fixed point of asymptotic safety, subsection 5.6.9. In contrast, the physical trajectories in the standard background field approximations hit a singular line at finite flow time, and are therefore not infrared complete. This singularity appears as a truncation artefact and is resolved if one properly accounts for the difference between the fluctuation and the background field. Moreover, if the scaling of the couplings in the vicinity of this fixed point is self-consistent, subsection 5.6.3, the infrared fixed point has classical properties, in the sense that Newtons constant and the cosmological constant do not depend on the energy scale.

In the coupling of gravity to Yang–Mills theories is discussed. In particular, we have investigated the interplay of gravitons and gluons in the far ultraviolet, where pure SU(N) gauge theories exhibit asymptotic freedom. It is found that the graviton induced interactions do not destroy this property as they contribute a strictly negative term to the beta function, chapter 7. Moreover, we find that the gluon fluctuations that contribute to graviton correlators are all local in the sense of section 5.2, subsection 8.1.2. However, preliminary results indicate that gluons in a large n limit might alter the fixed point structure in the gravity sector.

There are several interesting projects that are built upon the results described above or generalize our framework. First of all, it would be interesting to go beyond third order in the vertex expansion. In doing so, one could test if this enlarged system shows a fixed point with more than one irrelevant direction. Moreover, this would close the flow equation for the propagator entirely. Another idea is to push the resolution of the momentum dependence

further by including a momentum dependent coupling $g(k, p)$, such that one can directly investigate the behavior of graviton interactions as a function of a physical, external momentum. Also the enhancement of the truncation with further curvature invariants is of interest. A particular example is for instance the propagator with all fourth order derivative invariants. Another aspect is the dependence on the expansion point in the vertex expansion, which can be investigated by expansion around non-flat backgrounds. A different direction is the application of our results to the phenomenology of quantum gravity, such as black hole physics, cosmology or imprints of gravitons in cross-sections at collider experiments. In particular, the dependence on external momenta can be of major importance in such studies. At the end of the day one is interested in describing all forces in one unified framework. In this spirit one of the most interesting questions is the coupling of gravity to the entire standard model. In this context one can address several issues. First of all, one needs to test the stability of the non-Gaussian fixed point in the gravity sector against inclusion of all gauge bosons and matter particles, and possibly the effects of beyond the standard model physics. Furthermore, the asymptotic safety condition can in principle reduce the free parameters of the standard model.

Transport Coefficients in the Quark–Gluon Plasma

The main result of the third and last part of this thesis, Part III, is the computation of the shear viscosity over entropy ratio in SU(3) gauge theory and an estimate for this quantity in full quantum chromodynamics. We present a strategy that allows for the determination of transport coefficients in non-Abelian plasmas in the perturbative, as well as in the non-perturbative regime. This strategy is based on analytical continuation of Euclidean correlation functions for the gluon field. We then use a Kubo relation, where the real–time correlation functions of the energy-momentum tensor are expanded with the help of an exact functional relation in terms of the fundamental fields. The resulting expression is used within the Schwinger-Keldysh formalism for Minkowski space correlators. With this at hand, we obtain the viscosity over entropy ratio η/s as a function of temperature. We find that this function has a minimum roughly at the critical temperature T_c. Below T_c the behavior resembles that of a gluon resonance gas, and at high temperatures the data is in good agreement with perturbation theory. The entire data for $\eta/s(T)$ can be fitted to a function that is a sum of the low and the high temperature part. Finally, we can use this expression for a qualitative estimate of $\eta/s(T)$ in QCD.
The setup presented in Part III can easily be applied to other transport coefficients such as the bulk viscosity. Furthermore, for a quantitative picture in full QCD, one has to include the quark sector right from the beginning, which requires the quark spectral function as an input. As η/s is directly related to experimental data, our results can then be used in hydrodynamical descriptions of the phenomenology of heavy–ion collisions.

Appendix

The metric in super-field space

In this appendix we closely follow [32]. In Chapter 1 we have introduced the condensed notation and the related super-field

$$\phi_{\mathbf{a}} = (\phi_{1,a_1}...\phi_{N,a_N})_{\mathbf{a}} \tag{A.1}$$

which consists of N arbitrary fields that can carry several group indices, related to particular field species. The metric $\gamma^{\mathbf{ab}}$ is then defined on the super-field space $\{\phi_{i,a_i}\}$, as direct sum of the sub-space metrics. In case of bosonic fields the metric is trivial, i.e. just the identity, and therefore we restrict the discussion to fermionic fields, where the metric is given by the epsilon-tensor.

For $\phi_{\mathbf{a}} = \{\psi, \bar{\psi}\}_{\mathbf{a}}$, with Grassmann fields ψ and $\bar{\psi}$, the fermionic metric reads

$$\gamma = \begin{pmatrix} 0 & 1 \\ -1 & 0 \end{pmatrix}. \tag{A.2}$$

Raising and lowering of indices is defined via

$$\phi^{\mathbf{a}} = \gamma^{\mathbf{ab}}\phi_{\mathbf{b}}$$

$$\phi_{\mathbf{a}} = \phi^{\mathbf{b}}\gamma_{\mathbf{ba}}. \tag{A.3}$$

Furthermore there are the crucial relations

$$\gamma_{\mathbf{b}}{}^{\mathbf{a}} = \gamma^{\mathbf{ac}}\gamma_{\mathbf{bc}} = \delta_b^a \tag{A.4}$$

and

$$\gamma^{\mathbf{a}}{}_{\mathbf{b}} = \gamma^{\mathbf{ac}}\gamma_{\mathbf{cb}} = (-1)^{\mathbf{ab}}\delta_b^a, \tag{A.5}$$

where

$$(-1)^{\mathbf{ab}} = \begin{cases} -1 & \text{if number of fermions odd in } \mathbf{a} \text{ and } \mathbf{b} \\ 1 & \text{otherwise.} \end{cases} \tag{A.6}$$

In the above example $\phi_{\mathbf{a}} = \{\psi, \bar{\psi}\}_{\mathbf{a}}$ we have one fermionic field corresponding to one index and acooringly get a minus sign.

General Flow of the Propagator with Super-fields

In this appendix we derive the structure of the flow equation of the two-point function for a general theory, i.e. with an arbitrary super-field ϕ. In order to do so, we take two functional derivatives of the flow equation for the effective action (3.9). In this derivation we need the functional derivative of the propagator, which is the inverse of $\Gamma^{(2)} + R$. As a mathematical object it is a matrix in super-field space and therefore carries two bold face-type of indices. For a general matrix A, we know that $AA^{-1} = 1$. Therefore the derivative of the inverse operator is given by $\frac{\delta A^{-1}}{\delta \phi} = -A^{-1} \frac{\delta A}{\delta \phi} A^{-1}$. Applying this formula with $A = G$ we arrive at

$$\frac{\delta}{\delta \phi_{\mathbf{a}}} G_{\mathbf{ij}} = -(-1)^{\mathbf{ai}} G_{\mathbf{ir}} \Gamma^{(3)\,\mathbf{raf}} G_{\mathbf{kj}} \gamma^{\mathbf{k}}{}_{\mathbf{f}}. \tag{B.1}$$

Note that there is no sum for the $(-1)^{\mathbf{ai}}$ terms. The desired flow equation is then calculated as follows,

$$
\begin{aligned}
\dot{\Gamma}^{(2)\,\mathbf{ab}} &= \frac{1}{2} \frac{\delta}{\delta \phi_{\mathbf{a}}} \frac{\delta}{\delta \phi_{\mathbf{b}}} \left(G_{\mathbf{ij}} \dot{R}^{\mathbf{ij}} \right) \\
&= -(-1)^{\mathbf{bi}} \frac{1}{2} \frac{\delta}{\delta \phi_{\mathbf{a}}} \left(G_{\mathbf{ir}} \Gamma^{(3)\,\mathbf{rbf}} G_{\mathbf{kj}} \right) \gamma^{\mathbf{k}}{}_{\mathbf{f}} \dot{R}^{\mathbf{ij}} \\
&= +(-1)^{\mathbf{bi}} (-1)^{\mathbf{ai}} \gamma^{\mathbf{n}}{}_{\mathbf{m}} \gamma^{\mathbf{k}}{}_{\mathbf{f}} \frac{1}{2} G_{\mathbf{il}} \Gamma^{(3)\,\mathbf{lam}} G_{\mathbf{nr}} \Gamma^{(3)\,\mathbf{rbf}} G_{\mathbf{kj}} \dot{R}^{\mathbf{ij}} \\
&\quad - (-1)^{\mathbf{bi}} (-1)^{\mathbf{ai}} \gamma^{\mathbf{k}}{}_{\mathbf{f}} \frac{1}{2} G_{\mathbf{ir}} \Gamma^{(4)\,\mathbf{rabf}} G_{\mathbf{kj}} \dot{R}^{\mathbf{ij}} \\
&\quad + (-1)^{\mathbf{ai}} (-1)^{\mathbf{bi}} (-1)^{\mathbf{ab}} (-1)^{\mathbf{af}} (-1)^{\mathbf{ak}} \gamma^{\mathbf{q}}{}_{\mathbf{p}} \gamma^{\mathbf{k}}{}_{\mathbf{f}} \frac{1}{2} G_{\mathbf{ir}} \Gamma^{(3)\,\mathbf{rbf}} G_{\mathbf{ko}} \Gamma^{(3)\,\mathbf{oap}} G_{\mathbf{qj}} \dot{R}^{\mathbf{ij}} \tag{B.2}
\end{aligned}
$$

where we omit terms of the form $(1)^{\mathbf{ab}} \times (1)^{\mathbf{ab}} = 1$.

We close this appendix with some comments on the equation derived above. If there is only one field species running in the loop, one can immediately see by rearranging dummy indices that the two terms containing $\Gamma^{(3)}$ are identical in this case. As the equation (I) is

written in the general super-field formalism, it holds for generic theories. Specifying the indices then returns the equation for the theory under consideration. Furthermore, we note that also the flow of the propagator is one-loop exact. This is obviously also true for the flow of vertex functions of arbitray order n.

Flow Equations

The modified threshold functions introduced in subsection 5.6.2 are given by:

$$\Phi_n^p[\eta](\omega) = \frac{1}{\Gamma(n)} \int_0^\infty dx\, x^n \frac{\dot{r}(x) - \eta(x)r(x)}{(x(1 + r(x)) + \omega)^p} .$$
(C.1)

With these threshold functions, the geometric flow equations in [79], improved by momentum-dependent anomalous dimensions, are given by

$$\dot{\overline{g}} = 2\overline{g} - \frac{\overline{g}^2}{2\pi} \left[\frac{2}{3}\Phi_1^1[\eta_h](\mu) + \frac{10}{3}\Phi_2^2[\eta_h](\mu) + \frac{5}{12}\Phi_1^1[\eta_c](0) + \frac{5}{4}\Phi_2^2[\eta_c](0) \right],$$
(C.2)

for the background coupling and

$$\dot{g} = 2g - \frac{g^2}{2\pi} \left[\frac{1}{3}\Phi_1^1[\eta_h](\mu) + \frac{20}{9}\Phi_2^2[\eta_h](\mu) + \frac{5}{24}\Phi_1^1[\eta_c](0) + \frac{5}{6}\Phi_2^2[\eta_c](0) \right.$$
$$\left. + \dot{\mu}\left(\frac{1}{6}\Phi_1^2[0](\mu) + \frac{10}{9}\Phi_2^3[0](\mu) \right) \right],$$
(C.3)

for the coupling related to the dynamical field. The flows of the two-point functions are given by the coefficient functions $I_\phi(p^2, q^2, M^2, \Lambda^{(n)})$ with the contributions from the pure graviton diagrams

$$I_h(p^2, q^2, M^2, \Lambda^{(n)}) = - \frac{6q^2(3p^2 + 6q^2 - 8\lambda^{(4)})}{(q^2(1 + r_1) + \mu)^2}$$
$$+ \frac{f_h(p, q, x, \lambda^{(3)})}{(q^2(1 + r_1) + \mu)^2((p^2 + 2pqx + q^2)(1 + r_2) + \mu)},$$
(C.4)

with

$$f_h(p, q, x, \lambda^{(3)}) = \frac{4q^2}{5(p^2 + 2pqx + q^2)} \times$$
$$\left(15p^6(1 + 2x^2) + 10p^5qx(7 + 8x^2) \right.$$
$$+ p^4q^2(21 + 208x^2 + 56x^4) + 140p^3q^3x(1 + 2x^2)$$
$$+ 4p^2q^4(7 + 76x^2 + 22x^4)$$
$$+ 8pq^5x(17 + 11x^2 + 2x^4)$$
$$+ 4q^6(7 + 6x^2 + 2x^4) - 4\lambda^{(3)}\left[15p^4(1 + 4x^2) \right.$$
$$+ 30p^3qx(3 + 4x^2) + p^2q^2(-9 + 248x^2 + 16x^4)$$
$$+ 20pq^3x(5 + 4x^2) + 20q^4(1 + 2x^2)\big]$$
$$+ 8(\lambda^{(3)})^2\left[15p^2(1 + x^2) + 20pqx(2 + x^2) \right.$$
$$\left. + 2q^2(9 + 2x^2 + 4x^4)\big]\right). \tag{C.5}$$

and the ghost parts

$$I_c(p^2, q^2, M^2, \Lambda^{(n)}) = -\frac{16\left(p^2(2 + x^2) + 6pqx + 3q^2\right)}{p^2 + 2pqx + q^2} \frac{1}{(1 + r_1)^2(1 + r_2)} \tag{C.6}$$

Here, we have introduced the short cuts $r_1 = r(q^2)$ and $r_2 = r(p^2 + 2pqx + q^2)$ and x is defined by $p_\mu q^\mu = 2pqx$.

The flow equation for the ghost two–point function is given by

$$\frac{\partial_t \Gamma^{(\bar{c}c)}(p^2)}{p^2 Z_c(p^2)} = g \int_0^\infty dq \int_{-1}^1 dx \sqrt{1 - x^2} \frac{4q^3}{3\pi^2}$$
$$\times \frac{p^2(3 + 6x^2) + pqx(-2 + 20x^2) + q^2(5 - 12x^2 + 16x^4)}{p^2 + 2pqx + q^2} \tag{C.7}$$
$$\times \left[\frac{\dot{r}_1 - \eta_c(q^2)r_1}{(1 + r_1)^2((p^2 + 2pqx + q^2)(1 + r_2) + \mu)} \right.$$
$$\left. + \frac{q^2(\dot{r}_1 - \eta_h(q^2)r_1)}{(q^2(1 + r_1) + \mu)^2(1 + r_2)} \right]. \tag{C.8}$$

Finally, the flow equation for λ from the one-point function is given by

$$\dot{\lambda} = -2\lambda + g\left[\int_0^\infty dq \frac{3q^7(1 + 2\lambda)}{4\pi} \frac{\dot{r}(q^2) - \eta_h(q^2)r(q^2)}{(q^2(1 + r(q^2)) + \mu)^2} \right.$$
$$\left. + \int_0^\infty dq \frac{q^3(3 - \lambda)}{3\pi} \frac{\dot{r}(q^2) - \eta_c(q^2)r(q^2)}{(1 + r(q^2))^2} \right]. \tag{C.9}$$

Projection procedure

Here, we want to argue why the projection procedure to obtain the flow equation for the mass and the integral equation for the graviton anomalous dimension is the physical one. First the anomalous dimension must be finite everywhere, in particular at the pole. Otherwise, the wave-function renormalization could be written as

$$Z_h(p^2) = (p^2 + \mu)^\omega \tilde{Z}_h(p^2) \tag{D.1}$$

with a nonzero parameter ω and $Z_h(-\mu)$ finite and nonzero. However, the wave-function renormalization should only determine the residue at the propagator pole. Thus, we assume that the anomalous dimension is finite.

Next, we consider the flow equation of the two-point function,

$$-\eta_h(p^2)(p^2 + \mu) + \dot{\mu} + 2\mu = \frac{\partial_t \Gamma^{(2h)}(p^2)}{Z_h(p^2)} \, . \tag{D.2}$$

We can evaluate this equation at an arbitrarily chosen fixed momentum, say ℓ, to obtain the β-function of the mass:

$$\dot{\mu} = -2\mu + \frac{\partial_t \Gamma^{(2h)}(\ell^2)}{Z_h(\ell^2)} + \eta_h(\ell^2)(\ell^2 + \mu). \tag{D.3}$$

Substracting this from the original equation leaves an integral equation for the anomalous dimension,

$$\eta_h(p^2) = -\frac{\frac{\partial_t \Gamma^{(2h)}(p^2)}{Z_h(p^2)} - \frac{\partial_t \Gamma^{(2h)}(\ell^2)}{Z_h(\ell^2)}}{p^2 + \mu} + \eta_h(\ell^2)\frac{\ell^2 + \mu}{p^2 + \mu} \, . \tag{D.4}$$

One easily sees that the right hand side of this equation diverges at $p^2 = -\mu$, if $\eta(\ell^2)$ is not chosen appropriately. As we already know that the anomalous dimension must be finite everywhere, we conclude that

$$\eta_h(\ell^2) = \frac{\frac{\partial_t \Gamma^{(2h)}(-\mu)}{Z_h(-\mu)} - \frac{\partial_t \Gamma^{(2h)}(\ell^2)}{Z_h(\ell^2)}}{\ell^2 + \mu} \, . \tag{D.5}$$

This can be reinserted into (D.4), leading to

$$\eta_h(p^2) = -\frac{\frac{\partial_t \Gamma^{(2h)}(p^2)}{Z_h(p^2)} - \frac{\partial_t \Gamma^{(2h)}(-\mu)}{Z_h(-\mu)}}{p^2 + \mu}\,, \tag{D.6}$$

which is the equation originally proposed in the main text. We can use the expression for $\eta_h(\ell^2)$ also for the flow equation of the mass, resulting in

$$\dot{\mu} = -2\mu + \frac{\partial_t \Gamma^{(2h)}(-\mu)}{Z_h(-\mu)}\,, \tag{D.7}$$

again reproducing the result from the main text. Thereby, we have shown, under the reasonable condition of a finite anomalous dimension, that our flow equations are unique.

Note that for a momentum independent wave–function renormalization there is no need for e.g. the mass term to be projected at the pole. In this case one can simply generalize equations (5.46) or (5.61) for the case with $\Lambda^{(3)} \neq \Lambda^{(2)}$ to yield for the running of the dimensionless mass gap parameter

$$\partial_t \mu = -2\mu + \eta_h \mu + \frac{32\pi}{Z_h}\text{Flow}^{(2h)}(p = 0) \tag{D.8}$$

Accordingly for the anomalous dimensions at arbitray subtraction points

$$\eta_\phi = -\frac{32\pi}{Z_\phi}\left(\frac{\text{Flow}^{(2\phi)}(p = p_\star) - \text{Flow}^{(2\phi)}(p = p_\bullet)}{p_\star^2 - p_\bullet^2}\right) \tag{D.9}$$

Infrared scaling analysis

Here, we discuss the IR divergence analysis in more detail. Before we can proof a recursion relation for the parameters α_n, we discuss some general properties of such a setting.

Prerequisites: The flow of a general n-point vertex function includes generic loop integrals with dimensionless external momenta p_i and loop momentum q of the form

$$
\int \frac{\mathrm{d}^4 q}{(2\pi)^4} \frac{f_n(q, p_i)}{(q^2(1 + r(q^2)) + \mu)^2} \times \\
\prod_{i=1}^{n-2} ((p_i + q)^2 (1 + r((q + p_i)^2)) + \mu)^{-1} ,
\tag{E.1}
$$

with a function $f_n(q, p_i)$ resulting from contractions of the tensor structure $\tilde{\mathcal{T}}$ defined in (5.11). Obviously, the divergences are strongest at vanishing external momenta $p_i = 0$. In this case, all internal propagators carry the loop momentum q and we are left with

$$
\int \frac{\mathrm{d}^4 q}{(2\pi)^4} \frac{f_n(q, p_i = 0)}{(q^2(1 + r(q^2)) + \mu)^n} .
\tag{E.2}
$$

Moreover, in the limit $\mu \to -1$, these divergences emerge from small momentum modes near $q = 0$. Consistent regulators need to fulfill

$$
\lim_{x \to 0} x(1 + r(x)) = 1 + \zeta x + \mathcal{O}(x^2)
\tag{E.3}
$$

with $\zeta > 0$, because otherwise, the denominator in (E.2) exhibits a zero for $\mu > -1$. The highest pole order is contained in the momentum-independent part $f_n^0 := f_n(q = 0, p_i = 0)$. Neglecting the angular integration, and by the above reasoning, the most divergent part of the integral takes the form

$$
\int_0^{\delta > 0} \mathrm{d}q \frac{q^3 f_n^0}{(q^2 + \epsilon)^n} ,
\tag{E.4}
$$

147

where we introduced $\epsilon = 1 + \mu$ for convenience. These expressions can be integrated which leads to a divergence structure of the form

$$
\int_0^{\delta > 0} dq \frac{q^3}{(q^2 + \epsilon)^n} \sim \begin{cases} \text{finite} & \text{if } n < 2 \\ \log \epsilon & \text{if } n = 2 \\ \epsilon^{2-n} & \text{if } n > 2 \end{cases} . \tag{E.5}
$$

In a simple Einstein Hilbert truncation one identifies the constant, momentum-independent parts of the n-point vertex functions $\lambda^{(n)}$ with the mass term (or with the cosmological constant), i.e. $\lambda^{(n)} = -\mu/2$ for all n. However, this approximation incorporates a scaling inconsistency, as we will see by the divergence analysis below.

The following analysis is based on a matching of terms in the limit $\epsilon \to 0$ on the RHS and the LHS of the flow equations for n-point vertex functions. As a generalization of the Einstein-Hilbert construction we allow for a power law behaviour in ϵ in the limit under consideration. In such an expansion, logarithmic contributions are sub-leading, do not change the power law and are therefore discarded. Moreover, we keep only the leading order terms, i.e. we assume a power law

$$
\lambda^{(n)} \overset{\epsilon \to 0}{\sim} \epsilon^{\alpha_n}, \ n \geq 3, \tag{E.6}
$$

and suppress terms of the form $\epsilon^{\tilde{\alpha}_n}$ with $\tilde{\alpha}_n > \alpha_n$, since we are interested in the limit $\epsilon \to 0$. Moreover, we observe that the ϵ-dependence of the function f_n^0 is completely stored in the parameters $\lambda^{(n)}$. Accordingly, these are the only terms that we have to take into account in an ϵ-scaling analysis. The generic form of a β-function for $\lambda^{(n)}$ is of the form

$$
\dot{\lambda}^{(n)} = -2\lambda^{(n)} + g \ (\text{loop} - \text{terms}), \tag{E.7}
$$

i.e. a canonical term and loop contributions which are always proportional to the gravitational coupling g. First, we show that the canonical term does not dominate the β-functions for $\lambda^{(n)}$ with $n = 2, 3, 4$ in the limit $\epsilon \to 0$. In order to do so, we assume that the canonical term in the beta functions for $\lambda^{(3)}$ dominates in the limit $\epsilon \to 0$, i.e. $\dot{\lambda}^{(3)} \overset{\epsilon \to 0}{\sim} -2\lambda^{(3)}$, which implies $\lambda^{(3)} \overset{\epsilon \to 0}{\sim} 1/k^2$. On the other hand, dominance of the canonical term means $\dot{\lambda}^{(3)} \overset{\epsilon \to 0}{\sim} \epsilon^{\alpha_3}$. From Figure E.1 and (E.5) we can can see that there is a diagram producing a term $\overset{\epsilon \to 0}{\sim} \epsilon^{3\alpha_3 - 2}$. Dominance of the canonical term then implies $\alpha_3 > 1$. In this case $\lambda^{(3)} \overset{\epsilon \to 0}{\to} 0$. This contradicts $\lambda^{(3)} \overset{\epsilon \to 0}{\sim} 1/k^2$ as long as there is no UV fixed point at $\epsilon = 0$. The same argument goes through for $\lambda^{(4)}$ by using the term $\overset{\epsilon \to 0}{\sim} \epsilon^{2\alpha_4 - 1}$ on the RHS of the respective flow equation. Thus, we know that the canonical term is sub-leading or of equal order as the loop terms. With a case-by-case analysis of $(\lambda_3 \lessgtr 1, \lambda_4 \lessgtr 1)$, one can show that $\alpha_4 < 1$. Then, using (E.13) below it can be deduced that the canonical term in the flow equation for λ^4 is indeed subleading and $\dot{\lambda}^4 \overset{\epsilon \to 0}{\sim} g$. Together with (E.15) this in turn implies that $\dot{\epsilon} \overset{\epsilon \to 0}{\sim} g$ and therefore, the canonical term in $\dot{\epsilon}$ is irrelevant as well. Accordingly either

$$
\alpha_4 < 0 \ \text{ or } \ \alpha_3 < 1/2, \tag{E.8}
$$

and additionally, the canonical term in $\dot{\lambda}^n$ for all n is sub-leading too, as both sides of the respective flow equation must be proportional to g.

Lemma 1: *Assuming the results in Prerequisites, in particular a power law*

$$\lambda^{(n)} \overset{\epsilon \to 0}{\sim} \epsilon^{\alpha_n}, \tag{E.9}$$

with $n \geq 3$, the hierarchy of flow equations implies

$$\alpha_4 \leq 2\alpha_3 - 1. \tag{E.10}$$

Proof: The flow of the two point function (evaluated at vanishing external momentum) leads to the relation

$$\dot{\mu} = \dot{\epsilon} \overset{\epsilon \to 0}{\sim} g \, \max\left\{ \left|\lambda^{(4)}\right|, \frac{(\lambda^{(3)})^2}{\epsilon} \right\} \tag{E.11}$$
$$\sim g \, \max\left\{ \epsilon^{\alpha_4}, \epsilon^{2\alpha_3 - 1} \right\},$$

where the terms in the curly brackets $\{\cdot, \cdot, ...\}$ indicate the leading contributions arising from the distinct diagrams. The diagrams generating the running of the three point function (see Figure E.1) lead to

$$\dot{\lambda}^{(3)} \overset{\epsilon \to 0}{\sim} g \, \max\left\{ \epsilon^{\alpha_5}, \epsilon^{\alpha_3 + \alpha_4 - 1}, \epsilon^{3\alpha_3 - 2} \right\}. \tag{E.12}$$

The next order in the hierarchy, the flow equation for $\Gamma^{(4h)}$, has the diagrammatic represen-
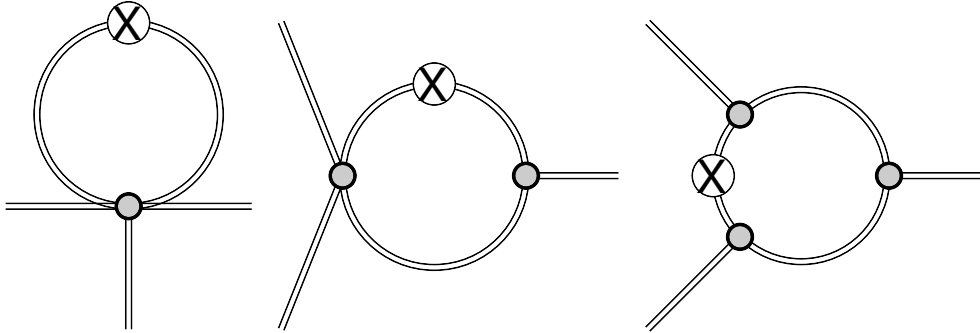
Figure E.1.: Diagrams contributing to the divergence analysis of the three-point function of the graviton.

tation Figure E.2. This means that the diagrams scale in the limit $\epsilon \to 0$ as

$$\dot{\lambda}^{(4)} \overset{\epsilon \to 0}{\sim} g \, \max\{ \epsilon^{4\alpha_3 - 3}, \epsilon^{2\alpha_3 + \alpha_4 - 2}, \\ \epsilon^{2\alpha_4 - 1}, \epsilon^{\alpha_3 + \alpha_5 - 1}, \epsilon^{\alpha_6} \}. \tag{E.13}$$

On the other hand, we can calculate $\dot{\lambda}^{(3)}$ and $\dot{\lambda}^{(4)}$ from (E.9), i.e. the LHS of the flow equation. Using (E.11), this yields

$$\dot{\lambda}^{(3)} \overset{\epsilon \to 0}{\sim} \epsilon^{\alpha_3 - 1} \dot{\epsilon} \overset{\epsilon \to 0}{\sim} g \, \max\left\{ \epsilon^{\alpha_3 + \alpha_4 - 1}, \epsilon^{3\alpha_3 - 2} \right\}, \tag{E.14}$$

and

$$\dot{\lambda}^{(4)} \overset{\epsilon \to 0}{\sim} \epsilon^{\alpha_4 - 1} \dot{\epsilon} \overset{\epsilon \to 0}{\sim} g \, \max\left\{ \epsilon^{2\alpha_4 - 1}, \epsilon^{\alpha_4 + 2\alpha_3 - 2} \right\}. \tag{E.15}$$
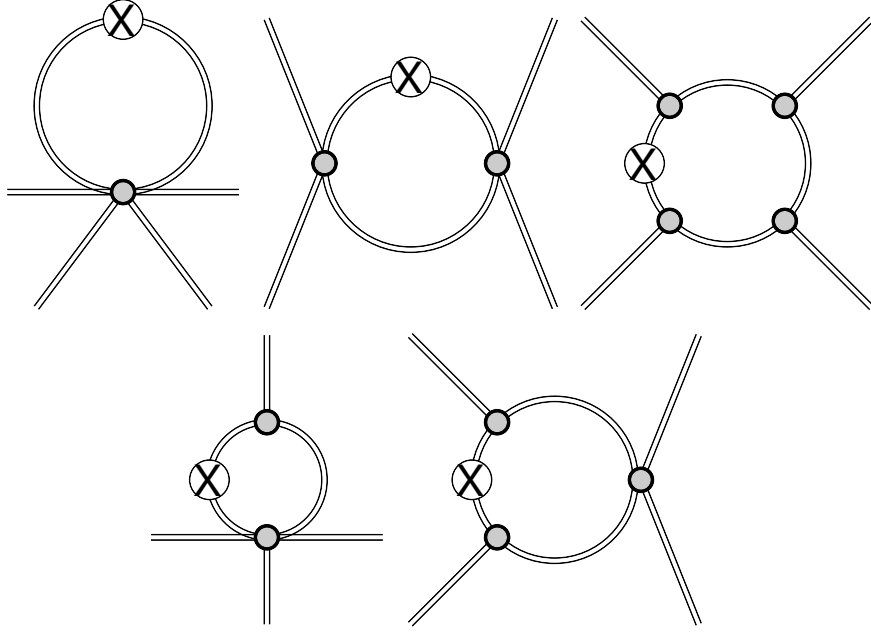
Figure E.2.: Diagrams contributing to the divergence analysis of the four-point function of the graviton.

Consistency requires matching of the leading terms on both sides of the flow equations.

If the leading term on the LHS is known, the matching condition induces inequalities on the RHS and we can obtain relations for α_n.

On the left hand sides of the flow equations for the three- and the four-point functions we have in each case two terms, (E.14) and (E.15). Let us now study the different cases for the leading terms. Considering the three-point function, the different cases can be written as

$$\alpha_3 + \alpha_4 - 1 \lesseqgtr 3\alpha_3 - 2 \, . \tag{E.16}$$

Analogously, from the LHS of the four-point function we obtain one of the "dual" relations

$$2\alpha_4 - 1 \lesseqgtr \alpha_4 + 2\alpha_3 - 2 \, . \tag{E.17}$$

Obviously, the above relations (E.16) and (E.17) are equivalent, i.e. if one of the relations $>, =, <$ is true, the corresponding relation holds for the other expression. Consequently, if we know the leading term on the LHS of the flow equation for $\Gamma^{(3h)}$, we know the leading term in the corresponding equation for $\Gamma^{(4h)}$ and vice versa. We proceed with a case-by-case analysis.

(i) Assume

$$\alpha_3 + \alpha_4 - 1 \geq 3\alpha_3 - 2 \, . \tag{E.18}$$

From the "dual" relation for the four point function we know that $\alpha_4 + 2\alpha_3 - 2$ is the dominant term on the LHS of $\dot{\lambda}^{(4)}$ and therefore also on the RHS, i.e. in (E.13). Hence, the inequality

$$\alpha_4 + 2\alpha_3 - 2 \leq 4\alpha_3 - 3 \tag{E.19}$$

necessarily holds. This inequality in turn implies $\alpha_4 \leq 2\alpha_3 - 1$, while (E.18) is equivalent to $\alpha_4 \geq 2\alpha_3 - 1$. We conclude that

$$\alpha_4 = 2\alpha_3 - 1 \,, \tag{E.20}$$

which is equivalent to the assumption $3\alpha_3 - 2 = \alpha_3 + \alpha_4 - 1$ while $3\alpha_3 - 2 < \alpha_3 + \alpha_4 - 1$ produces a contradiction.

With (E.20) we have checked two of the three cases, i.e. under the $\geq$ assumption only the $=$ sign is a consistent solution. The term involving α_5 is subject to the condition

$$\alpha_5 \geq \alpha_3 + \alpha_4 - 1 \,. \tag{E.21}$$

Let us study the other case:
  (ii) Assume

$$\alpha_3 + \alpha_4 - 1 < 3\alpha_3 - 2 \,. \tag{E.22}$$

Comparing with (E.12), we find that the equation for $\dot{\Gamma}^{(3h)}$ is trivially consistent with this assumption. Moreover, the assumption that $2\alpha_4 - 1$ is the leading term (which is equivalent to assumption (E.22)) is consistent with the first three diagrams in (E.13). Again, the terms involving α_5 and α_6 are appropriately constrained, see remark 2 below, and we can constitute that (E.22) is indeed a consistent assumption. Including both cases, this leads to the relation

$$\alpha_4 \leq 2\alpha_3 - 1 \,, \tag{E.23}$$

and proves the lemma. $\square$

Remark 1: This means that from $\dot{\Gamma}^{(3h)}$ and $\dot{\Gamma}^{(4h)}$ we obtain an inequality that constrains the relation between α_3 and α_4, which are at this stage free parameters.

Remark 2: Lemma 1 with (E.8) implies

$$\alpha_4 < 0 \tag{E.24}$$

always, thus α_3 cannot be constrained solely by the analysis above.

Remark 3: Moreover, we cannot fix α_n for $n > 4$ with the equations for the three- and the four-point function. However, since equations (E.14) and (E.15) are independent of α_4 and α_5, these terms cannot be the leading contributions in the limit under consideration, i.e. they cannot generate the power law. This implies

$$\alpha_5 \geq \alpha_4 + \alpha_3 - 1 \,. \tag{E.25}$$

Applying the same logic to the four-point function, we arrive at

$$\alpha_6 \geq 2\alpha_4 - 1 \,. \tag{E.26}$$

In order to further constrain the parameters α_n with $n > 4$, we proceed by analyzing the running of $\Gamma^{(nh)}$.

Lemma 2: *Under the same conditions as in Lemma 1, we obtain the recursion relation for $n \geq 5$:*

$$\alpha_n = \alpha_{n-2} + \alpha_4 - 1 \,. \tag{E.27}$$

E. Infrared scaling analysis

$1/\chi$	$\alpha_3 = -0.1$	$\alpha_3 = -0.2$	$\alpha_3 = -0.3$	$\alpha_3 = -0.4$	$\alpha_3 = -0.5$
20	$\mu_* = -0.698$ $g_* = 0.799$	$\mu_* = -0.704$ $g_* = 0.787$	$\mu_* = -0.713$ $g_* = 0.769$	$\mu_* = X$ $g_* = X$	$\mu_* = X$ $g_* = X$
50	$\mu_* = -0.681$ $g_* = 0.837$	$\mu_* = -0.682$ $g_* = 0.834$	$\mu_* = -0.684$ $g_* = 0.830$	$\mu_* = -0.686$ $g_* = 0.824$	$\mu_* = -0.689$ $g_* = 0.817$
100	$\mu_* = -0.675$ $g_* = 0.848$	$\mu_* = -0.676$ $g_* = 0.846$	$\mu_* = -0.677$ $g_* = 0.845$	$\mu_* = -0.678$ $g_* = 0.843$	$\mu_* = -0.679$ $g_* = 0.840$
2000	$\mu_* = -0.671$ $g_* = 0.857$	$\mu_* = -0.671$ $g_* = 0.857$	$\mu_* = -0.671$ $g_* = 0.857$	$\mu_* = -0.671$ $g_* = 0.857$	$\mu_* = -0.671$ $g_* = 0.857$

Table E.1.: UV fixed point values for different parameters χ and α_3 with exponential regulator and $a = 4$. X indicates that no fixed point is found for these parameter values.

Proof: In general, assumption (E.9) together with (E.11) leads to

$$\dot{\lambda}^{(n)} \overset{\epsilon \to 0}{\sim} g \, \epsilon^{\alpha_n - 1} \dot{\epsilon}$$
$$\overset{\epsilon \to 0}{\sim} g \max \left\{ \epsilon^{\alpha_n + \alpha_4 - 1}, \epsilon^{\alpha_n + 2\alpha_3 - 2} \right\}. \tag{E.28}$$

The canonical term can be dropped since $\alpha_4 < 0$. Lemma 1 ensures that the leading term is always given by $\epsilon^{\alpha_n + \alpha_4 - 1}$. Accordingly, all terms generated by the diagrams on the RHS of the flow equation must be smaller or equal to this term. For every n, the flow equation for $\Gamma^{(nh)}$ contains a diagram with 2 four-point vertices, one $(n-2)$-vertex and 4 internal propagators. Hence, we can conclude

$$\alpha_n + \alpha_4 - 1 \leq 2\alpha_4 + \alpha_{n-2} - 2. \tag{E.29}$$

Moreover, we can generalize the results (E.25) and (E.26), by considering the diagram with only one vertex, more precisely, an $(n+2)$-vertex. Again, consistency requires

$$\alpha_{n+2} \geq \alpha_n + \alpha_4 - 1 \tag{E.30}$$

or equivalently $\alpha_n \geq \alpha_{n-2} + \alpha_4 - 1$. Combining this result with (E.29) proves lemma 2. □

Remark 4: Lemma 2 yields a recursion relation connecting all α_n with α_4 and α_3. We are therefore left with two free parameters, with the constraint (E.24). Moreover, we can give explicit, non-recursive, expressions for α_n, depending on whether n is odd or even. The difference $\Delta\alpha$ between α_n and α_{n-2} is obviously

$$\Delta\alpha = \alpha_4 - 1, \tag{E.31}$$

and therefore independent of n. For n even we can express any α_n as

$$\alpha_n = \alpha_4 + \left(\frac{n-4}{2} \right) \Delta\alpha$$
$$= \left(\frac{n}{2} - 1 \right) \alpha_4 - \left(\frac{n}{2} - 2 \right), \, n \text{ even}, n \geq 6, \tag{E.32}$$

which can be rewritten as

$$\alpha_{2n} = (n-1)\alpha_4 - (n-2), \ n \geq 3.$$
(E.33)

For n odd we can do the same thing, starting with α_3 and adding multiples of $\Delta\alpha$ in order to arrive at

$$\alpha_{2n+1} = \alpha_3 + (n-1)\alpha_4 - (n-1), \ n \geq 2.$$
(E.34)

Estimating α_3

Following the argument in subsection 5.6.3, there is a transition regime between Einstein-Hilbert-type of solutions with $\lambda^{(2)} = \lambda^{(3)}$ and an IR regime where they differ as the trajectories approach $\epsilon = 0$. The simplest form of such a transition is a sharp switch between the two solutions at a scale k_0 when the trajectories bend over to the separatrix and are attracted towards the IR fixed point. Such a sharp cross-over between these two regions is certainly different from the true behaviour, and it also differs from our ansatz (5.92). However, this type of transition shares the essential features with the true solution and can thus provide a reasonable estimate. At the transition scale k_0 we have the connection conditions

$$\lambda^{(3)}(k_0) = \lambda^{(2)}(k_0) = -\frac{1}{2}\mu(k_0) \tag{F.1}$$

and

$$\dot{\lambda}^{(3)}(k_0) = \dot{\lambda}^{(2)}(k_0) = -\frac{1}{2}\dot{\epsilon}(k_0). \tag{F.2}$$

Using the power law (E.6) we have the simple relation for the logarithmic derivative

$$\frac{\left(\lambda^{(3)}\right)'}{\lambda^{(3)}} = \frac{\alpha_3}{\epsilon}, \tag{F.3}$$

where $'$ denotes the derivative with respect to ϵ. The scale derivative can be expressed as

$$\dot{\lambda}^{(3)} = \left(\lambda^{(3)}\right)' \dot{\epsilon}. \tag{F.4}$$

Evaluating the above equation at $k = k_0$ and combining it with (F.2) yields

$$\left(\lambda^{(3)}\right)'\Big|_{k=k_0} = -\frac{1}{2}. \tag{F.5}$$

This in turn can be used together with (F.2) when evaluating (F.3) at $k = k_0$. Keeping in mind that $\epsilon = 1 + \mu$, this results in

$$\alpha_3 = \frac{1 + \mu(k_0)}{\mu(k_0)}. \tag{F.6}$$

Together with $\alpha_4 = 2\alpha_3 - 1$ this fixes all α_n. From the phase diagram, one infers that the onset of this transition is near $\mu \approx -0.9$ independent of the chosen parameters. This gives

$$\alpha_3 \approx -1/9 \,. \tag{F.7}$$

Not sticking to the equality does not alter the results qualitatively.

Functional form of $\lambda^{(n)}$

Here we construct explicit expressions for the functions $\lambda^{(n)}$. In addition to the singularity structure, there are further constraints to be fulfilled by such an ansatz. In the following we show that

$$
\begin{aligned}
\lambda^{(n)} &= -\frac{\mu}{2}\left[1 + \mathrm{sgn}(\mu)\,\chi\left|\frac{\mu}{1+\mu}\right|^{-\alpha_n}\right] \\
&= -\frac{\mu}{2}(1 + \delta\lambda^{(n)})
\end{aligned}
\tag{G.1}
$$

is consistent with all constraints. In the above formula χ is an arbitrary parameter. From perturbation theory we know that in the Gaussian limit $\mu \to 0$, we need to recover an Einstein-Hilbert solution. Indeed, (G.1) entails $\lambda^{(n)} = -\mu/2$ for all n in the vicinity of $\mu = 0$ as long as $\alpha_n < 0$. In addition to that, it is clear that the correction cannot contain further powers of g, since this would interfere with the singularity structure. Furthermore, the correction should be inherently dimensionless. With these conditions, a quantity proportional to powers of the ratio $\mu/(1 + \mu)$ is everything we have at hand. In the end, we are left with two (constrained) free parameters, namely $\alpha_3 \le 0$ and $\chi \in \mathbb{R}\backslash 0$. The proportionality factor χ is in general different for all $\lambda^{(n)}$ and can in principle be calculated from higher order vertex functions. In our truncation we choose a uniform constant for simplicity. The IR structure is unaffected by the value of χ, but a large χ might alter the UV regime. Note that the scaling analysis is true in the IR limit only. Consequently, we expect a small χ which does not interfere with the UV regime.

Anomalous dimensions in the IR

Both anomalous dimensions need to vanish at the IR fixed point for it to be classical. For the ghost anomalous dimension, this is the case as long as $g/\epsilon \to 0$, which is equivalent to saying that $\alpha_3 < 0$, in accordance with our estimate above. On the other hand, the vanishing of the graviton anomalous dimension is seen as follows: First, as shown in [1], the terms quadratic in the external momentum in the flow cancel. Thus, the flow goes to a constant as the external momentum goes to infinity, and no divergences can appear there. Next, the flow equation for the mass can be rewritten as

$$\dot{\mu} = -2\mu + \frac{\partial_t \Gamma^{(2h)}(0)}{Z_h(0)} + \eta_h(0)\mu \,. \tag{H.1}$$

We know that in the IR for $\mu \to -1, g \to 0$, $\dot{\mu}$ vanishes. This can be achieved in 3 different ways: either the flow vanishes and the anomalous dimension at zero cancels the canonical scaling, or both the flow and the anomalous dimension cancel the canonical scaling, or only the flow remains finite. First assume that the flow vanishes in the limit $\mu \to -1, g \to 0$. We know that the leading order contribution comes from a term $\sim g\lambda^{(4)}$, all other terms have smaller divergences and thus vanish in the limit $g \to 0$. If this term vanishes, however, then the flow is 0 everywhere, thus also the anomalous dimension would vanish everywhere, and we would end up with no fixed point. On the other hand, assume that $g\lambda^{(4)}$ remains finite in our limit, then still all other terms in the flow vanish, and thus the flow is a nonzero constant. This in turn implies that the graviton anomalous dimension must vanish as it is a finite difference of the flow. We conclude that $\eta_h(p^2) = 0$ at the IR fixed point.

Flow of the Three-Point Fuction with Super-Fields

In this appendix we derive the flow equations of the three-point function with super-fields, i.e. a representation of Flow$^{(3)}$ in terms of propagators and vertices for a theory with arbitrary field content. For the propagator we have presented the derivation in Appendix B. In order to arrive at an analog expression for the three-point function we take a further derivative of with respect to the fields and arrive at

$$
\begin{aligned}
\dot{\Gamma}^{(3)\mathbf{abc}} = -\frac{1}{2}(-1)^{\mathbf{i,abc}}\Big\{ &\Big[G_{\mathbf{id}}\Gamma^{(3)\mathbf{dae}}G_{\mathbf{fg}}\Gamma^{(3)\mathbf{gbh}}G_{\mathbf{kl}}\Gamma^{(3)\mathbf{lcm}}G_{\mathbf{nj}}\gamma_{\mathbf{e}}^{\mathbf{f}}\gamma_{\mathbf{h}}^{\mathbf{k}}\gamma_{\mathbf{m}}^{\mathbf{n}} \\
&+ \text{Permutation}\big[(-1)^{(\mathbf{a,bef})}(\mathbf{a}\leftrightarrow\mathbf{b})\big] + \text{Permutation}\big[(-\mathbf{1})^{(\mathbf{a,bcefhk})}(\mathbf{a}\to\mathbf{c}\to\mathbf{b}\to\mathbf{a})\big] \\
&+ \text{Permutation}\big[(-1)^{(\mathbf{b,chk})}\big((\mathbf{b}\leftrightarrow\mathbf{c}) + (-1)^{(\mathbf{a,cef})}(\mathbf{a}\to\mathbf{c}\to\mathbf{b}\to\mathbf{a}) \\
&+ (-1)^{(\mathbf{a,bcefhk})}(\mathbf{a}\leftrightarrow\mathbf{c})\big)\big]\Big] \\
&- \Big[G_{\mathbf{id}}\Gamma^{(4)\mathbf{dabe}}G_{\mathbf{fg}}\Gamma^{(3)\mathbf{gch}}G_{\mathbf{kj}}\gamma_{\mathbf{e}}^{\mathbf{f}}\gamma_{\mathbf{h}}^{\mathbf{k}} \\
&+ \text{Permutation}\big[(-1)^{(\mathbf{a,bef})}(\mathbf{ab}\to\mathbf{b},\mathbf{c}\to\mathbf{ac}) + (\mathbf{ab}\to\mathbf{a},\mathbf{c}\to\mathbf{bc}) \\
&+ (-1)^{(\mathbf{a,bcef})}(\mathbf{ab}\to\mathbf{bc},\mathbf{c}\to\mathbf{a}) + (-1)^{(\mathbf{b,c,ef})}(\mathbf{ab}\to\mathbf{ac},\mathbf{c}\to\mathbf{b}) \\
&+ (-1)^{(\mathbf{b,cef})}(-1)^{(\mathbf{a,cef})}(\mathbf{ab}\to\mathbf{c},\mathbf{c}\to\mathbf{ab})\big]\Big] \\
&+ G_{\mathbf{id}}\Gamma^{(5)\mathbf{dabce}}G_{\mathbf{fi}}\gamma_{\mathbf{e}}^{\mathbf{f}}\Big\}\dot{R}^{\mathbf{ij}}.
\end{aligned}
$$

In the above equation we have introduced several short hand notations, namely

$$
(-1)^{(\mathbf{a,bc})} := (-1)^{(\mathbf{a,b})}(-1)^{(\mathbf{a,c})}, \tag{I.1}
$$

and analogous for more indices. Additionally, the permutations relate to the previous term that is written explicitly but with the given index replacements, where replacements of the form $(\mathbf{ab}\to\mathbf{c})$ mean that the order of the corresponding vertex is reduced by one and vive versa.

Analytic flow equations

In a specification precudure, where we use projections at $p = 0$ only, the system of flow equations is completely analytic, for symmetric, as well as for the asymmetric configuration. The corresponding equations with identifications $G^{(3)} \equiv G^{(4)} \equiv G^{(5)} \equiv G_N$ and $\Lambda^{(3)} \equiv \Lambda^{(4)} \equiv \Lambda^{(5)}$ which close the system of equations are then given by

$$
\begin{aligned}
\dot{g} = & (2 + 3\eta_h)g + \frac{g^2}{\pi}\left(-\frac{5(6 - \eta_h)}{42(\mu_h + 1)^2} \right. \\
& + \frac{2\lambda^{(4)}(62(6 - \eta_h) - 195(4 - \eta_h)\lambda^{(3)}) + 62(6 - \eta_h)\lambda^{(3)} - 15(8 - \eta_h)}{63(\mu_h + 1)^3} \\
& + \frac{39(8 - \eta_h) - 232(6 - \eta_h)\lambda^{(3)}}{252(\mu_h + 1)^3} + \frac{17 + 272\lambda^{(4)} - 4\lambda^{(3)}(161\lambda^{(4)} + 8)}{42(\mu_h + 1)^4} \\
& + \frac{2772(4 - \eta_h)\lambda^{(3)3} + 1000(6 - \eta_h)\lambda^{(3)2} - 705(8 - \eta_h)\lambda^{(3)} + 90(10 - \eta_h)}{210(\mu_h + 1)^4} \\
& \left. - \frac{523 - 2\lambda^{(3)}(4\lambda^{(3)}(374\lambda^{(3)} - 615) + 1415)}{105(\mu_h + 1)^5} + \frac{3(190 + 13\eta_c)}{140} \right),
\end{aligned}
\tag{J.1}
$$

for Newtons coupling from the asymetric three–point function, wihle the momentum–independent part reads

$$
\begin{aligned}
\dot{\lambda}^{(3)} = & -2\lambda^{(3)} + \frac{3}{2}\eta_h\lambda^{(3)} - \frac{1}{2}(\frac{\dot{g}}{g} - 2)\lambda^{(3)} + \frac{g}{2\pi}\left(\frac{12 - \eta_c}{5} + \frac{8 - \eta_h - 4(6 - \eta_h)\lambda_5}{4(1 + \mu_h)^2} \right. \\
& + \frac{3(8 - \eta_h)\lambda^{(4)} - 16(6 - \eta_h)\lambda^{(3)}\lambda^{(4)}}{3(1 + \mu_h)^3} \\
& \left. - \frac{11(12 - \eta_h) - 72(10 - \eta_h)\lambda^{(3)} + 120(8 - \eta_h)\lambda^{(3)2} - 80(6 - \eta_h)\lambda^{(3)3}}{120(1 + \mu_h)^4} \right).
\end{aligned}
\tag{J.2}
$$

J. Analytic flow equations

From the two–point functions we obtain for the evaluation at $p = 0$

$$
\dot{\mu}_h = (\eta_h - 2)\mu_h + \frac{g}{\pi}\left(\frac{8(6 - \eta_h)\lambda^{(4)} - 3(8 - \eta_h)}{12(1 + \mu_h)^2}\right.
$$
$$
\left. + \frac{21(10 - \eta_h) - 120(8 - \eta_h)\lambda^{(3)} + 320(6 - \eta_h)\lambda^{(3)2}}{180(1 + \mu_h)^3} - \frac{10 - \eta_c}{5}\right),
$$

(J.3)

and from the derivatve at $p = 0$

$$
\eta_h = \frac{g}{4\pi}\left(\frac{6 - \eta_h}{(1 + \mu_h)^2} - \frac{6(8 - \eta_h) + 8(6 - \eta_h)\lambda^{(3)} - 36(4 - \eta_h)\lambda^{(3)2}}{9(1 + \mu_h)^3}\right.
$$
$$
\left. + \frac{17 + 8\lambda^{(3)}(9\lambda^{(3)} - 8)}{3(1 + \mu_h)^4} - \eta_c\right)
$$

(J.4)

$$
\eta_c = -\frac{g}{9\pi}\left(\frac{8 - \eta_h}{(1 + \mu_h)^2} + \frac{8 - \eta_c}{1 + \mu_h}\right).
$$

(J.5)

For the symmetric configuration the gravitational coupling takes the form

$$
\dot{g} = (2 + 3\eta_h)g + \frac{g^2}{19\pi}\left(-\frac{47(6 - \eta_h)}{6(1 + \mu_h)^2} + \frac{16(1 - 3\lambda^{(3)})\lambda^{(4)}}{(1 + \mu_h)^4}\right.
$$
$$
+ \frac{45(8 - \eta_h) + 472(6 - \eta_h)\lambda^{(4)} - 120\lambda^{(3)}(2(6 - \eta_h) + 3(4 - \eta_h)\lambda^{(4)})}{18(1 + \mu_h)^3}
$$
$$
+ \frac{147(10 - \eta_h) - 1860(8 - \eta_h)\lambda^{(3)} + 3380(6 - \eta_h)\lambda^{(3)2} + 25920(4 - \eta_h)\lambda^{(3)3}}{90(1 + \mu_h)^4}
$$
$$
\left. + 2\frac{-299 + 1780\lambda^{(3)} - 3640\lambda^{(3)2} + 2336\lambda^{(3)3}}{15(1 + \mu_h)^5} - \frac{50 - 53\eta_c}{10}\right)
$$

(J.6)

Spectral Representation and Correlation Functions in the Real-Time Formalism

---

This appendix is based on my internal notes, [193], which were already presented in [175]. In this section we provide the basic definitions and theorems underlying our real-time study.
Definitions:
Correlation functions at finite temperature are defined as thermal ensemble averages according to

$$\langle A_1...A_n \rangle := \frac{\operatorname{Tr}\left(e^{-\beta H} A_1...A_n\right)}{\operatorname{Tr} e^{-\beta H}}, \tag{K.1}$$

for appropriately defined operators $A_1...A_n$.

In the real-time formalism, n-point correlation functions are tensors with respect to the contour indices $\{+, -\}$ and are therefore objects with 2^n components. For the two-point function

$$G = \begin{pmatrix} G_{++} & G_{+-} \\ G_{-+} & G_{--} \end{pmatrix}, \tag{K.2}$$

these components are defined by

$$
\begin{aligned}
G_{-+}(x,y) &:= -i\,\langle \varphi(x)\varphi(y) \rangle =: G_>(x,y) \\
G_{+-}(x,y) &:= -i\,\langle \varphi(y)\varphi(x) \rangle =: G_<(x,y) \\
G_{++}(x,y) &:= -i\,\langle T\varphi(y)\varphi(x) \rangle =: G_F(x,y) \\
G_{--}(x,y) &:= -i\,\langle \tilde{T}\varphi(y)\varphi(x) \rangle =: G_{\tilde{F}}(x,y),
\end{aligned} \tag{K.3}
$$

where T denotes the time ordering operator and $\tilde{T}$ the anti-time ordering operator. Using the definition of the retarded propagator the one above one obtains

$$G_R(x,y) = G_{++}(x,y) - G_{+-}(x,y). \tag{K.4}$$

Symmetry relations for the propgator:

The components $G_{i,j}$ of the propagator obey some very convenient relations. In particular,

$$G^*_{-+}(x,y) = -G_{+-}(x,y). \tag{K.5}$$

First we note that for a real, classical scalar field, the corresponding quantum field is a self-adjoint operator (at least symmetric), i.e. $\varphi^\dagger = \varphi$, and so is the Hamiltonian. Then we can deduce

$$G^*_{-+}(x,y) = \left(-i\,\frac{\mathrm{Tr}\left(e^{-\beta H}\varphi(x)\varphi(y)\right)}{\mathrm{Tr}\,e^{-\beta H}}\right)^* = i\sum_n \frac{\langle f_n, e^{-\beta H}\varphi(x)\varphi(y)f_n\rangle^*}{\mathrm{Tr}\,e^{-\beta H}}$$

$$= i\sum_n \frac{\langle e^{-\beta H}\varphi(x)\varphi(y)f_n, f_n\rangle}{\mathrm{Tr}\,e^{-\beta H}} = i\sum_n \frac{\langle f_n, \varphi(y)^\dagger\varphi(x)^\dagger\left(e^{-\beta H}\right)^\dagger f_n\rangle}{\mathrm{Tr}\,e^{-\beta H}}$$

$$= i\sum_n \frac{\langle f_n, e^{-\beta H}\varphi(y)\varphi(x)f_n\rangle}{\mathrm{Tr}\,e^{-\beta H}} = -G_{+-}(x,y), \tag{K.6}$$

which proves the claim. In the above proof f_n is a complete set of asymptotic states and we have used that the operators are symmetric and that the exponential of a symmetric operator is again symmetric. Moreover, we have used the cyclicity of the trace.

The above identity can also be proven using the machinery of thermo-field dynamics, where one constructs a finite temperature vacuum state $f_{0,\beta}$. With such a state one can simply generalize the definition of correlation functions at zero temperature to finite temperature ones by

$$\langle A_1...A_n\rangle := \langle f_{0,\beta}, A_1...A_n f_{0,\beta}\rangle. \tag{K.7}$$

With this formalism at hand we can prove the above relation via

$$G^*_{-+}(x,y) = \left(-i\langle f_{0,\beta}, \varphi(x)\varphi(y)f_{0,\beta}\rangle\right)^* = i\langle\varphi(x)\varphi(y)f_{0,\beta}, f_{0,\beta}\rangle$$

$$= i\langle f_{0,\beta}, \varphi(y)^\dagger\varphi(x)^\dagger f_{0,\beta}\rangle = i\langle f_{0,\beta}, \varphi(y)\varphi(x)f_{0,\beta}\rangle = -G_{+-}(x,y). \tag{K.8}$$

By Fourier transform we can write in momentum space

$$G^*_{-+}(p,q) = \mathscr{FT}\left\{G_{-+}(x,y)\right\}^* = \left(\int_x\int_y e^{ipx}e^{ipy}G_{-+}(x,y)\right)^*$$

$$= \int_x\int_y e^{-ipx}e^{-ipy}G^*_{-+}(x,y) = -\int_x\int_y e^{-ipx}e^{-ipy}G_{+-}(x,y) = -G_{+-}(-p,-q). \tag{K.9}$$

Note that we drop the tilde that indicates the Fourier transform since we write out the arguments explicitly. Under the assumption that the system is space-time translation invariant, the position space propagator is not an arbitrary function of (x,y), but depends only on the difference, i.e.

$$G(x,y) = G(x-y). \tag{K.10}$$

Therefore we can Fourier-transform with respect to $z := x - z$ according to

$$\mathscr{FT}\left\{G(x-y)\right\} = \int_z e^{ipz}G(z) = G(p). \tag{K.11}$$

With this at hand, and using the obvious relation $G_{-+}(x, y) = G_{+-}(y, x)$, which now translates into $G_{-+}(z) = G_{+-}(-z)$ we immediately arrive at

$$G_{-+}(p) = \int_z e^{ipz} G_{-+}(z) = \int_z e^{ipz} G_{+-}(-z) = \int_z e^{-ipz} G_{+-}(z)$$
$$= G_{+-}(-p) \tag{K.12}$$

and therefore

$$G^*_{-+}(p) = \left(\int_z e^{ipz} G_{-+}(z) \right)^* = \int_z e^{-ipz} G^*_{-+}(z) = -\int_z e^{-ipz} G_{+-}(z) = -\int_z e^{-ipz} G_{-+}(-z)$$
$$= -\int_z e^{ipz} G_{-+}(z) = -G_{-+}(p). \tag{K.13}$$

Spectral Representation:
We first derive the spectral representation for two-point functions. With a complete set f_i of generalized eigenfunctions of H with eigenvalues E_i, this is derived as follows,

$$G_{-+}(x, y) = \frac{-i}{Z_\beta} \operatorname{Tr} \left(e^{-\beta H} \varphi(x) \varphi(y) \right) = \frac{-i}{Z_\beta} \sum_n \langle f_n, e^{-\beta H} \varphi(x) \varphi(y) f_n \rangle$$
$$= \frac{-i}{Z_\beta} \sum_n \sum_m e^{-\beta E_n} \langle f_n, \varphi(x) f_m \rangle \langle f_m, \varphi(y) f_n \rangle$$
$$= \frac{-i}{Z_\beta} \sum_n \sum_m e^{-\beta E_n} \langle f_n, e^{-iPx} \varphi(0) e^{iPx} f_m \rangle \langle f_m, e^{-iPy} \varphi(0) e^{iPy} f_n \rangle$$
$$= \frac{-i}{Z_\beta} \sum_n \sum_m e^{-\beta E_n} \langle e^{iPx} f_n, \varphi(0) e^{iHx} f_m \rangle \langle e^{iPy} f_m, \varphi(0) e^{iPy} f_n \rangle$$
$$= \frac{-i}{Z_\beta} \sum_n \sum_m e^{-\beta E_n} e^{ip_n x} e^{-ip_m x} e^{ip_m y} e^{-ip_n y} \langle f_n, \varphi(0) f_m \rangle \langle f_m, \varphi(0) f_n \rangle$$
$$= \frac{-i}{Z_\beta} \sum_n \sum_m e^{-\beta E_n} e^{ip_n(x-y)} e^{-ip_m(x-y)} \left| \langle f_n, \varphi(0) f_m \rangle \right|^2 ,$$

with the partition function

$$Z_\beta = \operatorname{Tr} e^{-\beta H}. \tag{K.14}$$

In the above equation we have used that the Energy-Momentum operator P has eigenvalues p and generates space-time translations and acts as

$$\varphi(0) = e^{iPx} \varphi(x) e^{-iPx} \tag{K.15}$$

on the fields. Moreover, we exploited that P is symmetric and used the anti-linearity of the complex inner product. We now define the spectral density of the $-+$ two-point function in momentum space as

$$\tilde{\rho}_{-+}(p) := \frac{1}{Z_\beta} \sum_n \sum_m e^{-\beta E_n} (2\pi)^4 \delta(p_n - p_m + p) \left| \langle f_n, \varphi(0) f_m \rangle \right|^2 , \tag{K.16}$$

which is obviously a real (in momentum space!), and positive(-semi) definite quantity. The two point function G_{-+} in momentum space is now obviously proportional to the spectral density:

$$
\begin{aligned}
G_{-+}(p) &= \frac{-i}{Z_\beta} \int_{(x-y)} e^{ip(x-y)} \sum_n \sum_m e^{-\beta E_n} e^{ip_n(x-y)} e^{-ip_m(x-y)} \left| \langle f_n, \varphi(0) f_m \rangle \right|^2 \\
&= -i \tilde{\rho}_{-+}(p).
\end{aligned}
\tag{K.17}
$$

Clearly, the above derivation can be repeated for G_{+-} just with x and y interchanged and one arrives at

$$
\tilde{\rho}_{+-}(p) := \frac{1}{Z_\beta} \sum_n \sum_m e^{-\beta E_n} (2\pi)^4 \delta(-p_n + p_m + p) \left| \langle f_n, \varphi(0) f_m \rangle \right|^2
\tag{K.18}
$$

and

$$
G_{+-}(p) = -i \tilde{\rho}_{+-}(p).
\tag{K.19}
$$

By using the symmetry of the delta function in (K.16), we can establish the obvious relation

$$
\tilde{\rho}_{+-}(p) = \tilde{\rho}_{-+}(-p).
\tag{K.20}
$$

Moreover, we can relabel the dummy indices m and n in (K.16), making use of the zero component of the delta function, which is nothing but energy conservation $E_m - E_n + p^0 = 0$, and using the invariance of the matrix element under interchange of m and n in order to arrive at

$$
\begin{aligned}
\tilde{\rho}_{-+}(p) &= \frac{1}{Z_\beta} \sum_m \sum_n e^{-\beta E_m} (2\pi)^4 \delta^{(4)}(p_m - p_n + p) \left| \langle f_m, \varphi(0) f_n \rangle \right|^2 \\
&= e^{\beta p^0} \tilde{\rho}_{+-}(p).
\end{aligned}
\tag{K.21}
$$

The above equation is obviously nothing else than the well-known KMS-condition, which is usually formulated for the two-point functions itself,

$$
G_{-+}(p) = e^{\beta p^0} G_{+-}(p),
\tag{K.22}
$$

and can also be obtained from the periodicity condition in time-direction. Note that this holds only in equilibrium, since the periodicity as well as our representation for the correlation functions with the density matrix $e^{-\beta H}$ do not hold in non-equilibrium. A more convenient quantity than the spectral densities defined above is the standard spectral function $\rho(p)$ known from QFT textbooks, since all components of the propagator matrix G, as well as the retarded and advanced ones can be expressed in terms of this spectral function. We thus define in position space

$$
\begin{aligned}
\rho(x,y) &:= \langle [\varphi(x), \varphi(y)] \rangle \\
&= \langle \varphi(x)\varphi(y) \rangle - \langle \varphi(y)\varphi(x) \rangle \\
&= i \left(G_{-+}(x,y) - G_{+-}(x,y) \right) \\
&= \tilde{\rho}_{-+}(x,y) - \tilde{\rho}_{+-}(x,y).
\end{aligned}
\tag{K.23}
$$

In terms of this spectral function the off-diagonal elements of the propagator are given by

$$
\begin{aligned}
G_{-+}(p) = -i\tilde{\rho}_{-+}(p) = &-i\,\frac{\rho(p)}{1-e^{-\beta p^0}} = -i\,\frac{\rho(p)\,e^{\beta p^0}}{e^{\beta p^0}-1} = -i\,\frac{\rho(p)\left(e^{\beta p^0}-1+1\right)}{e^{\beta p^0}-1} \\
= &-i\left(\rho(p)+\frac{\rho(p)}{e^{\beta p^0}-1}\right) = -i\,\rho(p)\left(1+n_\beta(p^0)\right),
\end{aligned}
\tag{K.24}
$$

and similarly

$$
G_{+-}(p) = -i\tilde{\rho}_{+-}(p) = -i\,\rho(p)\,n_\beta(p^0),
\tag{K.25}
$$

with the Bose-Einstein distribution

$$
n_\beta(p^0) = \frac{1}{e^{\beta p^0}-1}.
\tag{K.26}
$$

Now we proceed to the diagonal elements. Considering the time-ordered, i.e. Feynman propagator and making the time-ordering explicit we have to deal with

$$
G_{++}(x,y) = -i\left(\theta(x^0-y^0)\langle\phi(x)\phi(y)\rangle + \theta(y^0-x^0)\langle\phi(y)\phi(x)\rangle\right),
\tag{K.27}
$$

with the Heaviside-theta function θ. The correlation functions appearing in (K.27) were already calculated above. However, the Fourier-transform is now a little more complicated due to the θ functions with pure time-arguments and we have to perform Fourier transformations for space arguments $\mathbf{z} := \mathbf{x} - \mathbf{y}$ and time arguments $z^0 := x^0 - y^0$ separately. Together with the identity for the θ-function the spectral representation for G_{++} is given by

$$
\begin{aligned}
G_{++}(p) = &\frac{-i}{Z_\beta}\int_{\mathbf{z}}\int_{z^0}e^{-i\mathbf{p}\mathbf{z}}e^{ip^0z^0}\theta(z^0)\sum_n\sum_m e^{-\beta E_n}e^{ip_n z}e^{-ip_m z}\left|\langle f_n,\varphi(0)f_m\rangle\right|^2 \\
&\frac{-i}{Z_\beta}\int_{\mathbf{z}}\int_{z^0}e^{-i\mathbf{p}\mathbf{z}}e^{ip^0z^0}\theta(-z^0)\sum_n\sum_m e^{-\beta E_n}e^{-ip_n z}e^{+ip_m z}\left|\langle f_n,\varphi(0)f_m\rangle\right|^2.
\end{aligned}
$$

We can make use of the integral representation of the θ function

$$
\theta(x) = \lim_{\epsilon\to 0}\frac{i}{2\pi}\int_\tau\frac{e^{-ix\tau}}{\tau+i\epsilon},
\tag{K.28}
$$

and

$$
\theta(-x) = \lim_{\epsilon\to 0}\frac{-i}{2\pi}\int_\tau\frac{e^{-ix\tau}}{\tau-i\epsilon},
\tag{K.29}
$$

which tells us how to deal with the above Fourier transforms with an appropriate $i\epsilon$-prescription. We first manipulate the first term in the above expression for $G_{++}(p)$, i.e. the

term proportional to $\theta(z^0)$, as

$$\frac{-i}{Z_\beta}\frac{i}{2\pi}\sum_m\sum_n e^{-\beta E_n}\left|\langle f_n,\varphi(0)f_m\rangle\right|^2\int_{\mathbf{z}}\int_{z^0}e^{iz^0\left(p^0+p_n^0-p_m^0\right)}e^{-i\mathbf{z}(\mathbf{p}+\mathbf{p_n}-\mathbf{p_m})}\int_{p^{0\prime}}\frac{e^{-iz^0 p^{0\prime}}}{p^{0\prime}+i\epsilon}$$

$$=\frac{-i}{Z_\beta}\frac{i}{2\pi}\sum_m\sum_n e^{-\beta E_n}\left|\langle f_n,\varphi(0)f_m\rangle\right|^2(2\pi)^3\delta^{(3)}\left(\mathbf{p}+\mathbf{p_n}-\mathbf{p_m}\right)$$

$$\times\int_{p^{0\prime}}\frac{1}{p^{0\prime}+i\epsilon}\int_{z^0}e^{iz^0\left(p^0-p^{0\prime}+p_n^0-p_m^0\right)}$$

$$=\frac{-i}{Z_\beta}\frac{i}{2\pi}\sum_m\sum_n e^{-\beta E_n}\left|\langle f_n,\varphi(0)f_m\rangle\right|^2(2\pi)^3\delta^{(3)}\left(\mathbf{p}+\mathbf{p_n}-\mathbf{p_m}\right)$$

$$\times\int_{p^{0\prime}}\frac{1}{p^{0\prime}+i\epsilon}(2\pi)\delta(p^0-p^{0\prime}+p_n^0-p_m^0)$$

$$=\frac{-i}{Z_\beta}\frac{i}{2\pi}\sum_m\sum_n e^{-\beta E_n}\left|\langle f_n,\varphi(0)f_m\rangle\right|^2(2\pi)^3\delta^{(3)}\left(\mathbf{p}+\mathbf{p_n}-\mathbf{p_m}\right)(2\pi)\frac{1}{p^0-p_n^0-p_m^0+i\epsilon}\,,$$

$$\text{(K.30)}$$

where the limit $\epsilon\longrightarrow 0$ is implicitly understood. In the end, we want to express the above in terms of the spectral function ρ, which contains a four dimensional θ-function. Therefore we rewrite the representation according to

$$\frac{-i}{Z_\beta}\frac{i}{2\pi}\sum_m\sum_n e^{-\beta E_n}\left|\langle f_n,\varphi(0)f_m\rangle\right|^2(2\pi)^3\delta^{(3)}\left(\mathbf{p}+\mathbf{p_n}-\mathbf{p_m}\right)$$

$$\times(2\pi)\int_{p^{0\prime}}\frac{1}{p^0-p^{0\prime}+i\epsilon}\delta(p^{0\prime}+p_n^0-p_m^0)$$

$$=\frac{1}{2\pi}\int_{p^{0\prime}}\frac{\tilde\rho_{-+}(p^{0\prime},\mathbf{p})}{p^0-p^{0\prime}+i\epsilon}\,.\qquad\text{(K.31)}$$

We can perform analog steps for the term proportional to $\theta(-z^0)$, which produces an additional overall minus sign and a minus sign in the $i\epsilon$ prescription due to the different integral representation of the θ-function. Furthermore, it interchanges the labels m and n in the delta functions. Obviously, this can then be expressed in terms of $\tilde\rho_{+-}(p^{0\prime},p^0)$, leading to

$$G_{++}(p)=\frac{1}{2\pi}\int_{p^{0\prime}}\left(\frac{\tilde\rho_{-+}(p^{0\prime},\mathbf{p})}{p^0-p^{0\prime}+i\epsilon}-\frac{\tilde\rho_{+-}(p^{0\prime},\mathbf{p})}{p^0-p^{0\prime}-i\epsilon}\right)\,.$$

Now we want two additional representations of the above, namely in terms of the usual spectral function ρ, and such that we regain the usual Feynman propagator in the limit $T\longrightarrow 0$. In order to do so, we use the Sokhotski-Plemelj theorem

$$\lim_{\epsilon\to 0}\int_x\frac{f(x)}{x-x_0\pm i\epsilon}=\mp i\pi f(x_0)+\mathscr{P}\int_x\frac{f(x)}{x-x_0}\,.\qquad\text{(K.32)}$$

Applying this to the above identity leads to

$$G_{++}(p) = \frac{1}{2\pi}\mathscr{P}\int_{p^{0'}}\left(\frac{\tilde{\rho}_{-+}(p^{0'},\mathbf{p}) - \tilde{\rho}_{+-}(p^{0'},\mathbf{p})}{p^0 - p^{0'}}\right) - \frac{1}{2\pi}i\pi\left(\tilde{\rho}_{-+}(p^0,\mathbf{p}) + \tilde{\rho}_{+-}(p^0,\mathbf{p})\right).$$

Using the KMS condition for the spectral densities and the definition $\rho = \tilde{\rho}_{-+} - \tilde{\rho}_{+-}$, we get the relation

$$\frac{1}{2\pi}i\pi\left(\tilde{\rho}_{-+}(p^0,\mathbf{p}) + \tilde{\rho}_{+-}(p^0,\mathbf{p})\right) = \frac{1}{2\pi}i\pi\left(\rho(p^0,\mathbf{p}) + 2\tilde{\rho}_{+-}(p^0,\mathbf{p})\right)$$
$$= \frac{1}{2\pi}i\pi\left(\rho(p^0,\mathbf{p}) + 2n_\beta(p^0)\rho(p^0,\mathbf{p})\right) = i\rho(p^0,\mathbf{p})\left(\frac{1}{2} + n_\beta(p^0)\right), \tag{K.33}$$

and therefore

$$G_{++}(p) = \frac{1}{2\pi}\mathscr{P}\int_{p^{0'}}\left(\frac{\rho(p^{0'},\mathbf{p})}{p^0 - p^{0'}}\right) - i\rho(p^0,\mathbf{p})\left(\frac{1}{2} + n_\beta(p^0)\right). \tag{K.34}$$

In addition to this, we can rewrite the representation such that the zero-temperature Feynman propagator appears, and that we get back the zero-temperature spectral representation of the time-ordered propagator. In order to achieve this, we, make use of the Sokhotski-Plemelj formula and rewrite the principal value again with an $i\epsilon$- prescription. We only consider the part with the principal value:

$$\frac{1}{2\pi}\mathscr{P}\int_{-\infty}^{\infty}\mathrm{d}p^{0'}\left(\frac{\rho(p^{0'},\mathbf{p})}{p^0 - p^{0'}}\right) = \frac{1}{2\pi}\int_{-\infty}^{\infty}\mathrm{d}p^{0'}\left(\frac{\rho(p^{0'},\mathbf{p})}{p^0 - p^{0'} + i\epsilon}\right) + \frac{1}{2\pi}i\pi\rho(p^0,\mathbf{p}).$$

Together with (K.50) we first state the intermediate result

$$G_{++}(p) = \frac{1}{2\pi}\int_{-\infty}^{\infty}\mathrm{d}p^{0'}\left(\frac{\rho(p^{0'},\mathbf{p})}{p^0 - p^{0'} + i\epsilon}\right) - in_\beta(p^0)\rho(p^0,\mathbf{p}), \tag{K.35}$$

which is also quite frequently used in the literature, and maybe the most convenient one. However, we proceed with bringing the above into the analog of the well-known zero-temperature form of the spectral representation of the time-ordered propagator as follows. Now we consider only the $i\epsilon$ part.

$$\begin{aligned}G_{++}(p) &= \frac{1}{2\pi}\int_{-\infty}^{\infty}\mathrm{d}p^{0'}\left(\frac{\rho(p^{0'},\mathbf{p})}{p^0 - p^{0'} + i\epsilon}\right) - in_\beta(p^0)\rho(p^0,\mathbf{p})\\[2mm]
&= \frac{1}{2\pi}\int_{-\infty}^{\infty}\mathrm{d}p^{0'}\left(\frac{p^0 + p^{0'} - i\epsilon}{\left(p^0 - \left(p^{0'} - i\epsilon\right)\right)\left(p^0 + \left(p^{0'} - i\epsilon\right)\right)}\right)\rho(p^{0'},\mathbf{p}) - in_\beta(p^0)\rho(p^0,\mathbf{p})\\[2mm]
&= \frac{1}{2\pi}\int_{-\infty}^{\infty}\mathrm{d}p^{0'}\left(\frac{p^0 + p^{0'} - i\epsilon}{(p^0)^2 - \left(p^{0'} - i\epsilon\right)^2}\right)\rho(p^{0'},\mathbf{p}) - in_\beta(p^0)\rho(p^0,\mathbf{p})\\[2mm]
&= \frac{1}{2\pi}\int_{-\infty}^{\infty}\mathrm{d}p^{0'}\left(\frac{p^0 + p^{0'} - i\epsilon}{(p^0)^2 - \left(p^{0'}\right)^2 + 2p^{0'}i\epsilon - i^2\epsilon^2}\right)\rho(p^{0'},\mathbf{p}) - in_\beta(p^0)\rho(p^0,\mathbf{p})\end{aligned}$$

$$\tag{K.36}$$

Now we use that the limit $\epsilon \longrightarrow 0$ is implicitly understood and that the $i\epsilon$ in the numerator does not change the value of the integral, since it is not connected to any pole description, i.e. there is no principle value description necessary. Hence we can drop it. Moreover, the term of order ϵ^2 in the denominator is sub-leading and can be dropped as well. Additionally, we want to rewrite the integral as an integral over $\left(p^{0\prime}\right)^2$ instead of $p^{0\prime}$. This transformation, however, is diffeomorphic only on the negative and the positive branch separately. Therefore we proceed with rewriting the above as

$$\frac{1}{2\pi}\int_{-\infty}^{\infty}\mathrm{d}p^{0\prime}\left(\frac{p^0+p^{0\prime}}{\left(p^0\right)^2-\left(p^{0\prime}\right)^2+2p^{0\prime}i\epsilon}\right)\rho(p^{0\prime},\mathbf{p})-in_\beta(p^0)\rho(p^0,\mathbf{p})$$

$$=\frac{1}{2\pi}\int_{-\infty}^{0}\mathrm{d}p^{0\prime}\left(\frac{p^0+p^{0\prime}}{\left(p^0\right)^2-\left(p^{0\prime}\right)^2+2p^{0\prime}i\epsilon}\right)\rho(p^{0\prime},\mathbf{p})$$

$$+\frac{1}{2\pi}\int_{0}^{\infty}\mathrm{d}p^{0\prime}\left(\frac{p^0+p^{0\prime}}{\left(p^0\right)^2-\left(p^{0\prime}\right)^2+2p^{0\prime}i\epsilon}\right)\rho(p^{0\prime},\mathbf{p})-in_\beta(p^0)\rho(p^0,\mathbf{p}). \qquad (K.37)$$

We now substitute the integration variable $p^{0\prime}$ in the integrals that range from $-\infty$ to 0 with $-p^{0\prime}$ and use $\rho(-p^0)=-\rho(p^0)$, leading to

$$=-\frac{1}{2\pi}\int_{\infty}^{0}\mathrm{d}p^{0\prime}\left(\frac{p^0}{\left(p^0\right)^2-\left(p^{0\prime}\right)^2-2p^{0\prime}i\epsilon}\right)\rho(-p^{0\prime},\mathbf{p})$$

$$+\frac{1}{2\pi}\int_{0}^{\infty}\mathrm{d}p^{0\prime}\left(\frac{p^0}{\left(p^0\right)^2-\left(p^{0\prime}\right)^2+2p^{0\prime}i\epsilon}\right)\rho(p^{0\prime},\mathbf{p})$$

$$+\frac{1}{2\pi}\int_{\infty}^{0}\mathrm{d}p^{0\prime}\left(\frac{p^{0\prime}}{\left(p^0\right)^2-\left(p^{0\prime}\right)^2-2p^{0\prime}i\epsilon}\right)\rho(-p^{0\prime},\mathbf{p})$$

$$+\frac{1}{2\pi}\int_{0}^{\infty}\mathrm{d}p^{0\prime}\left(\frac{p^{0\prime}}{\left(p^0\right)^2-\left(p^{0\prime}\right)^2+2p^{0\prime}i\epsilon}\right)\rho(p^{0\prime},\mathbf{p})-in_\beta(p^0)\rho(p^0,\mathbf{p})$$

and further manipulations yield

$$= -\frac{1}{2\pi} \int_0^\infty \mathrm{d}p^{0\prime} \left(\frac{p^0}{(p^0)^2 - (p^{0\prime})^2 - 2p^{0\prime}i\epsilon} \right) \rho(p^{0\prime}, \mathbf{p})$$

$$+ \frac{1}{2\pi} \int_0^\infty \mathrm{d}p^{0\prime} \left(\frac{p^0}{(p^0)^2 - (p^{0\prime})^2 + 2p^{0\prime}i\epsilon} \right) \rho(p^{0\prime}, \mathbf{p})$$

$$+ \frac{1}{2\pi} \int_0^\infty \mathrm{d}p^{0\prime} \left(\frac{p^{0\prime}}{(p^0)^2 - (p^{0\prime})^2 - 2p^{0\prime}i\epsilon} \right) \rho(p^{0\prime}, \mathbf{p})$$

$$+ \frac{1}{2\pi} \int_0^\infty \mathrm{d}p^{0\prime} \left(\frac{p^{0\prime}}{(p^0)^2 - (p^{0\prime})^2 + 2p^{0\prime}i\epsilon} \right) \rho(p^{0\prime}, \mathbf{p}) - in_\beta(p^0)\rho(p^0, \mathbf{p})$$

$$= -\frac{1}{2\pi} \int_0^\infty \mathrm{d}p^{0\prime} \left(\frac{p^0}{(p^0)^2 - (p^{0\prime})^2 - i\epsilon} \right) \rho(p^{0\prime}, \mathbf{p}) \tag{K.38}$$

$$+ \frac{1}{2\pi} \int_0^\infty \mathrm{d}p^{0\prime} \left(\frac{p^0}{(p^0)^2 - (p^{0\prime})^2 + i\epsilon} \right) \rho(p^{0\prime}, \mathbf{p})$$

$$+ \frac{1}{2\pi} \int_0^\infty \mathrm{d}p^{0\prime} \left(\frac{p^{0\prime}}{(p^0)^2 - (p^{0\prime})^2 - i\epsilon} \right) \rho(p^{0\prime}, \mathbf{p})$$

$$+ \frac{1}{2\pi} \int_0^\infty \mathrm{d}p^{0\prime} \left(\frac{p^{0\prime}}{(p^0)^2 - (p^{0\prime})^2 + i\epsilon} \right) \rho(p^{0\prime}, \mathbf{p}) - in_\beta(p^0)\rho(p^0, \mathbf{p}), \tag{K.39}$$

where we dropped the $2p^{0\prime}$ in the $i\epsilon$ parts in the last step since now all integrals are performed over an interval with $p^{0\prime} > 0$ and the sign of the $i\epsilon$ terms is therefore fixed. Since the limit $\epsilon \longrightarrow 0$ is implicitly understood, using $\pm i\epsilon$ is just as good as $\pm i2p^{0\prime}\epsilon$. In the expressions above, we can apply the integral transformation

$$u : p^{0\prime} \longrightarrow u\left(p^{0\prime} \right) = \left(p^{0\prime} \right)^2, \tag{K.40}$$

which is now a diffeomorphism. The measure obviously transforms as

$$\mathrm{d}p^{0\prime} = \frac{\mathrm{d}u}{2p^{0\prime}}, \tag{K.41}$$

and we arrive at

$$G_{++}(p) = -\frac{1}{2\pi}\frac{1}{2}\int_0^\infty \mathrm{d}u \left(\frac{p^0}{\sqrt{u}} \frac{\rho(\sqrt{u}, \mathbf{p})}{(p^0)^2 - u - i\epsilon} \right) + \frac{1}{2\pi}\frac{1}{2}\int_0^\infty \mathrm{d}u \left(\frac{p^0}{\sqrt{u}} \frac{\rho(\sqrt{u}, \mathbf{p})}{(p^0)^2 - u + i\epsilon} \right) \tag{K.42}$$

$$+ \frac{1}{2\pi}\frac{1}{2}\int_0^\infty \mathrm{d}u \left(\frac{\rho(\sqrt{u}, \mathbf{p})}{(p^0)^2 - u - i\epsilon} \right) + \frac{1}{2\pi}\frac{1}{2}\int_0^\infty \mathrm{d}u \left(\frac{\rho(\sqrt{u}, \mathbf{p})}{(p^0)^2 - u + i\epsilon} \right) - in_\beta(p^0)\rho(p^0, \mathbf{p}).$$

In addition to the integration over $\left(p^{0'}\right)^2$ and the squares in the denominator, which are already present in the equation above, we ultimately want a representation that is entirely based on the Feynman $+i\epsilon$ description. Using the Sokhtsky Plemely theorem we can rewrite the above in the desired way. Note that the principal value parts in the terms proportional to p^0 cancel each other, and therefore these terms contribute only terms with delta functions. This is expected, since if we had dropped the $i\epsilon p^{0'}$ terms in the denominator in (K.36), i.e. if we had a standard principal value, this principal value would be zero in the first place since there are integrations over a symmetric interval while the spectral function is antisymmetric and all other terms symmetric. In the other terms the $p^{0'}$ in the nominator makes the entire thing symmetric and non-vanishing. Hence, this cancellation of the principal values is just a manifestation of this fact and we are left with "pole-contributions" of these terms only. In total, we manipulate the equation according to

$$
\begin{aligned}
G_{++}(p) =& -\frac{1}{2\pi}\frac{1}{2}i\pi \int_0^\infty du\, \rho(\sqrt{u},\mathbf{p})\frac{p^0}{\sqrt{u}}\,\delta\left(u-\left(p^0\right)^2\right)\\
& -\frac{1}{2\pi}\frac{1}{2}i\pi \int_0^\infty du\, \rho(\sqrt{u},\mathbf{p})\frac{p^0}{\sqrt{u}}\,\delta\left(u-\left(p^0\right)^2\right)\\
& +\frac{1}{2\pi}\frac{1}{2}\mathscr{P}\mathscr{V} \int_0^\infty du\, \frac{\rho(\sqrt{u},\mathbf{p})}{\left(p^0\right)^2-u} + \frac{1}{2\pi}\frac{1}{2}i\pi \int_0^\infty du\, \rho(\sqrt{u},\mathbf{p})\,\delta\left(u-\left(p^0\right)^2\right)\\
& +\frac{1}{2\pi}\frac{1}{2}\int_0^\infty du\, \frac{\rho(\sqrt{u},\mathbf{p})}{\left(p^0\right)^2-u+i\epsilon} - in_\beta(p^0)\rho(p^0,\mathbf{p})\\
=& -\frac{1}{2\pi}\frac{1}{2}i\pi \int_0^\infty du\, \rho(\sqrt{u},\mathbf{p})\frac{p^0}{\sqrt{u}}\,\delta\left(u-\left(p^0\right)^2\right)\\
& -\frac{1}{2\pi}\frac{1}{2}i\pi \int_0^\infty du\, \rho(\sqrt{u},\mathbf{p})\frac{p^0}{\sqrt{u}}\,\delta\left(u-\left(p^0\right)^2\right)\\
& +\frac{1}{2\pi}\frac{1}{2}\int_0^\infty du\, \frac{\rho(\sqrt{u},\mathbf{p})}{\left(p^0\right)^2-u+i\epsilon}\\
& +\frac{1}{2\pi}\frac{1}{2}i\pi \int_0^\infty du\, \rho(\sqrt{u},\mathbf{p})\,\delta\left(u-\left(p^0\right)^2\right) + \frac{1}{2\pi}\frac{1}{2}i\pi \int_0^\infty du\, \rho(\sqrt{u},\mathbf{p})\,\delta\left(u-\left(p^0\right)^2\right)\\
& +\frac{1}{2\pi}\frac{1}{2}\int_0^\infty du\, \frac{\rho(\sqrt{u},\mathbf{p})}{\left(p^0\right)^2-u+i\epsilon} - in_\beta(p^0)\rho(p^0,\mathbf{p})\\
=& -\frac{i}{2}\int_0^\infty du\, \rho(\sqrt{u},\mathbf{p})\frac{p^0}{\sqrt{u}}\,\delta\left(u-\left(p^0\right)^2\right) + \frac{i}{2}\int_0^\infty du\, \rho(\sqrt{u},\mathbf{p})\,\delta\left(u-\left(p^0\right)^2\right)\\
& +\frac{1}{2\pi}\int_0^\infty du\, \frac{\rho(\sqrt{u},\mathbf{p})}{\left(p^0\right)^2-u+i\epsilon} - in_\beta(p^0)\rho(p^0,\mathbf{p}).
\end{aligned}
\tag{K.43}
$$

We have not carried out the delta-functions yet, since they contain a little subtlety. For the following analysis, it is little more convenient to use $u = \left(p^{0'}\right)^2$. Before we have introduced the integral transformation, the $p^{0'}$ integrals were along the positive real line, $\implies p^{0'} > 0$. The delta functions contain the squares, $\delta\left(\left(p^{0'}\right)^2 - \left(p^0\right)^2\right)$, but the argument of ρ is

without the square, i.e. $\rho(p^{0'}, \mathbf{p})$. Since $p^{0'} > 0$, the delta functions enforce

$$p^0 = p^{0'} > 0 \qquad \text{or} \qquad p^0 = -p^{0'} < 0. \qquad (\text{K.44})$$

First, we consider $p^0 > 0, \Longleftrightarrow p^0 = p^{0'}$:
In this case, obviously

$$\frac{p^0}{\sqrt{u}} = \frac{p^0}{p^{0'}} = 1, \qquad (\text{K.45})$$

and the two terms in the first line after the last equality sign in (K.43) cancel, and we are left with the last line.
Now we consider $p^0 < 0, \Longleftrightarrow p^0 = -p^{0'}$:
In this case the above fraction is -1 and the two terms do not cancel, but are equal. Considering these two terms together with the last term, we see that for the $p^0 = -p^{0'}$ case in the delta function

$$-\frac{i}{2} \int_0^\infty du\, \rho(\sqrt{u}, \mathbf{p}) \frac{p^0}{\sqrt{u}} \delta\left(u - \left(p^0\right)^2\right) + \frac{i}{2} \int_0^\infty du\, \rho(\sqrt{u}, \mathbf{p}) \delta\left(u - \left(p^0\right)^2\right) - i n_\beta(p^0)\rho(p^0, \mathbf{p})$$
$$= i\rho(-p^0, \mathbf{p}) - i n_\beta(p^0)\rho(p^0, \mathbf{p}) = -i\rho(p^0, \mathbf{p}) - i n_\beta(p^0)\rho(p^0, \mathbf{p}) = i n_\beta(-p^0)\rho(p^0, \mathbf{p})$$
$$= i n_\beta\left(|p^0|\right)\rho(p^0, \mathbf{p}), \qquad (\text{K.46})$$

where the last equality is true since $p^0 < 0$. Therefore, we write the final result as

$$G_{++}(p) = \frac{1}{2\pi} \int_0^\infty d\left(p^{0'}\right)^2 \frac{1}{\left(p^0\right)^2 - \left(p^{0'}\right)^2 + i\epsilon} \rho(p^{0'}, \mathbf{p}) - i\,\mathrm{sgn}(p^0)\, n_\beta\left(|p^0|\right)\rho(p^0, \mathbf{p}). \qquad (\text{K.47})$$

In the limit $T \longrightarrow 0$ the distribution function $n_\beta(p^0)$ becomes zero and we are left with the integral only, which is just the usual spectral representation in zero-temperature QFT. We can also evaluate the above for the case of a free massive scalar field, where the spectral function is just given by

$$\rho_{\text{free}}(p^2) = 2\pi\,\mathrm{sgn}(p^0)\,\delta\left(p^2 - m^2\right) = 2\pi\,\mathrm{sgn}(p^0)\,\delta\left(\left(p^0\right)^2 - \mathbf{p}^2 - m^2\right), \qquad (\text{K.48})$$

and we get

$$G_{++,\text{free}}(p) = \frac{1}{p^2 - m^2 + i\epsilon} - 2\pi i\,\delta\left(p^2 - m^2\right) n_\beta\left(|p^0|\right), \qquad (\text{K.49})$$

which is exactly the result given e.g. in [188]. In the limit $T \longrightarrow 0$ we get the standard Feynman propagator in $T = 0$ perturbative QFT. Note that usually the Feynman propagator is defined just as the correlation function $\langle T\varphi(x)\varphi(y)\rangle$, and the free propagator is then i times the above result, while we calculated $-i\langle T\varphi(x)\varphi(y)\rangle$. So if we multiply the usual result with the i in the numerator with $-i$, we get our above result, which is a consistency check that all signs and factors if i are correct. The convention we have used is the same as the one in [188].

The spectral representation for $G_{--}(p)$ can be obtained exactly in the same way as the one for $G_{++}(p)$, just with the role of the θ functions interchanged due to anti-time ordering instead of time-ordering. Looking at the derivation, it is easy to see that the thermal part

remains unchanged, but the principle value part gets an additional minus sign compared to (K.50), and, if written with an $i\epsilon$ prescription, we now have a $-i\epsilon$, in contrast to (K.35). Therefore

$$G_{--}(p) = -\frac{1}{2\pi}\mathscr{P}\mathscr{V}\int_{p^{0'}}\left(\frac{\rho(p^{0'},\mathbf{p})}{p^0-p^{0'}}\right) - i\rho(p^0,\mathbf{p})\left(\frac{1}{2}+n_\beta(p^0)\right)$$

$$= -\frac{1}{2\pi}\int_{-\infty}^{\infty}dp^{0'}\left(\frac{\rho(p^{0'},\mathbf{p})}{p^0-p^{0'}-i\epsilon}\right) - in_\beta(p^0)\rho(p^0,\mathbf{p}). \qquad (K.50)$$

Now we turn the representations for the retarded an advanced propagators. These are defined as

$$G_R(x,y) = G_{++}(x,y) - G_{+-}(x,y), \qquad (K.51)$$

and

$$G_A(x,y) = G_{++}(x,y) - G_{-+}(x,y). \qquad (K.52)$$

We can use the results obtained above in order to get the spectral representations

$$G_R(p) = \frac{1}{2\pi}\int_{-\infty}^{\infty}dp^{0'}\left(\frac{\rho(p^{0'},\mathbf{p})}{p^0-p^{0'}+i\epsilon}\right) = \frac{1}{2\pi}\mathscr{P}\mathscr{V}\int_{-\infty}^{\infty}dp^{0'}\left(\frac{\rho(p^{0'},\mathbf{p})}{p^0-p^{0'}}\right) - \frac{1}{2}i\,\rho(p^0,\mathbf{p}),$$

$$(K.53)$$

and

$$G_A(p) = \frac{1}{2\pi}\int_{-\infty}^{\infty}dp^{0'}\left(\frac{\rho(p^{0'},\mathbf{p})}{p^0-p^{0'}+i\epsilon}\right) + i\,\rho(p^0,\mathbf{p})$$

$$= \frac{1}{2\pi}\mathscr{P}\mathscr{V}\int_{-\infty}^{\infty}dp^{0'}\left(\frac{\rho(p^{0'},\mathbf{p})}{p^0-p^{0'}}\right) + \frac{1}{2}i\,\rho(p^0,\mathbf{p}) = \frac{1}{2\pi}\int_{-\infty}^{\infty}dp^{0'}\left(\frac{\rho(p^{0'},\mathbf{p})}{p^0-p^{0'}-i\epsilon}\right).$$

$$(K.54)$$

Note that there are no thermal distributions functions in the retarded or advanced propagator, and therefore the free causal propagators $G_{R,\text{free}}$ and $G_{A,\text{free}}$ are temperature independent, since the free spectral functions has this property. The full retarded and advanced propagators get of course a temperature dependence from the full spectral function.

From the spectral representation (K.53) of the retarded propagator it is obvious that

$$\rho(p^0,\mathbf{p}) = -2\,\text{Im}G_R. \qquad (K.55)$$

Danksagung

CHAPTER 12

Lists

List of Figures

Bibliography

[1] N. Christiansen, D. F. Litim, J. M. Pawlowski, and A. Rodigast, "Fixed points and infrared completion of quantum gravity," *Phys.Lett.* **B728** (2014) 114–117, arXiv:1209.4038 [hep-th].

[2] N. Christiansen, B. Knorr, J. M. Pawlowski, and A. Rodigast, "Global Flows in Quantum Gravity," arXiv:1403.1232 [hep-th].

[3] N. Christiansen, M. Haas, J. M. Pawlowski, and N. Strodthoff, "Transport Coefficients in Yang–Mills Theory and QCD," arXiv:1411.7986 [hep-ph].

[4] N. Christiansen, B. Knorr, J. M. Pawlowski, and A. Rodigast *in preparation* (2014) .

[5] R. Feynman, "Mathematical formulation of the quantum theory of electromagnetic interaction," *Phys.Rev.* **80** (1950) 440–457.

[6] S. Weinberg, "A Model of Leptons," *Physical Review Letters* **19** (Nov., 1967) 1264–1266.

[7] A. Salam and J. Ward, "On a gauge theory of elementary interactions," *Il Nuovo Cimento* (1961) .

[8] S. Glashow, "Partial Symmetries of Weak Interactions," *Nucl.Phys.* **22** (1961) 579–588.

[9] H. Fritzsch, M. Gell-Mann, and H. Leutwyler, "Advantages of the Color Octet Gluon Picture," *Phys.Lett.* **B47** (1973) 365–368.

[10] A. Einstein, "Die Feldgleichungen der Gravitation," *Sitzungsberichte der Preussischen Akademie der Wissenschaften zu Berlin, 844* (1915) .

[11] C. M. Will, "The confrontation between general relativity and experiment," *Living Reviews in Relativity* (2006) . http://www.livingreviews.org/lrr-2006-3.

[12] G. 't Hooft and M. Veltman, "One-loop divergencies in the theory of gravitation," *Annales de L'Institut Henri Poincare Section Physique Theorique* **20** (1974) 69–94.

[13] M. H. Goroff, A. Sagnotti, and A. Sagnotti, "Quantum gravity at two loops," *Physics Letters B* **160** (Oct., 1985) 81–86.

[14] K. Stelle, "Renormalization of Higher Derivative Quantum Gravity," *Phys.Rev.* **D16** (1977) 953–969.

[15] J. Gomis and S. Weinberg, "Are Nonrenormalizable Gauge Theories Renormalizable?," *Nucl. Phys.* **B469** (1996) 473–487, arXiv:hep-th/9510087.

[16] J. F. Donoghue, "Introduction to the effective field theory description of gravity," arXiv:gr-qc/9512024 [gr-qc].

[17] C. P. Burgess, "Quantum gravity in everyday life: General relativity as an effective field theory," *Living Rev. Rel.* **7** (2004) 5, arXiv:gr-qc/0311082.

[18] J. F. Donoghue, "Leading quantum correction to the Newtonian potential," *Phys. Rev. Lett.* **72** (1994) 2996–2999, arXiv:gr-qc/9310024.

[19] N. Christiansen, "Towards Ultraviolet Stability in Quantum Gravity, Dipoma Thesis,".

[20] D. F. Litim, "Fixed points of quantum gravity," *Phys. Rev. Lett.* **92** (2004) 201301, arXiv:hep-th/0312114.

[21] M. Niedermaier and M. Reuter, "The Asymptotic Safety Scenario in Quantum Gravity," *Living Rev.Rel.* **9** (2006) 5.

[22] R. Percacci, "Asymptotic Safety," arXiv:0709.3851 [hep-th]. to appear in 'Approaches to Quantum Gravity: Towards a New Understanding of Space, Time and Matter' ed. D. Oriti, Cambridge University Press.

[23] A. Codello, R. Percacci, and C. Rahmede, "Investigating the Ultraviolet Properties of Gravity with a Wilsonian Renormalization Group Equation," *Annals Phys.* **324** (2009) 414–469, arXiv:0805.2909 [hep-th].

[24] D. F. Litim, "Renormalisation group and the Planck scale," *Phil.Trans.Roy.Soc.Lond.* **A369** (2011) 2759–2778, arXiv:1102.4624 [hep-th].

[25] M. Reuter and F. Saueressig, "Quantum Einstein Gravity," *New J.Phys.* **14** (2012) 055022, arXiv:1202.2274 [hep-th].

[26] S. Nagy, "Lectures on renormalization and asymptotic safety," arXiv:1211.4151 [hep-th].

[27] D. F. Litim and J. M. Pawlowski, "On gauge invariant Wilsonian flows," *World Sci.* (1999) 168–185, arXiv:hep-th/9901063 [hep-th].

[28] J. Berges, N. Tetradis, and C. Wetterich, "Non-perturbative renormalization flow in quantum field theory and statistical physics," *Phys. Rept.* **363** (2002) 223–386, arXiv:hep-ph/0005122.

[29] K. Aoki, "Introduction to the nonperturbative renormalization group and its recent applications," *Int.J.Mod.Phys.* **B14** (2000) 1249–1326.

[30] C. Bagnuls and C. Bervillier, "Exact renormalization group equations. An Introductory review," *Phys.Rept.* **348** (2001) 91, `arXiv:hep-th/0002034 [hep-th]`.

[31] J. Polonyi, "Lectures on the functional renormalization group method," *Central Eur.J.Phys.* **1** (2003) 1–71, `arXiv:hep-th/0110026 [hep-th]`.

[32] J. M. Pawlowski, "Aspects of the functional renormalisation group," *Annals Phys.* **322** (2007) 2831–2915, `arXiv:hep-th/0512261 [hep-th]`.

[33] H. Gies, "Introduction to the functional RG and applications to gauge theories," *Lect.Notes Phys.* **852** (2012) 287–348, `arXiv:hep-ph/0611146 [hep-ph]`.

[34] B.-J. Schaefer and J. Wambach, "Renormalization group approach towards the QCD phase diagram," *Phys.Part.Nucl.* **39** (2008) 1025–1032, `arXiv:hep-ph/0611191 [hep-ph]`.

[35] O. J. Rosten, "Fundamentals of the Exact Renormalization Group," *Phys.Rept.* **511** (2012) 177–272, `arXiv:1003.1366 [hep-th]`.

[36] J. M. Pawlowski, "The QCD phase diagram: Results and challenges," *AIP Conf.Proc.* **1343** (2011) 75–80, `arXiv:1012.5075 [hep-ph]`.

[37] M. M. Scherer, S. Floerchinger, and H. Gies, "Functional renormalization for the BCS-BEC crossover," `arXiv:1010.2890 [cond-mat.quant-gas]`.

[38] J. Braun, "Fermion Interactions and Universal Behavior in Strongly Interacting Theories," *J.Phys.* **G39** (2012) 033001, `arXiv:1108.4449 [hep-ph]`.

[39] W. Metzner, M. Salmhofer, C. Honerkamp, V. Meden, and K. Schönhammer, "Functional renormalization group approach to correlated fermion systems," *Reviews of Modern Physics* **84** (Jan., 2012) 299–352, `arXiv:1105.5289 [cond-mat.str-el]`.

[40] I. Boettcher, J. M. Pawlowski, and S. Diehl, "Ultracold atoms and the Functional Renormalization Group," *Nuclear Physics B Proceedings Supplements* **228** (July, 2012) 63–135, `arXiv:1204.4394 [cond-mat.quant-gas]`.

[41] B. Delamotte, "An Introduction to the Nonperturbative Renormalization Group," in *Lecture Notes in Physics, Berlin Springer Verlag,* J. Polonyi and A. Schwenk, eds., vol. 852 of *Lecture Notes in Physics, Berlin Springer Verlag*, p. 49. 2012. `cond-mat/0702365`.

[42] L. Fister, "On the phase diagram of OCD with dynamical quarks, PhD Thesis,".

[43] U. Ellwanger, "The Running Gauge Coupling in the Exact Renormalization Group Approach," *Z.Phys.C76* (Feb., 1997) , `arXiv:hep-ph/9702309`.

[44] M. Pernici and M. Raciti, "Wilsonian flow and mass-independent renormalization," *Nuclear Physics B* (Oct., 1998) .

[45] M. Bonini, G. Marchesini, and M. Simionato, "Beta function and flowing couplings in the exact Wilson renormalization group in Yang-Mills theory," *Nuclear Physics B* (Feb., 1997) .

[46] D. F. Litim and T. Plehn, "Signatures of gravitational fixed points at the LHC," *Phys. Rev. Lett.* **100** (2008) 131301, arXiv:0707.3983 [hep-ph].

[47] E. Gerwick, D. Litim, and T. Plehn, "Asymptotic safety and Kaluza-Klein gravitons at the LHC," *Phys. Rev.* **D83** (2011) 084048, arXiv:1101.5548 [hep-ph].

[48] S. Weinberg, "Asymptotically Safe Inflation," *Phys. Rev.* **D81** (2010) 083535, arXiv:0911.3165 [hep-th].

[49] A. Bonanno, A. Contillo, and R. Percacci, "Inflationary solutions in asymptotically safe f(R) theories," *Class. Quant. Grav.* **28** (2011) 145026, arXiv:1006.0192 [gr-qc].

[50] A. Contillo, "Evolution of cosmological perturbations in an RG-driven inflationary scenario," *Phys. Rev.* **D83** (2011) 085016, arXiv:1011.4618 [gr-qc].

[51] M. Hindmarsh, D. Litim, and C. Rahmede, "Asymptotically Safe Cosmology," *JCAP* **1107** (2011) 019, arXiv:1101.5401 [gr-qc].

[52] A. Bonanno and M. Reuter, "Renormalization group improved black hole spacetimes," *Phys. Rev.* **D62** (2000) 043008, arXiv:hep-th/0002196.

[53] K. Falls, D. F. Litim, and A. Raghuraman, "Black Holes and Asymptotically Safe Gravity," *Int.J.Mod.Phys.* **A27** (2012) 1250019, arXiv:1002.0260 [hep-th].

[54] K. Falls and D. F. Litim, "Black hole thermodynamics under the microscope," arXiv:1212.1821 [gr-qc].

[55] B. Koch, C. Contreras, P. Rioseco, and F. Saueressig, "Black holes and running couplings: A comparison of two complementary approaches," arXiv:1311.1121 [hep-th].

[56] F. Saueressig, N. Alkofer, G. D'Odorico, and F. Vidotto, "Black holes in Asymptotically Safe Gravity," arXiv:1503.06472 [hep-th].

[57] D. F. Litim, "Mind the gap," *Int. J. Mod. Phys.* **A16** (2001) 2081–2088, arXiv:hep-th/0104221.

[58] S. Weinberg, "ULTRAVIOLET DIVERGENCES IN QUANTUM THEORIES OF GRAVITATION," *General Relativity: An Einstein centenary survey, Eds. Hawking, S.W., Israel, W; Cambridge University Press* (1979) 790–831.

[59] C. Wetterich, "Exact evolution equation for the effective potential," *Phys.Lett.* **B301** (1993) 90–94.

[60] M. Reuter, "Nonperturbative Evolution Equation for Quantum Gravity," *Phys. Rev.* **D57** (1998) 971–985, arXiv:hep-th/9605030.

[61] E. Manrique, S. Rechenberger, and F. Saueressig, "Asymptotically Safe Lorentzian Gravity," *Phys.Rev.Lett.* **106** (2011) 251302, `arXiv:1102.5012 [hep-th]`.

[62] D. F. Litim, "Fixed Points of Quantum Gravity and the Renormalisation Group," `arXiv:0810.3675 [hep-th]`.

[63] D. Benedetti, "On the number of relevant operators in asymptotically safe gravity," *Europhys.Lett.* **102** (2013) 20007, `arXiv:1301.4422 [hep-th]`.

[64] K. Falls, D. Litim, K. Nikolakopoulos, and C. Rahmede, "A bootstrap towards asymptotic safety," `arXiv:1301.4191 [hep-th]`.

[65] J. A. Dietz and T. R. Morris, "Redundant operators in the exact renormalisation group and in the f(R) approximation to asymptotic safety," *JHEP* **1307** (2013) 064, `arXiv:1306.1223 [hep-th]`.

[66] K. Falls, D. F. Litim, K. Nikolakopoulos, and C. Rahmede, "Further evidence for asymptotic safety of quantum gravity," `arXiv:1410.4815 [hep-th]`.

[67] R. Percacci and D. Perini, "Constraints on matter from asymptotic safety," *Phys. Rev.* **D67** (2003) 081503, `arXiv:hep-th/0207033`.

[68] J. E. Daum, U. Harst, and M. Reuter, "Non-perturbative QEG Corrections to the Yang-Mills Beta Function," `arXiv:1005.1488 [hep-th]`.

[69] A. Eichhorn and H. Gies, "Light fermions in quantum gravity," `arXiv:1104.5366 [hep-th]`.

[70] S. Folkerts, D. F. Litim, and J. M. Pawlowski, "Asymptotic freedom of Yang-Mills theory with gravity," *Phys.Lett.* **B709** (2012) 234–241, `arXiv:1101.5552 [hep-th]`.

[71] U. Harst and M. Reuter, "QED coupled to QEG," *JHEP* **05** (2011) 119, `arXiv:1101.6007 [hep-th]`.

[72] P. Donà, A. Eichhorn, and R. Percacci, "Matter matters in asymptotically safe quantum gravity," `arXiv:1311.2898 [hep-th]`.

[73] G. Narain and R. Percacci, "Renormalization Group Flow in Scalar-Tensor Theories. I," *Class. Quant. Grav.* **27** (2010) 075001, `arXiv:0911.0386 [hep-th]`.

[74] T. Henz, J. M. Pawlowski, A. Rodigast, and C. Wetterich, "Dilaton Quantum Gravity," *Phys.Lett.* **B727** (2013) 298–302, `arXiv:1304.7743 [hep-th]`.

[75] D. Benedetti, P. F. Machado, and F. Saueressig, "Asymptotic safety in higher-derivative gravity," *Mod. Phys. Lett.* **A24** (2009) 2233–2241, `arXiv:0901.2984 [hep-th]`.

[76] N. Ohta and R. Percacci, "Higher Derivative Gravity and Asymptotic Safety in Diverse Dimensions," *Class.Quant.Grav.* **31** (2014) 015024, `arXiv:1308.3398 [hep-th]`.

[77] M. Demmel, F. Saueressig, and O. Zanusso, "RG flows of Quantum Einstein Gravity on maximally symmetric spaces," `arXiv:1401.5495 [hep-th]`.

[78] A. Codello, G. D'Odorico, and C. Pagani, "Consistent closure of RG flow equations in quantum gravity," `arXiv:1304.4777 [gr-qc]`.

[79] I. Donkin and J. M. Pawlowski, "The phase diagram of quantum gravity from diffeomorphism-invariant RG-flows," `arXiv:1203.4207 [hep-th]`.

[80] P. Fischer and D. F. Litim, "Fixed points of quantum gravity in extra dimensions," *Phys. Lett.* **B638** (2006) 497–502, `arXiv:hep-th/0602203`.

[81] A. Eichhorn, "On unimodular quantum gravity," *Class.Quant.Grav.* **30** (2013) 115016, `arXiv:1301.0879 [gr-qc]`.

[82] A. Eichhorn, "The Renormalization Group flow of unimodular f(R) gravity," *JHEP* **1504** (2015) 096, `arXiv:1501.05848 [gr-qc]`.

[83] E. Manrique and M. Reuter, "Bimetric Truncations for Quantum Einstein Gravity and Asymptotic Safety," *Annals Phys.* **325** (2010) 785–815, `arXiv:0907.2617 [gr-qc]`.

[84] E. Manrique, M. Reuter, and F. Saueressig, "Bimetric Renormalization Group Flows in Quantum Einstein Gravity," *Annals Phys.* **326** (2011) 463–485, `arXiv:1006.0099 [hep-th]`.

[85] D. Becker and M. Reuter, "En route to Background Independence: Broken split-symmetry, and how to restore it with bi-metric average actions," `arXiv:1404.4537 [hep-th]`.

[86] M. Shaposhnikov and C. Wetterich, "Asymptotic safety of gravity and the Higgs boson mass," *Phys.Lett.* **B683** (2010) 196–200, `arXiv:0912.0208 [hep-th]`.

[87] O. Antipin, J. Krog, M. Mojaza, and F. Sannino, "A Stable Extension with(out) Gravity," `arXiv:1311.1092 [hep-ph]`.

[88] B. Koch and F. Saueressig, "Structural aspects of asymptotically safe black holes," *Class.Quant.Grav.* **31** (2014) 015006, `arXiv:1306.1546 [hep-th]`.

[89] B. Koch and F. Saueressig, "Black holes within Asymptotic Safety," `arXiv:1401.4452 [hep-th]`.

[90] E. J. Copeland, C. Rahmede, and I. D. Saltas, "Asymptotically Safe Starobinsky Inflation," `arXiv:1311.0881 [gr-qc]`.

[91] L. Abbott, "Introduction to the Background Field Method," *Acta Phys.Polon.* **B13** (1982) 33.

[92] D. F. Litim and J. M. Pawlowski, "On gauge invariance and Ward identities for the Wilsonian renormalization group," *Nucl.Phys.Proc.Suppl.* **74** (1999) 325–328, `arXiv:hep-th/9809020 [hep-th]`.

[93] D. F. Litim and J. M. Pawlowski, "Wilsonian flows and background fields," *Phys.Lett.* **B546** (2002) 279–286, `arXiv:hep-th/0208216 [hep-th]`.

[94] J. M. Pawlowski, "On Wilsonian flows in gauge theories," *Acta Phys.Slov.* **52** (2002) 475.

[95] D. F. Litim and J. M. Pawlowski, "Renormalization group flows for gauge theories in axial gauges," *JHEP* **0209** (2002) 049, `arXiv:hep-th/0203005 [hep-th]`.

[96] J. Braun, H. Gies, and J. M. Pawlowski, "Quark Confinement from Color Confinement," *Phys.Lett.* **B684** (2010) 262–267, `arXiv:0708.2413 [hep-th]`.

[97] J. M. PAWLOWSKI, "ON WILSONIAN FLOWS IN GAUGE THEORIES," *International Journal of Modern Physics A* **16** no. 11, (2001) 2105–2110, `http://www.worldscientific.com/doi/pdf/10.1142/S0217751X01004785`. `http://www.worldscientific.com/doi/abs/10.1142/S0217751X01004785`.

[98] I. H. Bridle, J. A. Dietz, and T. R. Morris, "The local potential approximation in the background field formalism," *JHEP* **1403** (2014) 093, `arXiv:1312.2846 [hep-th]`.

[99] J. A. Dietz and T. R. Morris, "Background independent exact renormalization group for conformally reduced gravity," *JHEP* **1504** (2015) 118, `arXiv:1502.07396 [hep-th]`.

[100] A. Eichhorn, H. Gies, and M. M. Scherer, "Asymptotically free scalar curvature-ghost coupling in Quantum Einstein Gravity," *Phys.Rev.* **D80** (2009) 104003, `arXiv:0907.1828 [hep-th]`.

[101] A. Eichhorn, "Faddeev-Popov ghosts in quantum gravity beyond perturbation theory," *Phys.Rev.* **D87** (2013) 124016, `arXiv:1301.0632 [hep-th]`.

[102] F. Marhauser and J. M. Pawlowski, "Confinement in Polyakov Gauge," `arXiv:0812.1144 [hep-ph]`.

[103] L. Fister and J. M. Pawlowski, "Confinement from Correlation Functions," *Phys.Rev.* **D88** (2013) 045010, `arXiv:1301.4163 [hep-ph]`.

[104] C. S. Fischer and J. M. Pawlowski, "Uniqueness of infrared asymptotics in Landau gauge Yang- Mills theory II," *Phys. Rev.* **D80** (2009) 025023, `arXiv:0903.2193 [hep-th]`.

[105] D. C. Brydges and G. Slade, "A Renormalisation Group Method. II. Approximation by Local Polynomials," *Journal of Statistical Physics* (Feb., 2015) , `arXiv:1403.7253 [math-ph]`.

[106] R. Bauerschmidt, D. C. Brydges, and G. Slade, "A Renormalisation Group Method. III. Perturbative Analysis," *Journal of Statistical Physics* (Feb., 2015) , `arXiv:1403.7252 [math-ph]`.

[107] J. A. M. Vermaseren, "New features of FORM," `arXiv:math-ph/0010025`.

[108] J. Martingarcia, R. Portugal, and L. Manssur, "The Invar tensor package," *Computer Physics Communications* **177** (Oct., 2007) 640–648, `arXiv:0704.1756 [cs.SC]`.

[109] C. Wetterich, "Challenges for Functional Renormalization, Talk given at the 6th International Conference on the Exact Renormalization Group,7.9.2012,".

[110] D. Schnoerr, I. Boettcher, J. M. Pawlowski, and C. Wetterich, "Error estimates and specification parameters for functional renormalization," *Annals Phys.* **334** (2013) 83–99, `arXiv:1301.4169 [cond-mat.quant-gas]`.

[111] U. Ellwanger, M. Hirsch, and A. Weber, "Flow equations for the relevant part of the pure Yang-Mills action," *Z.Phys.* **C69** (1996) 687–698, `arXiv:hep-th/9506019 [hep-th]`.

[112] J. M. Pawlowski, D. F. Litim, S. Nedelko, and L. von Smekal, "Infrared behaviour and fixed points in Landau gauge QCD," *Phys. Rev. Lett.* **93** (2004) 152002, `arXiv:hep-th/0312324`.

[113] C. S. Fischer and H. Gies, "Renormalization flow of Yang-Mills propagators," *JHEP* **10** (2004) 048, `arXiv:hep-ph/0408089`.

[114] C. S. Fischer, A. Maas, and J. M. Pawlowski, "On the infrared behavior of Landau gauge Yang-Mills theory," *Annals Phys.* **324** (2009) 2408–2437, `arXiv:0810.1987 [hep-ph]`.

[115] L. Fister and J. M. Pawlowski, "Yang-Mills correlation functions at finite temperature," `arXiv:1112.5440 [hep-ph]`.

[116] M. Mitter, J. M. Pawlowski, and N. Strodthoff, "Chiral symmetry breaking in continuum QCD," *Phys.Rev.* **D91** (2015) 054035, `arXiv:1411.7978 [hep-ph]`.

[117] T. R. Morris, "Derivative expansion of the exact renormalization group," *Phys.Lett.* **B329** (1994) 241–248, `arXiv:hep-ph/9403340 [hep-ph]`.

[118] N. Christiansen, "IR-completion of Asymptotic Safety, Talk given at the International Asymptotic Safety Seminar,5.11.2012,".

[119] D. F. Litim, "Optimised renormalisation group flows," *Phys. Rev.* **D64** (2001) 105007, `arXiv:hep-th/0103195`.

[120] A. Bonanno and M. Reuter, "Cosmology with selfadjusting vacuum energy density from a renormalization group fixed point," *Phys.Lett.* **B527** (2002) 9–17, `arXiv:astro-ph/0106468 [astro-ph]`.

[121] C. Contreras and D. F. Litim, "in preparation," (2014) , `in preparation`.

[122] D. Litim and A. Satz, "Limit cycles and quantum gravity," `arXiv:1205.4218 [hep-th]`.

[123] R. Kress, "Linear Integral Equations," *New York: Springer Verlag.* (1989) .

[124] R. Courant and D. Hilbert, "Methods of Mathematical Physics 1," *Wiley.* (1989) .

[125] H. Bueckner, "A Special Method of Successive Approximations for Fredholm Integral Equations," *Duke Mathematical Journal.* **13** (1948) 197–206.

[126] V. Branchina, K. A. Meissner, and G. Veneziano, "The Price of an exact, gauge invariant RG flow equation," *Phys.Lett.* **B574** (2003) 319–324, `arXiv:hep-th/0309234 [hep-th]`.

[127] J. M. Pawlowski, "Geometrical effective action and Wilsonian flows," `arXiv:hep-th/0310018 [hep-th]`.

[128] G. Vilkovisky, "The Unique Effective Action in Quantum Field Theory," *Nucl.Phys.* **B234** (1984) 125–137.

[129] C. Burgess and G. Kunstatter, "ON THE PHYSICAL INTERPRETATION OF THE VILKOVISKY-DE WITT EFFECTIVE ACTION," *Mod.Phys.Lett.* **A2** (1987) 875.

[130] S. Huggins, G. Kunstatter, H. Leivo, and D. Toms, "THE VILKOVISKY-DE WITT EFFECTIVE ACTION FOR QUANTUM GRAVITY," *Nucl.Phys.* **B301** (1988) 627.

[131] B. S. DeWitt, "THE EFFECTIVE ACTION," *Quantum Field Theory and Quantum Statistics, Vol. 1, Batalin, I.A. (Ed.) et al.* (1988) 191–222.

[132] A. Rebhan, "The Vilkovisky-DeWitt effective action and its application to Yang-Mills theories," *Nuclear Physics B* **288** (1987) 832–857.

[133] D. F. Litim, "Optimization of the exact renormalization group," *Phys.Lett.* **B486** (2000) 92–99, `arXiv:hep-th/0005245 [hep-th]`.

[134] A. Eichhorn and H. Gies, "Ghost anomalous dimension in asymptotically safe quantum gravity," *Phys. Rev.* **D81** (2010) 104010, `arXiv:1001.5033 [hep-th]`.

[135] K. Groh and F. Saueressig, "Ghost wave-function renormalization in Asymptotically Safe Quantum Gravity," *J. Phys.* **A43** (2010) 365403, `arXiv:1001.5032 [hep-th]`.

[136] N. Christiansen, J. Meibohm, J. M. Pawlowski, and M. Reichert *in preparation* (2015) .

[137] S. P. Robinson and F. Wilczek, "Gravitational correction to running of gauge couplings," *Phys. Rev. Lett.* **96** (2006) 231601, `arXiv:hep-th/0509050`.

[138] A. R. Pietrykowski, "Gauge dependence of gravitational correction to running of gauge couplings," *Phys. Rev. Lett.* **98** (2007) 061801, `arXiv:hep-th/0606208`.

[139] D. J. Toms, "Quantum gravity and charge renormalization," *Phys. Rev.* **D76** (2007) 045015, `arXiv:0708.2990 [hep-th]`.

[140] D. Ebert, J. Plefka, and A. Rodigast, "Absence of gravitational contributions to the running Yang-Mills coupling," *Phys. Lett.* **B660** (2008) 579–582, `arXiv:0710.1002 [hep-th]`.

[141] Y. Tang and Y.-L. Wu, "Gravitational Contributions to the Running of Gauge Couplings," *Commun. Theor. Phys.* **54** (2010) 1040–1044, `arXiv:0807.0331 [hep-ph]`.

[142] D. J. Toms, "Quantum gravitational contributions to quantum electrodynamics," *Nature* **468** (2010) 56–59, `arXiv:1010.0793 [hep-th]`.

[143] S. Folkerts, "Asymptotic Safety for Gravity coupled to Yang–Mills Theory: An RG Study," *Diploma thesis, Heidelberg* (2009) .

[144] P. Braun-Munzinger and J. Wambach, "The Phase Diagram of Strongly-Interacting Matter," *Rev.Mod.Phys.* **81** (2009) 1031–1050, `arXiv:0801.4256 [hep-ph]`.

[145] K. Fukushima and T. Hatsuda, "The phase diagram of dense QCD," *Rept.Prog.Phys.* **74** (2011) 014001, `arXiv:1005.4814 [hep-ph]`.

[146] A. S. Kronfeld, "Twenty-first Century Lattice Gauge Theory: Results from the QCD Lagrangian," *Ann.Rev.Nucl.Part.Sci.* **62** (2012) 265–284, `arXiv:1203.1204 [hep-lat]`.

[147] **PHENIX Collaboration** Collaboration, K. Adcox *et al.*, "Formation of dense partonic matter in relativistic nucleus-nucleus collisions at RHIC: Experimental evaluation by the PHENIX collaboration," *Nucl.Phys.* **A757** (2005) 184–283, `arXiv:nucl-ex/0410003 [nucl-ex]`.

[148] **STAR Collaboration** Collaboration, J. Adams *et al.*, "Experimental and theoretical challenges in the search for the quark gluon plasma: The STAR Collaboration's critical assessment of the evidence from RHIC collisions," *Nucl.Phys.* **A757** (2005) 102–183, `arXiv:nucl-ex/0501009 [nucl-ex]`.

[149] **ALICE Collaboration** Collaboration, K. Aamodt *et al.*, "Elliptic flow of charged particles in Pb-Pb collisions at 2.76 TeV," *Phys.Rev.Lett.* **105** (2010) 252302, `arXiv:1011.3914 [nucl-ex]`.

[150] T. K. Nayak, "Heavy Ions: Results from the Large Hadron Collider," *Pramana* **79** (2012) 719–735, `arXiv:1201.4264 [nucl-ex]`.

[151] P. Braun-Munzinger, J. Stachel, and C. Wetterich, "Chemical freezeout and the QCD phase transition temperature," *Phys.Lett.* **B596** (2004) 61–69, `arXiv:nucl-th/0311005 [nucl-th]`.

[152] R. Rapp and H. van Hees, "Heavy Quark Diffusion as a Probe of the Quark-Gluon Plasma," `arXiv:0803.0901 [hep-ph]`.

[153] U. Heinz and R. Snellings, "Collective flow and viscosity in relativistic heavy-ion collisions," *Ann.Rev.Nucl.Part.Sci.* **63** (2013) 123–151, `arXiv:1301.2826 [nucl-th]`.

[154] R. Venugopalan, "From many body wee parton dynamics to perfect fluid: a standard model for heavy ion collisions," *PoS* **ICHEP2010** (2010) 567, `arXiv:1012.4699 [hep-ph]`.

[155] B. V. Jacak and B. Muller, "The exploration of hot nuclear matter," *Science* **337** (2012) 310–314.

[156] P. Romatschke and U. Romatschke, "Viscosity Information from Relativistic Nuclear Collisions: How Perfect is the Fluid Observed at RHIC?," *Phys.Rev.Lett.* **99** (2007) 172301, arXiv:0706.1522 [nucl-th].

[157] P. Huovinen and D. Molnar, "The Applicability of causal dissipative hydrodynamics to relativistic heavy ion collisions," *Phys.Rev.* **C79** (2009) 014906, arXiv:0808.0953 [nucl-th].

[158] H. Song and U. W. Heinz, "Multiplicity scaling in ideal and viscous hydrodynamics," *Phys.Rev.* **C78** (2008) 024902, arXiv:0805.1756 [nucl-th].

[159] C. Zhou, Y. Ma, D. Fang, G. Zhang, J. Xu, *et al.*, "Correlation between elliptic flow and shear viscosity in intermediate-energy heavy-ion collisions," *Phys.Rev.* **C90** no. 5, (2014) 057601, arXiv:1411.5409 [nucl-th].

[160] L. P. Csernai, J. Kapusta, and L. D. McLerran, "On the Strongly-Interacting Low-Viscosity Matter Created in Relativistic Nuclear Collisions," *Phys.Rev.Lett.* **97** (2006) 152303, arXiv:nucl-th/0604032 [nucl-th].

[161] T. Hirano and M. Gyulassy, "Perfect fluidity of the quark gluon plasma core as seen through its dissipative hadronic corona," *Nucl.Phys.* **A769** (2006) 71–94, arXiv:nucl-th/0506049 [nucl-th].

[162] P. Kovtun, D. T. Son, and A. O. Starinets, "Viscosity in strongly interacting quantum field theories from black hole physics," *Phys.Rev.Lett.* **94** (2005) 111601, arXiv:hep-th/0405231 [hep-th].

[163] M. Haas, L. Fister, and J. M. Pawlowski, "Gluon spectral functions and transport coefficients in Yang–Mills theory," *Phys.Rev.* **D90** no. 9, (2014) 091501, arXiv:1308.4960 [hep-ph].

[164] G. Aarts and J. M. Martinez Resco, "Transport coefficients, spectral functions and the lattice," *JHEP* **0204** (2002) 053, arXiv:hep-ph/0203177 [hep-ph].

[165] Z. Xu and C. Greiner, "Shear viscosity in a gluon gas," *Phys.Rev.Lett.* **100** (2008) 172301, arXiv:0710.5719 [nucl-th].

[166] H. B. Meyer, "A Calculation of the shear viscosity in SU(3) gluodynamics," *Phys.Rev.* **D76** (2007) 101701, arXiv:0704.1801 [hep-lat].

[167] H. B. Meyer, "Transport properties of the quark-gluon plasma from lattice QCD," *Nucl.Phys.* **A830** (2009) 641C–648C, arXiv:0907.4095 [hep-lat].

[168] R. Lang and W. Weise, "Shear viscosity from Kubo formalism: NJL model study," *Eur.Phys.J.* **A50** (2014) 63, arXiv:1311.4628 [hep-ph].

[169] R. Marty, E. Bratkovskaya, W. Cassing, J. Aichelin, and H. Berrehrah, "Transport coefficients from the Nambu-Jona-Lasinio model for $SU(3)_f$," *Phys.Rev.* **C88** (2013) 045204, arXiv:1305.7180 [hep-ph].

[170] B. A. Gelman, E. V. Shuryak, and I. Zahed, "Ultracold strongly coupled gas: A near-ideal liquid," *Phys.Rev.* **A72** (2005) 043601, `arXiv:nucl-th/0410067 [nucl-th]`.

[171] J. E. Thomas, "Is an Ultra-Cold Strongly Interacting Fermi Gas a Perfect Fluid?," *Nuclear Physics A* **830** (Nov., 2009) 665–672, `arXiv:0907.0140 [cond-mat.quant-gas]`.

[172] T. Schaefer, "Fluid Dynamics and Viscosity in Strongly Correlated Fluids," `arXiv:1403.0653 [hep-ph]`.

[173] K. Kamikado, N. Strodthoff, L. von Smekal, and J. Wambach, "Real-time correlation functions in the $O(N)$ model from the functional renormalization group," *Eur.Phys.J.* **C74** (2014) 2806, `arXiv:1302.6199 [hep-ph]`.

[174] S. Strauss, C. S. Fischer, and C. Kellermann, "Analytic structure of the Landau gauge gluon propagator," *Phys.Rev.Lett.* **109** (2012) 252001, `arXiv:1208.6239 [hep-ph]`.

[175] M. Haas, "Spectral functions in finite temperature SU(3) gauge theory and applications to transport phenomena.," *PhD thesis, Heidelberg* (2014) .

[176] R. Kubo, "Statistical-Mechanical Theory of Irreversible Processes. I. General Theory and Simple Applications to Magnetic and Conduction Problems," *Journal of the Physical Society of Japan* **12** no. 6, (1957) 570–586, `http://dx.doi.org/10.1143/JPSJ.12.570`. `http://dx.doi.org/10.1143/JPSJ.12.570`.

[177] R. Zubarev and O. Morozov, "Statistical Mechanics of Non-equilibrium Processes Vol. 2: Relaxation and Hydrodynamics Processes," *Akademie Verlag GmbH.* (1996) .

[178] L. Kadanoff and P. Martin, "Hydrodynamic equations and correlation functions.," *Annals Phys.* **24,419** .

[179] J. S. Schwinger, "Brownian motion of a quantum oscillator," *J.Math.Phys.* **2** (1961) 407–432.

[180] L. Keldysh, "Diagram technique for nonequilibrium processes," *Zh.Eksp.Teor.Fiz.* **47** (1964) 1515–1527.

[181] J. Berges, "Introduction to nonequilibrium quantum field theory," *AIP Conf. Proc.* **739** (2005) 3–62, `arXiv:hep-ph/0409233`.

[182] A. Kamenev, "Many-body theory of non-equilibrium systems," *eprint arXiv:cond-mat/0412296* (Dec., 2004) , `cond-mat/0412296`.

[183] N. Landsman and C. van Weert, "Real and Imaginary Time Field Theory at Finite Temperature and Density," *Phys.Rept.* **145** (1987) 141.

[184] K.-c. Chou, Z.-b. Su, B.-l. Hao, and L. Yu, "Equilibrium and Nonequilibrium Formalisms Made Unified," *Phys.Rept.* **118** (1985) 1.

[185] A. Niemi and G. Semenoff, "Finite Temperature Quantum Field Theory in Minkowski Space," *Annals Phys.* **152** (1984) 105.

[186] T. Evans, "N point finite temperature expectation values at real times," *Nucl.Phys.* **B374** (1992) 340–372.

[187] R. Kobes, "A Correspondence Between Imaginary Time and Real Time Finite Temperature Field Theory," *Phys.Rev.* **D42** (1990) 562–572.

[188] A. K. Das, *Finite temperature field theory*. World Scientific, Singapore, 1997. Singapore, Singapore: World Scientific (1997) 404 p.

[189] P. C. Martin and J. Schwinger, "Theory of Many-Particle Systems. I," *Physical Review* **115** (Sept., 1959) 1342–1373.

[190] H. Matsumoto and H. Umezawa, "Thermo field dynamics of a quantum algebra," *Physics Letters A* **103** (July, 1984) 405–407.

[191] H. Matsumoto, I. Ojima, and H. Umezawa, "Perturbation and renormalization in thermo field dynamics," *Annals of Physics* **152** (Feb., 1984) 348–375.

[192] H. Matsumoto, Y. Nakano, and H. Umezawa, "Free energy in thermo field dynamics," **31** (Mar., 1985) 1495–1498.

[193] N. Christiansen, "Internal notes.," *PhD thesis, Heidelberg* (2015) .

[194] R. Silver, D. Sivia, and J. Gubernatis, "Maximum-entropy method for analytic continuation of quantum Monte Carlo data," *Phys.Rev.* **B41** (1990) 2380–2389.

[195] J. Gubernatis, M. Jarrell, R. Silver, and D. Sivia, "Quantum Monte Carlo simulations and maximum entropy: Dynamics from imaginary-time data," *Phys.Rev.* **B44** (1991) 6011–6029.

[196] S. Borsanyi, G. Endrodi, Z. Fodor, S. Katz, and K. Szabo, "Precision SU(3) lattice thermodynamics for a large temperature range," *JHEP* **1207** (2012) 056, arXiv:1204.6184 [hep-lat].

[197] S. Jeon, "Hydrodynamic transport coefficients in relativistic scalar field theory," *Phys.Rev.* **D52** (1995) 3591–3642, arXiv:hep-ph/9409250 [hep-ph].

[198] S. Jeon and L. G. Yaffe, "From quantum field theory to hydrodynamics: Transport coefficients and effective kinetic theory," *Phys.Rev.* **D53** (1996) 5799–5809, arXiv:hep-ph/9512263 [hep-ph].

[199] P. B. Arnold, G. D. Moore, and L. G. Yaffe, "Transport coefficients in high temperature gauge theories. 2. Beyond leading log," *JHEP* **0305** (2003) 051, arXiv:hep-ph/0302165 [hep-ph].

[200] J. L. Richardson, "The Heavy Quark Potential and the Upsilon, J/psi Systems," *Phys.Lett.* **B82** (1979) 272.

[201] F. Karbstein, A. Peters, and M. Wagner, "$\Lambda_{\overline{\text{MS}}}^{(n_f=2)}$ from a momentum space analysis of the quark-antiquark static potential," *JHEP* **1409** (2014) 114, `arXiv:1407.7503 [hep-ph]`.

[202] A. Nesterenko, "Quark - anti-quark potential in the analytic approach to QCD," *Phys.Rev.* **D62** (2000) 094028, `arXiv:hep-ph/9912351 [hep-ph]`.

[203] A. Nesterenko, "Analytic invariant charge in QCD," *Int.J.Mod.Phys.* **A18** (2003) 5475–5520, `arXiv:hep-ph/0308288 [hep-ph]`.

[204] F. Schrempp, "Tracking QCD instantons," *J.Phys.* **G28** (2002) 915–926, `arXiv:hep-ph/0109032 [hep-ph]`.

[205] J. O. Andersen, L. E. Leganger, M. Strickland, and N. Su, "The QCD trace anomaly," *Phys.Rev.* **D84** (2011) 087703, `arXiv:1106.0514 [hep-ph]`.

[206] L. von Smekal, K. Maltman, and A. Sternbeck, "The strong coupling and its running to four loops in a minimal MOM scheme," *Phys. Lett.* **B681** (2009) 336–342, `arXiv:0903.1696 [hep-ph]`. miniMOM.

[207] M. Haas, A. Maas, and J. M. Pawlowski, ",", *in preparation* (2014) .

[208] J.-W. Chen, Y.-F. Liu, Y.-K. Song, and Q. Wang, "Shear and bulk viscosities of a weakly coupled quark gluon plasma with finite chemical potential and temperature: Leading-log results," *Phys.Rev.* **D87** no. 3, (2013) 036002, `arXiv:1212.5308 [hep-ph]`.

[209] P. B. Arnold, G. D. Moore, and L. G. Yaffe, "Transport coefficients in high temperature gauge theories. 1. Leading log results," *JHEP* **0011** (2000) 001, `arXiv:hep-ph/0010177 [hep-ph]`.

[210] P. B. Arnold and C.-x. Zhai, "The Three loop free energy for high temperature QED and QCD with fermions," *Phys.Rev.* **D51** (1995) 1906–1918, `arXiv:hep-ph/9410360 [hep-ph]`.

[211] J. O. Andersen, E. Braaten, and M. Strickland, "Hard thermal loop resummation of the free energy of a hot quark - gluon plasma," *Phys.Rev.* **D61** (2000) 074016, `arXiv:hep-ph/9908323 [hep-ph]`.

[212] N. Demir and S. A. Bass, "Shear-Viscosity to Entropy-Density Ratio of a Relativistic Hadron Gas," *Phys.Rev.Lett.* **102** (2009) 172302, `arXiv:0812.2422 [nucl-th]`.